Membrane separation of anions in concentrated electrolytes

by

Edvard Sivertsen

Thesis submitted in partial fulfillment of the requirements for
the academic degree *Doktor Ingeniør*.

Department of Chemical Engineering
Norwegian University of Science and Technology (NTNU)
Trondheim, Norway

September 2001

Abstract

This thesis deals with a new possible nanofiltration process, where the objective is to remove sulphate ions present in trace amounts from a concentrated magnesium chloride brine. Ideally, the nanofiltration membrane will retain the divalent sulphate ions, whereas the monovalent chloride ions will pass through the membrane. In spite of the increasing use of nanofiltration the separation and transport mechanisms are not well understood and the retention models are not very accurate.

The magnesium chloride concentration in the experiments varies from 0.1 to 5 molal, whereas the sulphate concentration changes between three levels, *i.e.* 0, 300 ppm and 3000 ppm. An extensive database containing experimentally measured chloride and sulphate ion retentions and volume fluxes is established using the Osmonics/Desal membranes Desal 5 DK and Desal G5. The effects of Reynolds number, temperature and pressure are investigated.

The observed chloride retentions are relatively low, less than 10%, whereas the observed sulphate retentions are somewhat higher, around 20-60%. Both ion retentions decrease with increasing magnesium chloride concentration and increasing temperature, whereas the ion retentions increase with increasing Reynolds number and pressure. The ions are believed to be separated by the dielectric exclusion mechanism and both the chloride and sulphate retentions fit the Spiegler-Kedem model and the finely-porous model nicely.

The observed volume fluxes decrease with increasing magnesium chloride concentrations, which can at least partially be explained by the increase in the viscosity, the decrease in the water activity inside the membrane and the osmotic pressure difference between the feed side and the permeate side of the membrane.

The concentration polarisation of the chloride ions decreases with increasing concentration and is negligible at 5 molal magnesium chloride concentration, but the concentration polarisation of the sulphate ions is believed to be significant even at this high magnesium chloride concentration level.

Preface

"Better is the enemy of good", Voltaire.

This thesis is submitted in partial fulfillment of the requirements for the degree *Doktor Ingeniør* at Norwegian University of Science and Technology. The degree also requires one full year of courses at graduate and postgraduate levels.

When doing basic research one can only plan for the activities not the results. Sometimes the obtained results give important information and sometimes you find yourself at a dead-end. New to the membrane science I stumbled and lost focus several times before I after approximately a year found a useful track. The thesis tries to reflect my thoughts around using membrane separation in concentrated electrolytes, where I in particular have stressed the subject of describing the electrolyte solutions both qualitatively and quantitatively. Unfortunately, I was not able to combine these results with membrane separation theories and the discussion remains on a quantitative level.

The experimental measured fluxes and ion retentions became to a certain degree very similar and much time and money could have been saved by using fewer experiments. But at least now we know for sure how the fluxes and retentions react when changing different operation parameters at high concentrations. I think this thesis makes the starting point I wanted when I started my study, and further, knowing what we know today the experimental plan would have looked quite different from the one I followed, *e.g.* I would have had a stronger focus on the membrane material and how to optimize this.

Since the results were obtained so late in my research period the thesis is written as a monograph in order to finish the writing not too far behind the schedule. However, some of the results were presented at the Euromembrane 2000 conference in Israel, where I had one oral presentation entitled "Direct measurements of the concentration polarisation phenomenon" and one poster entitled "Retention measurements in concentrated salt solutions". Further, I have started to write a series of articles, which will present the results discussed in this thesis. The articles will be submitted to an international membrane journal.

Acknowledgements

I am grateful to my supervisor Norvald Nesse for our many discussions, your encouraging feedback and for always taking the time to listen to a frustrated student. I really appreciate your cheerful nature and your short, good, unscientific anecdotes.

I will also thank my secondary supervisor Ole Værnes, Roger I. Hagen and Per Oscar Wiig at SINTEF Chemical Engineering for valuable discussions, especially during the first period of my study, and Birger Langseth, Per Engseth, Oddmund Wallevik and Torgeir Lunde at Norsk Hydro for encouraging feedback at the project meetings.

Other people that have helped me to various extent and to whom I am thankful are Thor Thorsen for taking the membrane photos in Chapter 5, Odd Ivar Hovin for help with building the apparatus, Berhanu A. Demessie for valuable discussions and proofreading of the thesis, Lars Erik Smith for help with the Unscrambler program, and, "my" diploma students Vetle Misje and Mats Vingereid who worked with the concentration polarisation unit. I will also say thanks to my "roommate" through four years Ivar J. Halvorsen for our everyday small chats putting everything in perspective and for help with computer related problems.

I am also grateful to the Norwegian Research Council and Norsk Hydro for financing my study, Nordisk Forskerutdanningsakademi for financing a four week long visit at the Technical University of Denmark (1997) and a three week long visit at the Lappeenranta University of Technology, Finland (1999), and Norges Tekniske Høgskole fund for financial support to participate at the Euromembrane 2000 conference in Israel.

Finally, I will thank Synnøve, Ellisiv, mom, dad, Sverre, Svein Kåre, Torun and Ole-Einar for all love and support. To my wife Synnøve and my daughter Ellisiv, who I love very much: *We finally made it!*

Contents

List of symbols

Roman

A_k	Effective membrane porosity [-]
a_i	Activity [-]
C^*	Membrane constant [m^3 m^{-2} s^{-1}]
C_i	Concentration outside the membrane [molar]
$\overline{C}_i$	Mean logarithmic concentration [molar]
c_i	Concentration inside the membrane [molar]
D	Diffusion coefficient [m^2 s^{-1}]
d_h	Hydraulic diameter,
	$d_h = 4$ flow area/wetted periphery [m]
E_p	Potential energy [J]
e	The charge of an electron [C]
F	The Faraday constant [C mol^{-1}]
F	Feed flow [m^3 s^{-1}]
F	Intermolecular force [N = J m^{-1}]
F_{ij}	Friction force [kg m mol^{-1} s^{-2}]
f_{ij}	Friction coefficient [kg mol^{-1} s^{-1}]
ΔG_{hyd}	Gibbs hydration energy [J mol^{-1}]
g	Rational osmotic coefficient [-]
H	Enthalpy [J mol^{-1}]
ΔH_{hyd}	Hydration enthalpy [J mol^{-1}]
ΔH_{lat}	Crystal lattice formation enthalpy [J mol^{-1}]
ΔH_s	Dissolution enthalpy [J mol^{-1}]
I	Ionic strength [molar] or [molal]
J_i	Flux [mol m^{-2} s^{-1}]
J_v	Volume flux [m^3 m^{-2} s^{-1}]
$K_{i,c}$	Hindrance factor for convection [-]
$K_{i,c}$	Hindrance factor for diffusion [-]
k	Boltzmann constant [J K^{-1}]

k	Mass transfer coefficient [m/s]
k_s	Partition coefficient, $k_s = c_s/C_s$ [-]
L	Membrane length [m]
L_{ij}	Phenomenological coefficients [mol^2 kg^{-1} m^{-3} s]
L_p	Water permeability [m^3 m^{-2} s^{-1} Pa^{-1}]
l	Membrane thickness [m]
M_i	Molecular [g mol^{-1}]
m_i	Concentration [molal]
N_A	The Avogadro number [mol^{-1}]
N_i	Total flux [mol m^{-2} s^{-1}]
n_i	Number of mol of component i [number]
P	Permeate flow [m^3 s^{-1}]
P_h	Local hydrodynamic permeability [m^{4}m^{-2}s^{-1}Pa^{-1}]
P_s	Local solute permeability [m^2 s^{-1}]
P	Pressure [Pa]
ΔP	Transmembrane pressure difference [Pa]
R	Gas constant [J K^{-1} mol^{-1}]
R	Retention coefficient [-]
R_{int}	Intrinsic retention coefficient [-]
R'	Retentate flow [m^3 s^{-1}]
Re	Reynolds number, $Re = d_h v\rho/\eta$ [-]
Re_w	Reynolds wall number, $Re_w = d_h u\rho_w/\eta_w$ [-]
r	Length coordinate [m]
r_s	Solute or ionic radius [m]
r_p	Pore radius [m]
S	Entropy [J mol^{-1} K^{-1}]
Sc	Schmidt number, $Sc = \eta/(\rho D)$ [-]
Sh	Sherwood number, $Sh = kd_h/D$ [-]
T	Absolute temperature [K]
t	Time [s]
U	Internal energy [J mol^{-1}]
ΔU_s	Streaming potential [V]
u	Velocity in the pores [m s^{-1}]
u_i	Mobility [mol m N^{-1} s^{-1}]
$\overline{V}_i$	Partial molar volume [m^3 mol^{-2}]
v	Velocity parallel to the membrane surface [ms^{-1}]
W	Hydration energy [J]
w_w	Mass of solvent, here: water [kg]
X_i	Thermodynamic force [kg m mol^{-1} s^{-2}]
$-X_d$	Effective volumetric membrane charge

	density [molar]
x	Length coordinate [m]
x_i	Mol fraction [-]
Δx	Membrane thickness [m]
z_i	Valence of ion i [-]

Greek

β_i	Convection factor in the extended Nernst-Planck equation [-]
Γ	Surface excess concentration [mol m^2]
γ	Surface tension [N m^{-2}]
γ_i	Activity coefficient [-]
Δ	Adjustment to the ionic radius [m]
δ	Boundary layer [m]
δ_c	Concentration boundary layer [m]
δ_{ij}	Kronecker delta [-]
ϵ	Dielectric constant [-]
ϵ^*	Membrane (surface) porosity [-]
ϵ_0	Permittivity in free space [kg^{-1} m^{-3} s^4 A^2]
ζ	Zeta potential [V]
η	Viscosity [Pa s]
κ	Debye parameter [m^{-1}]
κ	Conductivity [μS cm^{-1}]
λ	Solute radius / membrane pore radius ratio [-]
λ'	Electrical conductivity [Ω^{-1} m^{-1}]
μ	Chemical potential [J mol^{-1}]
ν	The number of ions a molecule dissociates into when it dissolves in a solvent [number]
π	Osmotic pressure [Pa]
$\Delta\pi$	Osmotic pressure difference over the membrane [Pa]
ρ	Density [kg m^{-3}]
ρ'	Volumetric charge density [C m^{-3}]
σ	Reflection coefficient [-]
τ	Membrane tortousity [-]
Φ	Steric factor [-]
ϕ	Practical osmotic coefficient [-]
ϕ'	Dissipation function [J m^{-3} s^{-1}]
χ	Surface potential [V]
ψ	Electrical potential [V]

ω	Solute permeability [mol kg^{-1} m^{-1} s]
∇	Laplace operator

Superscripts

e	Excess
id	Ideal
∞	Infinity
^{0}	Standard state
$'$	Feed side of the membrane (mass transfer coefficients) or used as a mark to distinguish variables with the same symbol
$''$	Permeate side of the membrane

Subscripts

b	Bulk
D	Donnan
d	Diffusive
f or F	Feed side of the membrane
i	Component i
j	Component j
MS	Maxwell Stefan model
m or M	Membrane
mix	Mixture
p	Pore
p or P	Permeate side of the membrane
r or R	Retentate side of the membrane
s	Solute or salt
tot	Total
v	Volume
w	Solvent, here: water

Chapter 1

Introduction

1.1 Motivation

As for other separation processes the objective of a membrane separation process is to achieve a particular separation. The main component in a membrane separation process is of course the membrane itself, which can be defined as *a selective barrier between two phases* (Mulder 1996). The membrane must be semi permeable which means that the membrane should allow passage of one component and hinder another due to physical and/or chemical properties.

The retention characteristics of nanofiltration membranes are placed between the reverse osmosis and the ultrafiltration membranes, which gives the opportunity to separate monovalent ions from divalent ones. Other substances with molar masses higher than approximately 300 g/mol will also be retained. The fluxes in nanofiltration are higher for a given pressure compared with the fluxes in reverse osmosis, which gives a higher production rate and a more cost effective process under the assumption that the same separation is achived. Nanofiltration has become a popular membrane process during its approximately twenty years of existence and has proved efficient in a large number of applications, *e.g.* in the water and waste water treatments, the pharmaceutical industry, the agriculture industry, food industry and so on. Due to its success in a great number of different processes new nanofiltration applications are still searched for and its limits is expanded in order to meet the future challenges, especially under harsh conditions and difficult separation processes.

In spite of the increasing use of nanofiltration the separation and transport mechanisms are not well understood and the retention models are not very accurate. On the other hand, it is important to have a basic understanding of these mechanisms in order to develop better membranes and to operate the process under optimal conditions, which can give lower membrane area, fewer membrane modules and an overall reduction in the costs.

This thesis deals with a new possible nanofiltration process, where the objective is to remove sulphate ions present in trace amounts from a concentrated magnesium chloride brine. Ideally, the nanofiltration membrane will retain the divalent sulphate ions, whereas the monovalent chloride ions will pass through the membrane. The difficulties arise when the chloride ion concentration increases, which gives a lower sulphate ion retention and a severe reduction in the volume flux. The thesis tries to enlighten some of these problems and discusses different aspects of the membrane separation process.

1.2 Main objectives

This work had two main objectives; 1) to obtain experimental measured fluxes and ion retentions at high salt concentrations under different operation conditions and 2) to bring clarity into the separation and transport mechanisms of chloride and sulphate ions occurring in membrane separation of a concentrated magnesium chloride solution containing traces of sulphate ions. The operation conditions chosen cover a large area of possible values, which are interesting from both an industrial and a scientific point of view. Possible separation and transport mechanisms are sought for among the already existing theories for nanofiltration and reverse osmosis processes.

This work had at the beginning a third objective which was to develop a new method to measure the concentration polarisation phenomena, since we were worried about the significance of the concentration polarisation effect, especially at high concentrations and multicomponent solutions. An apparatus using a new method to measure the concentration polarisation was built, but the measured concentration polarisation at low concentration was not satisfactory measured and verified and the new method has not been applied at high concentrations or multicomponent solutions. Most of the work with this apparatus has been performed by two students, which did their diploma thesis on the subject.

1.3 Thesis outline

The thesis consists of two parts, where the first part contains the following chapters:

Chapter 2 is an introduction to the field of membrane separation and its basic definitions. A literature survey is also included in this chapter giving the reported results regarding membrane separations of concentrated solutions and some selected papers on the membrane permeation of chloride and sulphate ions. It should be emphasized that the first part of this chapter is tended to readers with limited knowledge of the membrane terminology.

Chapter 3 is a survey of the membrane transport theories and separation mechanisms in reverse osmosis and nanofiltration. The derivation of some of the models has been shown in detail in order to show the principles behind the models, which are considered important from a historical point of view, or, to better understand the underlying separation mechanisms in the models, or, to clarify the assumptions the models are based on.

Chapter 4 starts with a short presentation of the liquid state and the unusual solvent properties of water, followed by a discussion of ions in aqueous solutions. To calculate the thermodynamic properties of concentrated solutions the Pitzer ion interaction model has been chosen and the model is presented in some detail. Some examples of the thermodynamic and physical properties have been given for the pure magnesium chloride and magnesium sulphate solutions and their ions.

Chapter 5 gives a presentation of the apparatus, the chemicals, the membranes, the procedures and the ion analysis used.

Chapter 6 shows all the measured fluxes and ion retentions and gives a short discussion of their validity. The optimal process conditions in order to achieve the best separation between chloride and sulphate ions are also discussed.

Chapter 7 discusses the experimental results in more detail using the theories and models in Chapters 3 and 4. Possible transport and separation mechanisms of concentrated salt solutions in membrane separation are suggested.

Finally, **Chapter 8** concludes part one of the thesis and presents the most important results. Some directions for future work are also included here.

The second part of the thesis contains only **Chapter 9**, which presents a new direct method for measuring the concentration polarisation phenomenon. The chapter stands "alone" from the rest of the thesis and consists of its own introduction, presentation of the new method, results, discussion and conclusion. Even if the concentration polarisation results obtained so far are limited and their validity are a subject of controversy, the presentation of the method is included in the thesis due to the new principles regarding the concentration measurements in the boundary layer.

The thesis also includes the **Appendices A-F**, which contain supplementary information and tabulated results.

Part I

Retention measurements

Chapter 2

Membrane separation processes

2.1 Introduction to membrane processes

The use of synthetic membranes in industrial separation processes is a rather new method. The use of membranes got its breakthrough in the early 1960s when membranes of a certain cellulose acetate mixture showed acceptable flux and selectivity (Reid and Breton 1959). The efficiency of the membrane process was further improved by the making of asymmetric membranes (Loeb and Sourirajan 1962). After these important discoveries the field of membrane separation has grown and is today used in a wide range of applications, *e.g.* desalination, waste water treatment and artificial kidneys.

The advantages of membrane processes compared to other separation processes are in a general sense the low energy consumption; the process can be run continuously; the process conditions are mild, *e.g.* low temperature; up-scaling is easy; the membrane processes can easily be combined with other separation processes; and, additives are normally not required (Mulder 1996). Concentration polarisation, membrane fouling, membrane lifetime, selectivity and flux are factors that can limit or reduce the efficiency of the membrane separation processes.

Membranes can be classified in many different ways depending on what criteria one chooses to use (Mulder 1996). A first division can be made between biological

and synthetic membranes. The biological membranes can be further divided into living and non-living membranes, where the first category are essential to all life on earth. If we concentrate on the solid, synthetic membranes, which are the most important types of membranes used in industrial applications, a further classification of the membranes can be made based on the structure. The membranes can be divided into symmetric and asymmetric, where the symmetric membranes consist of only one layer, whereas the asymmetric membranes consist of a dense toplayer supported by a porous support. A very important class of the asymmetric membranes are the composite membranes, where the toplayer and support are made of different polymer material. The dense skin layer is responsible for the selectivity, whereas all layers contribute to the flow resistance. The symmetric and asymmetric membranes can be further divided into porous and non porous membranes, and while the porous membranes have physical pores which transport the fluids, the transport in non porous membranes occur through the membrane matrix itself.

Microfiltration, ultrafiltration, nanofiltration and reverse osmosis are all pressure driven membrane processes which differ in membrane pore size. The pore diameter in microfiltration membranes are in the range 100-1000 nm, in ultrafiltration membranes 5-100 nm, in nanofiltration membranes 1-10 nm and in reverse osmosis membranes below 1 nm. The microfiltration and ultrafiltration membranes contain physical pores and are characterised as porous membranes, whereas the characterisation of nanofiltration and reverse osmosis membranes as porous or non porous is a subject of controversy since the pore diameter is very small. In most cases an *effective pore diameter* can be determined from experiments and used as a picture of the membrane pore size. The applied pressure differences in membrane processes are proportional to the pore size. In microfiltration processes the applied pressure difference is around 0.1 bar while in reverse osmosis processes the pressure difference is typically in the range 60-100 bar.

In order to get a component to be transported through the membrane a *driving force* is needed. The driving force can be a concentration difference, a temperature difference, an electrical potential difference or a pressure difference between the feed or retentate side of the membrane and the permeate side of the membrane (refer figure 2.1). For example, dialysis and membrane contactors use a concentration difference over the membrane to create transport of the permeable components; membrane distillation uses a temperature difference; electrodialysis and membrane electrolysis use a electrical difference and microfiltration, ultrafiltration, nanofiltration and reverse osmosis use a pressure difference.

The transport through the membrane is passive when it is along the gradient of the force, while the transport is active when it is against the gradient of the force. Active transport is only possible when energy is added to the system. The system will reach equilibrium when the potential difference over the membrane has become zero and there are no external forces. Systems at equilibrium are not interesting in industrial applications since there is no net flow.

A simple schematic presentation of a membrane separation system is given in figure 2.1. The feed or inlet stream enters the membrane module where some components will penetrate the membrane and some will not. The stream leaving the membrane system is called the retentate while the mass going through the membrane is called the permeate.

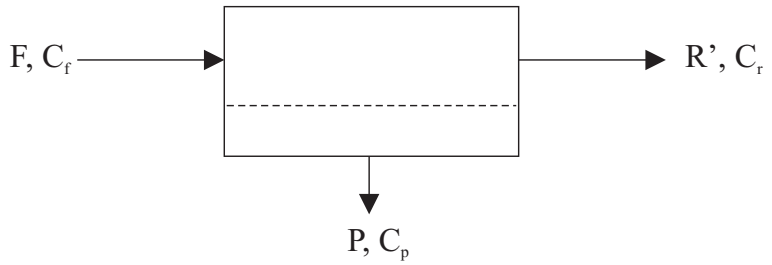

Figure 2.1: A schematic presentation of a membrane separation process showing the feed (F), retentate (R') and permeate (P).

A simple mass balance over the membrane system gives

$$F * C_f = R' * C_r + P * C_p \tag{2.1}$$

where the F, R' and P are the feed, retentate and permeate mass flows and C_f, C_r and C_p are their concentrations, respectively. The efficiency of the membrane separation process is given by the *retention coefficient* defined by

$$R = \frac{C_f - C_p}{C_f} = 1 - \frac{C_p}{C_f} \tag{2.2}$$

In most cases the separation of a solute from a solvent will lead to a phenomenon called *concentration polarisation*, *i.e.* the concentration at the membrane surface is higher (or lower) than the concentration in the bulk stream. In such cases an *intrinsic retention coefficient* is defined as

$$R_{int} = \frac{C_m - C_p}{C_m} = 1 - \frac{C_p}{C_m} \tag{2.3}$$

where C_m is the concentration at the membrane surface on the feed (or retentate) side.

2.2 Mass transfer through asymmetric membranes

2.2.1 General considerations of mass transfer in membrane processes

In order to understand the separation processes and obtain better efficiency different transport mechanisms and models have been proposed and developed. Transport models based on a phenomenological description and models based on a proposed mechanism such as the sieve mechanism, the wetted surface mechanism, the solution diffusion mechanism, the preferential sorption capillary flow mechanism and electrostatic interactions, will be thoroughly discussed in chapter 3. However, some aspects about the membrane separation process can be discussed in general terms as follows.

Figure 2.2 shows how the concentration (or chemical potential) can vary through an asymmetric membrane. The mass transfer has to be considered in different regions which are from left to right; feed or retentate bulk region, concentration boundary layer at the retentate side with thickness δ_c, membrane surface region at the retentate side, membrane skin layer with thickness l_1, surface region between the skin layer and support layer, membrane support layer with thickness l_2, membrane surface region at the permeate side and the permeate bulk region.

The concentration of the solute rejected by the membrane will gradually increase near the membrane surface and a concentration boundary layer is formed. At steady state conditions the convective and diffusive transport through the boundary layer equals the solute transport through the membrane, and the film theory discussed in section 2.2.2 gives an exponential concentration profile in this region.

It exists an equilibrium at the membrane surface between the concentration just outside and the concentration just inside the membrane surface. The ratio between the two concentrations is called the partition coefficient[1]. Part of the separation effect can in some models, *e.g.* the solution diffusion model described in section 3.3.4, be explained by the difference in solute and solvent partition coefficients. Since the two surfaces in asymmetric membranes consist of two different materials, the partition coefficients at the retentate side and the permeate side of the membrane are most likely different.

Several phenomena occur inside an asymmetric membrane. Most of the separation occurs in the dense skin layer and therefore the concentration profile in this layer is steep. The transport is caused by diffusion, convection or another expected transport mechanism. Since the flow resistance is high the skin layer should be as thin as possible in order to increase the permeability. Most probably the solubility of the solute in the skin layer is different from the solubility in the support layer and a partition coefficient exists between the two phases. The partition coefficient shown in figure 2.2 is greater than one, *i.e.* the solubility in the support layer is greater than the solubility in the skin layer. The support layer acts as a support for the skin layer and will not contribute much to the separation. The concentration profile will be flat and the transport mechanism is believed to be convective pore flow. The concentration profiles in the membrane shown in the figure are linear but this may not be the case in real membranes.

The final region defined in figure 2.2 is the permeate bulk with constant concentration at steady state conditions.

A complete mass transfer model should include the changes in the chemical potential profile in all regions, but in practice some simplifications have to be made since it is difficult to obtain parameters for the intermediate region between the two membrane layers and for the skin and support layers alone. In this study, the mass transfer model will include the concentration boundary layer on the retentate side, the surface region at the retentate side, the membrane skin layer with a thought modified membrane thickness l_3, the membrane surface region at the permeate side with the same partition coefficient as the retentate side and a well mixed permeate bulk region. The simplified model is shown with dashed line in figure 2.2.

[1] Other common names for the partition coefficient are solubility or distribution coefficient. The partition coefficient can be defined as the ratio between the solute concentration inside and outside of the membrane, $K_s = c_m/C_m$, where c_m is the concentration just inside the membrane surface whereas C_m is the concentration just outside the membrane surface.

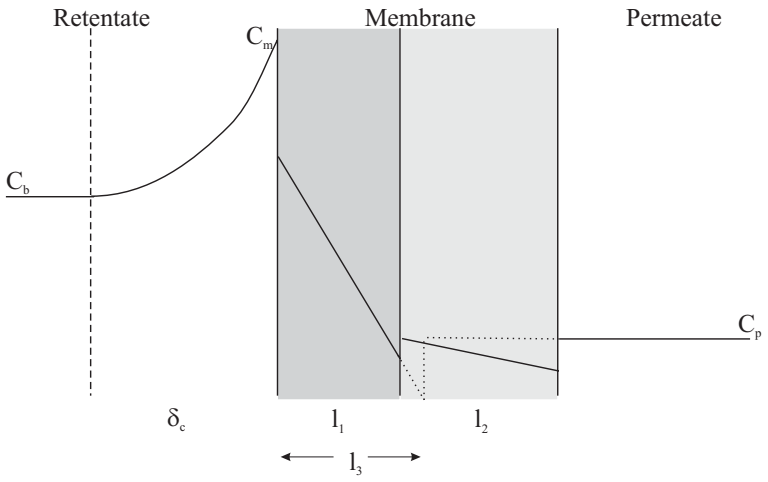

Figure 2.2: Concentration profile through an asymmetric membrane. The solid line gives the profile for the full mass transfer model while the dashed line is a simplified model.

2.2.2 Concentration polarisation

The main idea of a membrane process is to separate a component from a mixture of components by having a semi permeable membrane that allows some components to pass through the membrane while other components are prohibited. The latter components will accumulate near the membrane surface and a concentration gradient is formed. The increase in the concentration at the membrane surface is referred to as concentration polarisation and will influence the separation process in several ways. First, an increase in the concentration polarisation will give a reduction in the driving pressure difference since the osmotic pressure increases, and second, the solute flux is increased since the concentration difference over the membrane increases. Both effects will give an increased solute concentration in the permeate and thereby a lower separation efficiency (Jonsson and Boesen 1984, Rautenbach and Albrecht 1989).

In concentrated solutions the concentration polarisation may cause supersaturation of the liquid at the membrane surface, which may lead to precipitation on the membrane surface with the possibility of pore blocking. This will of course influence the product quality and production rate.

Special models have been developed to calculate the concentration polarisation phenomenon, *e.g.* the film model, the gel model, the osmotic pressure model, the boundary layer model and different filtration models (Mulder 1996). The film model is widely in use and is a good starting point when investigating the phenomena occuring in the concentration boundary layer, and some details of the model will be given (Mulder 1996, Jonsson and Boesen 1984).

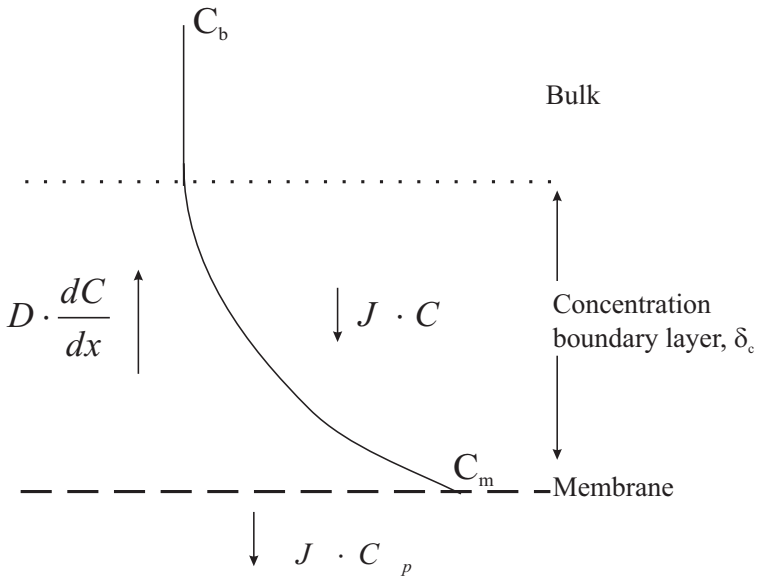

Figure 2.3: Mass transfer in the concentration boundary layer and through the membrane.

Figure 2.3 shows the concentration profile near the membrane surface at steady state conditions. The convective and diffusive transport through the film equals the solute transport through the membrane giving the mass balance

$$J_v\, C + D\, \frac{dC}{dx} = J_v\, C_p \tag{2.4}$$

where the J_v is the volume flux, C_p is the concentration in the permeate and D is the diffusion coefficient. The boundary conditions are

$$x = 0 \quad \Rightarrow \quad C = C_m \tag{2.5}$$

$$x = \delta_c \quad \Rightarrow \quad C = C_b \tag{2.6}$$

where the δ_c is the concentration boundary layer thickness. Equation 2.4 can be

rearranged and integrated to give

$$\ln\left[\frac{C_m - C_p}{C_b - C_p}\right] = \frac{J_v\,\delta_c}{D} \tag{2.7}$$

or

$$\frac{C_m - C_p}{C_b - C_p} = \exp\left(\frac{J_v\,\delta_c}{D}\right) = \exp\left(\frac{J_v}{k}\right) \tag{2.8}$$

where $D/\delta_c = k$ is the mass transfer coefficient. Introducing the definition for the intrinsic retention coefficient given in Equation 2.3 and rearranging, Equation 2.8 can be written

$$\frac{C_m}{C_b} = \frac{\exp(J_v/k)}{R_{int} + (1 - R_{int})\exp(J_v/k)} \tag{2.9}$$

which is called the concentration polarisation modulus. Equation 2.8 can be presented in a linearized form (Jonsson and Boesen 1977, Jonsson and Boesen 1984)

$$ln\left(\frac{1-R}{R}\right) = ln\left(\frac{1-R_{int}}{R_{int}}\right) + \frac{J_v}{k} \tag{2.10}$$

and since the mass transfer coefficient normally is a function of the Reynolds number this equation can be written

$$ln\left(\frac{1-R}{R}\right) = ln\left(\frac{1-R_{int}}{R_{int}}\right) + b\frac{J_v}{Re^a} \tag{2.11}$$

where a is a parameter giving the dependency of the Reynolds number on the mass transfer coefficient (approximately 0.33 for laminar flow and 0.75-0.8 for turbulent flow). If $ln((1-R)/R)$ is plotted versus J_v/Re^a at constant volume flux and different velocities a straight line should be obtained from where the concentration at the membrane wall can be determined from the intercept with the ordinate axis. An estimate of the mass transfer coefficient can now be obtained if Equation 2.8 is used together with the experimentally obtained concentrations and volume fluxes. The main problem with this method is to do the measurements in such a way that the intrinsic retention is constant (Jonsson and Boesen 1984).

The mass transfer coefficient can also be calculated from correlations found in the literature. The general correlation is given by

$$Sh = a\,Re^b\,Sc^c\,\frac{d_h}{L}^d \tag{2.12}$$

where $Sh = kd_h/D$ is the Sherwood number, $Re = d_h v\rho/\eta$ is the Reynolds number, $Sc = \eta/\rho D$ is the Schmidt number, $d_h = 4$ (area)/(wetted periphery) is the hydraulic diameter and a, b, c and d are constants. Further, D is the diffusion coefficient, v flow velocity, L is the length of the channel, ρ is the density and η is the viscosity. In this study the coefficients given by Mulder (1996) will be used in order to approximate the mass transfer coefficients. For laminar flow in a channel the mass transfer correlation becomes

$$Sh = 1.85\,(Re\,Sc\,d_h/L)^{0.33} \tag{2.13}$$

while for turbulent flow it is

$$Sh = 0.04\,Re^{0.75}\,Sc^{0.33} \tag{2.14}$$

Gekas and Hallstrøm (1987) have given an extended summary of different mass transfer correlations based on Sherwood, Schmidt and Reynolds numbers under turbulent cross flow. They also discussed the effect of different variables such as changes in viscosity and diffusion coefficients due to the concentration polarisation layer, membrane surface roughness and flux through the membrane (porosity and suction), and suggested several modifications of the correlations when they are used in membrane separation processes. In general, Gekas and Hallstrøm concluded that roughness increases the friction factor and hence the mass transfer coefficient, whereas the porosity of the membrane enhances the mass transfer coefficient, stabilizes the laminar flow and changes the limit where the laminar flow changes to turbulent flow approximately from a Reynolds number of 2300 to a Reynolds number around 4000.

The effect of flux on the mass transfer coefficient has been studied by several authors (refer Gekas and Hallstrøm (1987)) and Bird *et al.* (1960) have derived a simple relationship between the mass transfer coefficients with and without suction at the walls based on the static film theory. The relationship reads

$$k_{J_v} = \frac{J_v}{1 - exp(-J_v/k)} \tag{2.15}$$

where k_{J_v} is the mass transfer coefficient in channels with wall suction. Brian (1966) compared the theoretical results from an eddy diffusivity model and the film model and found that these models are identical and an expression for the concentration polarisation can be written

$$\frac{C_m - C_p}{C_b - C_p} = exp\left(\frac{J_v}{v}\frac{1}{f/2}\,Sc^{2/3}\right) \tag{2.16}$$

where v is the cross-flow velocity and $f/2$ is the Fanning friction factor. The equation has been successfully used by Sherwood *et al.* (1967) and is valid for low fluxes (approximately in the range $5 * 10^{-6} - 5 * 10^{-5}$ m/s) and Schmidt numbers in the range around 600-800. Thomas (1973) has also discussed how the flux influences the mass transfer coefficient in reverse osmosis and found the relationship

$$\frac{k_{J_v}}{k} = \frac{0.1}{\sqrt{2}} Re^{0.06} Re_w^{0.5} Sc^{0.42} \tag{2.17}$$

where Re_w is the Reynolds number at the membrane wall, which is calculated using the pore velocity[2]. The relationship was derived using salt solutions, high fluxes ($> 10^{-4}$ m/s) and Schmidt numbers around 600.

2.3 Literature survey

In this work a concentrated salt solution is defined as a solution having a concentration higher than 1 molal or 1 molar, and with this in mind only a few publications have been found which discuss the separation of concentrated salt solutions by membrane technology. On the other hand, the literature treating the membrane separations of sodium chloride and to some extent sodium sulphate, magnesium chloride and magnesium sulphate is enormous. This section presents the articles found covering membrane technology and concentrated salt solutions and *some* of the articles giving experimental results on the separation of chloride and sulphate ions in nanofiltration and reverse osmosis.

2.3.1 Membrane separations of concentrated salt solutions

Stegen *et al.* (2001) developed a radial distribution model of ions in pores with a surface charge. The model is applied to a Nafion sulfonic layer and the membrane surface charge and pore diameter have been estimated from sorption data of the sodium ion. Using a sodium chloride brine (consisting of 3 molar sodium chloride and trace amounts of the ions sulphate, magnesium and iron, amongst others) the radial pore concentration profiles have been calculated. The results showed

[2] The volume flux can be used instead of the pore velocity when the surface porosity of the membrane is high. The surface porosity is defined as the total area of all the pores divided by the total membrane area.

that near the negative membrane surface a competition between the positive ions takes place, whereas the negative ions are preferably located near the center of the pore. Both the sodium and magnesium ions showed a local maximum in the concentration profile.

Freger *et al.* (2000) worked with separation of concentrated lactic acid (2% w/v) and sodium chloride (up to 17% w/v) mixtures on aromatic polyamide nanofiltration membranes. The retention of the salt was generally low, whereas the lactate retention was maximal at neutral pH and decreased with increasing salt concentration and temperature. The flux was found to decrease with the salt concentration and increase with the temperature. Freger *et al.* explained the temperature effect on the flux with an increase in the activation energy and the salt concentration effect with a shrinkage of the skin layer due to a reduction in the water activity or by a screening of the repulsion effect of the fixed charges which increases with the number of ions, or both of these. The reduction in lactate retention with increasing temperature was explained by an increase in the sorption of lactate/lactic acid by the membrane, since neither the charge repulsion nor the sieve mechanism show any temperature dependency.

The same strong decrease in the flux as the salt concentration increases were observed by Nystrøm *et al.* (1995) using 0.1-20% sodium chloride solutions and aromatic polyamide and substituted poly(vinyl alcohol) nanofiltration membranes. The flux decline was believed to be caused by the osmotic pressure and to some extent the viscosity of the solution since both quantities increase with the salt concentration. The salt retention decreased strongly with the salt concentration, being less than 10% for solutions with concentration higher than 5%. The sodium chloride retention is somewhat lower than the magnesium chloride retention at equivalent chloride concentrations, a result Nystrøm *et al.* related to the difference in the hydrated ion sizes of sodium and magnesium ions and to the differences in the specific binding to the membrane surface.

Turek and Gonet (1996) discussed the use of nanofiltration and reverse osmosis to remove divalent ions from coal-mine brines containing around 129 kg/m^3 total dissolved solids (TDS). The composition of the coal-mine brines was mainly sodium chloride, but also some calcium, potassium and sulphate ions were present. Different membranes from Nitto-Denko, Osmonic, Dow and Desalination gave different retentions, which were in the area of 90-95% for the sulphate ions, 75-80% for the magnesium ions and 70-75% for the calcium ions.

Friebe and Moritz (1994) investigated the electrical properties and the distri-

bution coefficients for a thin cellulose acetate membrane for different 1 molar salt solutions. The membrane resistance differed in several orders of magnitude, whereas the dielectric constant differed considerably for different salt solutions. The mean distribution coefficient of sodium chloride and sodium sulphate among other salts were experimentally measured at 1 molar concentration and differed by an order of magnitude. The general conclusion was that an increase in the partition coefficient was found for increasing ionic radius and decreasing valency, which supports the theory of dielectric exclusion.

Bontha and Pintauro (1994) formulated a molecular-level equilibrium partition coefficient model to fit the single and multi component ion adsorption by a Nafion 117 cation exchange membrane. The model predictions fitted the experimental results at 0.1-1 molar alkali chloride solutions well, and as the total salt concentration in the bulk increased the membrane ion concentration also increased giving a lower salt retention.

Sabbatovskii *et al.* (1993) showed experimental results for 1 and 2 molar sodium chloride and 1 molar calcium chloride solutions. They used a polyethylene polyamine and polyethylene imine reverse osmosis membrane with polyester backing. The flux and selectivity decreased with increasing ionic strength, where the flux is at least an order of magnitude lower than the pure water flux and the retentions were around 10-30%. In their theoretical discussion Sabbatovskii *et al.* used a capillary osmotic counterflow model without concentration polarisation and their model predictions were good. They also claimed that the electrochemical separation meachanism is not working at these high concentrations and that the separation should be explained by a structural mechanims or the possibility of making ion pairs which have a lower retention. Sabbatovskii *et al.* have also measured an effective pore size which is dependent on the concentration and explained the decrease in pore size with increasing concentration by a reversible compaction of the selective layer due to the difference in osmotic pressure. Finally, Sabbatovskii *et al.* have estimated the diffusion coefficents inside the membrane from the retention coefficients and found a significant decrease, in some cases two orders of magnitude, compared with the bulk diffusion coefficients.

Tsuru *et al.* (1991*b*) used a negatively charged reverse osmosis membrane with skin layer of sulfonated polyether sulfone and polysulfone backing to separate single electrolytes at different concentrations up to 1 molar. The retention of pure sodium chloride, potassium chloride, magnesium chloride, calcium chloride, sodium sulphate and magnesium sulphate solutions decreased with increasing concentration, where the retention of the chlorides became less than 10% at 1

molar and the retention of the sulphates ended up around 80% at 0.1 molar.

Both Berezkin *et al.* (1991) and Aitkuliev *et al.* (1984) reported separation results in various electrolytes using reverse osmosis membranes (poly(ethylene terphthalate), glass and cellulose acetate) and concentrations changing from 10^{-5} to 1 molar. The selectivity decreased when the electrolyte concentration increased, *e.g.* the salt retention decreased from 99% to 1% when the sodium chloride concentration changed from 10^{-3} to 1 molar. The effect of pH, membrane pore size and pressure on the selectivity were also discussed.

Pusch (1980) reported the retention of ions in a multicomponent solution (ternary and quaternary) using different cellulose acetate reverse osmosis membranes and derived a model based on the irreversible thermodynamics. The ion retentions and the fluxes were measured as a function of the salt concentration and operating pressure using sodium chloride and sodium sulphate or nickel chloride and nickel sulphate or ammonium chloride or ammonium sulphate. The chloride concentration was varying, whereas the sulphate concentration was held on a constant level.

Heyde *et al.* (1975) measured the partition coefficients for cellulose acetate reverse osmosis membranes and different single electrolyte solutions at concentrations in the range 0.05-2 molar. Temperature, pH, concentration, electrolyte type and ion pairing influenced their experimentally measured partition coefficients. Further, the partition coefficients were related to the fixed charge of the membrane, the dielectric exclusion mechanism, the ion pairing which diminish the first two effects due to lower effective charge and the membrane swelling or shrinkage which influcence the effective dielectric constant of the membrane. The reported partition coefficients for sodium chloride, sodium sulphate and magnesium chloride decreased, whereas for magnesium sulphate it increased with increasing concentration. The partition coefficient for sodium chloride increased with temperature at low concentrations but at a concentration of 0.1 molar this tendency changed and the partition coefficient decreased with temperature. The partition coefficient for magnesium chloride decreased as the temperature increased. Magnesium chloride was also found to shrink the cellulose acetate membrane. In general, Heyde *et al.* concluded that at higher concentrations the dielectric exclusion of ions become dominant, and that the partition coefficients of ions decrease with increasing solute charge and increase with increasing ionic size.

Govindan and Sourirajan (1966) and Agrawal and Sourirajan (1969) reported separation experiments for 12 different inorganic and two organic solutes using re-

verse osmosis cellulose acetate membranes. Both the flux and retention decreased with increasing concentration, and in terms of their solute transport parameter, $D/K\delta$, sulphate had a lower transport parameter than chloride by an order of magnitude for both sodium and magnesium salts. Agrawal and Sourirajan (1970) extended the analysis to mixed salt solutions with a common ion.

2.3.2 Membrane permeation of chloride and sulphate ions in single and mixed electrolytes

Afonso and Pinho (2000) found for a composite nanofiltration membrane that the salt retentions are in agreement with the Donnan exclusion principle and that the membrane effective charge depends on the salt nature and concentration. For a given set of operation conditions the salt retention in single electrolyte solutions increased following the order magnesium chloride, magnesium sulphate and sodium sulphate. The higher retention of magnesium sulphate compared with the retention of magnesium chloride was explained by an increase in the anion charge density and hence membrane anion repulsion. Equivalently, the higher retention of sodium sulphate compared with the retention of magnesium sulphate is due to the decrease in the cation charge density which will give less attractive forces between the ions and the membrane. Further, Afonso and de Pinho related the decrease in the salt retention when the salt concentration increases to a cation shield effect on the membrane's negatively charged groups which increase with increasing salt concentration. This effect will be more evident for the chloride ion compared to the sulphate ion since the latter has a higher charge density. Another interesting observation done by Afonso and de Pinho is that the measured salt retention for low Reynolds numbers decreases as the operation pressure increases.

Dey *et al.* (2000) measured the selectivity of two nanofiltration membranes with single and mixed electrolytes. For single electrolyte solutions sodium sulphate had retentions around 95% whereas sodium chloride had retentions around 60%. In mixed solutions of chloride and sulphate ions the chloride retention declined and the decline is greater with increasing molar ratios of sulphate to chloride ions in the feed.

Ernst *et al.* (2000) measured the zeta potential and the retention of a polyethersulfone nanofiltration membrane in single salt solutions of sodium sulphate and potassium chloride. In the case of sodium sulphate they found that selective adsorption of sulphate ions gave an increase in the salt retention at low concentrations (up to 10^{-3} molar), whereas a further increase in the salt concentration

gave decrease in retention due to specific adsorption of sodium ions. The latter gave a shift in the isoelectric point to higher pH values with increasing sodium sulphate concentration and the zeta potential turned positive at high concentrations. In the case of potassium chloride no preferential adsorption of the ions was observed and the electrostatic properties of the membrane were only affected by the dissociation of the surface groups.

Xu and Leburn (1999) investigated the effect of pH, ionic strength and solute type on the separation by a charged nanofiltration membrane and single salt solutions. When pH was less than 5.5 and the membrane was positively charged, the increasing salt retention order was sodium chloride, sodium sulphate and magnesium chloride; when pH was greater than 9.0 and the membrane was negatively charged, the increasing retention order was magnesium chloride, sodium chloride and sodium sulphate; and when the pH was in the range 5.5 to 9.0 the increasing retention order was sodium chloride, magnesium chloride and sodium sulphate. When the membrane is charged the retention results can be explained by the Donnan exlusion mechanism whereas in the intermediate pH region the retention results can be explained by a steric or sieve mechanism.

Schaep *et al.* (1998*b*) and Schaep *et al.* (1998*a*) investigated the influence of ion size and charge on different nanofiltration membranes. The use of a polysulfone membrane with zirconia as backing material showed a retention behaviour that can be explained by the Donnan exlusion mechanism when comparing the salts sodium sulphate, calcium chloride and magnesium sulphate. For a positively and a negatively charged polymeric nanofiltration membranes with effective pore size around 0.4 nm, the increasing salt retention sequence was found to be inversely proportional to the salt diffusion coefficents in water, *i.e.* sodium chloride, magnesium chloride and sodium sulphate. For a negatively charged membrane with twice the pore size compared with the other two membranes the increasing salt retention sequence magnesium chloride, sodium chloride, magnesium sulphate and sodium sulphate, was explained by the Donnan exlusion mechanism and hence determined by charge effects. Further, Schaep *et al.* suggested that for higher concentrations (up to 0.75 eq/l) the retention is mainly determined by the anion charge, whereas the charge of the cation seems to be less important.

Schaep *et al.* (1999) analysed the salt retention results further and combined them with the Donnan steric partitioning pore model and the Nernst-Planck equations and evaluated the effective membrane charge density. They showed that the membrane charge density is not constant and depends very much on the salt and its concentration due to ion adsorption onto the membrane material,

and the ion adsorption could be described by linear isotherms. For membranes made of sulfonated polyethersulfone, cellulose acetate and polypiperazine amide magnesium salts can lead to positive membranes. Later, Schaep *et al.* (2000) showed with adsorption experiments that the change in the effective membrane charge can not be explained by an ion adsorption mechanism alone. Tsuru *et al.* (1991*b*) also calculated the effective membrane charge for both a negatively charged reverse osmosis membrane with skin layer of sulfonated polyether sulfone and polysulfone backing. The effective membrane charge increased with the bulk concentration and varied with the type of electrolyte.

Peeters *et al.* (1998) performed retention measurements with single salt solutions of calcium chloride, sodium chloride and sodium sulphate solutions on 21 different polymeric nanofiltration membranes, and showed that the membranes could be divided into two different categories depeding on separation mechanims, *i.e.* membranes where the retention is determined with a Donnan exclusion mechanism and membranes where the retention is determined by differences in diffusion coefficients between the salts.

Sata *et al.* (1998) measured the change in permselectivity between sulphate and chloride ions through an anion exchange membrane with the hydrophilicity of the membrane. The observed increase in the transport number of sulphate ions relative to the chloride ions when the membrane was made more hydrophilic is explained by an increase in the uptake of sulphate ions in the membrane rather than changes in the ions' mobility, since an increased water content of the membrane will enhance the solubilitiy of the strongly hydrated sulphate ions and not so much the non-hydrated chloride ions. The hydrophilicity of the anion exchange membrane is therefore an effective way of controlling the permselectivity.

Saracco (1997) used a electrodialysis application to separate different cation and anion pairs. When separating sulphate from chloride and keeping the sulphate concentration constant, the separation was enhanced by decreasing the applied current density and increasing the chloride concentration. The results were found to follow a combined solution-diffusion and kinetic model.

Tsuru *et al.* (1991*a*), Tsuru *et al.* (1991*b*) and Bowen and Mukhtar (1996) reported experimental results of the separation of ions in reverse osmosis and nanofiltration, and fitted the data to the extended Nernst-Planck equations. Cellulose acetate, polyethersulfone and sulfonated polyethersulfone membranes were used and the mixed electrolyte experiment was carried out at constant total concentration. In the case of sodium chloride and sodium sulphate the sulphate

retention was constant whereas the chloride retention decreased as the concentration of sulphate increased. In the low flux region the chloride retention became negative. A decrease in the total concentration led to increase in all retentions (both chloride and sulphate). The results were the same for a mixture of sodium sulphate and sodium hydroxide but in solutions containing sodium choride and magnesium chloride and magnesium chloride and hydrogen chloride the magnesium retention was more or less constant whereas the sodium and hydrogen retentions decreased but never became negative. Good model predictions were obtained.

Jonsson and Benavente (1992) and Benavente and Jonsson (1993) measured the salt retention, the membrane potential, the diffusion and the electrical resistances in both a composite membrane and its polysulfone porous backing using sodium chloride, sodium sulphate, magnesium chloride and magnesium sulphate single salt solutions. They found that 92% of the total flux resistance was due to the selective skin layer and comparing the results of sulphate salts to chloride salts showed that in the skin layer the sulphate ions had a lower specific solute permeability than the chloride ions (about 50%), whereas there were practicaly no differences in the solute permeabilities in the porous layer.

Mariñas and Selleck (1992) used two reverse osmosis membranes to separate multicomponent electrolyte solutions containing sulphate, chloride, magnesium and sodium with a maximum total concentration of 0.9 molar, in additon to trace amounts of sodium hydrogen biselenite (up to 90 ppm), sodium selenate (up to 90 ppm) and sodium nitrate (up to 30 ppm). Both membranes removed selenate whereas the first membrane (aromatic poly(ether/urea)) gave better retention for nitrate and the other membrane (aromatic with free carboxylic gropus) gave better retention of biselenite. Mariñas and Selleck suggested that magnesiun sulphate will move through the membrane as an ion pair rather than ions since the ion pair constant increases due to lower dielectric constant inside the membrane. The retention of magnesium sulphate decreased as the chloride concentration increased.

Higa *et al.* (1990) and Higa *et al.* (1991) investigated the ion permeation in charged membranes and multicomponent electrolyte solutions with emphasis of the membrane charge density dependency. Their theoretical models based on the Donnan equilibrium and Nernst-Planck equations gave good predictions of the experimental results. They concluded that the counterion with the highest valence is the most important for ion permeation in multicomponent solutions and that the direction of multivalent ion transport changes with charge density.

Chapter 3

Separation and transport in nanofiltration and reverse osmosis

3.1 Classification of the transport models

Membrane transport models have been derived from two independent approaches. The first category of models assumes a separation or transport mechanism and calculates the fluxes according to these mechanisms. The second category of transport models is based on the theory of irreversible thermodynamics, also referred to as non-equilibrium thermodynamics (Soltanieh and Gill 1981).

In the first category of transport models the physico-chemical properties of the membrane itself and the solution are part of the transport models and knowledge about such properties are important. For example, the model can be dependent on one or several of the quantities: the porosity, the tortuosity and the pore size of the membrane, the membrane solubility and the diffusivities of the components involved in the process. If the parameters involved in the model are known, a prediction of the membrane separation can of course be obtained.

The second category of transport models treats the membrane as a black box and assumes that the transport processes are slow and close to equilibrium. The methods based on the irreversible thermodynamics are considered as more fun-

damental models than the mechanistic models and are particularly useful when coupling between the transport of each component occurs.

In some cases a further classification of the transport models can be appropriate and a distinction between discontinuous and continuous models is made (Soltanieh and Gill 1981). The discontinuous models appear when no information about the membrane is available and all gradients are replaced with difference quantities. On the other hand, if structural information about the membrane exists, transport models can be applied on a local level within the membrane and the models are called continuous.

3.2 Irreversible thermodynamics

This section is not meant to be a complete introduction to the field of irreversible thermodynamics, but to give readers new to the topic an introduction and others a short revisit to the basic equations. The reader is refered to *e.g.* Prigogine (1955), Lakshminarayanaiah (1969), Haase (1969) or Soltanieh and Gill (1981) for more details.

3.2.1 Dissipation function and flux equations

The total entropy will increase in an irreversible process, whereas in a reversible process there will be no change in the total entropy. The entropy production in an irreversible process gives a dissipation of energy, *i.e.* energy is lost. Since transport through a membrane is an irreversible process, entropy is produced. The entropy production can be calculated from the dissipation function, ϕ', which is given by the equation

$$\phi' = T\frac{dS}{dt} = \sum_i J_i X_i \tag{3.1}$$

where J_i and X_i are the conjugated fluxes and forces, respectively, T is the temperature, S is the entropy and t is the time. The membrane is used as a frame of reference and all fluxes are given relative to the membrane. The transfer of heat and electrical charge with appropriate conjugated forces must also be included in the dissipation function.

An important assumption in the irreversible thermodynamics is to assume that the system can be divided into several subsystems, where each subsystem is not far from local equilibrium. A linear relationship between the fluxes and forces can be assumed when the system is close to equilibrium, *i.e.*

$$J_i = \sum_j L_{ij} X_j \tag{3.2}$$

where the sum includes all forces X_j acting in the system, whereas L_{ij} is the phenomenological coefficients. For instance, in a system with three components the flux equations can be written as

$$J_1 = -L_{11}\nabla\mu_1 - L_{12}\nabla\mu_2 - L_{13}\nabla\mu_3 \tag{3.3}$$
$$J_2 = -L_{21}\nabla\mu_1 - L_{22}\nabla\mu_2 - L_{23}\nabla\mu_3 \tag{3.4}$$
$$J_3 = -L_{31}\nabla\mu_1 - L_{32}\nabla\mu_2 - L_{33}\nabla\mu_3 \tag{3.5}$$

where the chemical potential of the components are used as forces. The main coefficients, L_{ii}, relate the conjugated forces and fluxes, *i.e.* give the contribution of a component on its own flux. The coupling or cross coefficients, L_{ij}, give the contribution from the force of one component on the flux of another component.

According to Onsager (Onsager 1931a, Onsager 1931b) the coupling coefficients are related to each other with the equation

$$L_{ij} = L_{ji} \qquad i, j = 1, 2, ..., \text{k and } j \neq i \tag{3.6}$$

which is called the Onsager Reciprocal Relations (ORR) and reduces the number of coefficients in the model. Further, since the entropy in an irreversible process must increase, Equation 3.1 must be positive-definite, *i.e.* $\phi' > 0$, which gives the two additional restrictions to the phenomenological coefficients

$$L_{ii} \geq 0 \tag{3.7}$$

and

$$L_{ii}L_{kk} \geq L_{ik}^2 \tag{3.8}$$

In other words, the main coefficients must be positive or zero and the coupling coefficients are limited in magnitude to the square root of the product between the corresponding main coefficients.

3.2.2 Kedem-Katchalsky model

One of the first membrane transport models based on the irreversible thermodynamics was developed by Kedem and Katchalsky (1958). This model has been widely used, discussed and modified by many authors (Kargol 2000) and the derivation of the Kedem and Katchalsky equations will be presented in some detail. Kedem and Katchalsky started with a two component system in which two solutions of the same solvent and solute are separated by a membrane. Using the index w for the solvent (water) and s for the solute (salt), the dissipation function can be written[1]

$$\phi' = J_w \Delta\mu_w + J_s \Delta\mu_s \tag{3.9}$$

where the fluxes and the change in the chemical potentials are one dimensional and perpendicular to the membrane. The chemical potential is defined by

$$\mu_i(T,P) = \mu_i^0(T,P^0) + RT \ln a_i + \overline{V}_i(P - P^0) + z_i F \psi \tag{3.10}$$

where μ_i^0 is the chemical potential at the standard state, T is the temperature, P is the pressure, R is the gas constant, a_i is the activity of component i, V_i is the partial molar volume of component i, z_i is the valency of component i, F is the Faraday constant and ψ is the electrical potential. If the membrane is not charged the electrical potential term, $z_i F\psi$, may be omitted and the chemical potential difference of water over the membrane can then be written

$$\Delta\mu_w = \overline{V}_w(P_2 - P_1) + RT(\ln a_{w,2} - \ln a_{w,1}) = \overline{V}_w(\Delta P - \Delta\pi) \tag{3.11}$$

where Equation 4.22 in Chapter 4 is used to correlate the osmotic pressure with the solvent activity. 1 refers to the feed side of the membrane, whereas 2 refers to the permeate side. A similar expression can be obtained for the chemical potential difference of the solute over the membrane

$$\Delta\mu_s = \overline{V}_s(P_2 - P_1) + RT(\ln a_{s,2} - \ln a_{s,1}) \tag{3.12}$$

To simplify this expression further one has to assume dilute solutions in order to use the van't Hoff equation

$$\pi = \nu C_s RT \tag{3.13}$$

[1] Kedem and Katchalsky (1963) showed that in a system containing ions the appropriate dissipation function becomes $\phi' = J_w\Delta\mu_w + J_s\Delta\mu_s + IE$, where E is the electromotive force acting in the system. In the absence of an electric current, *i.e.* $I = 0$, the dissipation function simplifies to $\phi' = J_w\Delta\mu_w + J_s\Delta\mu_s$. The derivation shown here are based upon the latter dissipation function in order to arrive at the famous Kedem-Katchalsky equations.

where ν is the number of ions in the salt molecule[2]. The second part of Equation 3.12 will then become

$$\frac{1}{RT}\Delta\mu_s^{\mathrm{a}} = \Delta(\ln a_s) \approx \ln\frac{C_{s,1}}{C_{s_2}} = \frac{C_{s,1}-C_{s,2}}{\overline{C}_s} = \frac{\Delta C_s}{\overline{C}_s} = \frac{1}{RT}\frac{\Delta\pi}{\overline{C}_s} \tag{3.14}$$

where

$$\overline{C}_s = \frac{C_{s,1}-C_{s,2}}{\ln\left(\frac{C_{s,1}}{C_{s,2}}\right)} \tag{3.15}$$

and the chemical potential difference of the solute finally becomes

$$\Delta\mu_s = \overline{V}_s\Delta P + \frac{\Delta\pi}{\overline{C}_s} \tag{3.16}$$

Substitution of Equations 3.11 and 3.16 into Equation 3.9 gives after some rearrangement the dissipation function

$$\phi' = (J_w\overline{V}_w + J_s\overline{V}_s)\Delta P + \left(\frac{J_s}{\overline{C}_s} - J_w\overline{V}_w\right)\Delta\pi \tag{3.17}$$

From this expression it is adjacent to define the total volume flux, J_v, by

$$J_v = J_w\overline{V}_w + J_s\overline{V}_s \tag{3.18}$$

and the diffusive flux, J_d, by

$$J_d = \frac{J_s}{\overline{C}_s} - J_w\overline{V}_w \tag{3.19}$$

with conjugated forces ΔP and $\Delta\pi$, respectively. The dissipation function can now be written

$$\phi' = J_v\Delta P + J_d\Delta\pi \tag{3.20}$$

with corresponding flux equations

$$J_v = L_{11}\Delta P + L_{12}\Delta\pi \tag{3.21}$$

$$J_d = L_{21}\Delta P + L_{22}\Delta\pi \tag{3.22}$$

[2]The van't Hoff equation for electrolytes is $\pi = iC_sRT$ where i is dependent on the degree of dissociation. For strong electrolytes that are completely dissociated i becomes equal to the number of ions, ν, formed from one molecule of the electrolyte.

L_{11} is called the hydrodynamic permeability of the membrane[3] and is normally written L_p. Further, the reflection coefficient, σ, is defined as

$$\sigma = -\frac{L_{12}}{L_{11}} \tag{3.23}$$

and is a measure of the selectivity of the membrane or, more precisely, its solute retention property. If σ equals 1 there is no solute transport and the membrane is an ideal semi permeable membrane, if σ equals 0 the membrane has no selectivity and no separation takes place, and, if the value of σ is between 0 and 1 the membrane is not completely semi permeable and there is some transport of the solute.

J_s is a more practical quantity than J_d to work with and a new expression for J_s can be obtained if Equation 3.19 is solved with respect to J_s. If the water flux J_w is replaced by Equation 3.18 the following relationship can be found between the solute, diffusive and volume fluxes

$$J_s(1 - \overline{V}_s\overline{C}_s) = (J_d + J_v)\overline{C}_s \tag{3.24}$$

If $\overline{V}_s\overline{C}_s \ll 1$ the solute flux expression can be simplified to

$$J_s = (J_d + J_v)\overline{C}_s \tag{3.25}$$

The volume flux given in Equation 3.21 can be rewritten using the definitions of the hydrodynamic permeability and the reflection coefficient, whereas the solute flux given by Equation 3.25 can be rearranged using Equations 3.21 and 3.22 to substitute J_v and J_d, respectively, and Equation 3.26 to eliminate the pressure. Finally, the Kedem-Katchalsky equations are obtained

$$J_v = L_p(\Delta P - \sigma\Delta\pi) \tag{3.26}$$
$$J_s = \omega\Delta\pi + (1 - \sigma)J_v\overline{C}_s \tag{3.27}$$

where

$$\omega = \frac{L_pL_{22} - L_{12}^2}{L_p}\,\overline{C}_s \tag{3.28}$$

is the solute permeability at zero volume flux

$$\omega = \left(\frac{J_s}{\Delta\pi}\right)_{J_v=0} \tag{3.29}$$

[3]Water permeability is another common name in aqueous solutions.

The coefficients, L_P, σ and ω can easily be determined from experiments (Mulder 1996). The hydrodynamic permeability coefficent, L_P, is the slope in a pressure-water flux diagramme. The determination of the other two parameters demands a rearrangment of Equation 3.27 to yield

$$\frac{J_s}{\Delta \overline{C}_s} = \nu RT\omega + (1-\sigma)J_v \frac{\overline{C}_s}{\Delta C_s} \tag{3.30}$$

where the van't Hoff equation $\pi = \nu RTC_s$ has been used to replace the osmotic pressure difference. A plot of $J_s/\Delta C_s$ against $J_v\overline{C}_s/\Delta C_s$ will have a slope equal to $1-\sigma$ and the intercept with the $J_s/\Delta C_s$-axis will be equal to $\nu RT\omega$.

Pusch has developed a retention-volume flux relationship based on the Kedem-Katchalsky model (Pusch 1977a, Pusch 1977b). He starts with the definition of the retention coefficient

$$R = 1 - \frac{C_P}{C_R} = 1 - \frac{J_s}{C_R J_v} \tag{3.31}$$

and uses Equation 3.27 to replace J_s and obtains the expression

$$R = 1 - \frac{\omega\Delta\pi + (1-\sigma)J_v\overline{C}_s}{C_R J_v} \tag{3.32}$$

which can be further rearranged into

$$R = 1 - \frac{(1-\sigma)\overline{C}_s}{C_R} - \left(\frac{L_{22}}{L_p} - \sigma^2\right)\frac{\overline{C}_s}{C_R}\frac{L_p\Delta\pi}{J_v} \tag{3.33}$$

when Equation 3.28 is used to replace ω. This equation shows that when J_v increases the retention reaches an asymptotic value of R^∞ expressed by

$$R^\infty = 1 - \frac{(1-\sigma)\overline{C}_{s,\infty}}{C_R} \tag{3.34}$$

where $\overline{C}_{s,\infty}$ is the mean salt concentration at infinite volume flux. Soltanieh and Gill (1981) have shown that $\overline{C}_{s\infty} \approx C_R$ in the high flux limit which means that $R^\infty \approx \sigma$. Using these two results and the assumption $\Delta\pi \approx \pi_R R$, where π_R is the osmotic pressure on the feed (retentate) side, Push obtained

$$\frac{1}{R} = \frac{1}{R^\infty} + \left[\frac{L_{22}}{L_P} - (R^\infty)^2\right]\frac{L_p\pi_f}{R^\infty}\frac{1}{J_v} \tag{3.35}$$

A plot of $1/R$ versus $1/J_v$ will give a straight line with the intercept equal to $1/R^\infty$ and the slope equal to $(L_{22}/L_p - (R^\infty)^2)L_p\pi_R/R^\infty$.

3.2.3 Spiegler-Kedem model

In the derivation of the Spiegler-Kedem model the starting point is the same as for the Kedem-Katchalsky model, but the generalized forces are now given as differential rather than differences (Spiegler and Kedem 1966). The differential analogous to the forces in Equations 3.11 and 3.12 can be written

$$-\frac{d\mu_w}{dx} = -\left(\overline{V}_w \frac{dP}{dx} + \frac{d\mu_w^c}{dx}\right) \tag{3.36}$$

$$-\frac{d\mu_s}{dx} = -\left(\overline{V}_s \frac{dP}{dx} + \frac{d\mu_s^c}{dx}\right) \tag{3.37}$$

where the term $\mu_i^c = RT \ln a_i$ and x is a length coordinate perpendicular to the membrane surface. The concentration dependent part of the chemical potential of the solvent can be expressed in terms of the osmotic pressure by Equation 4.22 in Chapter 4 and becomes $d\mu_w^c = -\overline{V}_w d\pi$. The concentration dependent part of the chemical potential of the solute can also be expressed in terms of the osmotic pressure by Equation 3.14 and becomes $d\mu_s^c = d\pi/c_s$. The differential forces then become

$$-\frac{d\mu_w}{dx} = -\left(\overline{V}_w \frac{dP}{dx} - \frac{d\pi}{dx}\right) \tag{3.38}$$

$$-\frac{d\mu_s}{dx} = -\left(\overline{V}_s \frac{dP}{dx} + \frac{1}{c_s}\frac{d\pi}{dx}\right) \tag{3.39}$$

The applied pressure and the osmotic pressure difference are in most cases of the same order of magnitude and since the partial molar volume of the solute is very much smaller than $1/c_s$, Equation 3.39 can be simplified into

$$-\frac{d\mu_s}{dx} \approx -\frac{1}{c_s}\frac{d\pi}{dx} \tag{3.40}$$

The local flux equations of the solvent and the solute can now be written

$$J_w = L_{11}\left(-\frac{d\mu_w}{dx}\right) + L_{12}\left(-\frac{d\mu_s}{dx}\right) \tag{3.41}$$

$$J_s = L_{21}\left(-\frac{d\mu_w}{dx}\right) + L_{22}\left(-\frac{d\mu_s}{dx}\right) \tag{3.42}$$

For dilute solutions the approximation $\overline{V}_w \approx 1/c_w$ is reasonable and when Equations 3.38 and 3.40 are substituted for the chemical potentials the flux equations

become

$$J_w = -L_{11}\overline{V}_w\left[\frac{dP}{dx} - \left(1 - \frac{L_{21}}{L_{11}}\frac{c_w}{c_s}\right)\frac{d\pi}{dx}\right] \tag{3.43}$$

$$J_s = \left(\frac{L_{21}^2}{c_s L_{11}} - \frac{L_{22}}{c_s}\right)\frac{d\pi}{dx} + \frac{L_{21}}{L_{11}\overline{V}_w}J_w\overline{V}_w \tag{3.44}$$

If the approximation $J_w\overline{V}_w \approx J_v$ is made, a comparison between Equation 3.43 multiplied on both sides with V_w and Equation 3.26 will give an expression for the local reflection coefficient

$$\sigma \approx 1 - \frac{L_{21}}{L_{11}}\frac{c_w}{c_s} \tag{3.45}$$

Further, the volume flux equation can be written

$$J_v = P_h\left(\frac{dP}{dx} - \sigma\frac{d\pi}{dx}\right) \tag{3.46}$$

where

$$P_h = -L_{11}\overline{V}_w^2 \tag{3.47}$$

is the local hydrodynamic permeability of the membrane. The solute flux in Equation 3.44 can be simplified into

$$J_s \approx \left(\frac{L_{21}^2}{c_s L_{11}} - \frac{L_{22}}{c_s}\right)\frac{d\pi}{dx} + (1-\sigma)c_s J_v \tag{3.48}$$

and using the van't Hoff equation the solute flux expression becomes

$$J_s \approx -P_s\frac{dc_s}{dx} + (1-\sigma)c_s J_v \tag{3.49}$$

where the local solute permeability, P_s, is defined by

$$P_s = \frac{\nu RT}{c_s}\left(\frac{L_{22} - L_{21}^2}{L_{11}}\right) \tag{3.50}$$

A further comparison between the flux equations from the Kedem-Katchalsky model and the Spiegler-Kedem model gives the following relationships between their parameters

$$L_p = \frac{P_h}{\Delta x} \tag{3.51}$$

and

$$\omega = -\frac{P_s}{\nu RT\Delta x} \tag{3.52}$$

where Δx is the membrane thickness.

A retention-volume flux relationship for the Spiegler-Kedem model can be derived using the expression $J_s = J_v C_P$ and assuming constant local solute permeability, P_s, reflection coefficient, σ, and fluxes J_s and J_v. Equation 3.49 can then be integrated over the membrane between the boundaries $x = 0$, $c_s = k_s C_R$ (feed or retentate side) and $x = \Delta x$, $c_s = k_s C_P$ (permeate side) to give

$$\frac{J_v(1-\sigma)\Delta x}{P_s} = \ln\left(\frac{C_P\sigma}{C_P - C_R(1-\sigma)}\right) \tag{3.53}$$

After introducing the definition of the retention coefficient, $R = 1 - \frac{C_P}{C_R}$, and some rearrangements the salt retention curve can be written

$$R = \frac{(1 - e^{-J_v(1-\sigma)\Delta x/P_s})\sigma}{1 - \sigma e^{-J_v(1-\sigma)\Delta x/P_s}} \tag{3.54}$$

where σ and $P_s/\Delta x$ are two unknown parameters.

3.2.4 Extended Nernst-Planck equation

The development of the extended Nernst-Planck equation is given by several authors, *e.g.* Schlögl (1964), but it is not until the last decade that its popularity has increased as part of the Donnan-steric-pore model, refer Section 3.3.9. The extended Nernst-Planck equation is a great simplification of the equations in irreversible thermodynamics, and still the model takes into account the diffusion, the migration and the convection mechanisms of the ion transport. The derivation given below is taken from Dresner (1972) who also thouroughly discusses the work of Schlögl.

Starting the analysis with n ions, water (solvent) and the membrane as the $n+2$ thermodynamic components the flux equations in a frame of reference fixed with respect to the membrane and in an irreversible thermodynamic notation, can be written

$$J_i = -L'_{iw}\frac{d\mu_w}{dx} - \sum_{k=1}^{n} L'_{ik}\frac{d\mu_k}{dx} \qquad i = w, 1..., n \tag{3.55}$$

where the index w refers to the water (solvent). If the flux equation of the water ($i = w$) is used to eliminate the $d\mu_w/dx$-term and the water flux is assumed to be equal to the total volume flux, $J_w = J_v$, the flux equations for the n ions become

$$J_i = -\sum_{k=1}^{n} \mathbf{L}'_{ik} \frac{d\mu_k}{dx} + \beta_i c_i J_v \tag{3.56}$$

where

$$\mathbf{L}_{ik} = L'_{ik} - \frac{L'_{iw} L'_{wk}}{L'_{ww}} = \mathbf{L}_{ki} \qquad \text{and} \qquad \beta_i c_i = \frac{L'_{iw}}{L'_{ww}} \tag{3.57}$$

The factor β_i was introduced by Dresner (1972) to take into account the influence of the membrane, creating greater generality into the flux equation compared to the equations given by Schlögl (1964) who negleted the membrane as a thermodynamic component and indirectly used $\beta_i = 1$. For example, if an interaction exists between the counterions and the membrane charges the motion of the counterions will most likely be slower than the motion of the water molecules and the factor $\beta_{\text{counterion}}$ will be less than 1.

To simplify Equation 3.56, Schlögl (1964) assumed that the ions only interact through the electrical field and not directly by collision or by affecting the motion of the water molecules. This implies that all the off-diagonal elements of the matrix $\mathbf{L}_{ik}$ will be equal to zero. Further, Schlögl used the general diffusive flux expression

$$J_i = L_{ii} \frac{\Delta \mu_i}{\Delta x} \approx \frac{L_{ii}}{\Delta x} \frac{RT \Delta c_i}{c_i} \tag{3.58}$$

and compared this with the Ficks first law

$$J_i = D_i \frac{\Delta c_i}{\Delta x} \tag{3.59}$$

and obtained the following equation for the main phenomenological coefficients

$$L_{ii} \approx \frac{D_i c_i}{RT} \tag{3.60}$$

Using the chemical potential given in Equation 3.10, where the activity has been replaced by the expression $a_i = \gamma_i c_i$ and the pressure term has been neglected, the extended Nernst-Planck equations can be written

$$J_i = -D_i \frac{dc_i}{dx} - c_i D_i \frac{d \ln \gamma_i}{dx} - \frac{z_i c_i D_i F}{RT} \frac{d\psi}{dx} + \beta_i c_i J_v \tag{3.61}$$

where the fluxes are dependent on the sum of contributions from the diffusion (first and second term), migration (third term) and convection (fourth term) mechanisms, respectively.

3.2.5 Summary of the irreversible thermodynamic models

The phenomenological coefficients, L_{ij}, are dependent of the concentration to various extent (Kedem and Katchalsky 1958, Spiegler and Kedem 1966, Jagur-Grodzinski and Kedem 1966, Soltanieh and Gill 1981), which gave the motivation for introducing the three alternative coefficients, L_p, σ and ω in the Kedem-Katchalsky equations. The coefficients in the Spiegler-Kedem model are even less dependent of the concentration (Spiegler and Kedem 1966) since the equations have been derived integrating the transport equations on a local level inside the membrane.

The models based on the irreversible thermodynamics presented are based upon the assumptions that the ORR are valid and that the transport is a function of the chemical potential difference only. When large pressure and concentration gradients across the membrane exist the application of the linear law is limited and for membrane processes the validity of the local equilibrium condition is questionable, which means that the ORR may not be true. Further, in many membrane processes the contribution of convection to the transport of components is significant and should be included in the transport models.

The derivation of both the Kedem-Katchalsky and the Spiegler-Kedem models assumed dilute (or ideal) solutions, *i.e.* the activity equals the concentration and the van't Hoff equation is valid. The extended Nernst-Planck equations are derived using the assumptions that the total volume flux equals the water flux and that the components only interact through the electrical potential. In solutions with high concentration and low retentions at least the first of these assumptions will fail.

Jagur-Grodzinski and Kedem (1966) have extended the Spiegler-Kedem model to apply also for asymmetric membranes and derived relationships between the overall reflection coefficient and the overall permeability of the membrane and the individual reflection coefficients and permeabilities of the skin and the support layers.

3.3 Transport models based on separation mechanisms

3.3.1 Friction model

The friction model was introduced in order to give the phenomenological coefficients in models based on the thermodynamics of irreversible processes a physical interpretation (Spiegler 1958). The friction model was later modified to apply for reverse osmosis and ultrafiltration membranes (Spiegler and Kedem 1966) and to include the effect of absorbed water onto the surface of the pores (Belfort 1976).

The model is based on the law of friction which balances the driving forces for any component in steady flow by the frictional forces exerted on it by the other components. The membrane itself is also regarded as a component, but usually the membrane is the reference component and its velocity is set equal to zero. The frictional forces are proportional to the mean relative velocities of the components, *i.e.*

$$F_{ij} = f_{ij}(u_i - u_j) \tag{3.62}$$

where f_{ij} is the friction coefficient between the components i and j, u_i and u_j are the mean velocities of the same components. If the total system consists of a membrane, water and salt, the total force acting on the water and the salt molecules can be written

$$F_w = (c_s/c_w)f_{sw}(u_w - u_s) + f_{wm}(u_w - u_m) \tag{3.63}$$

$$F_s = f_{sw}(u_s - u_w) + f_{sm}(u_s - u_m) \tag{3.64}$$

where the coefficient f_{ws} has been replaced according to the force balance $c_i f_{ij} = c_j f_{ji}$ and the membrane is used as reference, *i.e.* $u_m = 0$. The relationship $J = uc$ can be used to introduce the solvent and solute fluxes and after some rearrangement the fluxes can be expressed as

$$J_w = \frac{(f_{sm} + f_{sw})c_w^2}{d}F_w + \frac{f_{sw}c_w c_s}{d}F_s \tag{3.65}$$

$$J_s = \frac{f_{sw}c_w c_s}{d}F_w + \frac{(f_{wm}c_w + f_{sw}c_s)c_s}{d}F_s \tag{3.66}$$

where $d = f_{sm}f_{wm}c_w + f_{sm}f_{sw}c_s + f_{sw}f_{wm}c_w$. The total volume flux, $J_v = \overline{V}_w J_w + \overline{V}_s J_s$, is a more convinent property than the water flux and can be written in terms of frictional forces and coefficients as

$$J_v = \frac{(f_{sm} + f_{sw})c_w^2\overline{V}_w + f_{sw}c_w c_s\overline{V}_s}{d}F_w + \frac{(f_{wm}c_w + f_{sw}c_s)c_s\overline{V}_s + f_{sw}c_w c_s\overline{V}_w}{d}F_s \tag{3.67}$$

The next step is to replace the forces F_w and F_s with the thermodynamic forces given in Equations 3.38 and 3.40 and compare the results with the equations given by the Spiegler-Kedem model, Equations 3.46 and 3.49. The following relationships between the frictional coefficients and the phenomenological coefficients σ, P_h and P_s can be obtained after some tedious rearrangments (Belfort 1976):

$$\sigma = 1 - \underbrace{\left[\frac{c_s/C_{s,b}}{c_w/C_{w,b}}\right]}_{\text{exclusion}} \underbrace{\left[\frac{1+(f_{wm}/f_{sw})(\overline{V}_s/\overline{V}_w)}{1+(f_{sm}/f_{sw})}\right]}_{\text{kinetic}} \tag{3.68}$$

$$P_h = \underbrace{\left[\frac{c_w}{C_{w,b}^2}\right]}_{\text{exclusion}} \underbrace{\left[\frac{1}{f_{wm}}\right] \left[\frac{1+f_{sm}/f_{sw}}{1+f_{sm}/f_{sw}(1+f_{ws}/f_{wm})}\right]}_{\text{kinetic}} \tag{3.69}$$

$$P_s = \underbrace{2RT \left[\frac{c_s}{C_{s,b}}\right]}_{\text{exclusion}} \underbrace{\left[\frac{1/f_{sm}}{1+f_{sw}/f_{sm}}\right]}_{\text{kinetic}} \tag{3.70}$$

where $C_{i,b}$ is the bulk concentration of component i. In the derivation of these equations dilute solutions and high retention membranes are assumed, which gives the simplifications $\overline{V}_w c_w \approx 1$, $\overline{V}_w c_w \gg \overline{V}_s c_s$ and $c_s \ll c_w$. The derivation has been simplifed further by using sodium chloride as salt, giving $\overline{V}_s/\overline{V}_w \sim 3/2$. Even though Equations 3.68, 3.69 and 3.70 are based upon several assumptions, some general remarks about the criteria for an efficient desalting membrane can be made.

First, note that the expressions for the coefficients σ, P_h and P_s have been divided into two dimensonless terms. The exclusion terms depend on the partition coefficients or the concentration ratios, while the kinetic term depends on the friction coefficients. In order to achive a good separation, σ should be close to unity. This can be obtained if the ratio between the partition coefficients, k_s/k_w, is small, which means that the membrane have larger solubility to water than to salt, and if the friction coefficients fulfill the statements $f_{sm} \gg f_{wm}$ and $f_{sm} \gg f_{sw}$, which means that the friction between the salt and the membrane must be much larger than both the frictions between the water and the membrane and the friction between the salt and the water.

If the exclusion part of Equations 3.68, 3.69 and 3.70 is equivalent to a solution part and the kinetic part is equivalent to a diffusion part, Mulder (1996) points

out that even in the concept of irreversibel thermodynamics and friction models, the selectivity is considered in terms of a solution-diffusion mechanism, which is discussed Section 3.3.4.

3.3.2 Maxwell-Stefan approach to mass transfer

Krishna and Wesselingh (1997) give an extensive presentation of the generalized Maxwell-Stefan approach to mass transfer in multicomponent solutions. In the Maxwell-Stefan approach the diffusion of different species in a multicomponent solution is dependent on the forces acting on the molecules and the corresponding force balances have similarities with the previously discussed friction model.

The Maxwell-Stefan analysis for mass transport inside porous structures and under the influence of external body forces, *i.e.* valid for membrane transport processes, summarizes into the transport equations (Krishna and Wesselingh 1997)

$$-\frac{c_i}{RT}\nabla_{T,P}\mu_i - \frac{c_i}{RT}\overline{V}_i\nabla P - \alpha_i' c_i \frac{B_0}{\eta D_{iM}^{eMS}}\nabla P - c_i z_i \frac{F}{RT}\nabla\psi = \sum_{j=1}^{n}\frac{x_j N_i - x_i N_j}{D_{ij}^{eMS}} + \frac{N_i}{D_{iM}^{eMS}} \quad (3.71)$$

where the terms on the right hand side correspond to the contribution from the concentration and pressure parts of the chemical potential, the viscous flow due to the pressure gradient and the electrical potential gradient, respectively. x_i is the mole fraction and the modified viscous selectivity factor, α_i', is defined by the equation

$$\alpha_i' = \alpha_i + \sum_{j=1}^{n} x_j \frac{D_{iM}^{eMS}}{D_{ij}^{eMS}}(\alpha_i - \alpha_j) \quad (3.72)$$

where α_i is the viscous selectivity factor. The viscous selectivity factor is introduced to give the membrane a semi permeable character, where $\alpha_i > 1$ for solutes traveling near the center of the pores, whereas $\alpha_i < 1$ for solutes strongly adsorbed onto the membrane wall and $\alpha_i = 0$ for solutes that cannot penetrate the membrane matrix. The permeability constant B_0 is a characteristic of the membrane and can, for some geometries, be calculated from theoretical considerations, *e.g.* B_0 can be calculated from Poiseuille flow through a cylindrical pore to yield

$$B_0 = r_p^2/8 \quad (3.73)$$

where r_p is the membrane pore radius. The effective diffusion coefficients D_{iM}^{eMS} represent the effective Knudsen diffusion coefficients and can be calculated from

$$D_{iM}^{eMS} = \frac{\epsilon}{\tau}\frac{2r_p}{3}\sqrt{\frac{8RT}{\pi M_i}} \tag{3.74}$$

where ϵ is the membrane porosity, τ is the membrane tortuosity and M_i is the molecular weight. The effective diffusion coefficients D_{ij}^{eMS} are the effective binary pair diffusion coefficients in the membrane and can be related to the corresponding free space values by the equation

$$D_{ij}^{eMS} = \frac{\epsilon}{\tau}D_{ij}^{MS} \tag{3.75}$$

Here D_{ij}^{MS} is the binary Maxwell-Stefan diffusivities in free space which can be calculated from the Ficks diffusion coefficients D_{ij} using the relationship

$$D_{ij} = D_{ij}^{MS}\Gamma \tag{3.76}$$

where Γ represents the thermodynamic non-ideal effects calculated by

$$\Gamma_{ij} = \delta_{ij} + x_i\frac{\partial ln\gamma_i}{\partial x_j} \tag{3.77}$$

δ_{ij} is the Kronecker delta which equals 1 when $i = j$ and 0 when $i \neq j$.

Krishna and Wesselingh (1997) have also indicated which terms in Equation 3.71 that will have significant contributions to the fluxes in different membrane separation processes. In reverse osmosis the Maxwell-Stefan transport equation reduces to

$$-\frac{c_i}{RT}\nabla_{T,P}\mu_i - \frac{c_i}{RT}\overline{V}_i\nabla P = \frac{N_i}{D_{iM}^{eMS}} \tag{3.78}$$

whereas in ultrafiltration it can be simplified to

$$-\alpha_i' c_i\frac{B_0}{\eta D_{iM}^{eMS}}\nabla P = \frac{N_i}{D_{iM}^{eMS}} \tag{3.79}$$

3.3.3 Sieve model

One of the first models presented to explain the separation of a solute from a solvent with the help of membranes is the sieve model discussed among others

by Banks and Sharples (1966) and Applegate and Antonson (1972). The model is based on the assumption that the membrane consists of a large number of parallel capillary tubes in which the flow is given by the pure pore flow, *i.e.* the Hagen-Poiseuille equation

$$J_v = \frac{\epsilon^* r^2}{8\eta\tau}\frac{\Delta P}{\Delta x} \tag{3.80}$$

where ϵ^* is the surface porosity, r is the pore radius, η is the viscosity, τ is the pore tortuosity, ΔP is the transmembrane pressure and Δx is the membrane thickness. The solute molecules are retained by the membrane by a sieving mechanism, where the pore diameter is less than the solute diameter. Pores of different diameters must exist for membranes with partial retention of the solute, where some of the pores are large enough to allow solute molecules to pass through the membrane.

Several different sieve model equations exist depending on the assumptions made (Banks and Sharples 1966). If the membrane exists of two types of pores, where the smallest pores only pass solvent molecules, whereas the largest pores pass both solvent and solute molecules, the sieve model becomes

$$J_v = k_1(\Delta P - \Delta\pi) + k_2\Delta P \tag{3.81}$$

$$J_s = k_2 C_R \Delta P \tag{3.82}$$

where the flow in the largest pores are controlled by the pressure difference, ΔP. The flux equations can be combined with the definition of the retention coefficient and the relationship $\Delta\pi = R\pi_R$, in order to obtain an expression for the retention coefficient following the sieve mechanism

$$R = \frac{k_1\pi_R + (k_1 + k_2)\Delta P - [(k_1\pi_R + (k_1 + k_2)\Delta P)^2 - 4k_1^2\pi_R\Delta P]^{1/2}}{2k_1\pi_R} \tag{3.83}$$

3.3.4 Solution-diffusion model

The solution-diffusion model was introduced by Lonsdale *et al.* (1965) and is based on the assumptions that both the solvent and the solute are dissolved in the membrane matrix and transported through the membrane by diffusion. The membrane is considered to be a homogeneous nonporous layer and the transport of the solvent and the solute molecules are uncoupled.

To derive a suitable set of equations, Lonsdale *et al.* (1965) started by assuming that the water flux can be given by the Ficks first law

$$J_w = -D_w \frac{dc_w}{dx} \tag{3.84}$$

where D_w is the diffusion coefficient of water inside the membrane. If the membrane-water solution obeys Henrys law, the chemical potential can be written $d\mu_w = -RTd\ln c_w = -RTdc_w/c_w$, and Equation 3.84 can be written

$$J_w = \frac{D_w c_w}{RT}\frac{d\mu_w}{dx} \approx \frac{D_w c_w}{RT}\frac{\Delta\mu_w}{\Delta x} \tag{3.85}$$

where the last approximation is valid for small changes in the chemical potential of water. Finally, the chemical potential can be substitued by the expression given in Equation 3.11 and the water flux expression can be written

$$J_w = \frac{D_w c_w \overline{V}_w}{RT\Delta x}(\Delta P - \Delta\pi) = L_p(\Delta P - \Delta\pi) \tag{3.86}$$

A corresponding equation can be obtained for the salt flux when the transport through the membrane is purely diffusive

$$J_s = -D_s\frac{dc_s}{dx} \approx -D_s k_s \frac{C_P - C_R}{\Delta x} = K_2(C_R - C_P) \tag{3.87}$$

where k_s is the distribution coefficient (or solubility coefficient) and K_2 is the permeability of the solute. The distribution coefficient relates the concentration in the membrane given by a lowercase c with the concentration just outside the membrane given by a uppercase C, $c = kC$, and is normally assumed independent of the concentration. If the equations for the water and salt fluxes, the definition of the retention and the equation $\Delta\pi = R\pi_R$ are combined, the retention expression becomes (Banks and Sharples 1966)

$$R = \{\Delta P + \pi_R + K_2/L_p - [(\Delta P + \pi_R + K_2/L_p)^2 - 4\pi_R\Delta P]^{1/2}\}/2\pi_R \tag{3.88}$$

The diffusion and solubility coefficients, and hence the permeabilitiy coefficients, are concentration dependent in non-ideal systems (Mulder 1996). *E.g.* the diffusion coefficients can be calculated from

$$D_i = D_{T,i}\left(\frac{d\ln a_i}{d\ln c_i}\right) \tag{3.89}$$

where $D_{T,i} = u_i RT$ is the thermodynamic diffusion coefficient and u_i is the mobility of component i.

3.3.5 Solution-diffusion-imperfection model

The solution-diffusion-imperfection model given by Sherwood *et al.* (1967) is an extension of the solution-diffusion model. The solution-diffusion-imperfection model adds a pore flow contribution to the water and solute fluxes, taking into account pores or defects in the membrane that have no separation effects. The equations for the total water and salt fluxes will be

$$N_w = J_w + K_3 \Delta P C_w = L_p(\Delta P - \Delta\pi) + K_3 \Delta P C_w \tag{3.90}$$

$$N_s = J_s + K_3 \Delta P C_R = K_2(C_R - C_P) + K_3 \Delta P C_R \tag{3.91}$$

The water permeation velocity, u_w, can be obtained by dividing both sides of Equation 3.90 with C_w. Assuming the water permeation velocity to be equal to the total permeation velocity, the total solute flux can be written

$$N_s = u_w C_P \tag{3.92}$$

and the flux equations in 3.90 and 3.91 can be written in terms of permeation velocity

$$u_w = K_1(\Delta P - \Delta\pi) + K_3 \Delta P \tag{3.93}$$

$$u_w C_P = K_2(C_R - C_P) + K_3 \Delta P C_R \tag{3.94}$$

Equations 3.93 and 3.94 can be used to obtain an expression for the retention as a function of the pressure

$$\begin{aligned} R = &\{\pi_R + K_2/K_1 + \Delta P(1 + K_3/K_1) - \\ &[(\pi_R + K_2/K_1 + \Delta P(1 + K_3/K_1))^2 - 4\pi_R \Delta P]^{1/2}\}/2\pi_R \end{aligned} \tag{3.95}$$

The main disadvantage with this model is that the K_i-parameters are concentration and pressure dependent (Soltanieh and Gill 1981).

3.3.6 Highly-porous and finely-porous models

The solute molecules are transported by diffusion in the solution-diffusion model and in the solution-diffusion-imperfection model the solute molecules are transported partially by diffusion and partially by convection (viscous pore flow). Whereas the solution-diffusion-imperfection model assumes the existence of defect pores which are responsible of the viscous flow, *the highly-porous model* assumes that the solute transport is a combination of both the diffusion and the

convection mechanisms in the same pores and that separation is achieved when the pore concentration differs from the feed concentration (Merten 1966). Further, the coupling between the transport of the solute and the solvent molecules are only through the viscous flow.

The total volume flux, $J_v = \epsilon^* u$, follows the Hagen-Poiseuille equation and the solute flux can be calculated by

$$N_s = c_s u + J_s \tag{3.96}$$

where ϵ^* is the surface porosity, u is the velocity of the pore fluid, c_s is the concentration (per unit membrane volume). In Equation 3.96 the $c_s u$-term gives the convective part of the solute flux, whereas the J_s-term is the diffusive part of the solute flux and is given by Fick's first law. If the total solute flux is assumed constant, $N_s = \epsilon^* u C_p$, Equation 3.96 can be integrated to give the concentration profile of the solute through the membrane. The integration constant can be determined using the the boundary condition at the feed side of the membrane, $x = 0$, $c_s = k_s' C_R$, and the concentration profile becomes

$$c_s = \frac{N_s}{u} + \left(k_s' C_R - \frac{N_s}{u} \right) \exp\left(\frac{ux}{D_s} \right) \tag{3.97}$$

The boundary condition at the permeate side of the membrane, $x = \tau \Delta x$, $c_s = k_s'' C_P$, can be used to find an expression for the retention coefficient

$$R = 1 - \frac{C_P}{C_R} = 1 - \frac{k_s' exp(u\tau\Delta x/D)}{k_s'' - \epsilon^* + \epsilon^* \, exp(u\tau\Delta x/D)} \tag{3.98}$$

where τ is the tortuosity of the membrane.

In *the finely-porous model* the pores in the membrane are too small to allow unrestricted viscous flow, *i.e.* significant friction exists between the membrane pore walls and the solute molecules (Pusch 1977a, Pusch 1977b). The friction will affect the diffusion process in the pores and the diffusive solute flux expression is modified to yield

$$J_s = u_{sw} c_s \left[- \left(\frac{\partial \mu_s}{\partial c_s} \right) \frac{dc_s}{dx} + F_{sm} \right] \tag{3.99}$$

where u_{sw} is the mobility of the solute in the membrane and F_{sm} is the frictional force acting between the solute and the membrane. The frictional force can be written

$$F_{sm} = -f_{sm} u_s = -f_{sm} N_s / c_s \tag{3.100}$$

In dilute solutions $(\partial\mu_s/\partial c_s) = RT/c_s$ and the diffusive solute flux expression becomes

$$J_s = \frac{RT}{f_{sw}}\frac{dc_s}{dx} - \frac{f_{sm}}{f_{sw}}N_s \tag{3.101}$$

The diffusive flux term, J_s, in Equation 3.96 can be replaced by Equation 3.101 and the total solute flux in the finely-porous model becomes

$$N_s = -D_{e,s}\frac{dc_s}{dx} + \frac{c_s}{b}u \tag{3.102}$$

where

$$D_{e,s} = \frac{RT}{f_{sw}b} \qquad \text{and} \qquad b = 1 + \frac{f_{sm}}{f_{sw}} \tag{3.103}$$

The factor b gives the influence of the membrane on the solute molecules and both the diffusive and convetive contributions in the total solute flux expression are reduced by this factor. The finely-porous model is identical to the highly-porous model when b equals 1 and the friction between the solute and the membrane becomes negligible.

When the total solute, $N_s = \epsilon^* u C_p$, permeation velocity, u, and the coefficients b and f_{sw} are constant, Equation 3.102 can be integrated with the same boundary condtions as for the highly-porous model to give the concentration profile and the retention coefficient of the solute, hence

$$c_s = \frac{N_s b}{u} + \frac{(k_s' C_R - k_s'' C_P)exp(ux/bD_{e,s})}{1 - exp(u\tau\Delta x/bD_{e,s})} \tag{3.104}$$

and

$$R = 1 - \frac{C_P}{C_R} = 1 - \frac{k_s' exp(u\tau\Delta x/bD_{e,s})}{k_s'' - b\epsilon^* + b\epsilon^*\ exp(u\tau\Delta x/bD_{e,s})} \tag{3.105}$$

Jonsson and Boesen (1975) used a similar finely-porous model, but based the model on the pore volume rather than the total membrane volume. Jonsson and Boesen assumed that $k_s' = k_s''$ and used the relationship $bD_{e,s} = D_{sw}$, where D_{sw} is known, and obtained good estimates of the unknown parameters $b\epsilon^*/k_s$ and $\tau\Delta x/\epsilon^*$ from retention versus volume flux data of different sugar solutions. Jonsson and Boesen also compared the finely-porous model with the solution-diffusion-imperfection model and found that the parameters of the finely-porous model are concentration independent, whereas the parameters in the solution-diffusion-imperfection model are concentration dependent, although both models fitted the data equally well.

3.3.7 Interactions between ionic solutions and charged surfaces and the Donnan exclusion mechanism

A charged surface in an electrolyte solution will affect the distribution of the nearby ions so that ions with an opposite charge of the surface will be attracted towards the surface, whereas ions with the same charge as the surface will be repelled off. The charge distribution in the solution leads to the formation of what is called the electrical double layer. According to the Gouy-Stern model, the electrical double layer consists of the Stern layer with thickness δ and the Gouy (diffusive) layer with infinite thickness as shown in Figure 3.1. For practical reasons the thickness of the diffusive layer is set equal to the inverse Debye length, $1/\kappa$, defined later in this section. Over the whole system the electrical neutrality condition still applies and must be fulfilled. The reader is directed to *e.g.* Hunter (1981) or Mørk (1994) for more details about the electrokinetic phenomena in general and to Pihlajamäki (1998) for the applications to membrane characterisation.

The variation of the electrical potential can be described by Poisson's equation (Mørk 1994)

$$\nabla^2\psi = -\frac{\rho'}{\epsilon_0\epsilon} \tag{3.106}$$

where ∇ is the Laplace operator, ψ is the electrical potential, ρ' is the volumetric charge density, ϵ_0 is the permittivity of vacuum and ϵ is the relative permittivity or the dielectric constant of the solution. The volumetric charge density can be calculated by the equation

$$\rho' = \sum_i e\, z_i\, n_i \tag{3.107}$$

where n_i is the local ion concentration (number of ions per unit volume). The local ion concentration is dependent on the electrical potential and is given by the Boltzmann's equation

$$n_i = n_i^0 exp(-z_i e\psi/kT) \tag{3.108}$$

where n_i^0 is the ion concentration far from the charged surface (bulk concentration). If Equations 3.106, 3.107 and 3.108 are combined the Poisson-Boltzmann equation is obtained

$$\nabla^2\psi = -\frac{e}{\epsilon_0\epsilon}\sum_i z_i n_i^0 exp(-z_i e\psi/kT) \tag{3.109}$$

Debye and Hückel simplified this expression further by assuming a small electrical potential and obtained

$$\nabla^2\psi = \kappa^2\psi \tag{3.110}$$

with the one dimensional Cartesian solution

$$\psi = \psi^m exp(-\kappa x) \tag{3.111}$$

which is called the Debye and Hückel approximation. Here ψ^m is the electrical potential at the charged surface and

$$\kappa = \left(\frac{4\pi e^2 \sum n_i z_i^2}{\epsilon_0 \epsilon kT}\right)^{1/2} = \left(\frac{8\pi e^2 N_a \rho_w}{1000\epsilon_0 \epsilon kT}\right)^{1/2} I^{1/2} \tag{3.112}$$

is the Debye parameter. The molal ionic strength, I, is defined by Equation 4.35 in Chapter 4.

The inverse Debye parameter is the distance from the charged surface to the point in the solution where the electrical potential has dropped to 1/e of the surface potential[4]. The inverse Debye parameter can be taken as an approximation of the electrical double layer thickness.

The electrical field near a charged surface will create a stationary plane inside the double layer which is called the surface of shear. The surface of shear separates the solution near the charged surface into a stationary phase and a phase moving with the external flow. The electrical potential at the surface of shear is called the zeta potential [5]. The application and measurements of the zeta potential in the characterization of membranes are thoroughly discussed by Pihlajamäki (1998).

When the electrolyte concentration increases the Debye length decreases and makes the electrical double layer more compact. *E.g.* in a 0.1 molal magnesium chloride solution the Debye length becomes approximately 5 nm, whereas in a 5 molal magnesium chloride solution the Debye length becomes approximately 0.5 nm, which is of the same size as a hydrated ion. When the surface potential is high[6], or when the electrolyte concentration is moderate to high, most of the change in the electrical potential will occur in the Stern layer (Mørk 1994).

[4]When the Gouy-Stern model is used the inverse Debye parameter is more precisely the distance from the Stern plane at position δ to the point in the solution where the electrical potential has dropped to 1/e of the Stern potential, see Figure 3.1.

[5]Also referred to as the electrokinetic potential.

[6]200 mV is in this context a high potential (Mørk 1994).

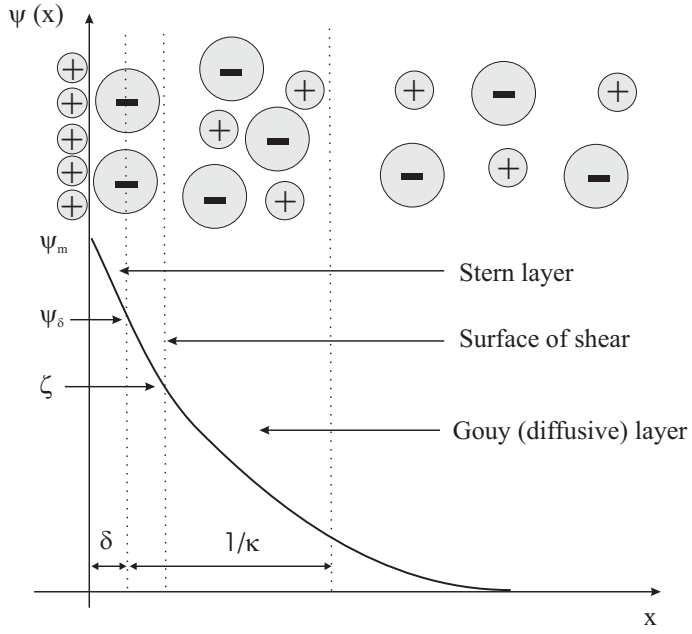

Figure 3.1: Illustration of the Gouy-Stern model and the distribution of ions near a charged surface (Mørk, 1994).

In both charged and uncharged membranes the interaction between the membrane and the ions can affect the partition coefficient and hence the separation. When a charged membrane is in contact with an electrolyte solution the counter-ions, which have the opposite charge as the membrane, will have a higher concentration in the membrane compared to the solution, whereas the co-ions, which have the same charge as the membrane, will have a lower concentration in the membrane. The concentration difference generates an electrical potential difference in order to maintain electrochemical equilibrium between the membrane and the solution. This potential is called the Donnan potential, ψ_D, and can be calculated by equation (Mulder 1996, Peeters *et al.* 1998)

$$\psi_D = \psi^m - \psi = \frac{RT}{z_i F} ln \left(\frac{a_i}{a_i^m} \right) \tag{3.113}$$

where a_i is the activity of ion i in the bulk solution just outside the membrane and a_i^m is the activity of ion i in the membrane. Equation 3.113 has been derived using the definition of the chemical potential given in Equation 3.10 and setting the chemical potential in the bulk solution equal to the chemical potential in the membrane phase. The Donnan potential will attract counter-ions, whereas

co-ions will be rejected.

Lakshminarayanaiah (1969) has combined Equation 3.113 with the electro neutrality conditions in the solution and in the membrane and obtained the following expression for the partition coefficient of the co-ions in a binary solution

$$k_B = \frac{c_B}{C_B} = \left(\frac{|z_B| C_B}{|z_B| c_B + |z_m| c_m} \right)^{|z_B|/|z_A|} \tag{3.114}$$

where c_m is the concentration of the membrane fixed charge, z_m is the valence of the membrane charge and the uppercase C is the concentration outside the membrane whereas the lowercase c is the concentration inside the membrane. Equation 3.114 shows that the co-ion partition coefficient is dependent on the salt concentration, the fixed charge concentration in the membrane, the valence of the co-ions and the valence of the counter-ions, *e.g.* an increase in the salt concentration in the solution and a decrease of the membrane fixed charge will give an increase in the concentration of the co-ions in the membrane and hence a lower retention.

3.3.8 Space-charge and fixed-charge models

The models used in the transport of ions through electrically charged membranes are based on either the *space-charge* or the *fixed-charge* theories (Hagmeyer and Gimbel 1999). The space-charge theory was developed by Morrison and Osterle (1965) and several models have been developed and discussed (Smith and Deen 1983, Westermann-Clark and Anderson 1983, Vonk and Smit 1983, Yaroshchuk and Vovkogon 1994*a*, Yaroshchuk and Vovkogon 1994*b*, Shenase *et al.* 1995, Wang *et al.* 1995*b*). The starting point is the Poisson-Boltzmann equation given by Equation 3.109 and the ion concentrations and the electrical potential may change both in the radial and the axial direction in the pores. The transport of ions are normally described by the extended Nernst-Planck equation, whereas the volumetric flow is calculated by the Navier-Stokes equations. The most serious disadvantages of this model are the complex mathematical calculations and the parameters that are difficult to estimate. Yaroshchuk (1995) has given a thorough presentation of the space-charge model in relation to other theories and discusses the optimal separation conditions of ions in Yaroshchuk (2000*a*) and Yaroshchuk (2000*b*).

The fixed-charge theory was proposed by Teorell (1935) and by Meyer and Sievers (1936) and is known as the Teorell-Meyer-Sievers (TMS) model. The TMS model

assumes uniform distribution of fixed charges in the membrane and is a special case of the more general space-charge theory. Several transport models have been derived using the fixed-charge theory in combination with the extended Nernst-Planck equation and the Donnan equilibrium potential (Tsuru *et al.* 1991*a*, Tsuru *et al.* 1991*b*, Wang *et al.* 1995*a*, Wang *et al.* 1995*b*, Wang *et al.* 1997, Peeters *et al.* 1998, Bowen and Mukhtar 1996, Bowen *et al.* 1997, Bowen and Mohammad 1998*a*, Hagmeyer and Gimbel 1999, Schaep *et al.* 1999). The Donnan-steric-pore model (Bowen *et al.* 1997, Bowen and Mohammad 1998*a*) will be discussed in some detail in Section 3.3.9 to show the principles of these models.

Wang *et al.* (1995*b*) have compared the space-charge and the TMS models and found that the TMS model agreed well with the space-charge model when the pore radius is much smaller than the Debye length, *i.e.* the radial electrical potential is more or less constant due to double layer overlap in the pore. Bowen *et al.* (1997) have shown how the radial electrical potential varies at different pore diameters and electrolyte concentrations and concluded that at small pores (less than 2 nm) and low concentations (less than 0.05 molar) the use of the simplified TMS model is justified.

3.3.9 Donnan-steric-pore and hybrid models

Bowen *et al.* (1997) and Bowen and Mohammad (1998*a*) derived the Donnan-steric-pore model (DSPM) based on the fixed-charge model and the extended Nernst-Planck equation. They also modified the diffusion, convection and distribution coefficients by introducing steric hindrance factors to describe the interaction between the penetrating molecules and the membrane pore walls. All variables are defined in terms of radially averaged quantities.

The transport through the membrane is calculated using the extended Nernst-Planck equation given in Equation 3.61, which can be rearranged to yield the concentration gradient

$$\frac{dc_i}{dx} = \frac{J_v}{D_i}\left(K_{i,c}c_i - C_{i,P}\right) - \frac{z_i c_i F}{RT}\frac{d\psi}{dx} \tag{3.115}$$

where the β_i-parameter has been replaced by the convective hindrance factor, $K_{i,c}$, and the relationship $J_i = J_v C_{i,P}$ has been used to replace J_i. Further, if no net current is transported through the membrane, *i.e.*

$$\sum_i J_i = 0 \tag{3.116}$$

an expression for the electrical potential gradient can be found, reading

$$\frac{d\psi}{dx} = \frac{\sum_{i=1}^{n} \frac{z_i J_v}{D_i} \left(K_{i,c} c_i - C_{i,P}\right)}{\frac{F}{RT} \sum_{i=1}^{n} z_i^2 c_i} \tag{3.117}$$

The hindrance factors and the modified diffusion coefficients have been reviewed by Deen (1987) and an appropriate set of definitions are given by the equations

$$K_{i,d} = K^{-1}(\lambda, 0) \qquad K_{i,c} = (2 - \Phi) G(\lambda, 0) \tag{3.118}$$

$$D_i = K_{i,d} D_{i,\infty} \tag{3.119}$$

where

$$K^{-1}(\lambda, 0) = 1.0 - 2.30\lambda + 1.154\lambda^2 + 0.224\lambda^3 \tag{3.120}$$

$$G(\lambda, 0) = 1.0 + 0.054\lambda - 0.988\lambda^2 + 0.441\lambda^3 \tag{3.121}$$

are the enhanced drag and the lag coefficient of a spherical solute moving inside a cylindrical pore, respectively. The steric factor, Φ, takes the finite size of the solute into account and is defined by the equation

$$\Phi = (1 - \lambda)^2 \tag{3.122}$$

where

$$\lambda = \frac{r_s}{r_p} \tag{3.123}$$

r_s and r_p are of course the radiuses of the solute and the membrane pores, respectively.

Equations 3.115 and 3.117 can be integrated between the boundary conditons

$$x = 0 \quad C_i = C_{i,m} \qquad \text{and} \qquad x = \Delta x \quad C_i = C_{i,P} \tag{3.124}$$

where $C_{i,m}$ and $C_{i,P}$ are the feed and permeate concentrations just outside the membrane. The concentrations inside the membrane can be found if the electro neutrality conditions in the bulk solution and inside the membrane are used together with a modified Donnan partitioning equation. The electro neutrality conditions in the bulk solution and inside the membrane can be expressed respectively as

$$\sum_{i=1}^{n} z_i C_i = 0 \qquad \text{and} \qquad \sum_{i=1}^{n} z_i c_i = -X_d \tag{3.125}$$

where as before the C_i is the concentration in the bulk solution, c_i is the concentration inside the membrane and $-X_d$ is the effective volumetric membrane charge density, which is assumed constant throughout the membrane. The Donnan equilibrium can also be modified to take steric effects into account and can be written

$$\frac{\gamma_i c_i}{\gamma_i^0 C_i} = \Phi exp\left(-\frac{z_i F}{RT}\Delta\psi_D\right) \tag{3.126}$$

where the steric factor Φ has been introduced.

The DSPM assumes the membrane to have pores (a heterogeneous membrane) in contrast to the *hybrid model* (HM) also discussed by Bowen *et al.* (1997), which assumes the membrane to be homogeneous. The HM differs from the DSPM only in the definition of the convective hindrance factor, $K_{i,c}$, which in the HM model becomes

$$K_{i,c} = G(\lambda, 0) \tag{3.127}$$

since the velocity profile through a homogeneous membrane is not fully developed in contrast to the velocity in membranes with pores.

3.3.10 Preferential-sorption-capillary-flow mechanism

The preferential sorption capillary flow mechanism was first proposed by Kimura and Sourirajan (1967) and is based on a generalised capillary-diffusion model for the transport of solute, whereas the solvent transport is proportional to the applied pressure. The transport equations become

$$N_w = L_p(\Delta P - \Delta\pi) \tag{3.128}$$

$$N_s = \frac{D_s k_s}{\Delta x}(C_R - C_P) \tag{3.129}$$

where Δx is the membrane thickness and $D_s k_s/\Delta x$ is the solute permeability factor dependent both on the concentration and the pressure (Soltanieh and Gill 1981). The mechanisms responsible for the separation are partially surface phenomena and partially by caplillary flow. An important assumption is that the membrane pores are only a few times bigger than the permeating molecules in order to enhance the importance of the membrane surface. The separation of different components occur when the membrane has a preferential sorption of one of the components, which will make the region close to the membrane rich

in this component so that only this component can have acess to the membrane pores.

In order to explain the physico-chemical criteria responsible of the separation Krasne and Eisenman (1973) suggested that the selectivity of the membrane was related to the relative free energy of interaction between the ions and the membrane. The free energy was written

$$\Delta\Delta G = \Delta G_I - \Delta G_B \tag{3.130}$$

where ΔG_I and ΔG_B is the free energy of ion-solvent interactions at the interface and in the bulk solution, respectively. The free energy of ion-solvent interaction can be expressed by the Born equation (Dickson *et al.* 1975, Dickson *et al.* 1976)

$$\frac{1}{\Delta G} = -\frac{1}{E} r_s - \frac{\Delta}{E} \tag{3.131}$$

where r_s is the ionic radius, Δ is adjustments to the ionic radius, $E = 1/2N_a(z_i e)^2$ $(1 - 1/\epsilon_w)$, N_a is the Avagadro number, z_i is the ion valence, e is the electronic charge and ϵ_w is the dielectric constant of the solvent. The solute permeability factor can then be related to the free energy of interaction by the equation

$$\frac{D_s k_s}{\Delta x} = C^* \exp\left[\sum_{i=1}^{n} (-\Delta\Delta G/RT)_i\right] \tag{3.132}$$

where C^* is a membrane constant depending on the pore distribution. When $(-\Delta\Delta G/RT)$ is positive energy is required to bring the ion from the bulk solution to the membrane surface, *i.e.* ions are rejected by the membrane, whereas when $(-\Delta\Delta G/RT)$ is negative the ions are attracted to the membrane.

Two other separation mechanisms should also be mentioned, which are the wetted surface mechanism and the desalination mechanism proposed by Luck (1984). The wetted surface or water clustering mechanism was proposed by Reid and Breton (1959) and further developed by Orofino *et al.* (1969). In this mechanism water adsorbs to the membrane through hydrogen bonds and hinders the solutes from entering the pores. The water molecules pass through the membrane by moving from a wetted site to another, whereas the solute molecules can only pass through the membrane by displacing water molecules from wetted sites, a process which requires much energy and therefore is unfavorable. On the other hand, Luck (1984) showed that the water structure inside desalination membranes differed from the water structure in the bulk solution, where the "modified" water structure inside the membrane makes the ion solubility lower and hence make

separation possible. Ions which solve easily will have a lower retention compared with ions less solvable, *e.g.* sulphate ions have a higher retention than chloride ions due to their higher hydration energy.

3.3.11 Dielectric exclusion mechanism

Based on the ideas of Sourirajan Glueckauf (1967) introduced the mechanism of *dielectric exclusion* into the context of membrane separation. The basis of the mechanism is that the membrane matrix will interact with the penetrating molecules and make the dielectric constant of the solution different from the dielectric constant in the bulk solutions. In most cases the dielectric constant within a membrane will be lower than the dielectric constant of a bulk solution, *i.e.* the molecules are more oriented due to the electric field of the membrane. The dielectric constant will affect the solubility of the solutes and the difference in the dielectric constant between the bulk solution and the membrane will have influence on the partition coefficient. Several authors have discussed and used the basic principles of the dielectric exclusion theory (Parsegian 1969, Hodgson 1970, Bean 1972, Dytnerskii *et al.* 1972, Dresner 1974, Heyde *et al.* 1975, Glueckauf 1976, Kornyshev *et al.* 1989, Min and Im 1990, Mariñas and Selleck 1992, Starov and Churaev 1993, Bontha and Pintauro 1994, Friebe and Moritz 1994, Hagmeyer and Gimbel 1998) as summarized by Yaroshchuk (2000*b*), who also gives a thorough presentation of the dielectric exclusion theory and discusses some of its interpretations.

To interpret the dielectric exclusion theory into a mathematical model Bontha and Pintauro (1994) added an extra term to the definition of the chemical potential given in Equation 3.10 and yielded

$$\mu_i(T,P) = \mu_i^0(T,P^0) + RT\ln a_i + \overline{V}_i(P-P^0) + z_iF\psi + \Delta_{hyd}G_i \qquad (3.133)$$

where $\Delta_{hyd}G_i$ is the hydration Gibbs free energy change associated with the transfer of an ion from vacuum to a given solution, which in this case is either the bulk solution or the membrane phase. The distribution of the ions between the membrane and the bulk solution can be found when the chemical potential in these two phases are set equal and all activity coefficients are assumed to be equal to 1, *i.e.*

$$\frac{c_i}{C_i} = exp\left(-\frac{z_iF\psi}{RT} - \frac{\Delta_{hyd}^m G_i - \Delta_{hyd}^b G_i}{RT}\right) = exp\left(-\frac{z_iF\psi}{RT} - \frac{\Delta W}{kT}\right) \qquad (3.134)$$

which can be compared to the Donnan potential given in Equation 3.113. Equation 3.134 shows that there are two terms that control the distribution of ions, *i.e.* the Donnan potential due to the charge of the membrane and the difference in the dielectric constant[7]. Born's model can be used to calculate the hydration energy

$$\Delta W = \frac{z_i^2 e^2}{8\pi\epsilon_0 r_i}\left(\frac{1}{\epsilon_b} - \frac{1}{\epsilon_p}\right) \tag{3.135}$$

where r_i is the ionic radius and ϵ_b and ϵ_m are the dielectric constants of the bulk solution and the pore solution, respectively. However, Parsegian (1969), Glueckauf (1976) and Mariñas and Selleck (1992) have shown that the dielectric constant of the membrane itself must be taken into account and suggest

$$\Delta W = \frac{z_i^2 e^2}{8\pi\epsilon_0 r_i}\left\{\frac{1}{\epsilon_b} - \left[\frac{1}{\epsilon_p} + \frac{0.393}{r_p/r_i\epsilon_m}\left(1 - \frac{\epsilon_m}{\epsilon_p}\right)^2\right]\right\} \tag{3.136}$$

where ϵ_m is the dielectric constant of the membrane. Hagmeyer and Gimbel (1998) use Born's model and let ϵ_p be a fitting parameter also including the effect of the membrane.

The presentation of the dielectric exclusion mechanism will end with the expression for the salt retention derived by Glueckauf (1976), which assumed spherical pores and obtained

$$R = 1 - \exp\left[-\frac{e^2 z_i^2}{2\epsilon_0\epsilon_p kT}\frac{(1-\alpha)Q}{r_p + \alpha r_i Q}\right] \tag{3.137}$$

where $Q = (\epsilon_p - \epsilon_m)/\epsilon_m$, ϵ_m is the dielectric constant of the membrane material, ϵ_p is the dielectric constant of the solution in the membrane pores, r_p is the pore radius, r_i is the radius of the ion, $\alpha = 1 - (1 + \kappa^2 r_p^2)^{-1/2}$, and, κ is the inverse Debye length defined by Equation 3.112.

3.4 Extensions to multicomponent solutions

The transport models derived for multicomponent solutions are often mathematically complicated and involve many interaction parameters. The general

[7] Equation 3.134 can in more general terms be written $c_i/C_i = exp(-W_{tot}/kT)$, where W_{tot} is the excess hydration energy. The problem that arises is to define an expression for the W_{tot} that can be used in practical calculations (Kornyshev *et al.* 1989).

irreversible thermodynamic approach presented in Section 3.2 can be used, but the model consists of a large number of phenomenological coefficients, L_{ij}, which also depend on the solute concentrations. The extended Nernst-Planck equation described in Section 3.2.4 provides a major simplification of the irreversibel thermodynamic flux equations and reduces the number of parameters by including the solute-solute interaction in the electrical potential. Both the Kedem-Katchalsky model (refer Section 3.2.2) and the Spiegler-Kedem model (refer Section 3.2.3) have been extended to multicomponent solutions (Galey and Bruggen 1970, Boesen and Jonsson 1978, Vonk and Smit 1983). On the other hand, the Maxwell-Stefan model is already applicable in multicomponent solutions, but the model suffers from the lack of relevant parameter data. Other models extended to multicomponent solutions are the solution-diffusion model (Soltanieh and Sahebdelfar 2001) and the preferential-sorption-capillary-flow model (Rangarajan *et al.* 1985).

A generalization of the Kedem-Katchalsky model has been given by Galey and Bruggen (1970) and Vonk and Smit (1983) and the solute fluxes can be written

$$J_i = \overline{c}_i(1-\sigma_i)J_v + \sum_{j=1}^{n} \omega_{ij}\Delta\pi_j \tag{3.138}$$

where ω_{ij} is the solute permeability also including the solute-solute interaction and σ_i is the reflection coefficient. The equation is valid in dilute solutions under isothermal conditions. Equation 3.138 can easily be extended to the Spiegler-Kedem model in multicomponent solutions which becomes (Boesen and Jonsson 1978, Vonk and Smit 1983)

$$J_i = c_i(1-\sigma_i)J_v - \sum_{j=1}^{n} P_{ij}\frac{dc_j}{dx} \tag{3.139}$$

where P_{ij} is the solute permeability. In a two-solute system Vonk and Smit (1983) derived the following expression for the retention coefficient

$$R_i = \frac{\sigma_{ij}(1-F_{ij})}{1-\sigma_{ij}F_{ij}} \qquad i \sim j \tag{3.140}$$

where

$$F_{ij} = exp[-J_v\Delta x\,(1-\sigma_{ij})/P_{ii}] \qquad i \sim j \tag{3.141}$$

and $i \sim j$ means that the equation for component j can be obtained by switching the indices. σ_{ij} is an effective reflection coefficient, which also includes the

interaction effects between the solutes. Also Boesen and Jonsson (1978) derived a retention expression in a two-solute system and found the relationship

$$R_i = R_i^0 - \left(\frac{P_{ij}}{P_{jj}}\right)\frac{(\sigma_j - R_j)J_v}{P_{ii} + J_v}\left(\frac{C_{j,R}}{C_{i,R}}\right) \qquad i \sim j \tag{3.142}$$

where R_i^0 is the retention in the single solute solution. Small fluxes were assumed in the derivation of this equation.

Soltanieh and Sahebdelfar (2001) wrote the multicomponent flux equations in the solution-diffusion model as

$$J_v = L_P(\Delta P - \Delta\pi_{tot}) \tag{3.143}$$

and

$$J_i = \sum_{j=1}^{n} K_{ij}(C_{j,R} - C_{j,P}) \tag{3.144}$$

where K_{ij} is the permeability including the solute-solute interaction. As for the other models an expression for the retention can be found (Lonsdale *et al.* 1974)

$$R_i = R_i^0 + \left(\frac{K_{ij}}{K_{ij} - K_{ii}}\right)(R_j^0 - R_i^0)\left(\frac{C_{j,R}}{C_{i,R}}\right) \tag{3.145}$$

Pusch (1980) used the irreversible thermodynamic approach and derived simplified flux equations and an equation for the retention coefficients

$$\frac{1}{R_i} = \frac{1}{R_i^\infty} + \sum_{j=1}^{n} \frac{P_{ij}\pi_{j,R}}{R_i^\infty J_v}\frac{R_j}{R_i} \tag{3.146}$$

where R_i^∞ is the retention at infinite volume flux ($J_v \to \infty$).

3.5 Concluding remarks

This review has shown that many possible separation mechanisms exist in a membrane separation process, and the separation may be a product of one or several of these mechanisms. Some of the mechanisms have proven useful in a particular set of conditions, whereas other mechanisms are less dependent on the conditions in the process. When the situation around a new process is investigated,

all separation mechanisms should be considered and regarded as possible, until experimental evidence points out the most likely mechanism(s).

Except for the Maxwell-Stefan approach, all transport equations are only valid in dilute solutions, but in many cases the equations have proven useful even if the concentrations are not "dilute". This assumption is necessary in order to derive at practically and mathematically feasible solutions and any attempt to extend the transport equations to concentrated solutions have ended at the point where the assumption of dilute solutions are made. Anyway, the Pitzer model has been discussed in some details in Chapter 4 in order to calculate the osmotic and activity coefficients in concentrated solutions, which will be useful in discussing the concentration versus the activity.

Chapter 4

Electrolyte solutions

4.1 The liquid state

Liquids are more difficult to deal with than gases or solids since there is neither complete disorder nor complete order in the molecular structure (Laidler and Meiser 1982). To make quantitative models the liquid state can be considered either as a nonideal gas or a disordered solid, where the first approach is better at temperatures near the critical point of the liquid whereas the latter approach is better at temperatures near the melting point. None of the approaches are good since the relative positions and orientations in liquids are difficult to define, which also means that it is difficult to calculate the macroscopic properties from the molecular interactions, *i.e.* the partition function for the liquids is usually hard to formulate.

Liquids exhibits some short range order but no long range order in the structure. The short range structure can partially be described by the *radial distribution function*, which specifies the number of entities found, on the average, at a specific distance from a particular point or entity. In liquids the short range order exists only over a few atomic or molecular diameters, and this distance decreases with increasing temperature.

Other factors required to fully describe the structure in liquids are the *coordination number* which is the mean number of nearest neighbors to a molecule, and the *angular correlation* between the nearest molecules (Conway 1981). Also, in

liquids making hydrogen bonds, such as water, the amounts of *broken* and *bent* hydrogen bonds present in the liquid can provide useful information.

The structure of liquids is dependent on the nature and strength of the *intermolecular forces*, which come into play when molecules approach each other close enough. The intermolecular forces can be separated into ion-ion, ion-dipole, ion-induced dipole, dipole-dipole, dipole-induced dipole, dispersion and repulsive forces. The first five types of forces occur when ions or dipoles are present in the liquid, while the dispersion forces are the result of a sudden unsymmetrical electron distribution in the electron cloud of a molecule which makes the molecule momentarily dipolar. This new dipole will induce a nearby molecule into another dipole and attraction between the dipoles occurs. The dipoles are in rapid fluctuation due to the rapid motion of the electron cloud, but on average the molecules experience an attractive force. Repulsive forces occur when two molecules are so close together that their electron clouds overlap, which will reduce the shielding effect of the nucleis and hence create a repulsive force between the molecules.

The relationship between the force and the potential energy between two molecules can be written

$$F = -\frac{dE_p}{dr} \tag{4.1}$$

where F is the intermolecular force, E_p is the potential energy and r is the distance between the molecules. The potential energy is set to zero when the molecules are separated by an infinite distance. The different intermolecular forces have different strength due to the different amounts of electrical charges involved and the forces decrease with different powers of the reciprocal distance between the interacting molecules, *e.g.* ion-ion forces depend on r^{-2}, ion-dipole forces depend on r^{-3} , ion-induced dipole forces depend on r^{-5}, dipole-dipole, dipole-induced dipole and dispersion forces depend on r^{-7} and repulsive forces depend on r^{-13} (Laidler and Meiser 1982).

4.2 Structure and solvent properties of water

Water is in possession of some unusual properties such as low density with corresponding high free volume, maximum density at 277 K, relatively high boiling point, high surface tension and high dielectric constant (Conway 1981). These properties are a result of the hydrogen bonds formed between water molecules.

The HOH bond angle in the water molecule is 105^o and the separation of a negative charge on the oxygen atom and a positive charge on each of the hydrgen atoms makes the water molecule an electric dipole. This strongly favours the making of hydrogen bonds in *three* dimensions.

The high dielectric constant of water is an effect of 1) the large dipole moment of the water molecule, 2) the availability of an electron lone pair on the oxygen atom that can act as an electron donor, and, 3) the high polarisation factor or high tendency to orient the molecules in response to an applied electric field. The high dielectric constant makes water a unique solvent for polar molecules and for salts which dissociate into ions.

The number density function[1] for water found by X-ray diffraction experiments is shown in Figure 4.1 (Narten *et al.* 1967). Since the number density is zero up to 250 pm, this distance can be regarded as the effective molecular diameter of the water molecule. Further, the relative density becomes one above 700 pm which means that there does not exist any structural order above this distance. The sharp peak located at a distance of 290 pm indicates the presence of the nearest neighbours, and when the number density is integrated over the volume shell at this distance, the coordination number becomes 4.4 molecules. This value is actually valid in the temperature range 277-473 K.

The structure of ordinary ice has also been determined by X-ray diffraction (Laidler and Meiser 1982). The O-O distance is found to be 276 pm and each water molecule is surrounded by four other molecules in a tetrahedral arrangement. In this ice structure there are no molecules corresponding to the peak at a distance of 350 pm found in the number density function for liquid water (refer Figure 4.1). In fact, this distance locates interstitial sites from each oxygen atom, and it seems reasonable to conclude that when ice melts some of the molecules move into these sites. This partial collaps of the tetrahedral structure when ice melts gives a contraction in the volume of about 9% (Laidler and Meiser 1982).

Several different *mixture* and *continuum* models have been used to calculate the structure and the thermodynamic properties of water, but the most promising model compared with X-ray data is given by *molecular dynamic simulation* (Conway 1981). Results from molecular dynamic simulations are still improved by more sophisticated models of the intermolecular forces and details in the struc-

[1] The number density, $\rho(r)$, relates to the radial distribution function, $g(r)$, by the equation $\rho(r) = g(r)dr/4\pi r^2 dr = g(r)/4\pi r^2$, and gives the number of atoms per unit of volume of a particular shell dr at distance r from a particular point.

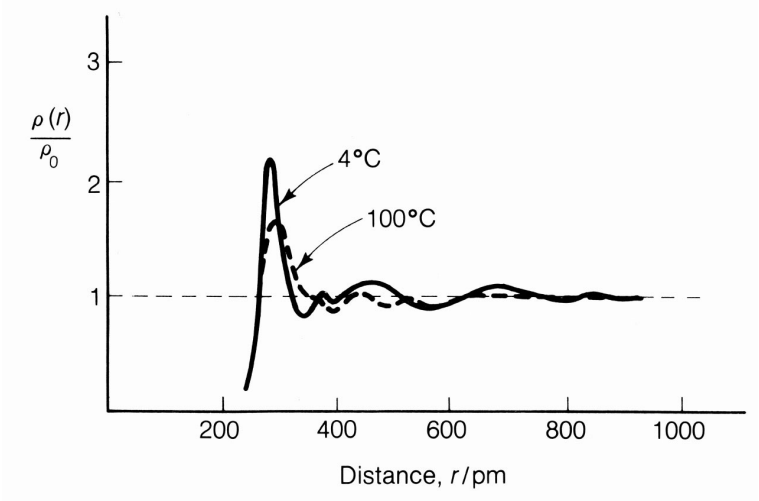

Figure 4.1: The relative number density as a function of distance calculated from X-ray diffraction experiments for water at 4 and 100 degrees Celsius. ρ_0 is the number density at large distances. From Narten et al. (1967).

ture of water are still discussed in the literature (Chialvo *et al.* 1998). Conway (1981) concludes that the structure of liquid water can be visualized "as a random, defective and highly strained network of hydrogen bonded molecules, filling space rather uniformly".

4.3 Ions in solution

4.3.1 The dissolution process of an ionic lattice

A salt consists of ions in a crystal lattice with a defined structure where the ions are held together by ionic forces. A spontaneous dissolution of the ionic lattice into dissolved ions usually occurs when a salt is mixed with water, and this process can be discussed in terms of the Gibbs energy of dissolution and hence the enthalpy and entropy of the dissolution process. The dissolution energy of an ion depends on many factors where the most important are the ion size; the ion charge; the sign of the charge; the locations of the charge bearing atoms in large molecules; the number of solvent molecules that can have direct access to the ion; the dipole and quadrapole[2] moments of the solvent molecules; and, the dielectric properties of the solvent (Conway 1981).

In a Born-Haber energy cycle the dissolution energy of the ions, ΔH_s, can be related to the energy of the crystal lattice formation, ΔH_{lat} and the hydration energy of the ions, ΔH_{hyd}. The Born-Haber enthalpy cycle can be written

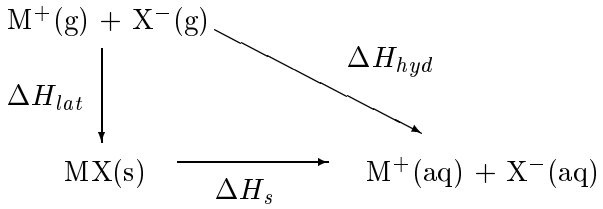

where g refers to the gas phase, aq to the aqueous phase and s to the ions in the crystal lattice. The enthalpy balance can then be written

$$\Delta H_s = \Delta H_{hyd} - \Delta H_{lat} \tag{4.2}$$

where both the enthalpy of crystal lattice formation and the enthalpy of hydration of ions in water are large negative quantities which give a relatively small enthalpy of the dissolution process, approximately in the range ± 42 kJ mol^{-1}

[2]The water molecule also forms a quadrapole moment because it actually consists of two points with negative charge (two electron lone pairs on the oxygen atom) and two points of positive charge (the two hydrogen atoms). The quadrapole moment is the electrical analogy to the moments of inertia (Millero 2001).

(Conway 1981). This means that when ions dissolve in polar solvents they return to approximately the same energy state experienced in the crystal lattice due to large energy interactions between ions and surrounding polar solvent molecules.

A simple model to interpret the thermodynamics of ions in solution was given by Max Born (Laidler and Meiser 1982), who considered the solvent as a continuous dielectric and the ion as a conducting sphere. The energy change when transferring the ion from a gas phase into a solvent equals the electrostatic Gibbs energy of hydration which can be calculated from Born's equation

$$\Delta G^0_{hyd} = G^0_{es} - G^0_{es}(vacuum) = \frac{z^2e^2}{8\pi\epsilon_0 r}\left(\frac{1}{\epsilon} - 1\right) \tag{4.3}$$

Here es means electrostatic, z is the valence of the ion, e is the electric charge, r is the radius of the ion, ϵ_0 is the permittivity of vacuum and ϵ is the dielectric constant of the solvent. Born's model is a rather simple model which does not include that the solvent molecules close to an ion will orient themselves and that the dielectric constant of the solvent will decrease nearby ions. More sophisticated models are therefore now in use (Conway 1981). However, in a plot of Gibbs hydration energy in water versus z^2/r, the Born's model shows good agreement with measured energies for univalent ions whereas the model predictions get worse when the ion charge increases and the ion radius decreases. Further, Born's model has been improved by changing the dielectric constant of the solvent close to ions. Indeed, the agreement between measured energies and calculated values from the model for divalent ions become better when the dielectric constant of water is decreased from 78 to 2 (Laidler and Meiser 1982). In other words, Born's model is very dependent on the local values of the dielectric constant and the assumption of treating the solvent as a continuum is not good.

The dielectric constant of a liquid is related to the tendency of the molecules to orient themselves in an electric field. Near ions a very high electrical field exists and this field causes almost complete orientation of the solvent molecules. The dielectric constant falls off to a value of approximately 2 when the solvent molecules get fully aligned, an effect known as *dielectric saturation* (Conway 1981). These arguments also apply for charged interfaces, *e.g.* membranes, where the dielectric constant can very rapidly fall from its normal bulk value to a much lower value close to the interface and, of course, inside a membrane.

Since the dielectric constant is a macroscopic property of a continuum liquid, the term dielectric constant near ions and interfaces should be regarded as a local effective polarizability parameter to describe the condition near the ion or interface. Since much of the Gibbs energy of hydration calulated from Born's

model is accounted for very close to the ion, *i.e.* 50% of the hydration energy is accounted for in the water layer with a thickness of one ionic radius whereas 83% of the hydration energy is accounted for in the water layer with a thickness of six ionic radiuses, it depends on the changes in the local dielectric constant. This means that an appropriate choice of the dielectric constant is of great importance when considering ionic solutions and hydration processes. Hasted *et al.* (1948) have measured the dielectric decrement in different aqueous solutions and some values are given in Table 4.2 at the end of this chapter. The ionic dielectric decrement values are additive and the dielectric constant of the solution can be calculated from the relationship $\epsilon = \epsilon_w + 2\overline{\delta}_\epsilon c$ when the concentration is lower than 2 molar.

4.3.2 Hydration number, the Frank and Wen model and Gurney's hydration co-spheres

The hydration number[3] of an ion in a solution is a widely used quantity to characterize the ion-solvent interaction present, but it is a controversy quantity due to its vague definiton and the relatively large differences between estimated values. Even if the hydration number is conventionally defined as the number of water molecules associated with an ion in the solution, problems arise when trying to decide which water molecules are satisfactorily associated and which are not. Bockris has given a useful definition of the hydration number and divided the hydration sphere into a *primary* and a *secondary* hydration layer (Conway 1981). The water molecules in the primary hydration layer are rather permanently associated with the ion and move along with it as one entity, whereas the water molecules in the secondary layer are more loosely affected by the ion and will not move along with it.

Several different experimental methods are available to measure the hydration numbers of ions. Methods used are statistical calculations from a distribution function, calculations from transport properties such as mobility measurements, calculations from measured thermodynamic properties such as activity coefficient, entropy, partial molar volume, compressibility and dielectric constant, and, from

[3]Conway (1981) makes a difference between the *hydration number* and the *coordination number* and defines the latter in terms of geometrical considerations and the hydration number in terms of the fraction α of the coordination number which have different properties compared with the properties of the bulk molecules. For strongly hydrated ions the hydration number equals the coordination numbers, while for weakly hydrated ions the hydration number approaches zero whereas the coordination number can still be a definite number.

spectroscopy measurements such as nuclear magnetic resonance (NMR). More details about each method are given in Conway (1981).

An illustrative example of the wide range of hydration numbers obtained by different methods is given by Burgess (1988), who listed the reported hydration number obtained by different methods for the magnesium ion in aqueous solutions. The reported hydration numbers are in the range 12-14 for transport number measurements; 10-13 for mobility measurements; 8 for conductivity measurements; 9 for diffusion measurements; 13 for entropy measurements; 5 for activity coefficient calculations; and 6 for calculation of the NMR peak areas. Marcus (1997) has tabulated averaged and recommended hydration numbers for a large number of ions and the values for the ions Mg^{2+}, Cl^{-} and SO_4^{2-} are given in Table 4.2 at the end of this chapter.

Another useful model of the solvent structure around ions in solutions was given by Frank and Wen (1957) and a sketch of this model is shown in Figure 4.2a. The Frank and Wen model distinguishes between three different zones around an ion in solution; 1) a hydration layer with ordered structure of water molecules, 2) a disorder layer where the water molecules are more randomly oriented than in ordinary water, and, 3) a bulk region where the ion has no influence on the water molecules.

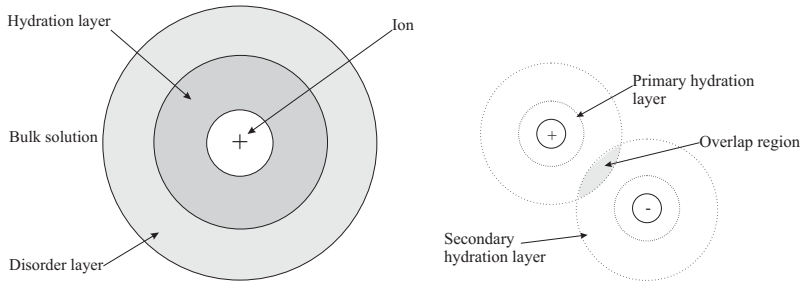

Figure 4.2: (a) The Frank and Wen model consisting of three zones. (b) Overlap between two Gurney hydration co-spheres.

Gurney (1960) treated ions in solution in terms of co-spheres, where the co-sphere around an ion was limited to those solvent molecules having an interaction energy

with the ion above a certain level, *e.g.* kT. For most ions the co-sphere radius would approximately be 2 or 3 water molecules. The probability that two co-spheres will overlap increases when the concentration increases. The solvent trapped between two spheres will be influenced by both ions, but when the ions are of the same sign the influence will to some extent vanish and release unbound water. The principle of Gurney's hydration co-sphere overlap is shown in Figure 4.2b. The critical concentration, C_G [mole/dm^3], at which Gurney co-spheres just overlap can be calculated using the equation

$$C_G = \frac{1}{N_A(2r_G)^3} \tag{4.4}$$

where N_A is the Avagadro number and r_G is the radius of the Gurney co-sphere. The latter is the sum between the ionic radius and the thickness of the hydration layer. If the co-spheres are arranged in a cubic lattice and the hydration layer thickness is set equal to the diameter of one water molecule, the critical concentration for sodium and magnesium ions is approximately one molar.

4.3.3 Ion association

Strong electrolytes were first assumed to be fully dissociated in solutions, but deviations from amongst other the Debye-Hückel-Onsager conductivity equation, have led to the conclusion that this assumption may not be strictly valid (Laidler and Meiser 1982). So, even if most strong electrolytes in water are highly dissociated (α = 0.90-0.99) there can be a significant degree of ion pairing at high concentrations.

The strong electrostatic attraction between positive and negative ions makes it possible for pairs of ions to become associated in solution. The bonds between ions that have formed such ion pairs must be distinguished from covalent bonds, since the latter bond type are permanent whereas in ion association there is a constant interchange between the ions forming the ion pair and the ions which are unassociated in the solution. Ion pairs are normally divided into three types (Conway 1981); 1) *solvent separated* ion pairs where the hydration sphere of the anion and cation are more or less retained (refer Gurney co-sphere overlap), 2) *solvent shared* ion pairs where some of the associated solvent molecules are released and where at least one solvent molecule is shared between the ions, and, 3) *contact* ion pairs in which the ions are in direct contact with each other.

Based on the Boltzmann equation, Bjerrum (refer Laidler and Meiser (1982))

derived an expression which gives the critical distance between two ions where the ions form an associated ion pair held together by coulombic forces. The electrostatic potential energy at this distance r_B is four times the mean kinetic energy per degree of freedom in the case of two univalent ions, and the probability that the ions are associated is significant. The Bjerrum distance, r_B, can be calculated from the equation

$$r_B = \frac{z_c z_a e^2}{8\pi\epsilon_0\epsilon kT} \tag{4.5}$$

where z_i is the valence of the cation and anion, e is electrostatic charge, ϵ_0 is the permittivity of vacuum and ϵ is the dielectric constant of the solvent. If the dielectric constant of water at 298 K is used this distance becomes 0.358 nm for two univalent ions, 0.716 nm for one univalent ion and one divalent ion and 1.432 nm for two divalent ions. A lower dielectric constant will of course increase these distances.

4.3.4 Structure making and structure breaking ions

The importance of solvent structural effects in the entropy of electrolyte solutions was first investigated by Frank and Robinson (1940) and Frank and Evans (1945), and led to the classification of ions as structure *makers* or structure *breakers*. Several different quantities can be used as criteria for classification, giving more or less the same result.

Frank and Robinson (1940) calculated the relative partial molal entropy of water in solutions which is defined as the difference between the actual partial molar entropy of water in a solution, $\overline{S}_w$, and the pure solvent entropy at its standard state, S_w^0. This quantity was used to predict the net structure effect in solvents when ions were added since an increase in the relative partial molal entropy of water will be equal to a breaking of the water structure and vise versa. Frank and Robinson showed that small ions like the magnesium ion have a small structure breaking tendency, especially compared with larger ions such as the sodium ion, and the results both for sodium chloride and sodium sulphate and for magnesium chloride and magnesium sulphate indicated that the sulphate ion has a smaller disruptive effect on the water structure than the chloride ion. The latter conclusion is related to the tetrahedral shape of the sulphate ion which rather easily fits into the water structure.

Later, Frank and Evans (1945) discovered the importance of the structural effects

in the entropy of electrolyte solutions and introduced the term *structural entropy.* Except for small ions, such as lithium and fluoride which has a decrease, the increase in the structural entropy indicates that most ions have a net structure breaking effect. This change in structure can be related to a change in the fluidity or viscosity[4] of a solution and is measured by the B-coefficient of the Jones-Dole equation for the viscosity given by

$$\frac{\eta}{\eta_w} = 1 + A_\eta \sqrt{c} + B_\eta c + ... \tag{4.6}$$

where η is the viscosity of the electrolyte solution, η_w is the viscosity of the water and c is the concentration given in molar. If the B_η-coefficients are positive the viscosity will increase and equivalently the fluidity will decrease and the ion is classified as a structure maker. From the B_η-coefficients listed in Table 4.2, the magnesium and sulphate ions are structure makers, whereas the chloride ion is a structure breaker. The same ion classification can be obtained by using the fluidity elevations, Δ_ϕ, given in Table 4.2 and measured by Bingham (1941).

Kaminsky (1957) discussed the temperature dependency of the B-coefficients of single ions in the temperature range 288-315.5 K. The magnesium ion has a positive and decreasing B-coefficient with increasing temperature, the sulphate ion has a positive and increasing value, whereas the chloride ion has a negative value which turns positive around 303 K.

Marcus (1997) classifies the ions as structure makers or breakers by using the average number of hydrogen bonds in which a water molecule participates, G_{HB}, and calculates the change in this number by an empirical model for the structural entropy. From Table 4.2, the magnesium ion can be regarded as a structure maker, the chloride ion is a structure breaker, whereas the sulphate ion is classified as a structure breaker. The classification of the sulphate ion is barely significant due to the accuracy of the method used.

4.3.5 Effect of increasing the electrolyte concentration

Generally, as the concentration increases the amount of free bulk water available for hydration decreases, a situation clearly demonstrated by calculating the number of water molecules per ion in divalent-univalent salts which becomes 185 water molecules for a 0.1 molal solution, 18.5 water molecules for a 1.0 molal

[4]The fluidity, ϕ is defined as the reciprocal viscosity, η, *i.e.* $\phi = 1/\eta$.

solution and 3.7 water molecules for a 5.0 molal solution. This leads to a competition over the water molecules between the ions and as a consequence the water activity decreases. This is the same as an increase in the osmotic coefficient as shown in Figure 4.3. For strongly hydrated ions, such as magnesium and sulphate ions, there is no free water at 5 molar solution. Bockris and Saluja (1972) measured the adiabatic compressibilities of several chloride salts and calculated the hydration number per salt as the concentration changed. The results for magnesium chloride are shown in Table 4.1, and the general conclusion is that the hydration number per ion will decrease as the concentration increases.

Table 4.1: Total and ionic hydration number (HN) for magnesium chloride as function of concentration at 298 K, from Bockris and Saluja (1972).

C [mol dm^{-3}]	Total HN	HN Mg^{2+}	HN Cl^{-}
0.05	12.8	10.1	1.4
0.09	12.3	9.7	1.3
1.05	10.1	8.1	1.0
2.11	8.4	6.8	0.8
4.22	6.1	5.1	0.5

The same effect was obtained by Stokes and Robinson (1973), who considered the hydration number as a distribution of successive stages, and showed how the distribution of hydration number to lithium chloride changed from a hydration number of 5 at 1 molal solution to a hydration number with a normal distribution around an average value of 2.5 at 20 molal solution. The results from molecular dynamic simulations with 0.55 molal and 2.2 molal sodium chloride solutions show a significant formation of a second hydration shell and a significant increase in the primary hydration number as the concentration decreases (Conway 1981).

The loss of free water with increasing concentration and the increase in probability that Gurney hydration co-spheres will overlap, results in an increase in the salt activity which is shown as an increase in the salt activity coefficient, see Figure 4.3. This increase in the activity coefficient is determined by the ion-ion coulombic forces and the ion-solvent interactions due to a change in the solvent activity[5].

[5] The fundamental Gibbs-Duhem equation for a solution $n_s d\mu_s + n_w d\mu_w = 0$, consisting of n_s moles of solute and n_w moles of solvent and where μ is the chemical potential, which relates the activities of the solvent and the solute in a solution.

4.4 Thermodynamics of concentrated electrolytes

This study has dealt with high electrolyte concentrations where the solutions are far from ideal and the activity coefficients are far from one. The thermodynamic properties at high concentrations can be modeled by a number of theories (Loehe and Donohue 1997). In this study the Pitzer model was chosen due to its simplicity and the wide variety of exsisting parameters. In the first sections some of the fundamental equations defining the thermodynamic properties of interest are given, while the Pitzer model is described in Section 4.4.5. The theory and the equations are taken from Pitzer (1995) unless stated otherwise.

4.4.1 Gibbs energy and definition of the chemical potential

One of Gibbs definitions given in 1875 is the equation defining what is now known as Gibbs energy

$$G \equiv U - TS + PV = H - TS \tag{4.7}$$

where G is the Gibbs energy, U the internal energy, T the absolute temperature, S the entropy, P the pressure, V the volume and H the enthalpy. If this equation is differentiated and the internal energy, $dU = dq + dw = TdS - PdV$, is introduced, the well-known thermodynamic relationship

$$dG = -SdT + VdP \tag{4.8}$$

is obtained. On the other hand, expecting the Gibbs energy to be dependent on the temperature, pressure and the mixture composition, the general differential can be written as

$$dG = \left(\frac{\partial G}{\partial T}\right)_{P,n_i} dT + \left(\frac{\partial G}{\partial P}\right)_{T,n_i} dP + \sum_i \left(\frac{\partial G}{\partial n_i}\right)_{P,T,n_{j\neq i}} dn_i \tag{4.9}$$

n_i is the number of moles of component i. If Equations 4.8 and 4.9 are compared, the following relationships can be found

$$-S = \left(\frac{\partial G}{\partial T}\right)_{P,n_i} \qquad \text{and} \qquad V = \left(\frac{\partial G}{\partial P}\right)_{T,n_i} \tag{4.10}$$

Further, the chemical potential can be defined as

$$\mu_i \equiv \left(\frac{\partial G}{\partial n_i}\right)_{P,T,n_j\neq n_i} \tag{4.11}$$

and the Gibbs energy can be expressed as

$$dG = -SdT + VdP + \sum_i \mu_i dn_i \tag{4.12}$$

4.4.2 Definitions of the activity, activitiy coefficient and osmotic coefficient

The chemical potential can be written

$$\mu_i - \mu_i^0 = RT \ln a_i \tag{4.13}$$

where μ_i^0 is the chemical potential at the standard state and a_i is the activity of component i. The activity can be divided into two parts

$$a_i = \gamma_i m_i \tag{4.14}$$

where γ_i is the activity coefficient and m_i the concentration given in molality.

When $m_i \to 0$, $a_{m,i} \to m_i$ and $\gamma_{m,i} \to 1$. This means that an ideal solution has the activity coefficient 1 and the activity is given by the concentration. The activity of the solvent (water, w) can in ideal (or very dilute) solutions be written

$$a_w = x_w = \left(1 + \frac{\sum_i m_i}{1000/M_w} \right)^{-1} \tag{4.15}$$

and the logaritmic activity can be approximated

$$\ln a_w = -\ln \left(1 + \frac{\sum_i m_i}{1000/M_w} \right) \cong -\frac{\sum_i m_i}{1000/M_w} \tag{4.16}$$

To deal with the problem that the solvent activity is very close to one in dilute solutions one defines the practical osmotic coefficient

$$\phi = -\left(\frac{1000/M_w}{\sum_i m_i} \right) \ln a_w \tag{4.17}$$

where a_w and M_w are the activity and molar weight of the solvent. The practical osmotic coefficient, ϕ, is distinguished from the rational osmotic coefficient, g, which is defined in terms of mole fraction as

$$\ln a_w = g \ln x_w \tag{4.18}$$

If Equation 4.17 is used to substitute the solvent activity, the chemical potential of the solvent given by Equation 4.13 simplifies to

$$\mu_w - \mu_w^0 = RT \ln a_w = -\frac{RTM_w\phi}{1000} \sum_i m_i \tag{4.19}$$

4.4.3 Osmotic pressure

A simple illustration of the osmotic pressure is given by a system containing pure solvent on one side and a solution on the other side of a semi permeable membrane. The membrane allows passage only of the solvent. If the pressure is the same on both sides of the membrane, the chemical potential of the solvent is less in the solution and solvent will flow through the membrane into the solution, a phenonenon commonly known as osmosis. The solvent flow will change the pressure in the solution and hence the chemical potential until equilibrium can be attained. This equilibrium can be written

$$d\mu_w = 0 = \frac{\partial \mu_w}{\partial P} dP + \frac{\partial \mu_w}{\partial m} dm \tag{4.20}$$

and inserting $(\partial \mu_w / \partial P)_T = \overline{V}_w$ and $d \ln f_w = d\mu_w / RT$, where $\overline{V}_w$ is the partial molar volume and f_w is the fugacity of the solvent, gives

$$0 = \overline{V}_w dP + RT d \ln f_w \tag{4.21}$$

which can be integrated from reference pressure P^0 to pressure P to give

$$\ln a_w = \frac{f_w}{f_w^0} = \frac{(P^0 - P)\overline{V}_w}{RT} \tag{4.22}$$

Further, substitution of Equation 4.17 gives the osmotic pressure in terms of the osmotic coefficient

$$\pi = P - P^0 = \phi \left(\frac{RTM_w}{1000 \overline{V}_w} \right) \sum_i m_i \tag{4.23}$$

Thus, the practical osmotic coefficient, ϕ, is a factor correcting the approximate expression to the true osmotic pressure.

4.4.4 Activity and osmotic coefficients in terms of Gibbs excess energy

A useful framework of equations is derived based on the definition of the excess Gibbs energy. This energy is defined as the difference between the actual Gibbs energy and the Gibbs energy of an ideal solution taken at the same temperature, pressure and composition, *i.e.*

$$G^E(T,P,x_i) = G(T,P,x_i) - G^{id}(T,P,x_i) \tag{4.24}$$

where the superscripts E and id mean excess and ideal, respectively. Taking the pure components at the same temperature and pressure as the reference states, the excess Gibbs energy for a mixing process can be written

$$G^E = \Delta_{mix}G - \Delta_{mix}G^{id} \tag{4.25}$$

$\Delta_{mix}G^{id}$ can be expressed as

$$\begin{aligned} \Delta_{mix}G^{id} &= \sum_i n_i(\mu_i - \mu_i^0) + n_w(\mu_w - \mu_w^0) \\ &= RT\sum_i n_i(\ln m_i - 1) \end{aligned} \tag{4.26}$$

The last equation is valid when using the expression for the solvent activity given in Equation 4.16. Further, by using the defintions given in Equations 4.13 and 4.19, a similar expression for the $\Delta_{mix}G$ can be found

$$\begin{aligned} \Delta_{mix}G &= \sum_i n_i(\mu_i - \mu_i^0) + n_w(\mu_w - \mu_w^0) \\ &= RT\left[\sum_i n_i \ln(\gamma_i m_i) - \phi\left(\frac{n_w}{1000/M_w}\right)\sum_i m_i\right] \end{aligned} \tag{4.27}$$

Remembering that $m_i = n_i/n_w \cdot 1000/M_w$, the last expression can be further simplified into

$$\Delta_{mix}G = RT\sum_i n_i\left[\ln(\gamma_i m_i) - \phi\right] \tag{4.28}$$

Then, finally, substitution of Equations 4.26 and 4.28 into Equation 4.25 gives

$$\frac{G^{Em}}{w_w RT} = \sum_i m_i\left(1 - \phi + \ln\gamma_i\right) \tag{4.29}$$

where $n_i = m_i \cdot w_w$ and w_w is the amount of solvent in kilograms. The superscript m states explicitly that the Gibbs excess energy is given in the molal system. The osmotic and activity coefficients can now be defined by differentiation of the G^{Em}-expression, giving

$$(\phi - 1) = -\left(\sum_i m_i\right)^{-1} \left(\frac{\partial(G^{Em}/RT)}{\partial w_w}\right)_{T,P,n_i} \tag{4.30}$$

$$\ln \gamma_i = \left(\frac{\partial(G^{Em}/RT)}{\partial n_i}\right)_{T,P,w_w,n_{j\neq i}} \tag{4.31}$$

4.4.5 Semi empirical equations (Pitzer model) for the activity and osmotic coefficients

To calculate the osmotic and activity coefficients from Equations 4.30 and 4.31 a model of the Gibbs excess energy is needed. The most acknowledged and practical model is the Pitzer ion interaction model, proposed by Pitzer (1973). The Gibbs excess energy is written

$$\frac{G^{Em}}{RT} = w_w f(I) + \frac{1}{w_w} \sum_{ij} \lambda_{ij}(I) n_i n_j + \frac{1}{w_w^2} \sum_{ijk} \mu_{ijk} n_i n_j n_k \tag{4.32}$$

and applies for a solution containing w_w kg of solvent and n_i, n_j, ... moles of solutes. The function $f(I)$ is dependent on the ionic strength, temperature and solvent properties and takes care of the long-range electrostatic forces and is given by

$$f = -\frac{4IA_\phi}{b} \ln(1 + bI^{1/2}) \tag{4.33}$$

where b is a universal constant with a value of 1.2 $\mathrm{kg}^{1/2}\mathrm{mol}^{-1/2}$ and A_ϕ is the Debye-Hückel parameter defined by

$$A_\phi = \frac{1}{3}\left(\frac{2\pi N_A \rho_w}{1000}\right)^{1/2} \left(\frac{e^2}{4\pi\epsilon_0 \epsilon kT}\right)^{3/2} \tag{4.34}$$

N_A is the Avagadro number, ρ_w is the solvent density, e is the electronic charge [C], ϵ_0 is the permittivity in free space, ϵ is the dielectric constant, k is the

Boltzmann constant and T is the absolute temperature. The ionic strength, I, is defined by

$$I = \frac{1}{2}\sum_i m_i z_i^2 \tag{4.35}$$

where m_i is the molality of species i with valence z_i.

λ_{ij} is also a function of ionic strength and expresses the short-range forces between species i and j.

Finally, the triple particle interaction, μ_{ijk}, is included, which is taken as a constant at a given temperature. It is also neglected when all the components are of the same sign due to mutual repulsion preventing short-range effects.

Only combinations of the λ's and μ's are allowed in order to get measurable variables. A set of appropriate definitions are:

$$B_{ca} = \lambda_{ca} + \frac{\nu_c}{2\nu_a}\lambda_{cc} + \frac{\nu_a}{2\nu_c}\lambda_{aa} \tag{4.36}$$

$$\Phi_{cc'} = \lambda_{cc'} - \frac{z_{c'}}{2z_c}\lambda_{cc} - \frac{z_c}{2z_{c'}}\lambda_{c'c'} \tag{4.37}$$

$$C_{ca} = \frac{3}{2}\left(\frac{\mu_{cca}}{z_c} + \frac{\mu_{caa}}{z_a}\right) \tag{4.38}$$

$$\psi_{cc'a} = 6\mu_{cc'a} - \frac{3z_{c'}}{z_c}\mu_{cca} - \frac{3z_c}{z_{c'}}\mu_{c'c'a} \tag{4.39}$$

with corresponding definitions for $\Phi_{aa'}$ and $\psi_{aa'c}$.

These expressions can be put into Equation 4.32 and the concentrations can be changed into molalities ($m_i = n_i/w_w$), which would give the following equation

for the Gibbs excess energy

$$\begin{aligned}\frac{G^{Em}}{w_w RT} = f(I) &+ 2\sum_c\sum_a m_c m_a \left[B_{ca} + \left(\sum_c m_c z_c\right) C_{ca}\right] \\ &+ \sum_{c>c'}\sum m_c m_{c'} \left[2\Phi_{cc} + \sum_a m_a \psi_{cc'a}\right] \\ &+ \sum_{a>a'}\sum m_a m'_a \left[2\Phi_{aa'} + \sum_c m_c \psi_{aa'c}\right] \\ &+ 2\sum_n\sum_c m_n m_c \lambda_{nc} + 2\sum_n\sum_a m_n m_a \lambda_{na} + ...\end{aligned} \tag{4.40}$$

where the subscripts c, a and n stand for cation, anion and neutral components, respectively. Further, the neutral-neutral interactions and 3-particle interaction involving a neutral component are omitted.

Equation 4.40 can be combinded with the defining Equations 4.30 and 4.31, and give expressions for the osmotic and activity coefficients:

$$\begin{aligned}(\phi - 1) = &\ -(\sum_i m_i)^{-1} \left(\frac{\partial(G^{Em}/RT)}{\partial w_w}\right)_{T,P,n_i} \\ = &\ \frac{2}{\sum_i m_i}\left(\frac{-A_\phi I^{3/2}}{1+bI^{1/2}} + \sum_c\sum_a m_c m_a (B^\phi_{ca} + ZC_{ca})\right. \\ &+\sum_{c<c'}\sum m_c m_{c'} (\Phi^\phi_{cc'} + \sum_a m_a \psi_{cc'a}) \\ &\left.+\sum_{a<a'}\sum m_a m_{a'} (\Phi^\phi_{aa'} + \sum_c m_c \psi_{caa'})\right)\end{aligned} \tag{4.41}$$

$$\begin{aligned}\ln\gamma_M = &\ \left(\frac{\partial(G^{Em}/RT)}{\partial n_M}\right)_{T,P,w_w,n_{i\neq M}} \\ = &\ z_M^2 F + \sum_a m_a(2B_{Ma} + ZC_{Ma}) + \sum_c m_c(2\Phi_{Mc} + \sum_a m_a \psi_{Mca}) \\ &+\sum_{a<a'}\sum m_a m_a \psi_{Maa'} + z_M \sum_c\sum_a m_c m_a C_{ca}\end{aligned} \tag{4.42}$$

$$\begin{aligned}\ln\gamma_X &= \left(\frac{\partial(G^{Em}/RT)}{\partial n_X}\right)_{T,P,w_w,n_{i\neq X}} \\ &= z_X^2 F + \sum_c m_c(2B_{cX} + ZC_{cX}) + \sum_a m_a(2\Phi_{Xa} + \sum_c m_c\psi_{cXa}) \\ &\quad + \sum_{c<c'}\sum m_c m_{c'}\psi_{cc'X} + |z_X|\sum_c\sum_a m_c m_a C_{ca}\end{aligned} \tag{4.43}$$

where

$$F = f^\gamma + \sum_c\sum_a m_c m_a B'_{ca} + \sum_{c<c'}\sum m_c m_{c'}\Phi'_{cc'} + \sum_{a<a'}\sum m_a m_{a'}\Phi'_{aa'} \tag{4.44}$$

Here the contributions of any neutral components are omitted. B' and Φ' are the ionic strenght derivative of B and Φ. Further, the following expressions are valid:

$$f^\gamma = \frac{1}{2}f'(I) = -A_\phi\left(\frac{I^{1/2}}{1+bI^{1/2}} + \frac{2}{b}\ln(1+bI^{1/2})\right) \tag{4.45}$$

$$Z = \sum_i m_i|z_i| \tag{4.46}$$

$$B^\phi_{ca} = B_{ca} + IB'_{ca} \tag{4.47}$$

$$C_{ca} = \frac{C^\phi_{ca}}{2|z_c z_a|^{1/2}} \tag{4.48}$$

The parameter B is given by

$$B_{ca} = \beta^{(0)}_{ca} + \beta^{(1)}_{ca}g(\alpha_1 I^{1/2}) + \beta^{(2)}_{ca}g(\alpha_2 I^{1/2}) \tag{4.49}$$

and it's derivative

$$B'_{ca} = \beta^{(1)}_{ca}g'(\alpha_1 I^{1/2}) + \beta^{(2)}_{ca}g'(\alpha_2 I^{1/2}) \tag{4.50}$$

For uni-uni and uni-di valent ion pairs $\alpha_1 = 2.0$ kg$^{1/2}$ mole$^{-1/2}$ and $\beta^{(2)}_{ca} = 0$, while for di-di valent (and higher valencies) electrolytes $\alpha_1 = 1.4$ kg$^{1/2}$ mole$^{-1/2}$ and $\alpha_2 = 12.0$ kg$^{1/2}$ mole$^{-1/2}$. Further, the function g is given by

$$g(x) = \frac{2[1-(1+x)exp(-x)]}{x^2} \tag{4.51}$$

and it's ionic strength derivative

$$g'(x) = -4x' \frac{1-(1+x+x^2/2)exp(-x)}{x^3} \tag{4.52}$$

Substitution of Equations 4.49, 4.50, 4.51 and 4.52 into Equation 4.47, gives

$$B^{\phi}_{ca} = \beta^{(0)}_{ca} + \beta^{(1)}_{ca} exp[-\alpha_1 I^{1/2}] + \beta^{(2)}_{ca} exp[-\alpha_2 I^{1/2}] \tag{4.53}$$

The parameter Φ^{ϕ}_{ij} where ij are either two different cations or two different anions is given by

$$\Phi^{\phi}_{ij} = \Phi_{ij} + I\Phi'_{ij} \tag{4.54}$$

where

$$\Phi_{ij} = \theta_{ij} + {}^{E}\theta_{ij}(I) \tag{4.55}$$

The parameter θ_{ij} is an adjustable parameter in the model, while the ${}^{E}\theta_{ij}$ is dependent on the ionic strength and accounts for electrostatic unsymmetrical mixing effects. It also depends on the charges and equals zero when the two interaction ions have the same charge. This gives the derivative of Φ equal to

$$\Phi'_{ij} = {}^{E}\theta'_{ij} \tag{4.56}$$

The parameter ${}^{E}\theta_{ij}$ is defined by

$${}^{E}\theta_{ij} = \left(\frac{z_i z_j}{4I}\right)\left[J(x_{ij}) - \frac{1}{2}J(x_{ii}) - \frac{1}{2}J(x_{jj})\right] \tag{4.57}$$

where

$$x_{ij} = 6 z_i z_j A_{\phi} I^{\frac{1}{2}} \tag{4.58}$$

The ionic strength derivative of ${}^{E}\theta_{ij}$ equals

$$\begin{aligned} {}^{E}\theta'_{ij} = \; & \left(\tfrac{z_i z_j}{4I}\right)\left[J'(x_{ij}) - 1/2J'(x_{ii}) - 1/2J'(x_{jj})\right] \\ & - \left(\tfrac{z_i z_j}{4I^2}\right)\left[J(x_{ij}) - 1/2J(x_{ii}) - 1/2J(x_{jj})\right] \end{aligned} \tag{4.59}$$

The function J contains the short-range potential and is very complicated. It can be approximated with numerical expressions, *i.e.* (Pitzer 1975)

$$J(x) = \frac{x}{4 + \frac{4.581}{x^{0.7237}} exp[-0.0120 x^{0.528}]} \tag{4.60}$$

This equation is straight forward to differentiate, remembering that x is also a function of I.

To sum up, the Pitzer model depends on the following adjustable parameters: $\beta_{ca}^{(0)}$, $\beta_{ca}^{(1)}$, $\beta_{ca}^{(2)}$ and C_{ca}^{ϕ} for each $c-a$ pair called the main parameters, and, θ_{ij} for each $c-c'$ and $a-a'$ pair and ψ_{ijk} for each $c-c'-a$ and $a-a'-c$ pair called the mixed parameters. All parameters including neutral components are omitted, but details about contribution from neutral solutes are treated in Pitzer (1995).

Recently the Pitzer model has been extended to apply also inside membranes as proposed by Stegen *et al.* (1999), where also the influence of the membrane has been taken into account. The fixed charged groups of the membrane are considered as ions of concentration m_m, and the activity coefficients inside the membrane can then be calculated by

$$\gamma_i^m = f_{\text{Pitzer}}(m_1^m, ..., m_n^m, m_m, f_{\text{shielding}}) \tag{4.61}$$

where m_i^m is the ion concentrations inside the membrane and $f_{\text{shielding}}$ corrects that the membrane charges perform a shielding effect upon each other. In order to use the model the Pitzer parameters have to be determined from experimental adsorption results and at this point very few literature data exist[6].

4.4.6 Temperature and pressure dependency

The temperature dependency of the thermodynamic properties are usually included in the Pitzer ion interaction parameters. Each parameter is given as a temperature dependent function and both the shape of this function and its parameters are determined from experimental results and curve-fitting. As can be seen from Appendix A, different functions apply to different electrolytes and different ion interaction parameters.

The pressure dependency of the activity coefficients could also be included in the Pitzer model, but since there is only a limited number of volumetric parameters available in the literature, this has not been done. Instead, from classical

[6] Stegen *et al.* (1999) have calculated the Pitzer parameters for a sulphonic DuPont membrane and a sodium chloride - sodium hydroxide solution.

thermodynamics the pressure dependency on activity coefficients can be written

$$\left(\frac{\partial \ln \gamma_i}{\partial P}\right)_T = \frac{\overline{V}_i - \overline{V}_i^{\infty}}{RT} \tag{4.62}$$

where $\overline{V}_i$ is the partial molar volume at a given temperature, pressure and concentration, and $\overline{V}_i^{\infty}$ is the partial molar volume at the same temperature and pressure but at infinte dilution[7].

[7]Pressure correction in the activity due to the change in reference state has been omitted, for details see Pitzer (1995).

4.5 Properties of $MgCl_2$ and $MgSO_4$ solutions

4.5.1 Calculated osmotic and activity coefficients

Mean activity[8] and osmotic coefficients for magnesium chloride and magnesium sulphate solutions were calculated using the Pitzer model described in Section 4.4.5. The results are given in Figure 4.3, where the model predictions at 298 K are compared with literature values from Lobo and Quaresma (1989). As can be seen, the model predictions are good.

An increase in temperature will give a decrease in both the activity and osmotic coefficients which can be seen in Figure 4.3. The effect of increasing the temperature is especially large at high salt concentrations.

4.5.2 Pressure dependency on activity coefficients

The pressure dependency on activity coefficients is given by Equation 4.62. Data for the partial molar volumes for magnesium chloride and magnesium sulphate solutions as function of concentration, temperature and pressure are given by Surdo *et al.* (1982) and Millero *et al.* (1982), and pressure corrections to the activity coefficients calculated from the Pitzer model at one bar can be estimated. Figure 4.4 shows mean activity coefficients at 1 and 50 bars at 298 and 318 K, respectively, and only at high magnesium sulphate concentration a minor difference can be observed due to the increased pressure. Therefore, the pressure dependency has been omitted when calculating the acitivity coefficients.

4.5.3 Phase diagrams for the system Mg-Cl-SO_4-H_2O

Phase diagrams for the system Mg-Cl-SO_4-H_2O at different temperatures are shown in Figure 4.5 (Wood 1975) and Figure 4.6 (Pabalan and Pitzer 1987). At 298 K (Figure 4.5) the stable solid phase of magnesium sulphate changes from the

[8] If one molecule of an electrolyte dissolves into $\nu = \nu_+ + \nu_-$ ions, where ν_+ is the number of positive ions and ν_- is the number of negative ions, then the mean activity coefficient, $\gamma_\pm$, can be calculated from $\gamma_\pm = (\gamma_+^{\nu_+}\ \gamma_-^{\nu_-})^{1/\nu}$, where γ_+ and γ_- are the activity coefficients for the positive and negative ions respectively.

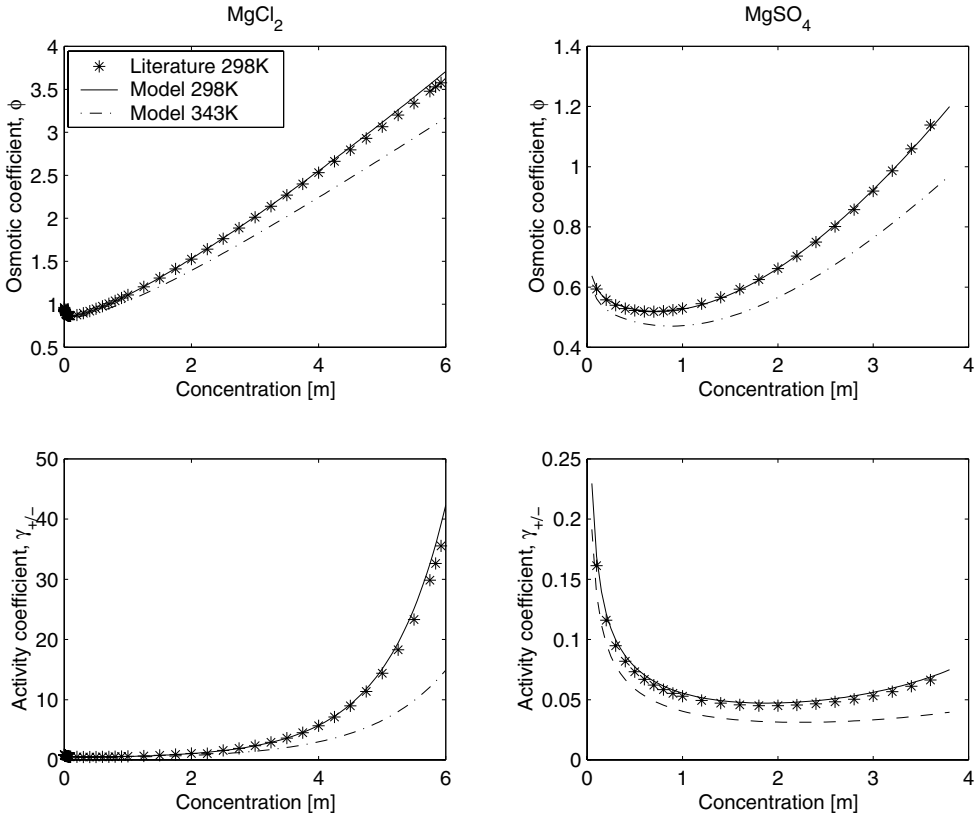

Figure 4.3: Mean activity and osmotic coefficients as function of concentration for magnesium chloride (left) and magnesium sulphate (right) solutions. Literature data from Lobo and Quaresma (1989).

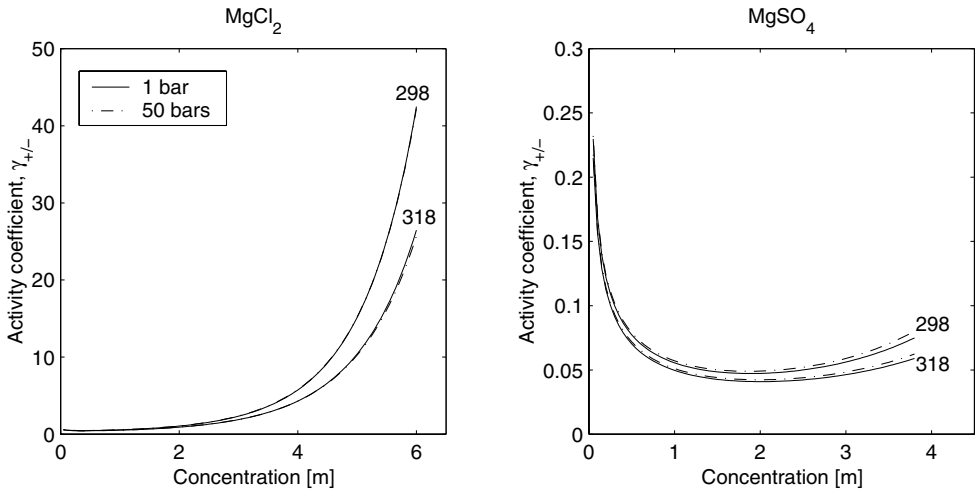

Figure 4.4: Mean activity coefficients as function of concentration calculated for 1 and 50 bars at 298 and 318 K for magnesium chloride (left) and magnesium sulphate (right) solutions.

hepta hydrate (epsomite) at low and intermediate magnesium chloride concentrations, through the hexa hydrate (hexhydrite) to the mono hydrate (kiserite) at the highest magnesium chloride concentrations. The phase diagram at 308 K in Figure 4.6 also shows a shift between different solid magnesium sulphate hydrates when the concentration of magnesium chloride increases, whereas at 273 K the only solid magnesium sulphate present is the hepta hydrate. The phase diagrams for the higher temperatures, 348 and 373 K, show that the only stable phase is the mono hydrate. At the temperatures considered in this section magnesium chloride precipitates as a hexa hydrate (bischofite).

The solubility of magnesium chloride in a pure magnesium chloride solution increases when the temperature increases, changing from approximately 5.5 molal at 273 K to approximately 7.8 molal at 373 K. The solubility of magnesium sulphate in a pure magnesium sulphate solution increases with increasing temperature until a maximum value of approximately 5.1 molal at 348 K. A further increase in the temperature gives a lower solubility of magnesium sulphate.

The highest concentrations used in this study are 5 molal magnesium chloride together with 0.04 molal magnesium sulphate (3000 ppm sulphate). For both temperatures, 298 and 343 K, the concentrations are in the soluble area of the

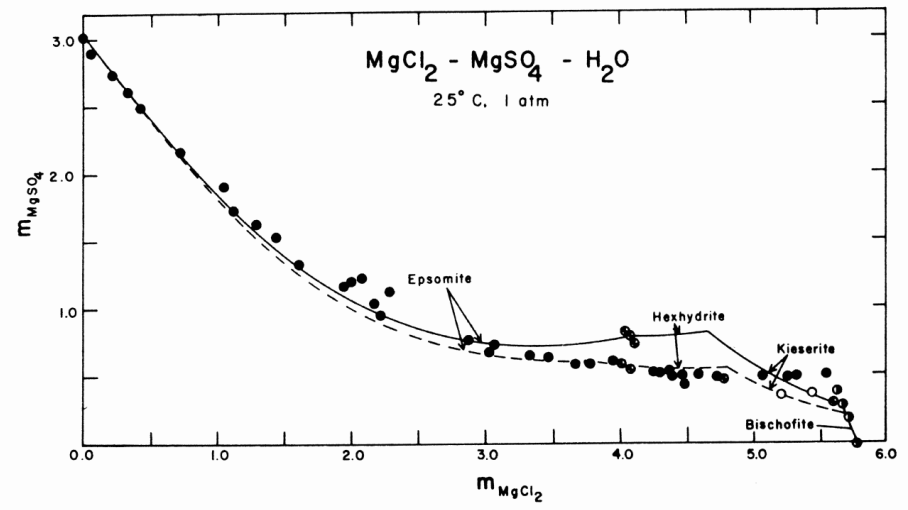

Figure 4.5: Phase diagram for the system Mg-Cl-SO_4-H_2O at 298 K, from Wood (1975).

phase diagram, but at the highest temperature the solution is closer to the solubility line. In this worst case scenario a moderate concentration polarisation of either of the two salts near the membrane surface can induce supersaturation and precipitation of solid minerals.

4.5.4 Viscosity, density and diffusion coefficient for pure $MgCl_2$ and $MgSO_4$ solutions

Density, viscosity and diffusion coefficients for pure magnesium chloride and magnesium sulphate solutions are shown in the Figures 4.7 and 4.8, where the data are from Lobo and Quaresma (1989). No magnesium chloride density data at 343 K was found in the literature, but the density data at 323 K is successfully fitted by the equation

$$\rho_T = \rho_{298K} \frac{\rho_{H_2O,T}}{\rho_{H_2O,298K}} \tag{4.63}$$

where the ρ_{298K} is magnesium chloride density at 298 K and this model is also assumed to be valid at 343 K. The magnesium chloride viscosity is successfully

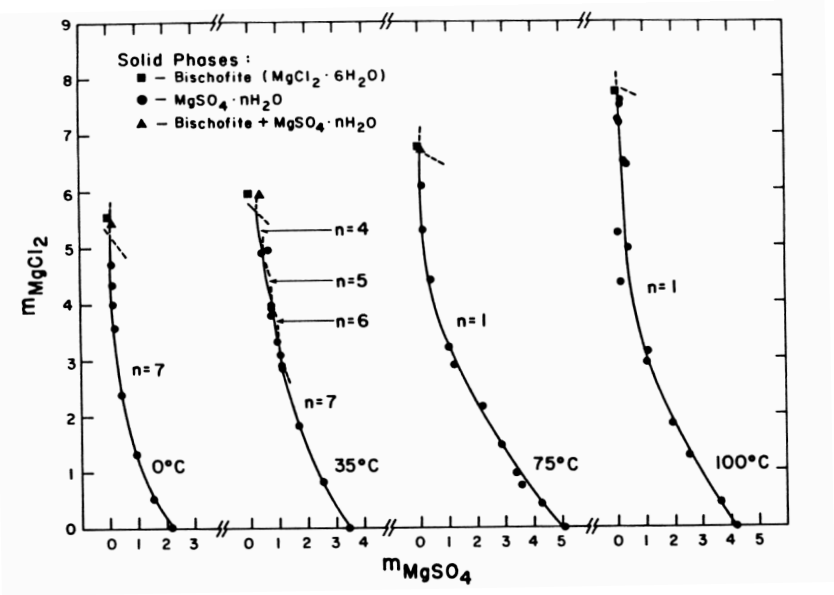

Figure 4.6: Phase diagram for the system Mg-Cl-SO_4-H_2O at 273, 308, 348 and 373 K, from Pabalan and Pitzer (1987).

fitted by the equation

$$\eta_T = \eta_{H_2O,T} \; e^{A(T)m} \tag{4.64}$$

where A is a temperature dependent parameter and m is the concentration given in molal. Predicted magnesium chloride densities and viscosities at 323 and 343 K are shown as solid lines in Figure 4.7. The density and viscosity of water at different temperatures can be found in Lide (1990).

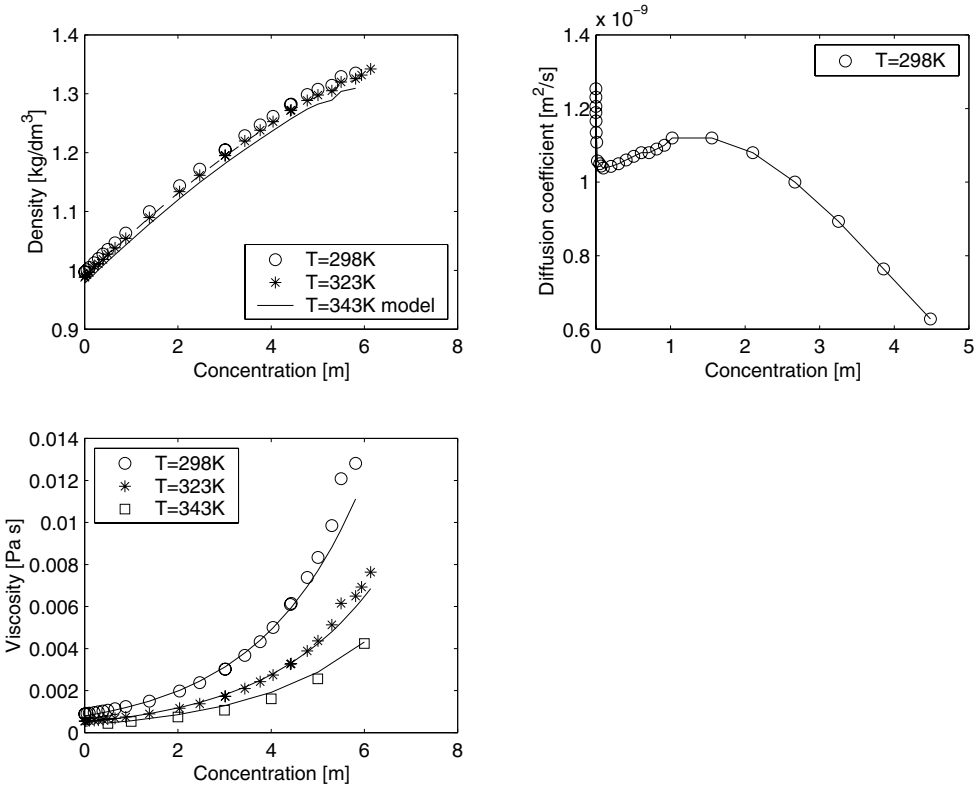

Figure 4.7: Density, viscosity and diffusion coefficient for magnesium chloride solutions, from Lobo and Quaresma (1989). The density (Equation 4.63) and the viscosity (Equation 4.64) solid lines are model predictions.

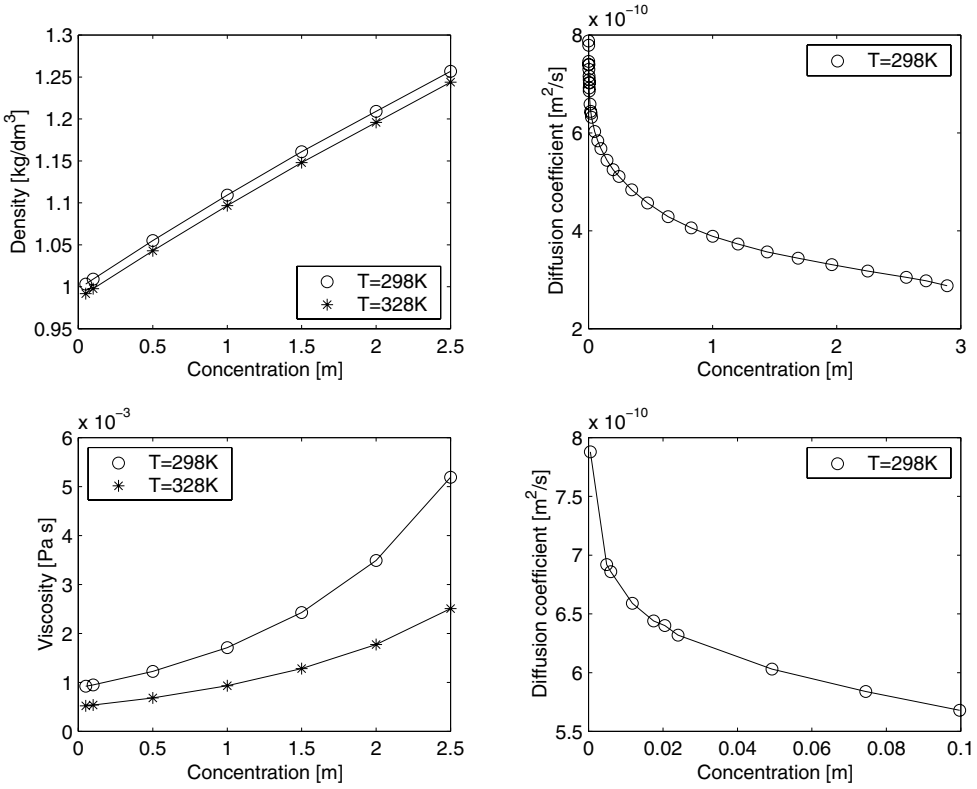

Figure 4.8: Density, viscosity and diffusion coefficient for magnesium sulphate solutions, from Lobo and Quaresma (1989).

Table 4.2: Physical properties of the Mg^{2+}, Cl^- and SO_4^{2-} ions in aqueous solutions.

	Mg^{2+}	Cl^-	SO_4^{2-}	$MgSO_4^0$
r_{cryst} [pm][1]	65	181	290	-
r_{hyd} [pm][1]	428	332	379	-
n[1,2]	9-14	2-4	3-10	15.3[3]
$n_{primary}$[1]	6	-	-	-
$n_{secondary}$[1]	8	-	-	-
ΔH_{hyd} [kJ mol^{-1}][2]	-1949	-367	-1035	-
ΔS_{hyd} [J K^{-1} mol^{-1}][2]	-331	-75	-200	-
ΔG_{hyd} [kJ mol^{-1}][2]	-1838	-347	-1090	-
λ^{∞} [cm^2 Ω^{-1} mol^{-1}][2]	106.1	76.4	160	-
D^{∞} [10^{-9} m^2 s^{-1}][2]	0.706	2.032	1.065	-
δ_{ϵ} [dm^3 mol^{-3}][4]	-24	-3	-7	-
B_{η} [dm^3 mol^{-1}][2]	0.385	-0.005	0.206	-
ΔG_{HB}[2]	0.78	-0.61	-0.21	-
Δ_{ϕ} [Pa^{-1} s^{-1}][5]	-36.5	0.28	-20.4	-

[1] Conway (1981)

[2] Marcus (1997)

[3] Millero (2001)

[4] Hasted *et al.* (1948)

[5] Bingham (1941)

Chapter 5

Experimental

5.1 Apparatus

5.1.1 Laboratory test unit

Experiments were carried out on the laboratory test unit shown schematically in Figure 5.1. The unit was built especially for this study, and due to the rather tough experimental conditions caused by the high temperature and the high salt concentration, thorough considerations were made when choosing materials. In addition the project had limited funds, so a trade off between costs and inertness of the materials was done.

The module consists of a feed tank (total volume 35 dm^3) with a heater (Watlow screw plug immersion heater, material Inconell 600, effect 2 kW) and a water heat exchanger, a pump (Hydra-Cell G10 XD, engine effect 3 kW), a bypass line, and a membrane flat-sheet cell. The membrane cell was placed inside an oven (Memmert ULE 600) to give good temperature control. The bypass line was controlled with a needle valve (Whitey union bonnet valve) and the main line was controlled with a back pressure valve (Tescom). To prevent corrosion the total area of steel in contact with the solution was kept at a minimum by using Teflon tubes, a feed tank made of glass fibre with an inside layer of vinyl ester and all parts made of steel were of quality stainless steel (SS316) or better.

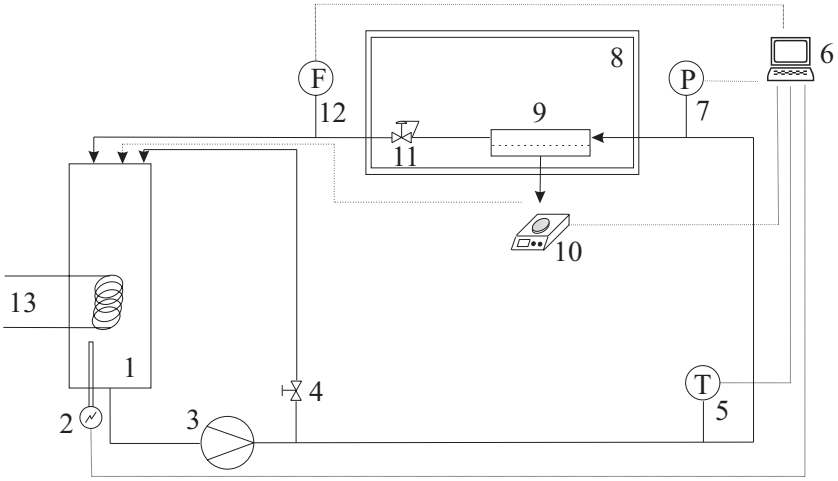

Figure 5.1: The laboratory test unit consists of (1) a feed tank, (2) a heater, (3) a pump, (4) a bypass line, (5) a temperature transmitter, (6) a computer, (7) a pressure transmitter, (8) an oven, (9) a membrane flat-sheet cell, (10) a weight balance, (11) a back pressure valve, (12) a flow meter and (13) a water heat exchanger. Temperature, pressure, flow rate and flux were automatically measured and the data stored in the computer.

The pressure transmitter (Keller type PR21, 0-100 bar, current output 4-20 mA) and temperature transmitter (PR type 5333A1, Pt-100, 0-100^{o}C, current output 4-20 mA) were placed upstream of the membrane cell, while the flow meter (Flomid-MC, Tecfluid, electro magnetic flow meter, 0-20 dm^3/minute, current output 4-20 mA) was connected to the main line downstream the membrane cell. The accumulated permeate was weighed on a balance (Explorer, Ohaus, capacity 0.00-410.00 grams).

The pressure, temperature, flow rate and flux were automatically measured and the data stored in a computer. The Field Point data acquisition system from National Instruments was used together with the program Labview. The process variables were normally sampled six times per minute. The computer also controlled the temperature by switching the heater on or off. Figure 5.2 shows the data file for one of the experiments where the temperature was 70 degrees Celsius and the flow rate at first was 1 dm^3/minute then changed to 4.5 dm^3/minute after 1.75 hours.

The experimental conditions were limited to a maximum pressure of 100 bar,

maximum temperature of 75 degrees Celsius and a maximum flow rate of 12 dm^3/minute due to the material properties and capacity of the pump.

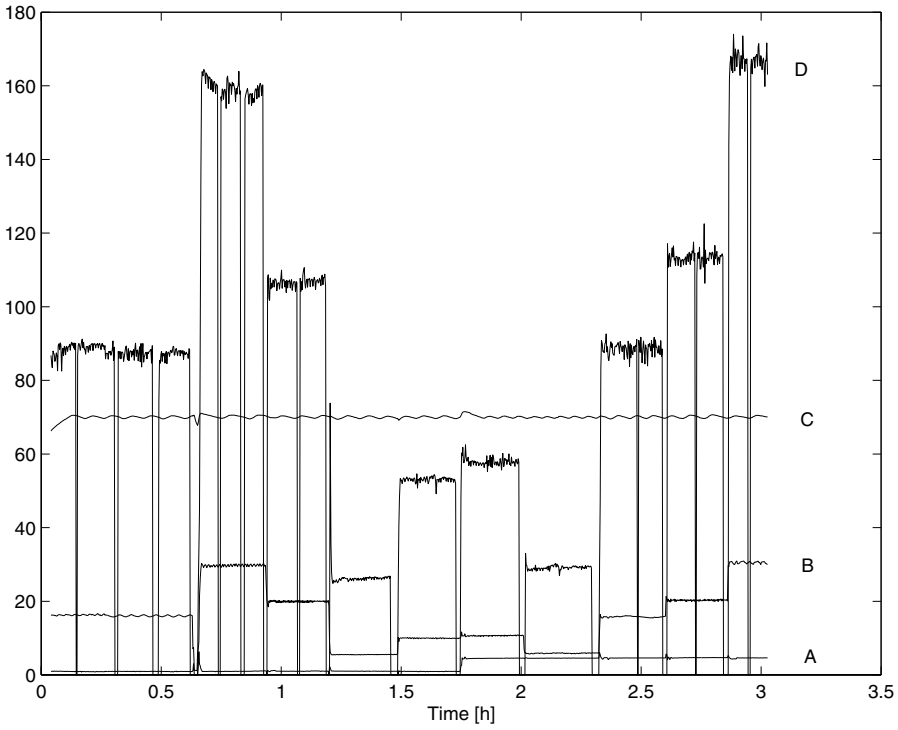

Figure 5.2: Logged experimental properties from one of the experiments. The computer did six measurements/minute. The four data series are; A: flow rate [dm^3/min], B: pressure [bar], C: temperature [^oC] and D: flux [g/m^2s].

5.1.2 Flat-sheet membrane cell

The membrane cell was a cross-flow flat-sheet stainless steel (SS316) membrane cell, which was specially designed and made for this study. A few sketches are shown in Figures 5.3, 5.4 and 5.5. The total active membrane area was 60 cm^2 (60 mm x 100 mm), and membranes with dimension 85 mm x 145 mm were cut from a larger sheet delivered from the membrane producer.

The channels perpendicular to the flow direction at the entrances in Figure 5.3,

distribute the feed to either side of the inlet or collect the fluid at the outlet. These channels are constructed to give a low pressure drop and therefore a flat velocity profile, giving quantitatively the fluid velocity along the cell wall to be at least 90% of the velocity in the middle of the cell when going from the inlet to the outlet. Figure 5.4 shows among other things the channels that collect the permeate below the membrane and the membrane support. A porous sintered metal plate in stainless steel (SS316) was used as a membrane support. The placement of this membrane support and the gasket sealing the membrane and the membrane cell, are shown in Figure 5.5.

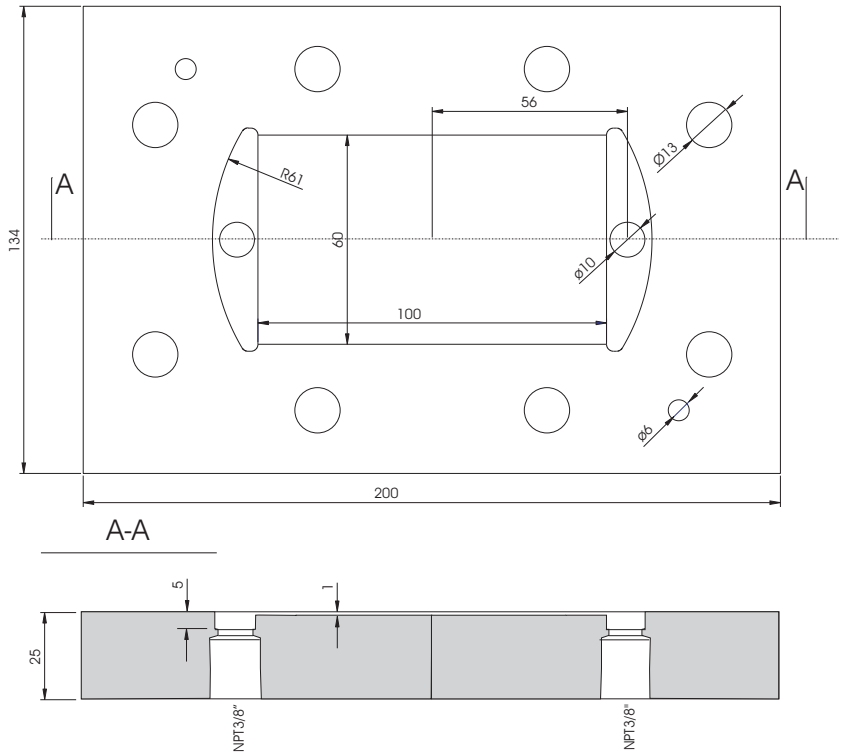

Figure 5.3: The top plate of the cross-flow flat-sheet membrane cell. All lengths in mm.

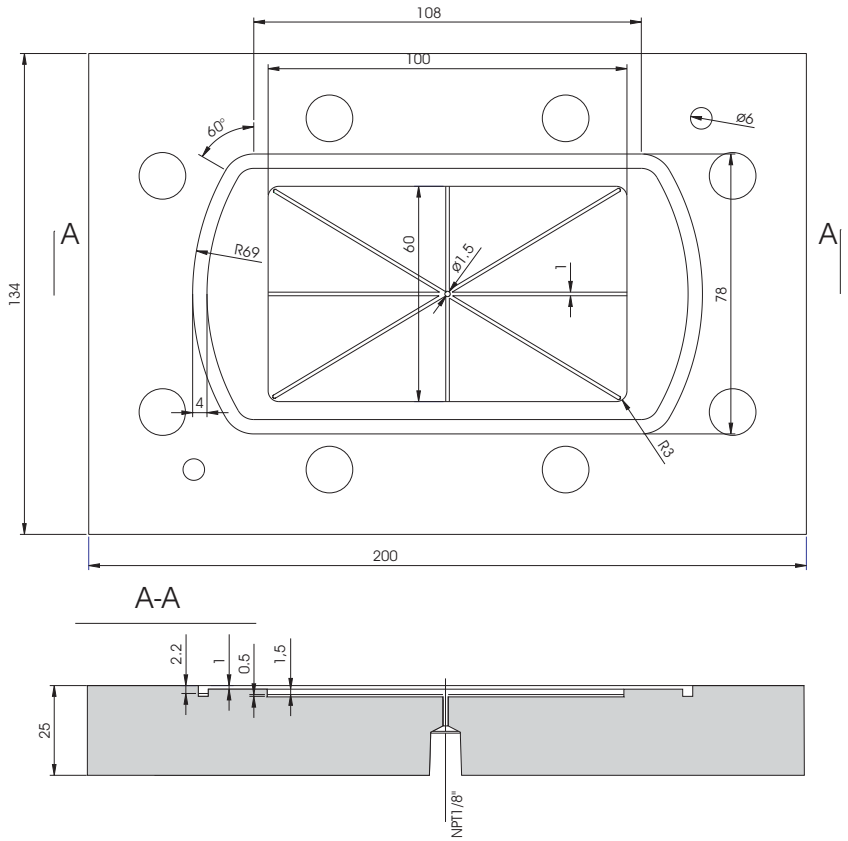

Figure 5.4: The bottom plate of the cross-flow flat-sheet membrane cell. All lengths in mm.

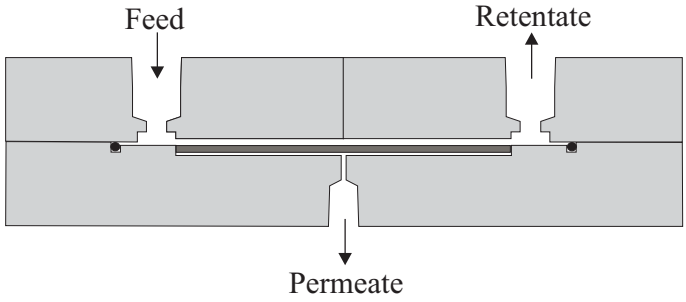

Figure 5.5: The profile of the cross-flow flat-sheet membrane cell showing the feed, the retentate and the permeate flows and the placement of the gasket and the membrane support.

5.2 Chemicals

The salt solutions were made of magnesium chloride from Prolabo (p.a. quality) and magnesium sulphate hepta hydrate from Merck (p.a. quality). The solvent was deionized water with conductivity less than 2 μS/cm and pH 7.

5.3 Characterization of membranes

Desal 5 DK and Desal G5 membranes from Osmonics/Desal were used in the study. Desal 5 DK is a nanofiltration membrane and Desal G5 is a tight ultrafiltration membrane. Both membranes are composite membranes consisting of several layers as shown in Figure 5.6. The photos are taken at magnification 300 after virgin membrane pieces had been soaked in a dye solution for five minutes and cut with a razor blade. Four visible layers can be seen for both membranes; a non-woven backing, a porous support and two skin layers (skin layer and skin layer support). From similar photos with dry membranes the thickness of the layers have been measured and the results are given in Table 5.1. According to the supplier both membranes have polyester backing and a polysulfone intermediary layer. The skin layers are proprietary, but the literature suggests that the skin support of the Desal 5 DK is a sulfonated polysulfone with a ultrathin skin layer of polypiperazineamide (Petersen 1993, Mänttäri 1999), while the skin layers of Desal G5 are made of an aromatic polyamide polymer (Palacio *et al.* 1999).

The water permeability, L_p, is defined as the coefficient relating the water flux and the pressure. This can be written as

$$J_w = L_p \Delta P \tag{5.1}$$

where J_w is the water flux and ΔP is the transmembrane pressure. The measured water fluxes plotted against the pressure for new membrane samples are shown in Appendix B, Figures B.1-B.6. The slopes are determined by a least square method and the calculated permeabilities for each sample are given in Tables B.1 and B.2. The averaged water permeabilities at 298 K and 343 K and their standard deviations are also shown in Table 5.1. The Desal 5 DK permeability at 298 K is around 50% higher than the values reported by the membrane producer, while for the Desal G5 the measured permeability is twice as high as the value reported by the supplier.

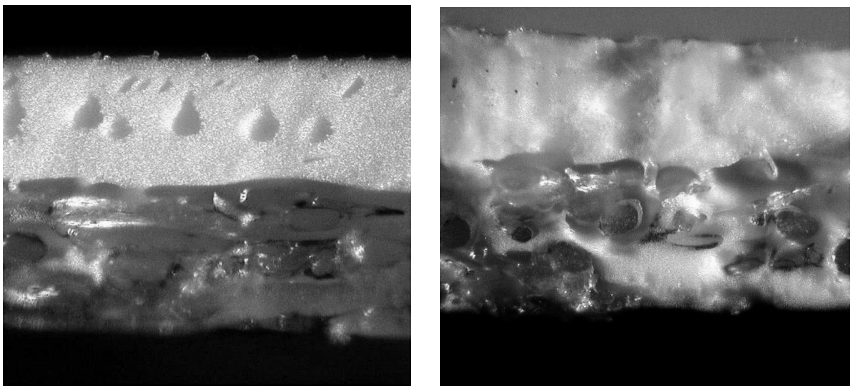

(a) (b)

Figure 5.6: Cross-section photos (magnification 300x) of a: Desal 5 DK and b: Desal G5 membranes. The membranes were soaked in a dye solutions for five minutes before cut with a razor blade.

The conctact angle hysteresis in water has been measured for both membranes. The measurements were done at the Laboratory of Technical Polymer Chemistry in Lappeenranta, Finland, using a vertical rod technique based on the Wilhelmy plate method. Small membrane pieces were put on a glas rod with diameter 2 cm and moved vertically up and down with a speed of 1 mm/minute, giving the receding and advancing angle, respectively. A video camera magnified the three phase (membrane, water and air) contact angle and the dynamic angle was measured. More details about the method and apparatus are given in Palacio *et al.* (1999).

The measured contact angles are given in Table 5.1, and since the values are lower than 90 degrees the membranes are characterized as hydrophilic. Since the values for Desal G5 are higher than the values for Desal 5 DK, Desal G5 is more hydrophobic than Desal 5 DK. Palacio *et al.* (1999) reported advancing and receding contact angle values for Desal G5 equal to 73 and 35 degrees, respectively, which are in good agreement with the angles found here.

At the Laboratory of Technical Polymer Chemistry in Lappeenranta, Finland, the streaming potential for both membranes were measured and the zeta potential

was calculated using the Helmholtz-Smoluchowski equation

$$\frac{\Delta U_s}{\Delta P} = \frac{\epsilon\epsilon_0\zeta}{\eta\lambda'} \tag{5.2}$$

where ζ is the zeta potential, ΔU_s is the streaming potential, ϵ_0 is the permittivity of free space, ϵ is the dielectric constant, η is the viscosity and λ' is the electrical conductivity. Two different flat-sheet membrane modules were used to measure the streaming potential *through* the pores and the streaming potential *along* the surface of the membranes. Details about the method and the apparatus used are given in Pihlajamäki (1998). The measurements were done at 25 degrees Celsius and 1 mM potassium chloride solution. The pH was adjusted in the range 2.5-7 by adding potassium hydroxide or hydrogen chloride in small amounts and the streaming potential was measured at five different pressures in the range of 0.1-1 bar. The measured streaming potentials were plotted versus the pressures, and the slopes were used to calculate the zeta potential from Equation 5.2.

The zeta potentials measured along the surface of the Desal G5 membrane are more or less equal to the potentials measured through the pores which can be seen in Figure 5.7. The zeta potentials are sligthly negative giving a small negative charge on the membrane in the pH range 2.5 - 7. The two measured zeta potentials for the Desal 5 DK membrane show different trends since the potentials along the membrane gets positive below pH 4, while the potential measured through the pores stays negative in the pH range covered. The zeta potentials measured along the membrane surface for the Desal 5 DK membrane agree well with the values reported by Hagmeyer and Gimbel (1999) for low pH, whereas above pH 5 Hagmeyer and Gimbels values are more negative than the values found here. The zeta potentials found through the pores for the Desal G5 membrane follow qualitatively as well as quantitatively similar experiments done by Nystrøm *et al.* (1989) on sulfonated polysulfone membranes, where the measured zeta potentials are stable at -5 mV in the pH range 3-7.

The molecular weight cut off (MWCO) of the Desal 5 DK membrane has been measured by Comstock (1989) and the pore radius has been calculated from experimental results from Wang *et al.* (1995*a*) and Bowen and Mohammad (1998*a*). The MWCO and the corresponding pore radius for the Desal G5 membrane are given by Palacio *et al.* (1999). All parameters are given in Table 5.1.

Further, the ratio of membrane thickness over the effective porosity of the membrane, $\Delta x/A_k$, is a useful parameter which can be calculated from the Hagen-

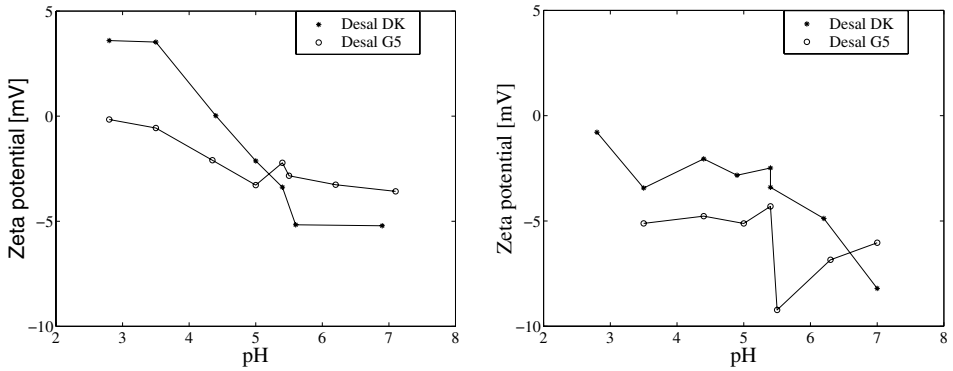

(a) (b)

Figure 5.7: Measured zeta potential (a) along the surface and (b) through the pores for the Desal 5 DK and Desal G5 membranes.

Poiseuille equation

$$J_w = \frac{r_p^2 \Delta P}{8\eta(\Delta x/A_k)} \tag{5.3}$$

when the water permeability, $L_p = J_w/\Delta P$, the pore radius, r_p, and the viscosity, η, are known. Using the reported values for the permeability, pore radius and viscosity, values for the $\Delta x/A_k$-parameters have been calculated and the results are shown in Table 5.1. The result for the Desal 5 DK membrane is of the same order as the values reported by Wang *et al.* (1995*a*) and Bowen and Mohammad (1998*a*), which are in the range 2-4 μm.

Table 5.1: Characteristic parameters of the membranes.

	Desal 5 DK	Desal G5
10^6 L_p^{298K} [m^3/m^2 s bar]	3.5 ± 0.5	1.0 ± 0.1
10^5 L_p^{343K} [m^3/m^2 s bar]	1.11 ± 0.03	0.19 ± 0.01
θ_{adv} [^{o}]	52 ± 3	69 ± 3
θ_{rec} [^{o}]	23 ± 2	33 ± 2
MWCO [g/mol]	200-300[1]	2000[2]
r_p [nm]	0.4-0.6[3]	2.82[2]
$\Delta x/A_k$ [μm]	1.0	108
Membrane thickness Δx [μm](dry)	≈185	≈200
Backing thickness [μm]	≈95	≈90
Support thichness [μm]	≈80	≈100
Skin support + skin thickness [μm]	≈10	≈10

[1] Comstock (1989)

[2] Palacio *et al.* (1999)

[3] Wang *et al.* (1995*a*), Bowen and Mohammad (1998*a*)

5.4 Procedures

5.4.1 Pretreatment of new membrane samples

All new membrane samples were wetted in water for 2.5 hours at 25 degrees Celsius and 20 bar, followed by half an hour at the same temperature and 40 bar. The water flux was then measured at different pressures (5, 10, 15, 20 and 40 bar), 25 degrees Celsius and Reynolds number between 1000-3000.

The retention characteristic of the membrane was measured after half an hour running using a 0.1 m magnesium chloride solution at 25 degrees Celsius, 30 bar and Reynolds number 1000. If the retention of the membrane sample varied from the retention measured on previous samples, the membrane sample was rejected. The salt concentration was determined by conductivity measurements (712 Conductometer, Metrohm, error $\pm$ 0.8%) and the calculated retention for the membrane samples are given in Tables B.1 and B.2 in Appendix B.

5.4.2 Experiments

A detailed operation procedure of how the experiments were carried out is given in Appendix C. At each temperature and flow rate level the pressure was changed in a random order to prevent statistical systematic errors. All reported values of temperatures, flow rates, pressures and fluxes, are averaged values from 15-20 measurements, and from the same measurements the standard deviations to the sampled properties were calculated.

The elapsed time from a change in the feed concentration until a new permeate concentration has stabilized, can be defined as the response time to the membrane cell. The response time was measured for different magnesium chloride concentrations and is shown in Figure 5.8. As the figure shows the response time is independent of the concentration and equals 50 grams accumulated permeate. The time from a change in the experimental conditions to a sample in the permeate can be taken, was set to be one and a half of the response time, that is 75 grams of permeate.

After the experiments were finished and the system was emptied, the apparatus was washed three times with 10 litres of deionized water. This normally gave

a conductivity in the third water less than 50 μS/cm, and the water flux at different pressures (5, 10, 15, 20 bar) was measured at 25 degrees Celsius. After the experiments with the highest concentration (5 molal), a fourth wash was needed to give a satisfing conductivity in the water.

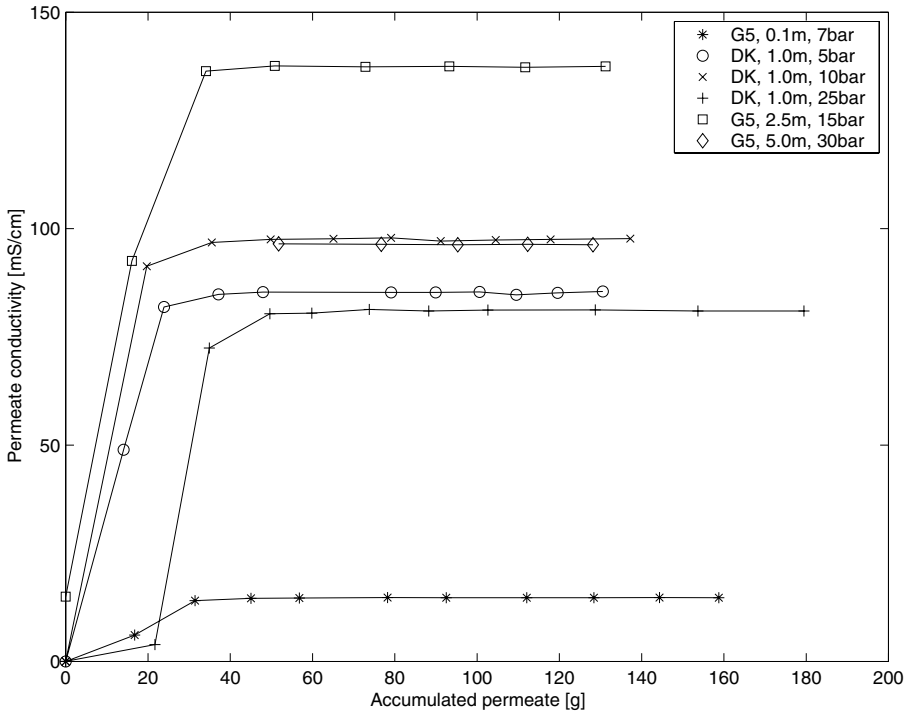

Figure 5.8: Measured conductivity in the permeate as a function of accumulated permeate when the feed was changed from water to a magnesium chloride solution.

5.4.3 Ion analysis

The chloride ion concentration was measured by the method of Mohr, *i.e.* precipitation of silver chloride. The accuracy in the determined chloride concentration was found to be better than 0.5%. This value is calculated from more than 50 samples that have been tested with 2 or more titrations.

The sulphate ion concentration was measured gravimetrically by precipiation of barium sulphate. The accuracy of the sulphate concentration was found to be

better than 3% when the concentration was around 300 ppm and better than 1% when the concentration was around 3000 ppm. The standard deviations were calculated from 10 different samples with concentrations around 300 ppm and 11 different samples with concentrations around 3000 ppm, which were tested twice. The analysis was performed by SINTEF, Inorganic Process Chemistry and Analysis.

The magnesium ion concentration was measured with atomic absorption spectroscopy with a Varian apparatus, model 400. The samples were diluted until the magnesium concentration was in the range 5-20 ppm. The accuracy of the magnesium concentration was found to be better than 1%, by calculating the standard deviation for 4 different samples that were tested twice. SINTEF Inorganic Process Chemistry and Analysis performed the analysis.

The pH was measured by a pH meter from Metrohm (model 744) with error $\pm$ 0.05 pH units. The measurements was done directly in the samples when the magnesium chloride concentration was equal to or less than 1 molal, otherwise the samples were diluted ten times with deionized water (pH 7) before the pH were measured and the pH in the original samples calculated.

5.5 Overview of the experiments

An overview of the experimental conditions is given in Table 5.2. For each experimental condition, that is for a given magnesium chloride concentration, magnesium sulphate concentration, temperature and Reynolds number the flux and ion retentions were measured at 5-7 different pressures. The pressure varied in the range 5 to 55 bars. Most of the experiments are done both on Desal 5 DK and Desal G5 membranes. In addition, one experiment with 1.0 molal magnesium chloride concentration and Desal 5 DK membrane was done with a sulphate concentration of 175 ppm.

All obtained results and accurate process variables are given in Appendices D and E, while the water flux measurements are shown in Appendix B.

Table 5.2: The experimental conditions are given by combinations of the flow rate and concentrations at each temperature level. The fluxes and the ion retentions are measured at 5-7 different pressures (in the range 5-55 bar), and most of the experiments have been done both on Desal 5 DK and Desal G5 membranes.

T=298 K	c_{MgCl_2} [m]	0.1	1.0	2.5	5.0
	$c_{SO_4^{2-}}$ [ppm]	0	0	0	0
		300	300	300	300
		3000	3000		3000
	Reynolds number	1000	1000	1000	750
		4500	4500	2500	
T=343 K	c_{MgCl_2} [m]		1.0	2.5	5.0
	c_{MgSO_4} [ppm]		0	0	0
			300	300	300
			3000		3000
	Reynolds number		1000	1000	750
			2000	2500	1500
			4500	5000	2500
			10000		

Chapter 6

Measured fluxes and ion retentions

The aim of this chapter is to give the reader a quick overview of all the results. The measured fluxes and ion retentions are shown in Figures 6.1-6.13. Each figure presents the measured data for a given temperature and magnesium chloride concentration. The first column shows the results for pure magnesium chloride solution, while the other columns show the results after addition of small amounts of magnesium sulphate. The first row shows the measured total volume flux, the second row shows the chloride ion retention, the third row shows the sulphate ion retention and the fourth row, if any, shows the magnesium ion retention. All data are plotted as function of the pressure. The figure captions also contain the identification number of all membrane samples used to produce the data shown in that figure and further information of each membrane sample can be found in Appendix B.

All raw data can be found in the Appendices D and E. The fluxes given in the appendices have been divided by the density of the permeate and the factor 1000 to convert the flux values from g/m^2s to m^3/m^2s. The retentions have been calculated using Equation 2.2 in Chapter 2 and the experimentally measured feed and permeate concentrations.

The standard deviation in the retention values has been calculated combining the standard deviations in the measured ion concentrations[1]. The standard deviation of the chloride concentration is 0.5% of the value, of the magnesium concentration better than 1% of the value and of the sulphate concentration better than 3% of the value when the sulphate concentration is around 300 ppm and better than 1% of the value when the sulphate concentration is around 3000 ppm. Calculated standard deviations of the retention values are shown as error bars in the figures. The standard deviation of the flux values are estimated to be less than 5% of the value.

6.1 Measured fluxes and ion retentions using Desal 5 DK membranes

The fluxes and ion retentions obtained using the Desal 5 DK membrane are given in the Figures 6.1-6.7. The figures show that the total volume flux is linearly dependent on the pressure in all cases. Some very small deviations from linearity can be observed at 1 molal magnesium chloride concentrations, high temperatures and high pressures and the deviations are believed to be pressure compaction, refer Section 6.6.

The figures show that the temperature has a considerable positive effect on the volume flux. When the temperature increases from 298 K to 343 K, the flux increases approximately 5 times. On the other hand, the magnesium chloride concentration has a large negative influence on the total volume flux. At 298 K the flux at 5 molal decreases approximately to 1/15 of the flux measured at 1 molal, whereas at 343 K the same flux ratio is 1/8. Further, neither the Reynolds number nor an addition of magnesium sulphate show any significant effect on the total volume flux.

The total volume flux plot for the pure magnesium chloride solution in Figure 6.3 shows a large difference between the measured fluxes at Reynolds 1000 and 4500 using the membrane sample DK-R3 and values measured at Reynolds number 2000 and 10000 using the membrane sample DK-R9. The retention results also show that the membrane sample DK-R9 is much tighter than membrane sample

[1] The standard deviation s_y of a function y can be calculated from the equation $s_y = \sqrt{(\frac{\partial y}{\partial x_1} s_{x_1})^2 + (\frac{\partial y}{\partial x_2} s_{x_2})^2 + ...}$, where x_1, x_2, ... are the variables with standard deviations s_{x_1}, s_{x_2}, ...

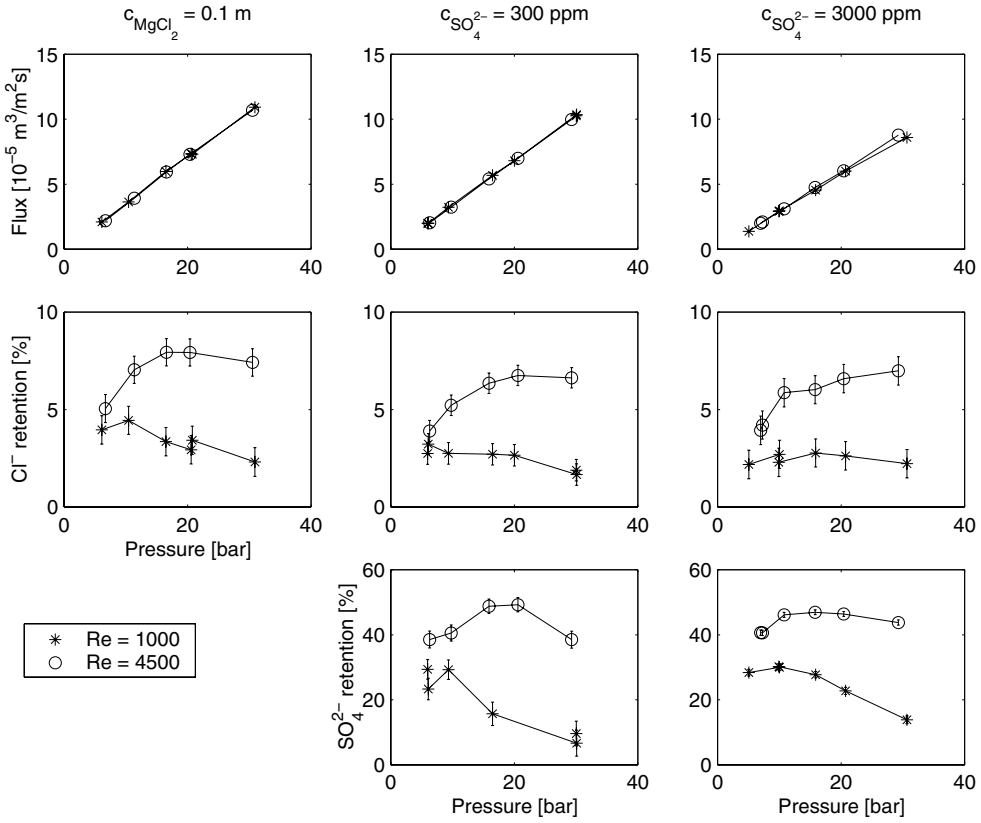

Figure 6.1: Measured fluxes and ion retentions using 0.1 molal magnesium chloride solutions, temperature 298 K and Desal 5 DK membrane samples DK-R3 in the first column, DK-R4 in the second column and DK-R6 in the third column.

DK-R3. This difference was the reason that a quality test was introduced to test the permeabilities and the retention characteristics of each membrane sample before it was used in experiments.

The chloride and sulphate ion retentions obtained using 0.1 and 1 molal magnesium chloride solutions and laminar flow are constant or slightly decreasing when the pressure increases, while at turbulent flow the retentions increase to a maximum limiting value with increasing pressure. The chloride retentions at 2.5 molal magnesium chloride concentration are weakly increasing with increasing pressure whereas the sulphate retentions are independent of the pressure. At 5 molal magnesium chloride concentration both ion retentions are independent of

the pressure. Both the chloride and the sulphate ion retentions seem to decrease when the temperature increases from 298 to 343 K, and further, the results indicate a decrease in the retentions when the chloride concentration increases. The effect of Reynolds number vanishes at high magnesium chloride solutions, refer Section 6.4.

The sulphate retention point at 175 ppm sulphate concentration, Reynolds number 1000 and pressure 5 bar in Figure 6.2 has a strange placement compared to the other retention patterns at this magnesium chloride concentration and most likely something has gone wrong in the laboratory. The statistical analysis discussed in Section 6.4 also indicated that something was wrong with this point.

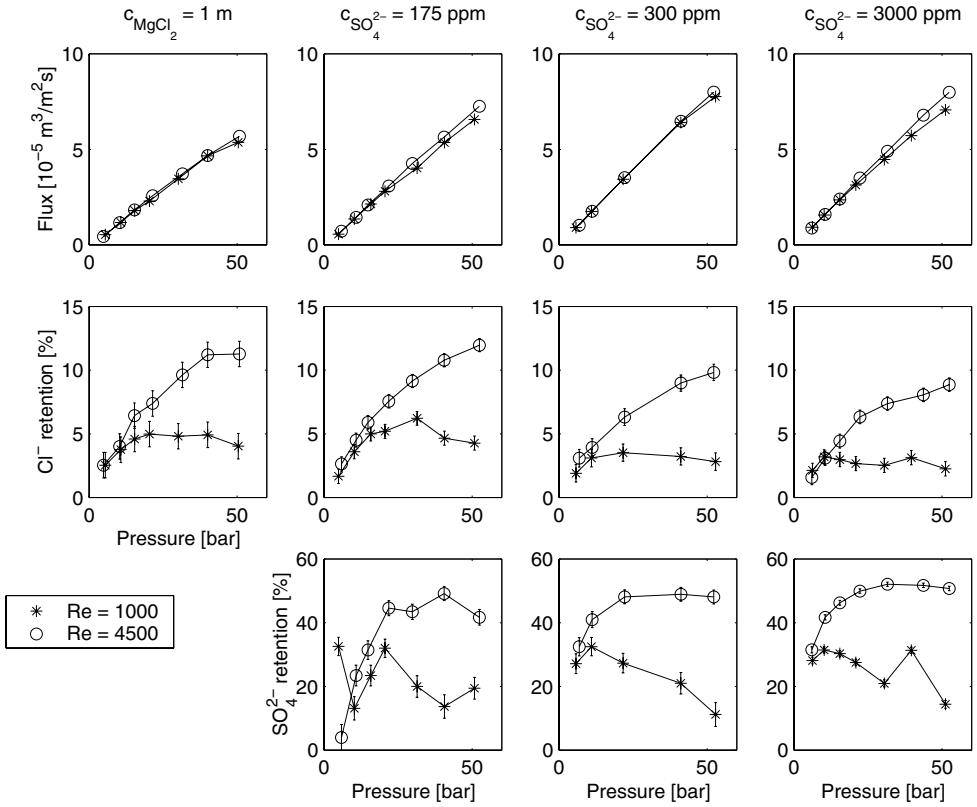

Figure 6.2: Measured fluxes and ion retentions using 1 molal magnesium chloride solutions, temperature 298 K and Desal 5 DK membrane sample DK-R8.

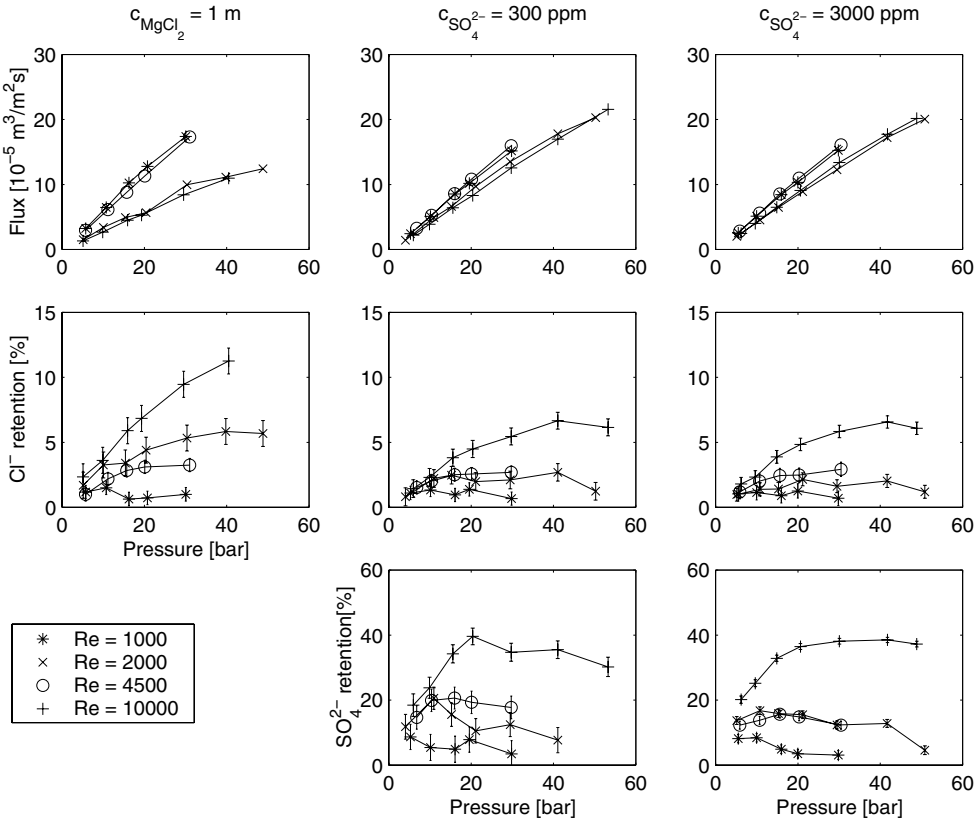

Figure 6.3: Measured fluxes and ion retentions using 1 molal magnesium chloride solutions, temperature 343 K and Desal 5 DK membrane samples DK-R3 (Re=1000/4500) and DK-R9 (Re=2000/10000) in the first column, DK-R6 (Re=1000/4500) and DK-R8 (Re=2000/10000) in the second column and DK-R6 (Re=1000/4500) and DK-R8 (Re=2000/10000) in the third column.

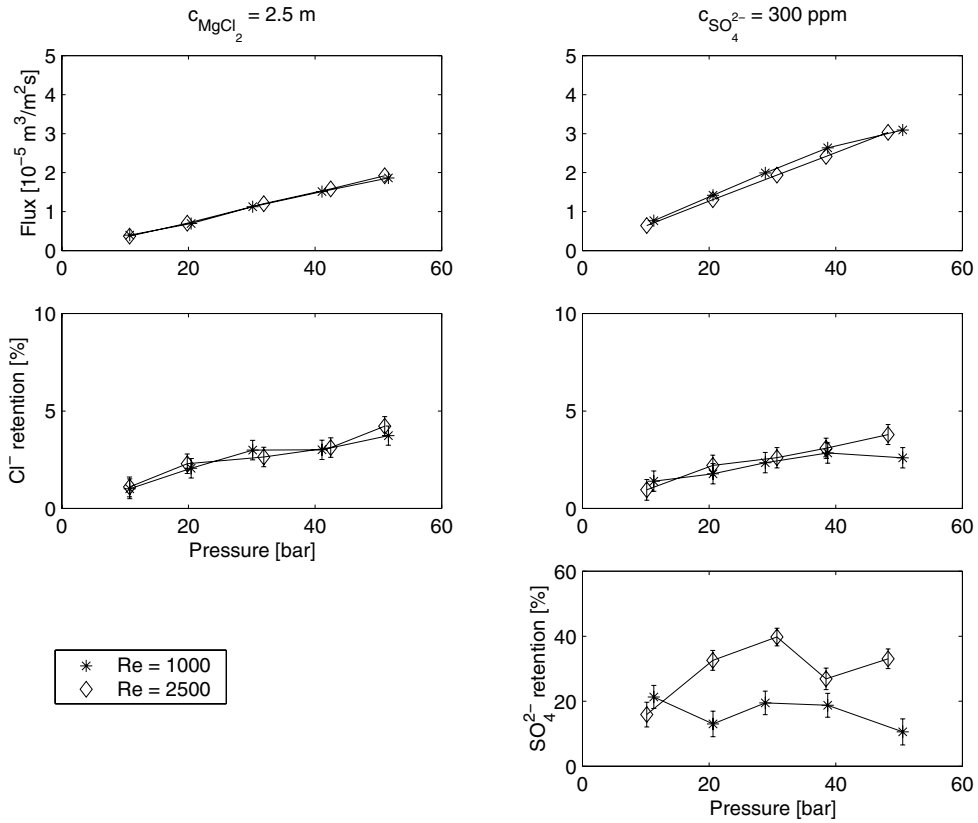

Figure 6.4: Measured fluxes and ion retentions using 2.5 molal magnesium chloride solutions, temperature 298 K and Desal 5 DK membrane samples DK-R1 in the first column and DK-R4 in the second column.

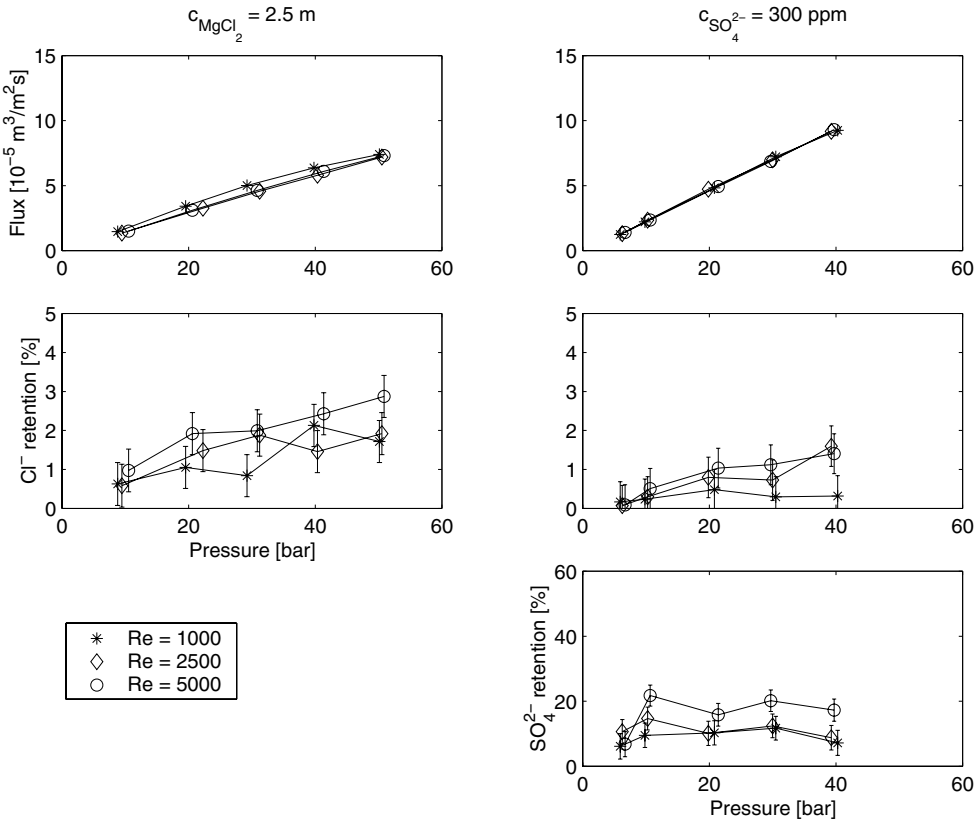

Figure 6.5: Measured fluxes and ion retentions using 2.5 molal magnesium chloride solutions, temperature 343 K and Desal 5 DK membrane samples DK-R1 in the first column and DK-R4 in the second column.

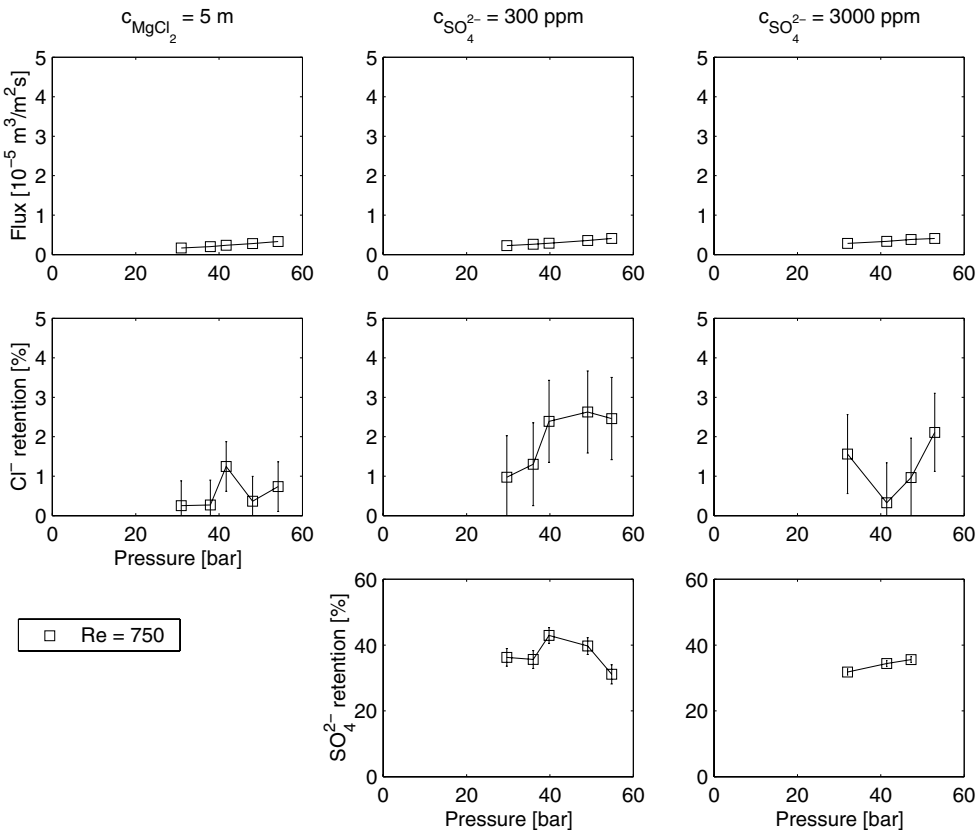

Figure 6.6: Measured fluxes and ion retentions using 5 molal magnesium chloride solutions, temperature 298 K and Desal 5 DK membrane samples DK-R1 in the first column, DK-R5 in the second column and DK-R6 in the third column.

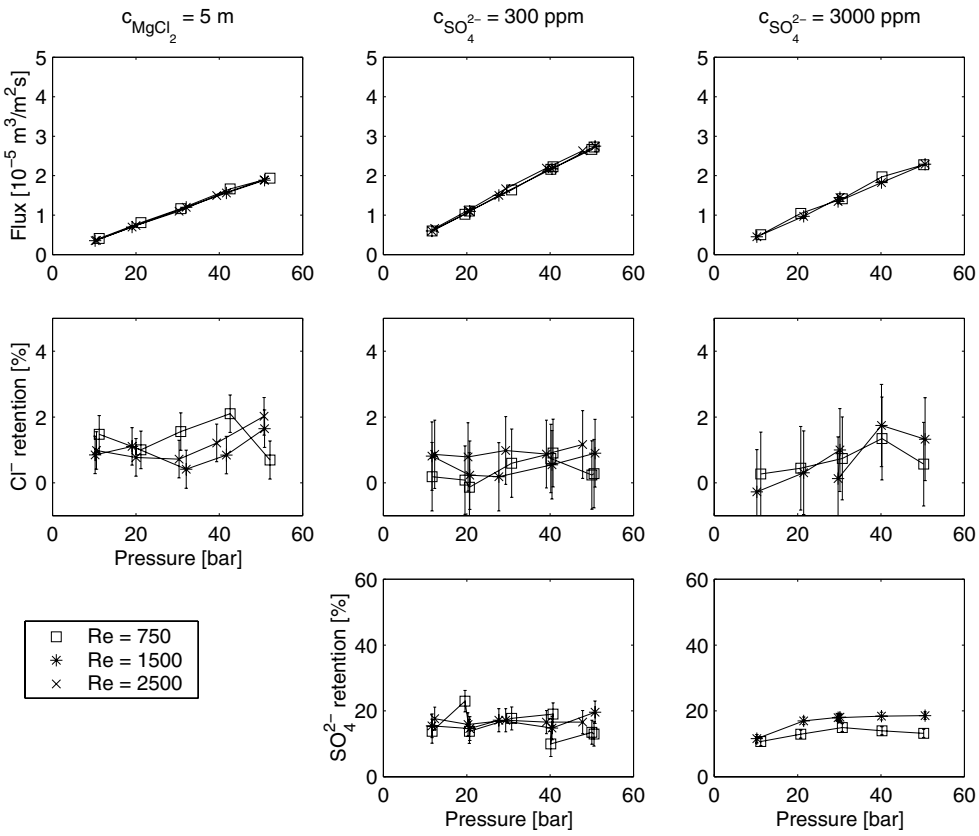

Figure 6.7: Measured fluxes and ion retentions using 5 molal magnesium chloride solutions, temperature 343 K and Desal 5 DK membrane samples DK-R1 in the first column, DK-R5 in the second column and DK-R6 in the third column.

6.2 Measured fluxes and ion retentions using Desal G5 membranes

The results obtained using the Desal G5 membrane are given in Figures 6.8-6.13. As for the Desal 5 DK membrane, the total volume flux is linearly dependent on the pressure. Some small deviations from linearity occur at high pressures and are most likely caused by further pressure compaction of the membrane sample at high temperature.

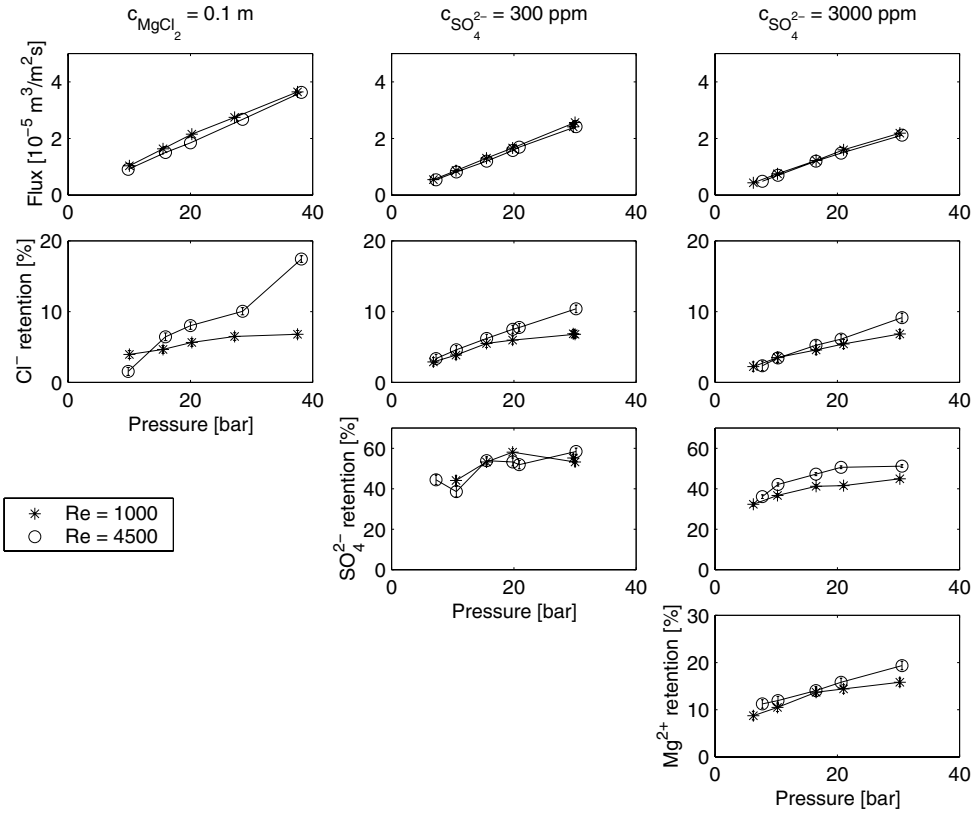

Figure 6.8: Measured fluxes and ion retentions using 0.1 molal magnesium chloride solutions, temperature 298 K and Desal G5 membrane samples G5-R2 in the first column, G5-R5 in the second column and G5-R6 in the third column.

A strange pressure-flux behavior can be seen in Figure 6.10 at 1 molal magnesium chloride concentration and temperature 343 K. First, at the 300 ppm sulphate level, Reynolds number 2000 and 50 bars, a sudden jump up in the flux value oc-

curs with a corresponding jump down in the ion retentions. Normally this would indicate a discrepancy or a hole in the membrane sample, but the next data series at Reynolds number 10000 show the initial pressure-flux and retention patterns. The same membrane sample was later used in the experiments with 3000 ppm sulphate concentration and the flux and the retention values at 298 K shown in Figure 6.9 were values comparable to the results with 3000 ppm sulphate concentration, whereas at temperature 343 K the permeability has increased drastically and the retentions are considerably lower compared to the values obtained with a different membrane sample.

The total volume flux increases approximately by a factor 2.5 when the temperature increases from 298 K to 343 in 1 and 2.5 molal magnesium chloride solutions. The Desal G5 membrane is completely impervious at 298 K and a magnesium chloride concentration of 5 molal. At 298 K the flux at 2.5 molal decreases approximately to 1/4 of the flux measured at 0.1 molal, whereas at 343 K the flux at 5 molal decreases by a factor 1/8 of the flux at 1 molal. Further, the measurements show that neither the Reynolds number nor an addition of magnesium sulphate has significant effect on the total volume flux.

Both the chloride and the sulphate ion retentions increase and reach a limiting value when the pressure increases. The retentions increase when the Reynolds number increases, but the effect of the Reynolds number vanishes when the magnesium chloride concentration increases. Both the chloride and the sulphate retentions decrease when the magnesium chloride concentration increases. The magnesium retentions shown in Figure 6.8 have values between the chloride and sulphate retentions, whereas in Figure 6.13 the magnesium retentions equal the chloride retentions.

Since transport of the most permeable component is enhanced by the presence of a less permeable component in multicomponent solutions, the former component can experience negative retention values at low fluxes. Figure 6.9 shows that the only negative chloride retention values obtained occur in a 1 molal magnesium chloride and 0.003 molal magnesium sulphate solution.

The chloride retention point at 35 bar and Reynolds number 4500 in Figure 6.8 and the point at 30 bar and Reynolds number 1000 in Figure 6.9 show large deviations from the rest of the data series and are most likely outliers where something has gone wrong during the analysis.

The measured total volume flux using Desal 5 DK membrane is much higher com-

pared to the flux measured using Desal G5 membrane. On the other hand, both the chloride and the sulphate retentions are higher for the Desal G5 membrane compared to the Desal 5 DK membrane.

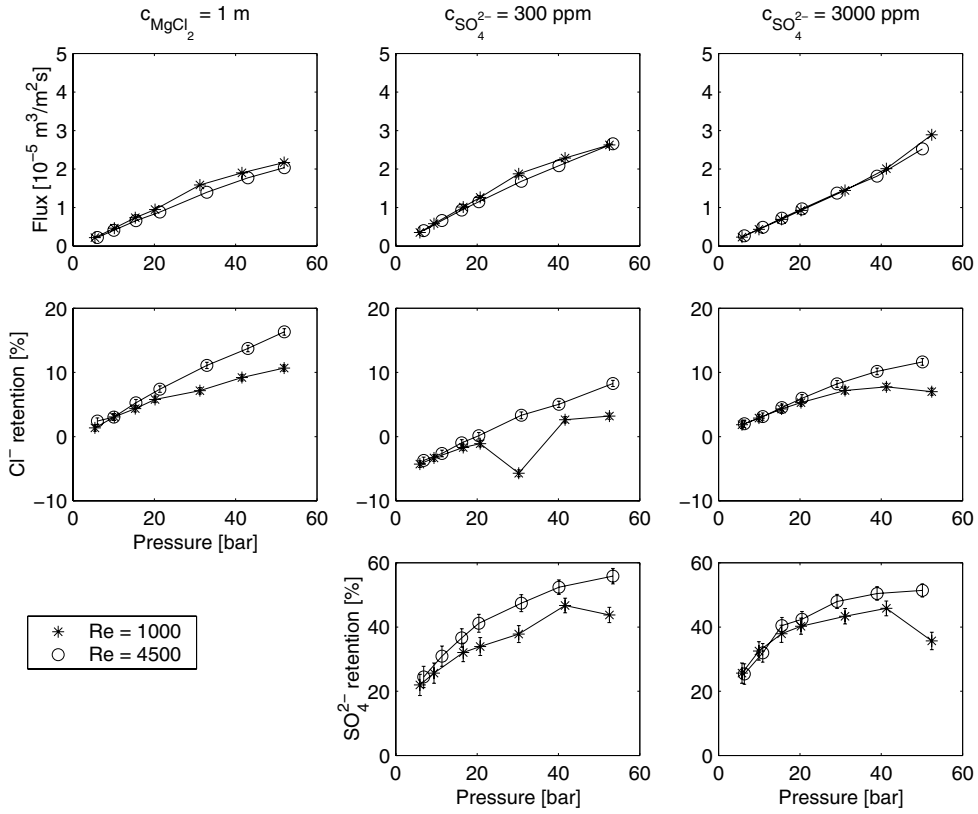

Figure 6.9: Measured fluxes and ion retentions using 1 molal magnesium chloride solutions, temperature 298 K and Desal G5 membrane samples G5-R9 in the first column and G5-R10 in the second and third columns.

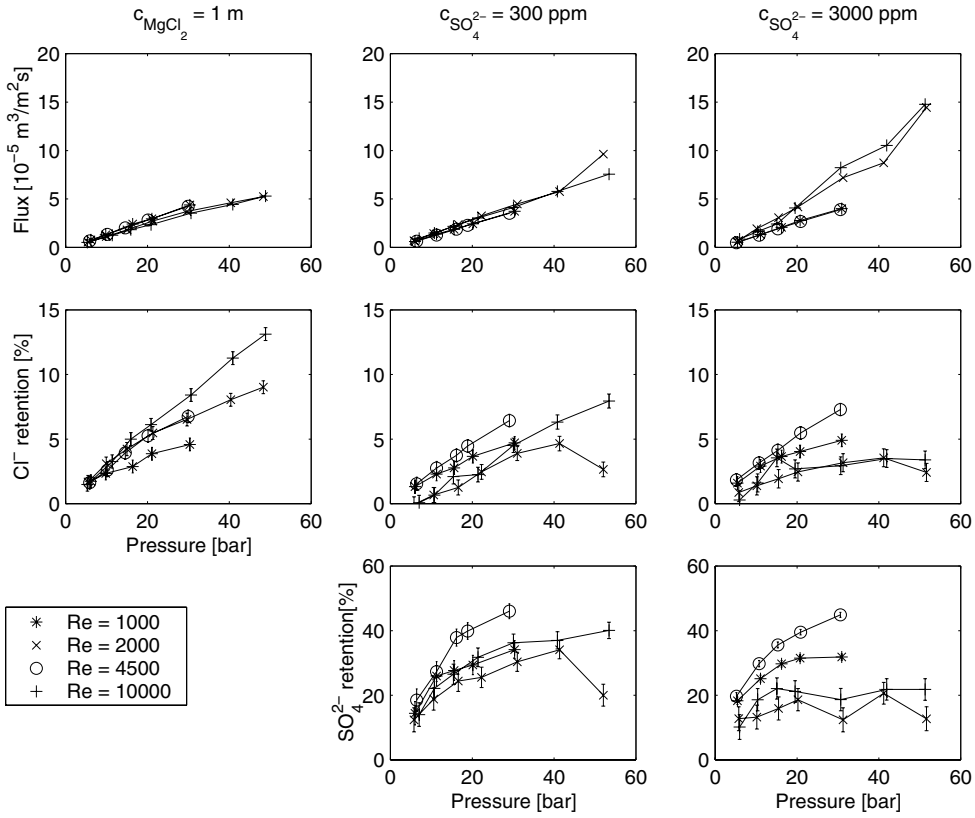

Figure 6.10: Measured fluxes and ion retentions using 1 molal magnesium chloride solutions, temperature 343 K and Desal G5 membrane samples G5-R2 (Re=1000/4500) and G5-R9 (Re=2000/10000) in the first column, G5-R5 (Re=1000/4500) and G5-R10 (Re=2000/10000) in the second column and G5-R7 (Re=1000/4500) and G5-R10 (Re=2000/10000) in the third column.

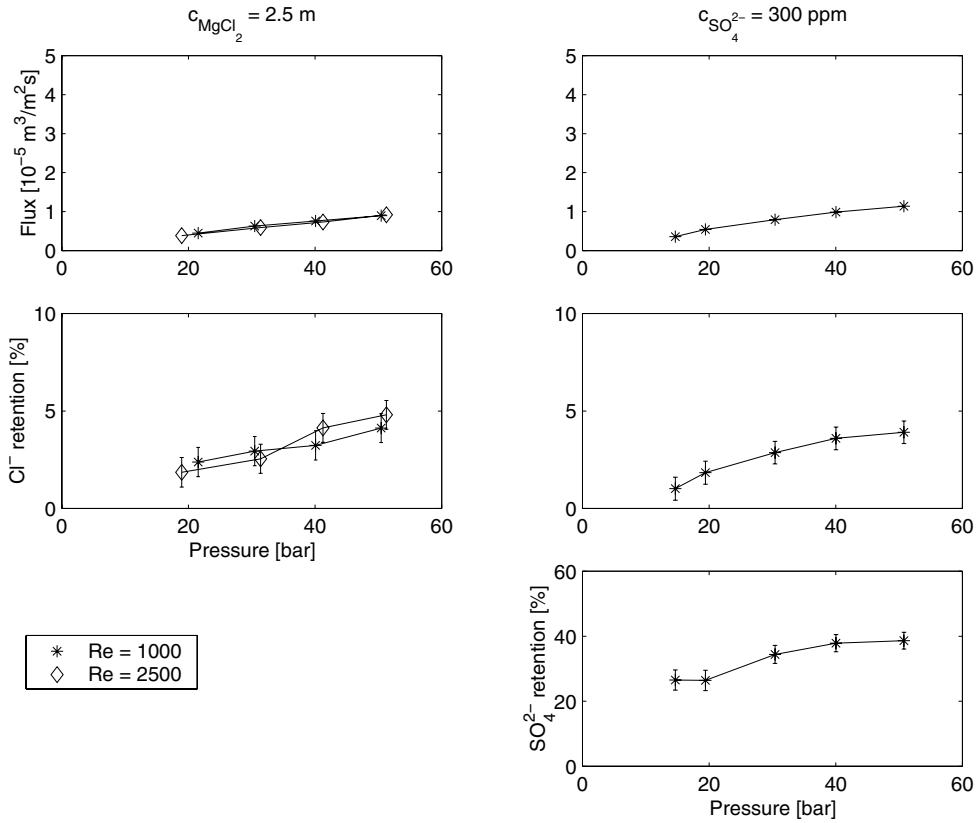

Figure 6.11: Measured fluxes and ion retentions using 2.5 molal magnesium chloride solutions, temperature 298 K and Desal G5 membrane samples G5-R1 in the first column and G5-R8 in the second column.

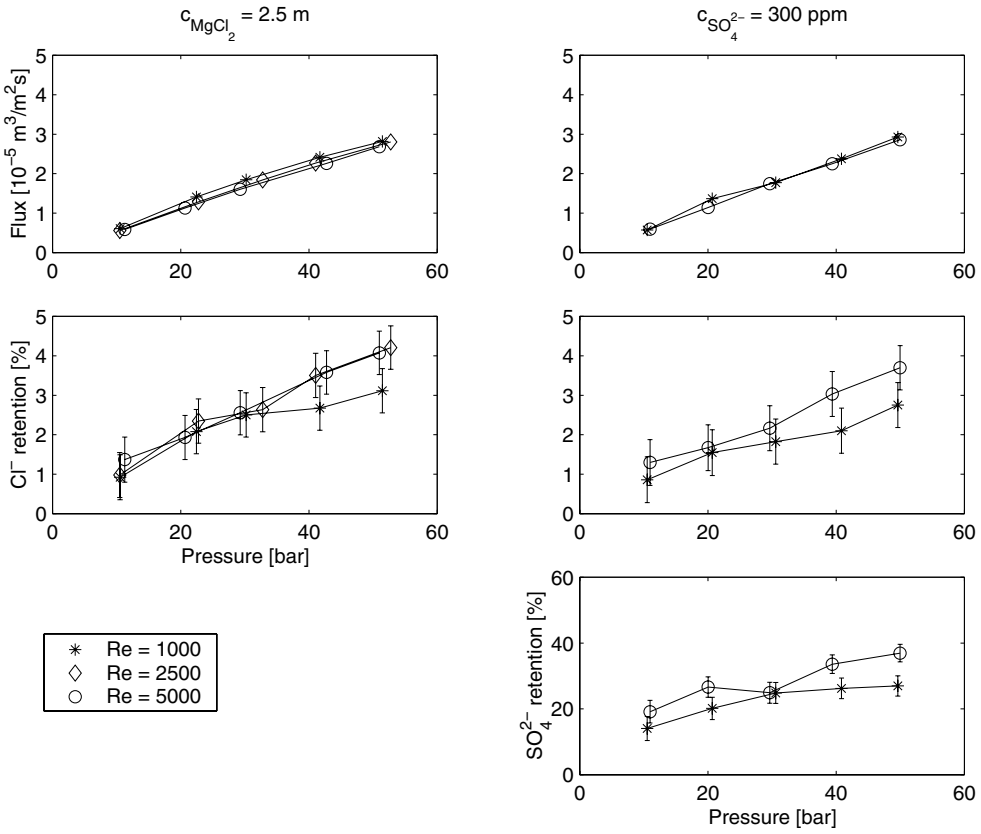

Figure 6.12: Measured fluxes and ion retentions using 2.5 molal magnesium chloride solutions, temperature 343 K and Desal G5 membrane samples G5-R1 in the first column and G5-R8 in the second column.

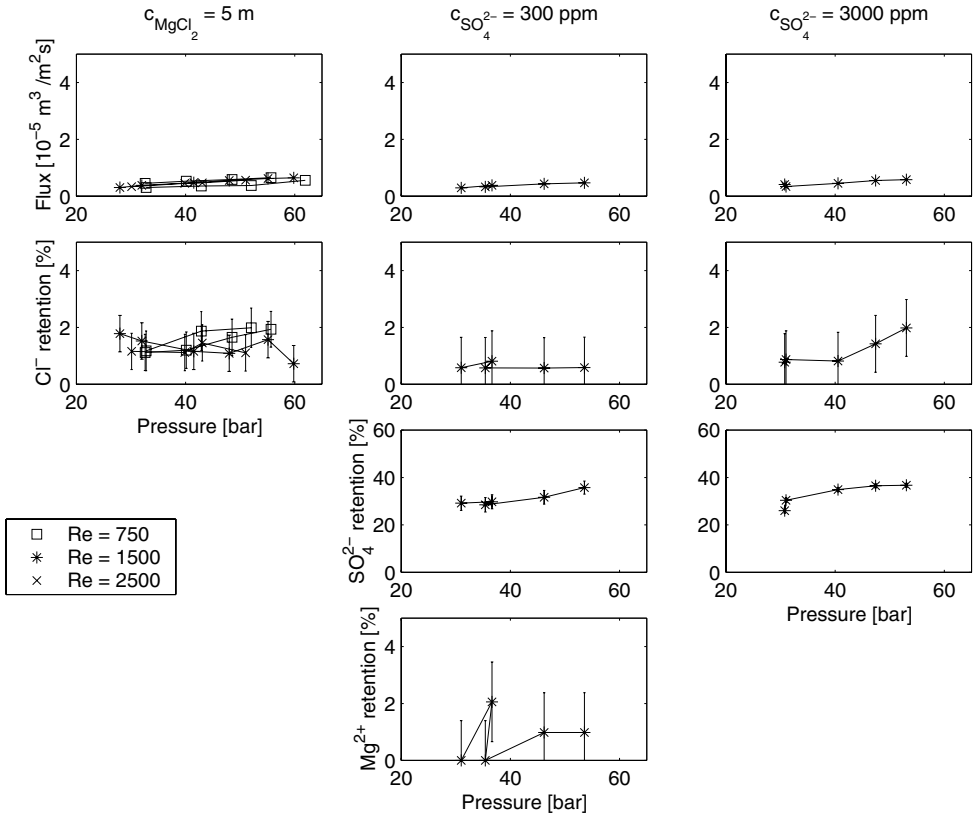

Figure 6.13: Measured fluxes and ion retentions using 5 molal magnesium chloride solutions, temperature 343 K and Desal G5 membrane samples G5-R1 (one of the data series at Re=1500) and G5-R2 in the first column, G5-R6 in the second column and G5-R8 in the third column.

6.3 Verification of the results

In experimental work there is always a possibility of making random and systematic errors and precautions should be made in order to avoid random errors and to remove the systematic errors.

The high salt concentrations were believed to have influence on the flow meter and the flow was measured manually at each magnesium chloride concentration level to check that the flow meter measured the correct values. No evidence

of concentration influence was found and the manually measured flow values corresponded with the values measured by the flow meter within the limits of uncertainties. The temperature transmitter and the pressure transmitter were calibrated by their producers and are believed to measure the temperature and pressure correctly. To eliminate any systematic errors in the weight balance the fluxes were calculated from the difference between two weight measurements.

The standard deviations in the ion retention and the flux values were calculated from several independent measurements as described in Chapter 5. It should be noted that the calculated standard deviation of the magnesium concentration is only based on duplicated measurements for four different samples, which from a statistical point of view is a small number of samples.

In two experiments the magnesium ion concentrations were determined in order to check the electro neutrality condition $\sum c_i z_i = 0$. The magnesium retentions are shown in Figures 6.8 and 6.13 and in the case of 0.1 molal magnesium chloride solution the calculated sums of concentration-valence products equal approximately -0.005 $\pm$ 0.02 molal both in the feed and the permeates, whereas at 5 molal magnesium chloride solution the sums equal approximately -0.3 $\pm$ 0.2 molal. In the first case the electro neutrality condition is fulfilled whereas in the latter case it is not. Neither the presence of inpurities or an error in the sulphate ion concentration can be responsible for such large negative deviations, which leads to the conclusion that an underestimation of the magnesium ions or an overestimation of the chloride ions may be the cause.

The determination of the equivalence point in Mohr's method corresponds to a slightly overestimation of the chloride concentration. The influence of this overestimation in the chloride concentration will increase when the chloride concentration in the samples increases and it has been estimated to be less than 0.001 molal at 0.2 molal chloride concentration and approximately 0.1 molal at 10 molal chloride concentration. The sums of the concentration-valence products at high magnesium chloride concentration become approximately -0.2 $\pm$ 0.2 molal after the chloride concentration has been corrected, and the electro neutrality condition is fulfilled within the limits of uncertainties. It should be pointed out that there still seems to be a systematic negative deviation in the calculated sums. Most likely the magnesium ion concentration is underestimated, but this effect has not been quantified. The overestimation of the chloride concentration affects both the feed and the permeate solutions equally due to the high chloride concentrations in the permeate and the calculated chloride retentions will be unaffected.

The reproducibility of the points measured twice in an experiment is good, refer Figure 6.1 for several examples of overlapping points. The reproducibility of the experiments are also good, *e.g.* the two retention series for the pure magnesium chloride solution at Reynolds number 750 in Figure 6.13, but there are also some deviations in the results, *e.g.* the retention results for the pure magnesium chloride solution in Figure 6.3.

The ion retentions have also been modified by the equation

$$R_{\text{mod}} = R_{\text{obs}} \frac{R^t_{\text{ave}}}{R^t_{\text{sample}}} \tag{6.1}$$

where R^t_{sample} is the salt retention measured in the test experiment for each new membrane sample and R^t_{ave} is their average. The salt retentions from the test experiments are given in Appendix B. Only small corrections in the retention values were obtained, whereas the patterns of the modified versus the unmodified retentions were the same. The multivariate statistical analysis discussed in Section 6.4 and in Appendix F also shows that there is no significant difference between the modified and the unmodified retention values and the following discussion will use the unmodified retention results.

6.4 Multivariate statistical analysis

A preliminary multivariate statistical analysis has been performed in Appendix F. It should be emphasized that the models used are only dependent on the main variables (temperature, Reynolds number, chloride concentration, sulphate concentration and pressure) and the terms containing the main variables squared and the main variables two factor interactions. The models presented in the appendix are the models giving the best fit to all the data without any further classification, *i.e.* better models can be obtained if the data are first divided into smaller data sets, *e.g.* into two data sets which contain the results at high and low temperature, respectively.

The analysis shows that most of the predicted retentions are too low and the models can only explain around 65-70% of the variation in the observations. The analysis indicates that for Desal 5 DK membrane the separation between the chloride and sulphate ions will be enhanced by a low Reynolds number and low pressure since the pressure has almost no influence on the sulphate retention whereas the chloride retention increases when the pressure increases. Both the chloride

and sulphate retentions will increase when the Reynolds number increases but the Reynolds number also has a strong negative effect on the sulphate retention through the interaction with the chloride concentration and should therefore be kept as low as possible. The statistical results can be misleading and comparing the statistical analysis results with the retention results given in Figures 6.8-6.13, show that both the chloride and sulphate ion retentions are independent of the Reynolds number and pressure at 5 molal magnesium chloride concentration. The conclusion is that at high magnesium chloride concentration the process should be operated at high pressure in order to increase the production rate, whereas the control of the Reynolds number is not important and can be set to any convenient value.

The results for the Desal G5 membrane give no clear difference between the models for chloride and sulphate ions, but there are indications that an increased chloride concentration has a stronger negative effect on the chloride retention than on the sulphate retention.

6.5 pH measurements

The measured pH values are tabulated in Appendices D and E. The pH was around 5 in the 5 molal magnesium chloride feed solutions and increased to approximately pH 6.5 when the magnesium chloride concentration decreased to 0.1 molal. In some experiments the pH in the feed had a tendency to increase during the experiments. The pH in the permeate are more or less the same as in the feed and no general relationships have been found with the pressure or the order the experiments were carried out.

In the pH range 5-7 the Desal 5 DK and Desal G5 membranes both have a small negative zeta potential with little variation, as can be seen from figure 5.7, chapter 5. This means that the membrane materials are more or less equally charged for all experiments and eventually any differences in the effective surface charge must come from specific ion adsorption.

6.6 Water flux measurements

The measured water fluxes are shown in Appendix B, Figures B.1-B.6. Some of the membrane samples show only the new water flux pressure relationship because the membrane samples had a tendency to break during the washing procedure due to fluid back stroke from the back pressure valve placed just downstream the membrane cell, refer Figure 5.1, Chapter 5.

The measured water fluxes for the DK-R1 membrane sample show that the initial water flux is fully recovered 24 hours after the experiment with 2.5 molal solution. The decrease in the water fluxes after the experiments with 2.5 and 5 molal solutions are concurrent. The same decrease in the water flux can be seen for DK-R4 and DK-R5. The DK-R6 membrane sample shows no decrease in the water flux after experiments with 0.1 molal solution and temperature 298 K, but after the experiment with 5 molal solution and 343 K the water flux drops. The DK-R8 shows a small increase in the water flux compared to the initial values after an experiment with 1 molal magnesium chloride solution and the water flux maintains the same level even after 10 days of storage in deionized water. The DK-R10, DK-R11 and DK-R12 have only been run with water but the water flux at 343 K has also been measured. The water flux measured after some time (1-3 hours) at 343 K and high pressure shows a decrease compared to the water flux measured immediately after reaching 343 K. Further, the water flux measured at 298 K immediately after cooling shows an equivalent drop compared to the initial water flux.

The results for the Desal G5 membrane samples show the same trends as the Desal 5 DK membrane. The measured water flux decreases after experiments with 1, 2.5 or 5 molal magnesium chloride solutions run at high temperatures, whereas the water flux does not change when the experiments have been run at low temperatures. The water flux experiments show similar decreases in the flux values at both high and low temperatures.

The observed water flux decrease for both membrane types is most likely caused by the high temperature and the high pressure which the membranes experience during the experiments. The decrease seems to be reversible, *i.e.* the initial water flux is recovered after the membrane sample has been stored in deionized water for some time (approximately 24 hours).

Chapter 7

Discussion of separation mechanisms and transport models

7.1 Concentration polarisation

7.1.1 Mass transfer coefficients

All discussion of the separation mechanisms and transport models in membrane separation processes are normally based upon a model of the concentration polarisation phenomena, since it is the concentration near the membrane surface that is important in order to determine the real retention characteristics of the membrane. Several authors have tried to measure the phenomena using both indirect and direct methods as discussed in Chapter 9. No general, reliable direct method exists so far and the predictions of concentration polarisation is based upon indirect methods, where the film theory presented in Section 2.2.2 can be used.

The bulk and permeate concentrations and the volume fluxes have been measured experimentally, whereas the mass transfer coefficient must be estimated by some sort of correlation before Equation 2.8 in Chapter 2 can be used to calculate the concentration near the membrane, C_m. As a first approximation the

correlations relating the mass transfer coefficient to the Reynolds number and the Schmidt number given in Equations 2.13 and 2.14 for laminar and turbulent flow, respectively, can be used, where the density, viscosity and diffusion coefficient of magnesium chloride solutions can be found in Figure 4.7, Chapter 4. Figure 7.1 shows the intrinsic retentions calculated using the mass transfer coefficients k, calculated from Equation 2.13, $k/2$ and $2 * k$ at different magnesium chloride concentrations, temperature 298 K and Reynolds number 1000 (750 at 5 molal). The intrinsic retentions calculated from the mass transfer coefficients $k/2$ and $2 * k$ are shown in order to see the effect of using a wrong mass transfer coefficient. There seems to be a considerable concentration polarisation at concentrations below 2.5 molal and hence the intrinsic retention differs from the observed retention given in Chapter 6. Further, there seems to be no significant concentration polarisation at 5 molal magnesium chloride concentration. However, the most striking result is that the intrinsic retentions depend so heavily on the mass transfer coefficient, which means that an accurate determination of the mass transfer coefficient is of major importance in order to get the right concentration at the membrane surface and the real retention characteristics of the membrane.

The calculated concentration polarisations using $k/2$ at 0.1 and 1 molal magnesium chloride concentrations and high fluxes are not feasible, since the concentration at the membrane surface exceeds the saturation concentration and solid magnesium chloride should precipitate. No solid material was observed on the membrane and neither was there observed any decrease in the flux due to pore blocking, so the mass transfer coefficients obtained from Equations 2.13 and 2.14 can most likely be taken as a lower limit. This statement is further supported by the mass transfer coefficient calculated using the linearized equation given in Equation 2.11 and using the data in Figure 6.3. Different $ln((1-R)/R)$ versus J_v/Re^a curves were constructed at constant pressure and at either laminar or turbulent flow. Since the curves were made of only two points each, which of course will give a perfect linear line, and varying intrinsic retentions, the determination of the mass transfer coefficient by this method is not very polite and the results must be used with care. Even so, approximately 15 mass transfer coefficient estimates were obtained using all the pressure levels and sulphate concentration levels, and the results indicated that the mass transfer coefficients at 1 molal magnesium chloride and temperature 343 K are approximately twice as large as the mass transfer coefficients calculated from the Sherwood correlations in Equations 2.13 and 2.14.

Also, one should remember that the Sherwood correlations for the mass transfer

coefficient are developed for non-porous duct flow and do not take into account that the flux will enhance the mass transfer coefficient (Gekas and Hallstrøm 1987). According to the presentation in Section 2.2.2 several modifications of the mass transfer coefficient and the film model exist and the presentation of the intrinsic retentions given in Sections 7.1.2 and 7.1.3 shows the calculated intrinsic retentions from these different models. As can be seen from Figures 7.3-7.10 large variations in the intrinsic retentions calculated from the different models occur. The results will be discussed in more detail in the next two sections.

Since the magnesium sulphate concentrations were low, the density and the viscosity of the mixed solutions have been approximated by the density and viscosity of the equivalent pure magnesium chloride solutions in the calculations. The worst case for this assumption is at 0.1 molal magnesium chloride and 0.032 molal magnesium sulphate, but as Figures 4.7 and 4.8 show the density and viscosity of the pure magnesium chloride and magnesium sulphate solutions at these low concentrations are very similar and close to the pure water values. The magnesium chloride diffusion coefficients are set equal to the values given in Figure 4.7 and any interaction with the magnesium sulphate is neglected. The density and viscosity values of the magnesium chloride as function of the concentration at 343 K are shown in Figure 4.7, but since no data of the diffusion coefficients at 343 K was found in the literature, a simple relationship based on the Stokes-Einstein equation was assumed (Reid *et al.* 1987)

$$D_T = D_{298} \frac{T \, \eta_{298}}{298 \, \eta_T} \tag{7.1}$$

which relates the diffusion coefficient at 298 K to the wanted diffusion coefficient at temperature T when the viscosity at both temperatures is known.

To calculate the concentration polarisation of the sulphate ions the same procedure was used. The main problem is to estimate the diffusion coefficient of magnesium sulphate in different magnesium chloride solutions. As a first approximation the diffusion coefficient of magnesium sulphate was set equal to the value that corresponds to a magnesium sulphate concentration equal to the magnesium chloride concentration in the solution under investigation, *e.g.* at 5 molal magnesium chloride the diffusion coefficient of magnesium sulphate was set equal to the value $3 * 10^{-10}$ m^2/s at 5 molal magnesium sulphate, refer Figure 4.8 in Chapter 4.

Since the mass transfer coefficient depends on the diffusion coefficient, the diffusion coefficient of the magnesium sulphate will have a great influence on the calculated intrinsic retention of the sulphate ions as shown in Figure 7.2. In the

0.1 molal magnesium chloride solution and 300 ppm sulphate concentration a diffusion coefficient ten times higher than the value found from Figure 4.8 will decrease the calculated intrinsic retention drastically, whereas a diffusion coefficient twice the literature value will increase the intrinsic retention (at Reynolds number 1000 the intrinsic retention become equal to 100%).

The physical properites such as density, viscosity and diffusion coefficient, will vary across the boundary layer as the concentration near the membrane increases. Gekas and Hallstrøm (1987) have discussed several different correction factors to account for changes in the physical properties and propose the factor $(Sc/Sc_w)^{0.11}$, where Sc_w is the Schmidt number calculated with the physical properties near the membrane surface. The correction factors calculated using the concentration polarisations at 0.1 and 2.5 molal and the model given by Bird *et al.* (1960) became around 0.999 and compensation of the mass transfer coefficient of this kind will therefore be neglected.

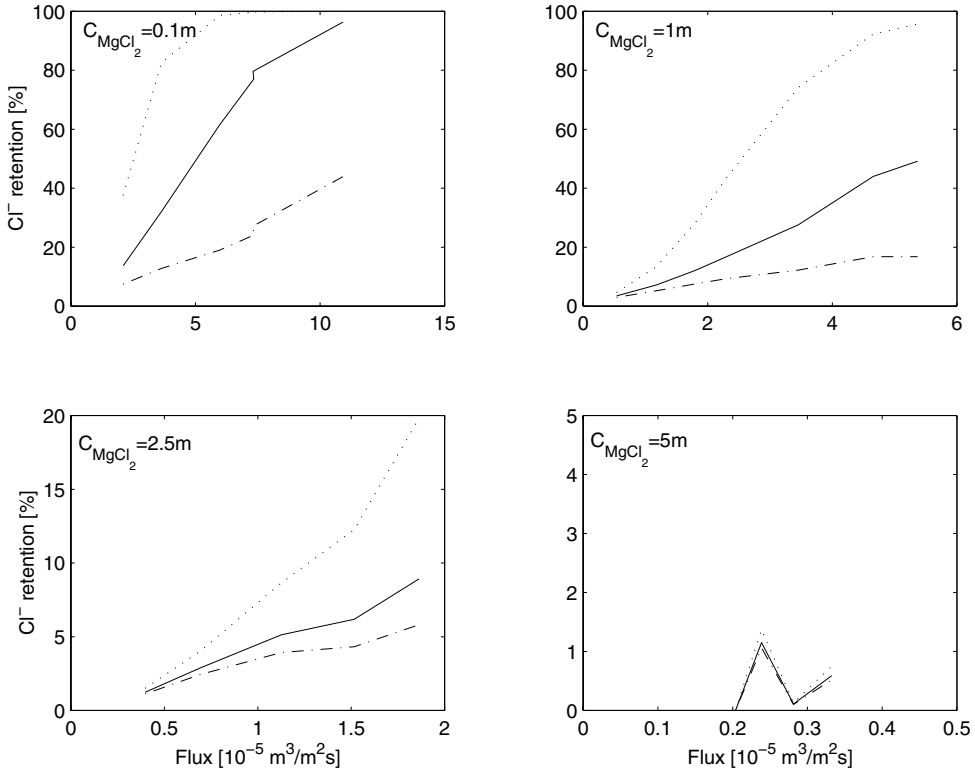

Figure 7.1: The intrinsic magnesium chloride retentions at different magnesium chloride concentrations showing the effect of different mass transfer coefficients. Experiments are done at temperature 298 K, Desal 5 DK membrane and Re=1000 (750 at 5 molal). (-) intrinsic retention calculated using the mass transfer coefficient, k, from Equation 2.13, (..) intrinsic retention using $k/2$, and, (-.) intrinsic retention using $2 * k$.

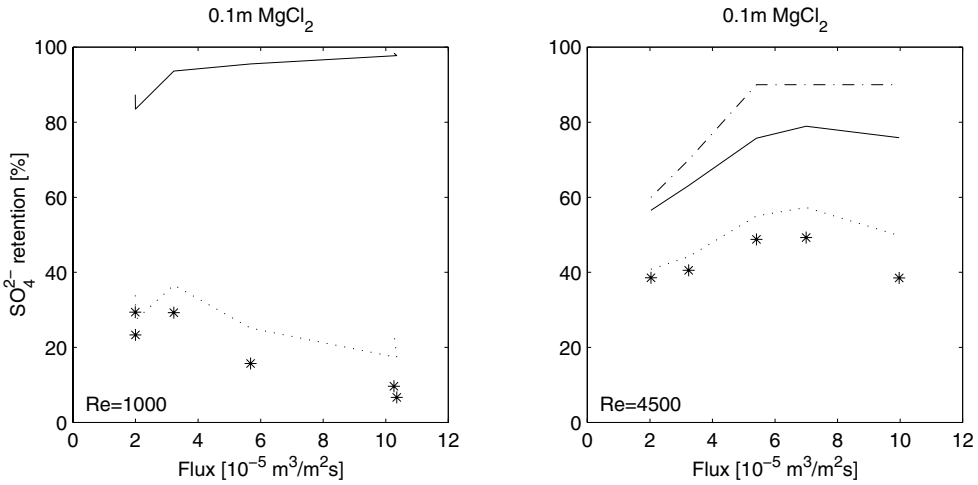

Figure 7.2: The intrinsic sulphate retentions calculated from the model of Brian (1966) using different magnesium sulphate diffusion coefficients at Re=1000 (left) and Re=4500 (right). Experiments are done at 0.1 molal magnesium chloride concentration, 300 ppm sulphate concentration, temperature 298 K and Desal 5 DK membrane. (*) observed retention, (-) intrinsic retention using $D_{MgSO_4} = 6 * 10^{-10} m^2/s$*, (...) intrinsic retention using* $10 * D$*, and, (.-.) intrinsic retention using* $D/2$*.*

7.1.2 Calculated $MgCl_2$ intrinsic retentions

This section presents the calculated intrinsic retentions of the chloride ions using different magnesium chloride concentrations, 300 ppm sulphate concentration and the Desal 5 DK membrane. Figures 7.3 and 7.4 show the results at 298 K, whereas Figures 7.5 and 7.6 show the results at 343 K. For each set of observed retentions the intrinsic retentions are calculated from different models, where the *dotted* lines give the intrinsic retentions calculated using k from Equations 2.13 or 2.14, the *dashed-dotted* lines give the intrinsic retentions calculated using Equation 2.15 (Bird *et al.* 1960), the *dashed* lines give the intrinsic retentions calculated using Equation 2.17 (Thomas 1973), and the *solid* lines give the intrinsic retentions calculated using Equation 2.16 (Brian 1966).

The figures show that the intrinsic retentions calculated by the Sherwood correlations given by Equations 2.13 or 2.14 and the intrinsic retentions calculated by the model of Thomas (1973) predict a very strong concentration polarisation, the intrinsic retentions calculated by the model of Brian (1966) predict a more moderate concentration polarisation, whereas the results from the model of Bird *et al.* (1960) predict only a modest concentration polarisation. A main problem with the model of Bird *et al.* is that the concentration polarisation at lower Reynolds numbers are lower than the concentration polarisation at higher Reynolds number, which is the opposite of what is expected from all theories. The difference between the models decreases when the Reynolds number increases and there is a slight decrease in the concentration polarisation when the temperature increases. The concentration polarisation also decreases with increasing magnesium chloride concentration.

Since the different concentration polarisation models give very different answers the remaining problem is to choose the most reasonable model. For low concentrations and low Reynolds number the model of Thomas (1973) and the use of the Sherwood correlations give far too high concentration polarisation values. It is hard to believe that a membrane with 2% observed retention should have an intrinsic retention around 80-90%. The model of Brian (1966) also predicts unreasonable high intrinsic retention values at high fluxes (around 40%), whereas the predicted concentration polarisations of the model of Bird *et al.* (1960) sound more reasonable (around 5%), but this method gives higher concentration polarisation values in the turbulent region than in the laminar region as stated before. If one ought to choose one model the model of Brian (1966) is recommended, since the validity region of this model fits best the conditions in the experiments. The model of Brian is valid in the flux range $5 * 10^{-6} - 5 * 10^{-5}$m/s, whereas the

fluxes in the experiments vary in the range $1 * 10^{-6} - 1.5 * 10^{-4}$m/s, which means that the highest fluxes exceed the limits of the models where we also observe the least reasonable intrinsic retentions. Further, the model of Brian is reported to be valid in the Schmidt number range 600-800, whereas the Schmidt numbers in the experiments varied in the range 200-10000. The Schmidt number of the 0.1 and 1 molal magnesium chloride solutions, where we find the highest intrinsic retentions, were around 790-980, which should match the validity region of the model well.

The Desal G5 membrane shows the same general trends in the intrinsic retentions as the Desal 5 DK membrane, but the concentration polarisations are much lower. Hence, the intrinsic magnesium chloride retentions will also be lower. For example, using the model of Brian (1966) at 298 K, 30 bar and 0.1 molal magnesium chloride concentration the calculated concentration polarisations of Desal 5 DK membrane were 1.56 and 1.22 at Reynolds numbers 1000 and 4500, respectively, whereas for the Desal G5 membrane the concentration polarisations were 1.08 and 1.04, respectively. Normally, one would assume that the intrinsic retentions of the Desal G5 membrane were higher than the intrinsic retentions of the Desal 5 DK membrane, since the observed retentions of the Desal G5 are slightly higher than the observed retentions of the Desal 5 DK. On the other hand, the fluxes of Desal G5 are also smaller than the fluxes of Desal 5 DK, which points in the direction of higher concentration polarisation since the mass transfer coefficient will be less enhanced, but Aitkuliev *et al.* (1984) argued that the concentration polarisation vanishes when the fluxes become low. Again the concentration polarisation models have problems in explaining the expected results.

The discussion has shown that there exists no good model prediction of the concentration polarisation phenomena and the calculated values are unreliable. However, at high magnesium chloride concentrations, *i.e.* 5 molal, the concentration polarisation seems to vanish and the Reynolds number has less effect on the retention. This is of course an indirect effect of the low retention found at high concentrations. Further, it seems resonable to take the flux into account at least at the lower concentrations where it is high.

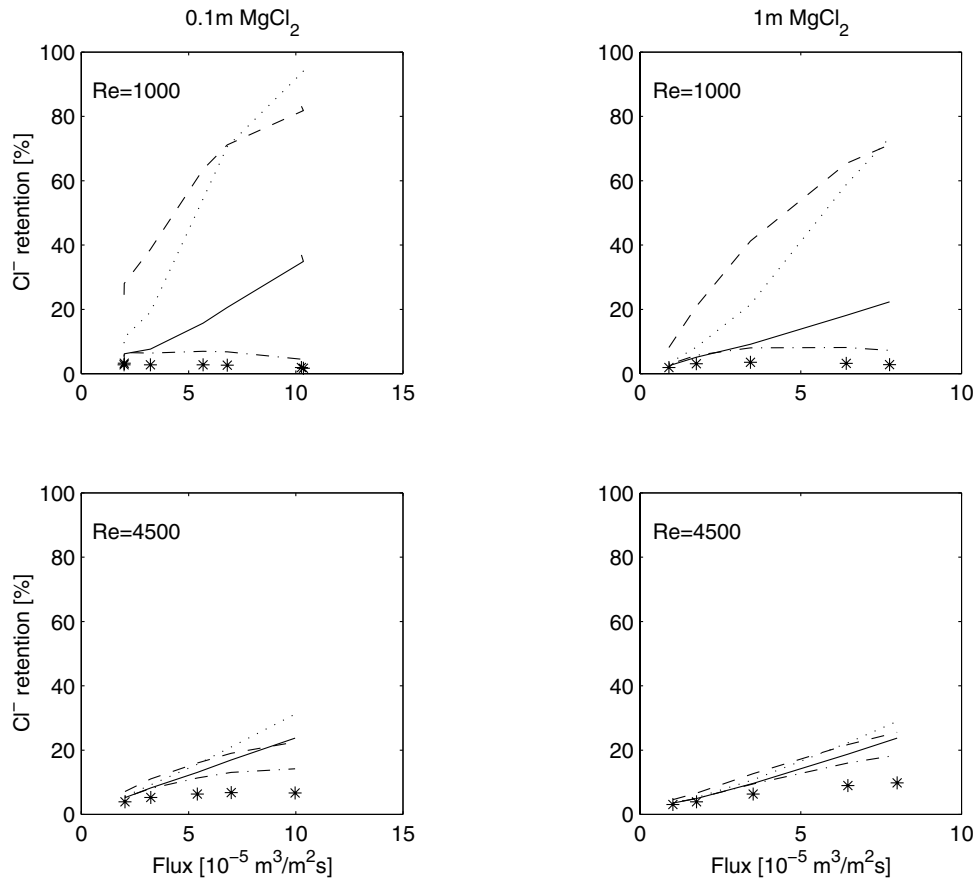

Figure 7.3: Calculated intrinsic chloride retentions at different Reynolds numbers, magnesium chloride solutions (0.1 and 1 molal), constant sulphate concentration (300 ppm), Desal 5 DK membrane and temperature 298 K. (*) observed retentions, (...) intrinsic retentions calculated with k from Equations 2.13 or 2.14, (.-.) calculated intrinsic retentions from Bird et al. (1960), Equation 2.15, (- -) calculated intrinsic retentions from Thomas (1973), Equation 2.17, and, (-) calculated intrinsic retentions from Brian (1966), Equation 2.16.

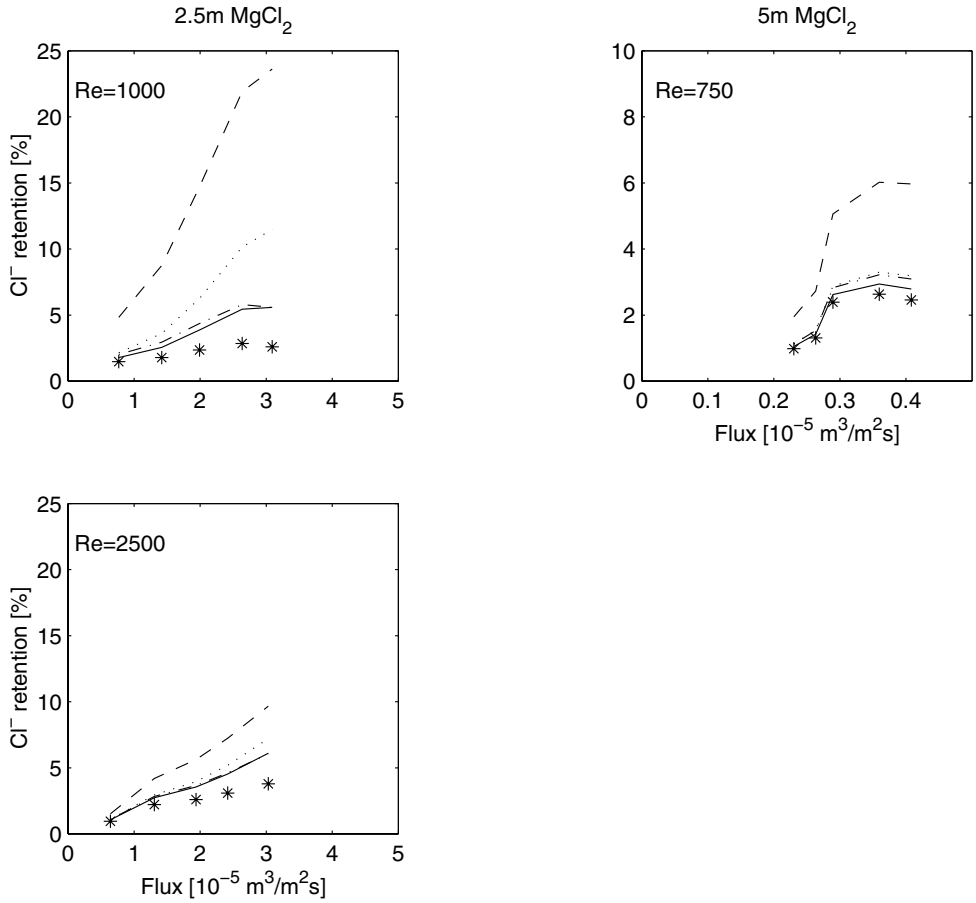

Figure 7.4: Calculated intrinsic chloride retentions at different Reynolds numbers, magnesium chloride solutions (2.5 and 5 molal), constant sulphate concentration (300 ppm), Desal 5 DK membrane and temperature 298 K. (*) observed retentions, (...) intrinsic retentions calculated with k from Equations 2.13 or 2.14, (.-.) calculated intrinsic retentions from Bird et al. (1960), Equation 2.15, (- -) calculated intrinsic retentions from Thomas (1973), Equation 2.17, and, (-) calculated intrinsic retentions from Brian (1966), Equation 2.16.

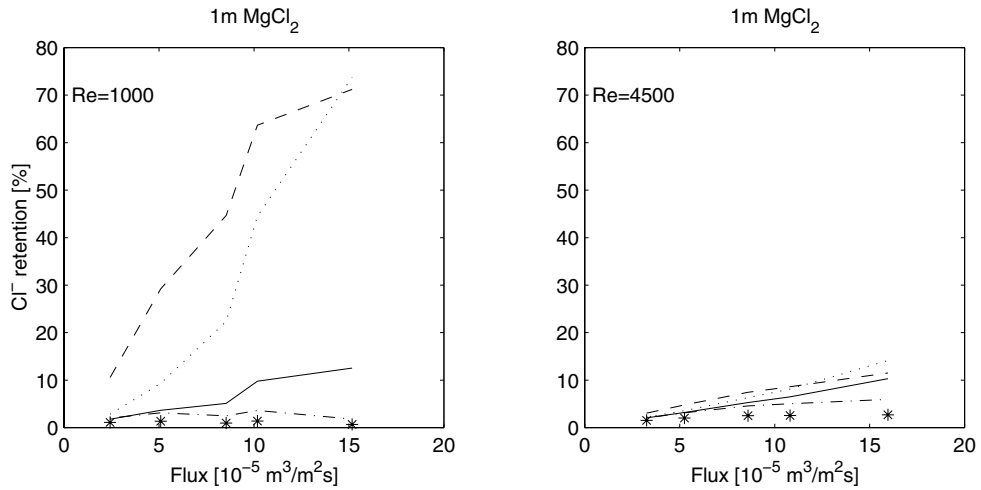

Figure 7.5: Calculated intrinsic chloride retentions at different Reynolds number, 1 molal magnesium chloride solution, constant sulphate concentration (300 ppm), Desal 5 DK membrane and temperature 343 K. (*) observed retentions, (...) intrinsic retentions calculated with k from Equations 2.13 or 2.14, (.-.) calculated intrinsic retentions from Bird et al. (1960), Equation 2.15, (- -) calculated intrinsic retentions from Thomas (1973), Equation 2.17, and, (-) calculated intrinsic retentions from Brian (1966), Equation 2.16.

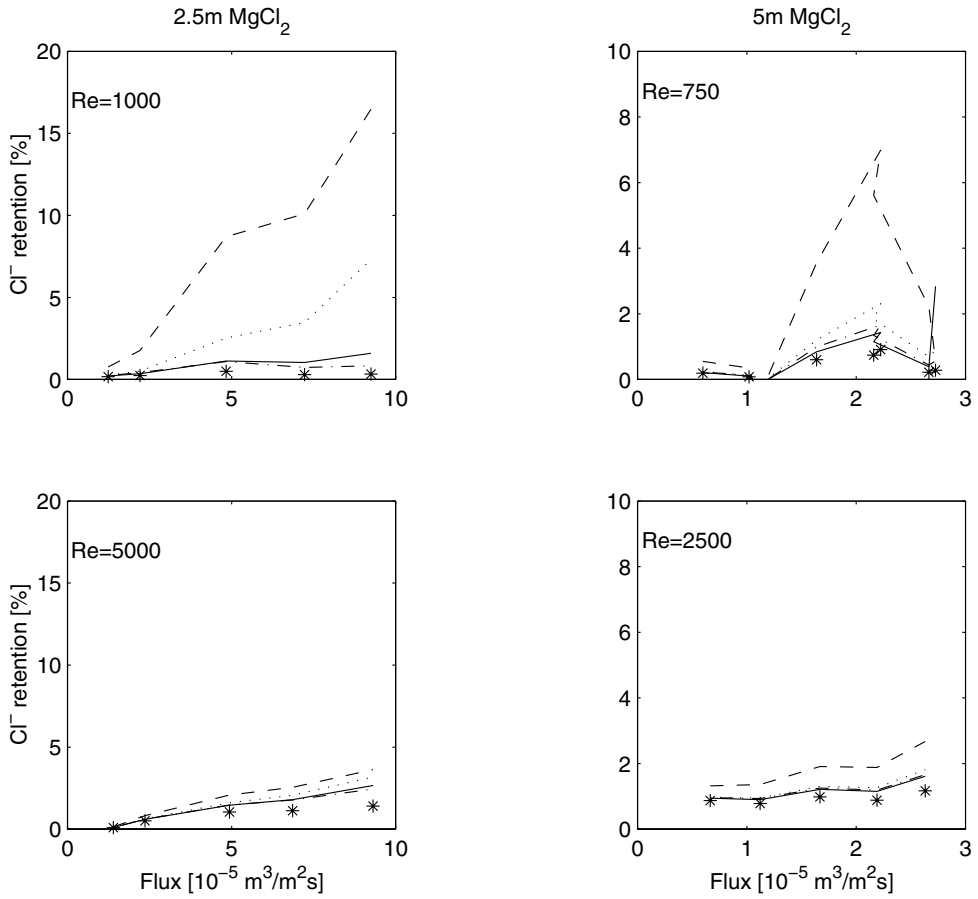

Figure 7.6: Calculated intrinsic chloride retentions at different Reynolds number, magnesium chloride solutions (2.5 and 5 molal), constant sulphate concentration (300 ppm), Desal 5 DK membrane and temperature 343 K. (*) observed retentions, (...) intrinsic retentions calculated with k from Equations 2.13 or 2.14, (.-.) calculated intrinsic retentions from Bird et al. (1960), Equation 2.15, (- -) calculated intrinsic retentions from Thomas (1973), Equation 2.17, and, (-) calculated intrinsic retentions from Brian (1966), Equation 2.16.

7.1.3 Calculated $MgSO_4$ intrinsic retentions

This section presents the calculated intrinsic retentions of the sulphate ions using different magnesium chloride concentrations, 300 ppm sulphate concentration and the Desal 5 DK membrane. Figures 7.7 and 7.8 show the results at 298 K, whereas Figures 7.9 and 7.10 show the results at 343 K. For each set of observed retentions the intrinsic retentions are calculated from different models, where the *dashed-dotted* lines give the intrinsic retentions calculated using Equation 2.15 (Bird *et al.* 1960), the *dashed* lines give the intrinsic retentions calculated using Equation 2.17 (Thomas 1973), and the *solid* lines give the intrinsic retentions calculated using Equation 2.16 (Brian 1966). The intrinsic retentions calculated using only the Sherwood correlations in Equations 2.13 or 2.14 are not shown since they all were close to 100%, unless in a few cases where they followed the trends of Thomas' model.

The figures show that the intrinsic retentions calculated at laminar flow conditions by the model of Thomas (1973) predict a very strong concentration polarisation, the intrinsic retentions calculated by the model of Brian (1966) predict a more moderate concentration polarisation, at least at low fluxes, whereas the results from the model of Bird *et al.* (1960) predict only a modest concentration polarisation. The same problem with the model of Bird *et al.* (1960) occurs here, since the model predicts a lower concentration polarisation at laminar flow compared with the concentration polarisation at turbulent flow, which is not physically correct. The difference between the models decreases when the Reynolds number increases and there is a slight decrease in the concentration polarisation when the temperature increases. The concentration polarisation also decreases with increasing magnesium chloride concentration and a small decrease in the concentration polarisation is also observed with increasing sulphate concentration at low magnesium chloride concentration, whereas at high concentration the opposite is true[1].

Again one can observe unreasonable high calculated intrinsic retentions at low Reynolds number, where the observed retentions are quite low, whereas at turbulent flow the three models seem to approach each other. The calculated sulphate intrinsic retentions using the Desal G5 membrane are lower than the corresponding intrinsic retentions calculated using results for the Desal 5 DK membrane.

As for the calculated magnesium chloride intrinsic retentions the results of the

[1] The results using the 3000 ppm sulphate concentration are not shown.

sulphate intrinsic retentions are uncertain. The concentration polarisation of the sulphate ions are much lower at high magnesium chloride concentration, *e.g.* the concentration polarisation modulus of the sulphate ion was equal to 14.5, 10.9, 1.4 and 1.06 at laminar Reynolds number, 298 K, 300 ppm sulphate concentration and 0.1, 1, 2.5 and 5 molal magnesium chloride concentration, respectively. In a worst case scenario the sulphate concentration at the membrane surface becomes 0.156 molal (approximately 10000 ppm sulphate) using the results calculated at 5 molal magnesium chloride and 3000 ppm sulphate concentration. If this value is compared with the phase diagrams given in Figures 4.5 and 4.6 in Chapter 4, one can see that at 298 K the concentrations are far from any saturation concentrations, whereas at 348 K the sulphate concentration is closer to the saturation concentration and the boundary where the precipitation of kiserate occur.

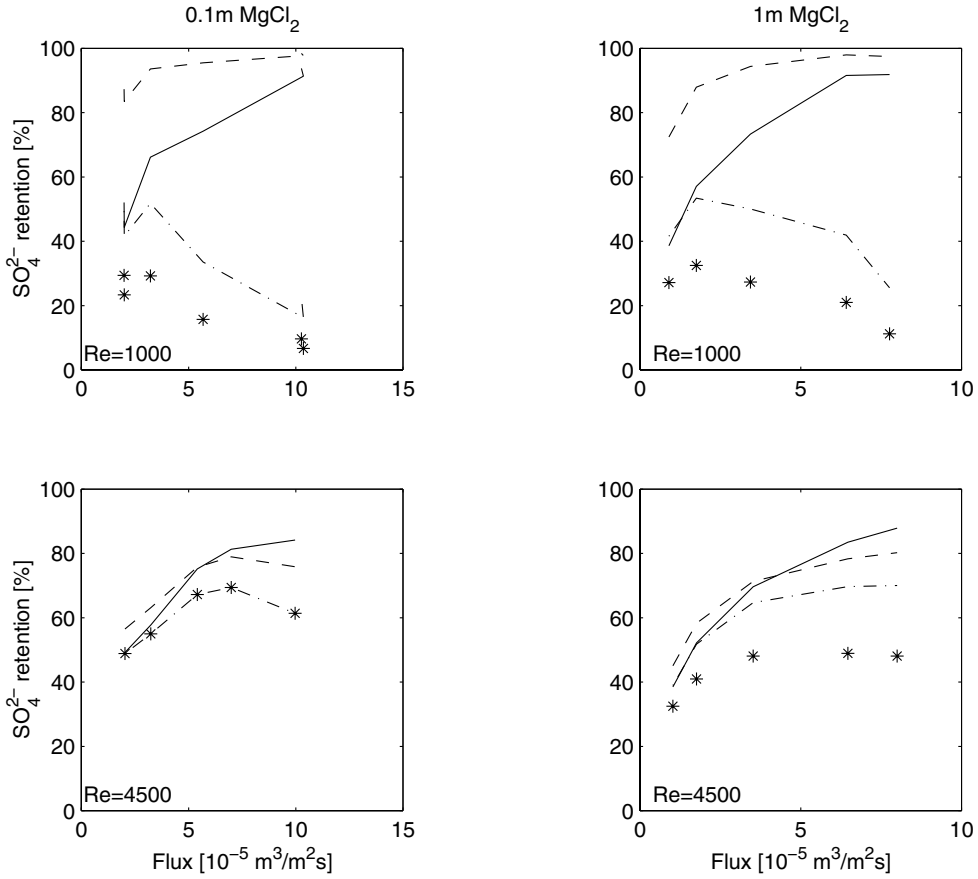

Figure 7.7: Calculated intrinsic sulphate retentions at different Reynolds numbers, magnesium chloride solutions (0.1 and 1 molal), constant sulphate concentration (300 ppm), Desal 5 DK membrane and temperature 298 K. (*) observed retentions, (.-.) calculated intrinsic retentions from Bird et al. (1960), Equation 2.15, (- -) calculated intrinsic retentions from Thomas (1973), Equation 2.17, and, (-) calculated intrinsic retentions from Brian (1966), Equation 2.16.

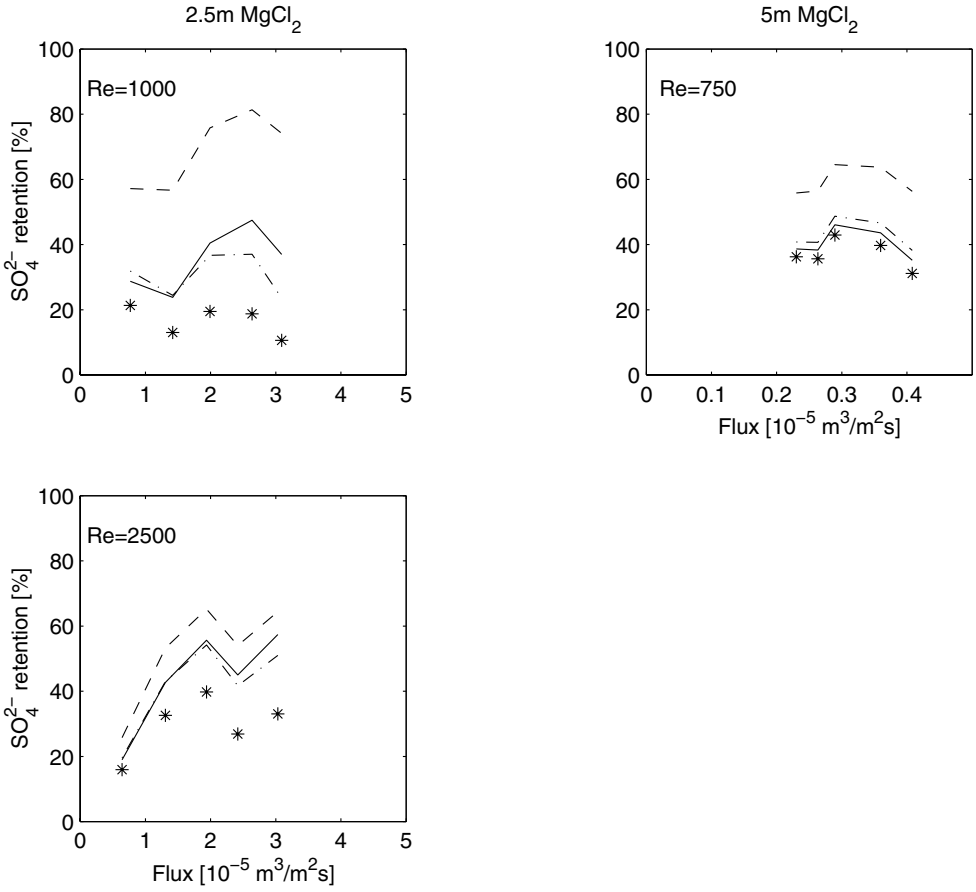

Figure 7.8: Calculated intrinsic sulphate retentions at different Reynolds numbers, magnesium chloride solutions (2.5 and 5 molal), constant sulphate concentration (300 ppm), Desal 5 DK membrane and temperature 298 K. (*) observed retentions, (.-.) calculated intrinsic retentions from Bird et al. (1960), Equation 2.15, (- -) calculated intrinsic retentions from Thomas (1973), Equation 2.17, and, (-) calculated intrinsic retentions from Brian (1966), Equation 2.16.

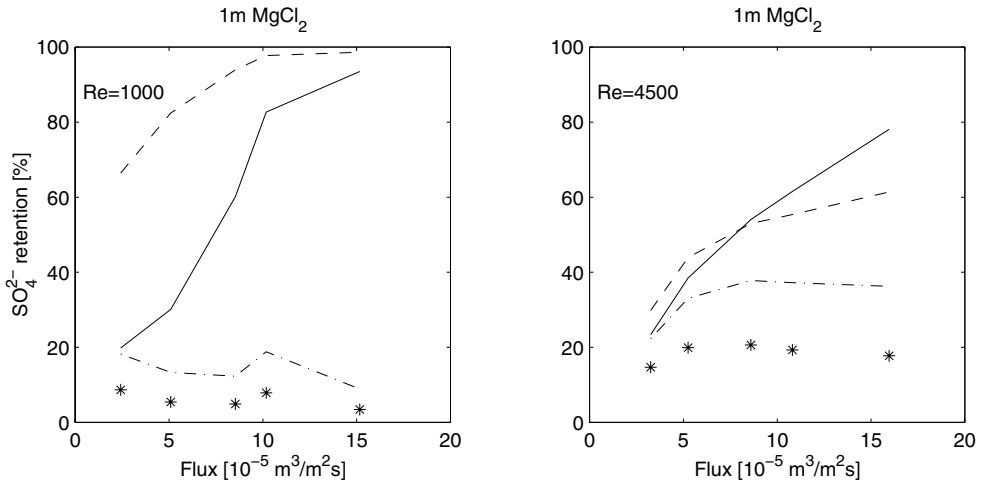

Figure 7.9: Calculated intrinsic sulphate retentions at different Reynolds numbers, 1 molal magnesium chloride solutions, constant sulphate concentration (300 ppm), Desal 5 DK membrane and temperature 343 K. (*) observed retentions, (.-.) calculated intrinsic retentions from Bird et al. (1960), Equation 2.15, (- -) calculated intrinsic retentions from Thomas (1973), Equation 2.17, and, (-) calculated intrinsic retentions from Brian (1966), Equation 2.16.

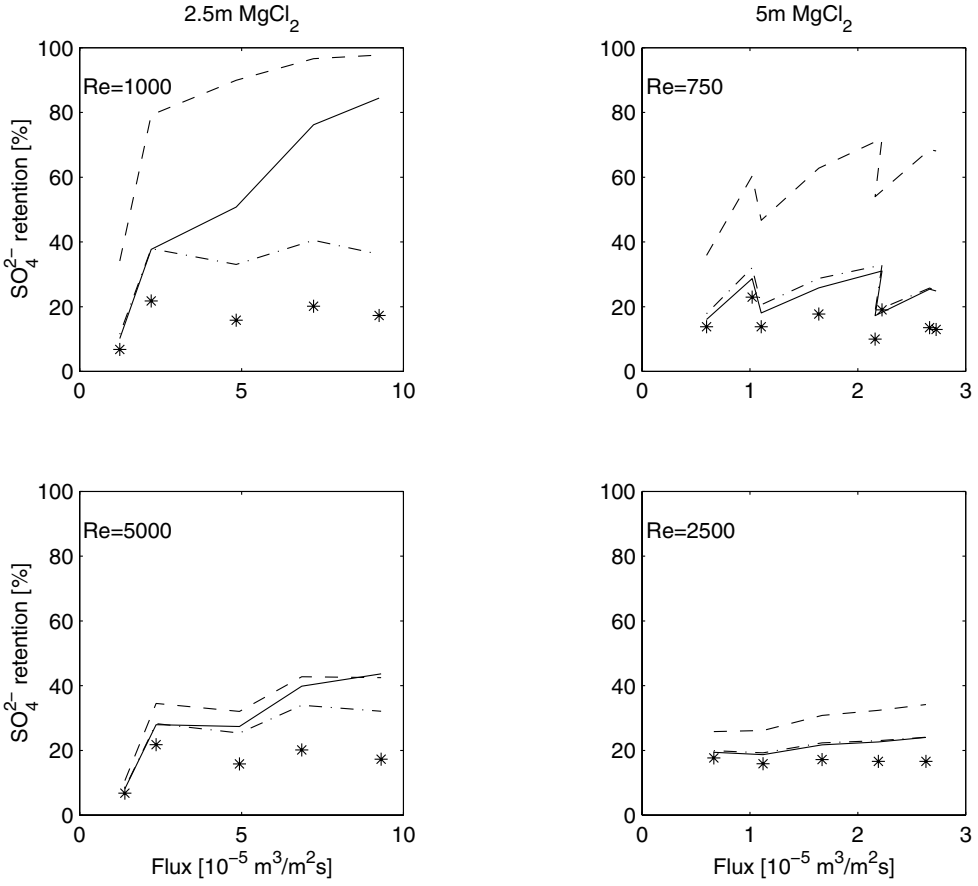

Figure 7.10: Calculated intrinsic sulphate retentions at different Reynolds numbers, magnesium chloride solutions (2.5 and 5 molal), constant sulphate concentration (300 ppm), Desal 5 DK membrane and temperature 343 K. (*) observed retentions, (.-.) calculated intrinsic retentions from Bird et al. (1960), Equation 2.15, (- -) calculated intrinsic retentions from Thomas (1973), Equation 2.17, and, (-) calculated intrinsic retentions from Brian (1966), Equation 2.16.

7.1.4 Osmotic pressure difference over the membrane with and without concentration polarisation

The osmotic pressure has been calculated using Equation 4.23 in Chapter 4, where the osmotic coefficient has been calculated using the Pitzer model described in the same chapter. The osmotic pressure differences have been calculated using both the bulk and the membrane surface concentration calculated from Brian's model and the results are shown in Figures 7.11 and 7.12, which give the results at 298 and 343 K, respectively. The concentration polarisation effect on the osmotic pressure difference is relatively small at 0.1 molal magnesium chloride solution, large at 1 molal magnesium chloride solution, whereas the effect at 2.5 and 5 molal magnesium chloride solutions are moderate. The effect of the concentration polarisation reduces at higher temperatures. Figure 7.13 shows the osmotic pressure as a function of the magnesium chloride concentration. The increase in the osmotic pressure with increasing concentration is enormous. The osmotic pressure differences observed at 5 molal magnesium chloride follow no particular curve and can probably be explained by the uncertainty in the chloride determination, since a small error in the chloride concentration will give a large error in the osmotic pressure and hence a large error in the osmotic pressure difference.

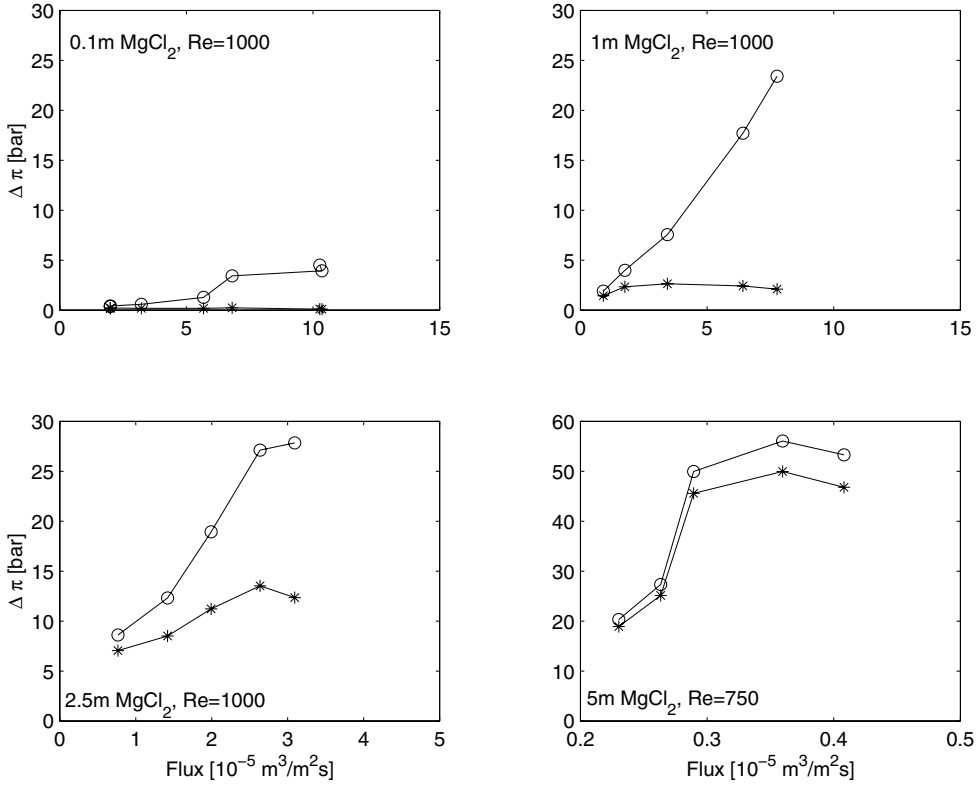

Figure 7.11: The osmotic pressure difference at different magnesium chloride concentrations, 300 ppm sulphate concentration, 298 K and Desal 5 DK membrane. (*) without concentration polarisation, and, (o) with concentration polarisation calculated from Brian's (1966) model.

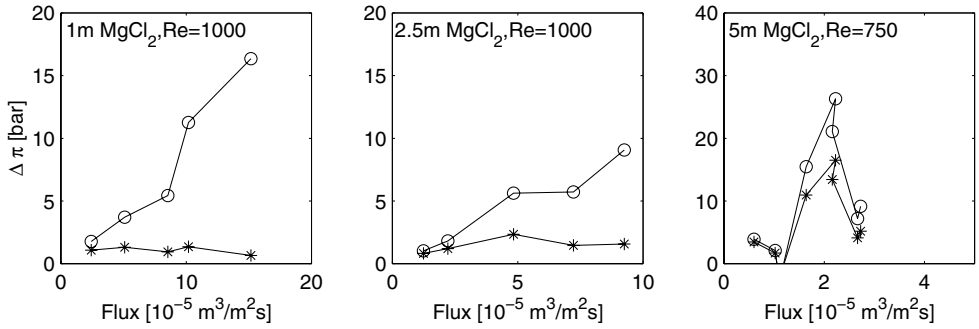

Figure 7.12: The osmotic pressure difference at different magnesium chloride concentrations, 300 ppm sulphate concentration, 343 K and Desal 5 DK membrane. (*) without concentration polarisation, and, (o) with concentration polarisation calculated from Brian's (1966) model.

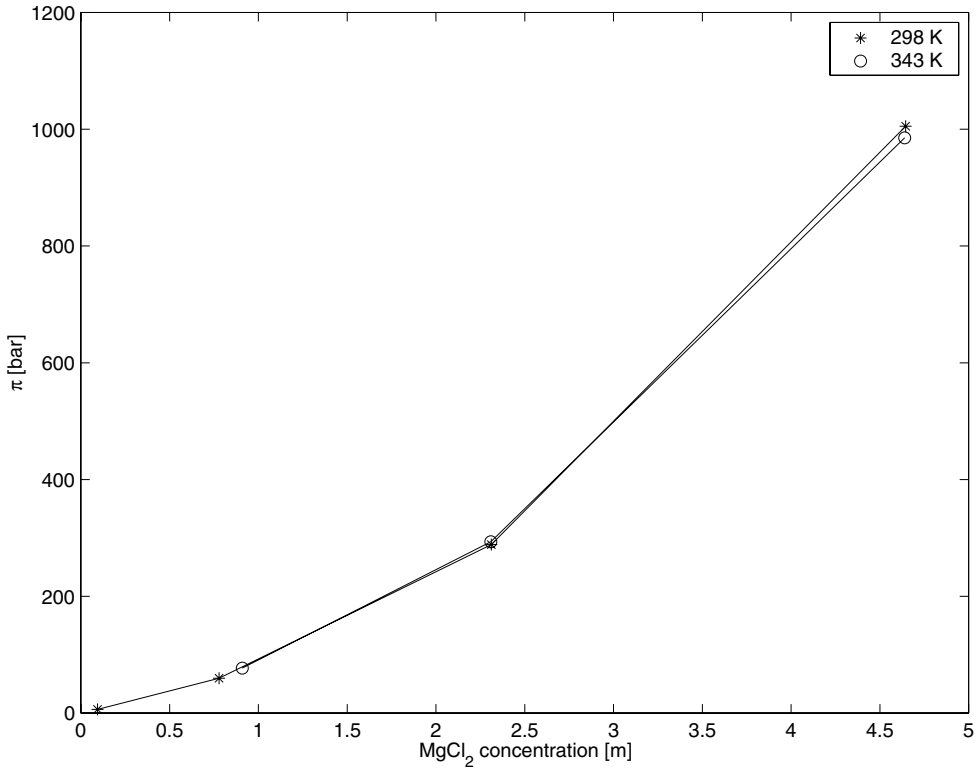

Figure 7.13: The osmotic pressure in different magnesium chloride solutions with 300 ppm sulphate calculated using Equation 4.23 and the Pitzer model described in Chapter 4.

7.2 Flux measurements

7.2.1 Observed volume flux reduction with increasing $MgCl_2$ concentration

The reduction in the volume flux as function of the pressure and the magnesium chloride concentration is shown in Figure 7.14. The volume flux at 0.1 molal magnesium chloride concentration is equal to the pure water flux at 298 K for both membranes, whereas for the other concentrations a significant reduction in the volume flux compared with the pure water flux is observed. Several explanations for this flux reduction with increasing salt concentration have been proposed in the literature. Nystrøm *et al.* (1995) related the flux reduction to the osmotic pressure difference, whereas Freger *et al.* (2000) related it to either the reduction in water activity or to the increased screening of the repulsion effect of the fixed charges in the membrane.

According to the Hagen-Poiseuille equation given in Equation 3.80 the volume flux will decrease when the viscosity increases and a correction to the water permeability coefficient can be calculated using the expression

$$L_{p,solution} = L_{p,w}\frac{\eta_w}{\eta_{solution}} \tag{7.2}$$

where the $L_{p,w}$ is the water permeability measured in pure water. Further, a correction of the water activity on the permeability can be calculated using the water activity in the bulk solutions. Setting the water activity in pure water equal to 1, the corrected permeability coefficient becomes

$$L'_{p,solution} = L_{p,w}\frac{\eta_w}{\eta_{solution}}a_w \tag{7.3}$$

where a_w is the water activity in the actual solution. Figure 7.15 shows the predicted fluxes using the Hagen-Poiseuille equation with the corrected permeabilities, where the water activity in different magnesium chloride solutions are given in Table 7.1. The solid lines are the observed fluxes versus the observed fluxes and deviations from this lines means that the predictions are either too high or too low. In the 0.1 molal magnesium chloride solution the predictions fit the observed volume fluxes nicely, whereas at higher concentrations the predictions are too high. In both the 2.5 molal magnesium chloride solution and especially in the 5 molal magnesium chloride solution the correction of the water activity improves the predictions, but there are still effects not accounted for. The water

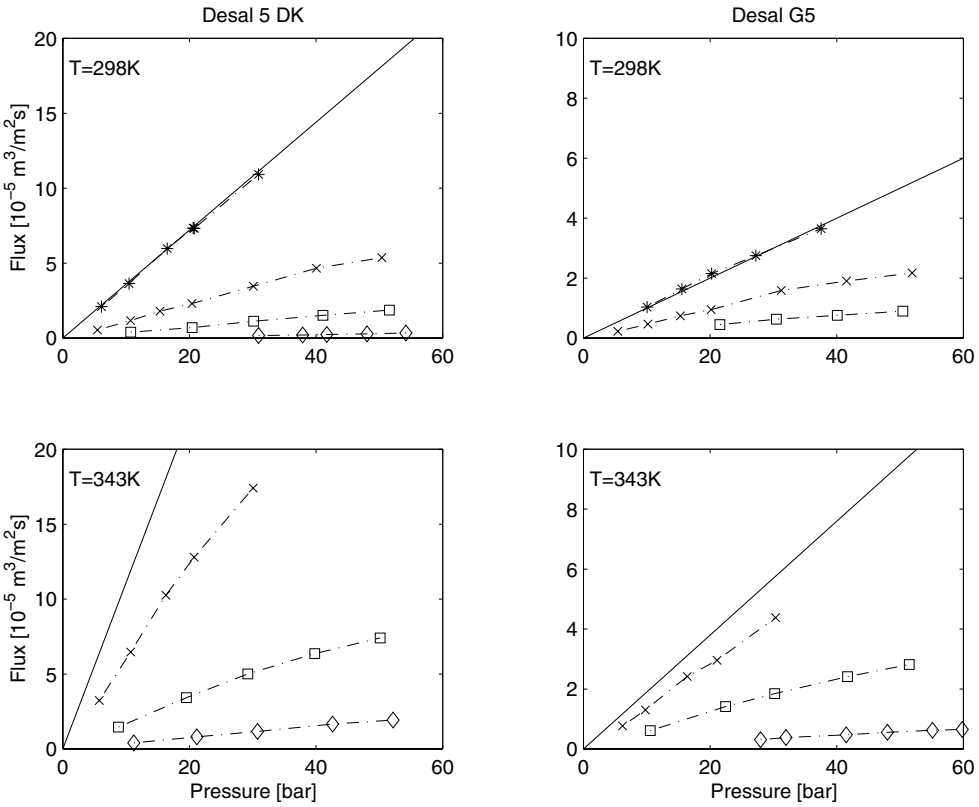

Figure 7.14: Volume flux reduction using the Desal 5 DK (left) and Desal G5 (right) membranes at different temperatures and Reynolds number 1000 (750). (-) water permeability, (∗) 0.1 molal $MgCl_2$, (x) 1 molal $MgCl_2$, (□) 2.5 molal $MgCl_2$, and, (◇) 5 molal $MgCl_2$.

activity used in the corrections are calculated in pure magnesium chloride solution and the interaction with the membrane is not taken into account, which of course may alter the predictions. It is reasonable to think that the presence of the membrane will lower the water activity even more and improve the volume flux predicitons further.

From the discussion in Section 7.3.4, the parameter $\tau\Delta x/\epsilon^*$ is decreasing with increasing salt concentration, which means that the effective membrane thickness decreases. This parameter can also be found in the Hagen-Poiseuille equation, refer Equation 3.80, and if it decreases the volume fluxes should also decrease, which will improve the volume flux prediction even further.

The difference in the osmotic pressure between the feed side and the permeate side is affecting the real pressure difference over the membrane, and the volume flux can be calculated using equation

$$J_v = L_p(\Delta P - \Delta\pi) \tag{7.4}$$

The osmotic pressure differences have been calculated using the Pitzer model described in Section 4.4 and discussed in Section 7.1.4. Figure 7.16 shows the observed fluxes and the predicted volume fluxes with and without concentration polarisation at different magnesium chloride solutions. The results at 5 molal are not shown, since the osmotic pressure differences varied very much and was believed to be caused by titration error, see discussion in Section 7.1.4. The volume flux predictions using the osmotic pressure difference without the concentration polarisation fit the observed fluxes best at the 0.1 molal magnesium chloride solution. The results at 1 molal magnesium chloride fit the volume flux predictions using the osmotic pressure difference with the concentration polarisation surprisingly well, whereas at 2.5 molal the best volume flux predictions are the ones without concentration polarisation.

The fluxes measured using the Desal 5 DK are much higher than the fluxes measured using the Desal G5 membrane, even if the pore diameter of the Desal 5 DK is much lower than the pore diameter of the Desal G5 membrane, refer Table 5.1. This difference in flux is due to the higher surface porosity of the Desal 5 DK membrane and the Desal 5 DK membrane is also more hydrophilic than the Desal G5, which will increase the water flux.

Table 7.1: Water activity in different magnesium chloride solutions calculated from the Pitzer model described in Section 4.4.

c_{MgCl_2} [molal]	0.1	1	2.5	5
a_w	0.9956	0.9575	0.8106	0.4811

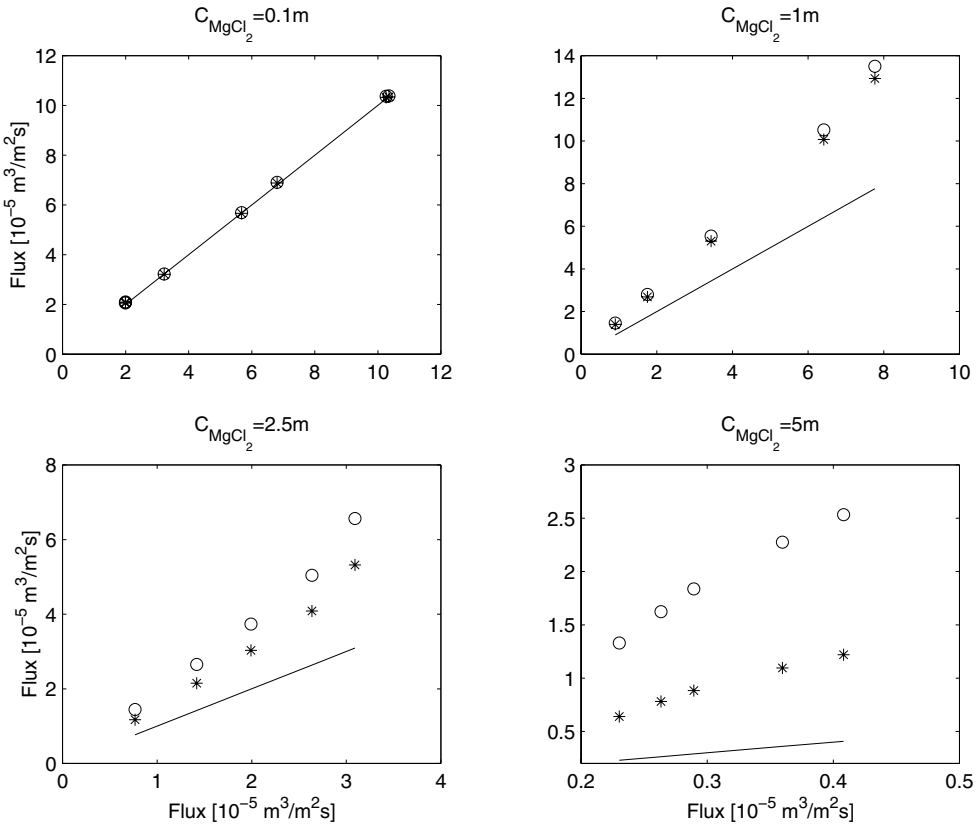

Figure 7.15: The predicted and observed volume fluxes at different magnesium chloride concentrations, 298 K and Desal 5 DK as a function of the observed volume fluxes. The solid lines are the observed fluxes versus the observed fluxes and deviations from this lines means that the predictions are either too high or too low. (-) observed volume flux, (o) predicted volume flux from the Hagen-Poiseuille equation with viscosity correction, (*) predicted volume flux from the Hagen-Poiseuille equation with viscosity and water activity corrections.

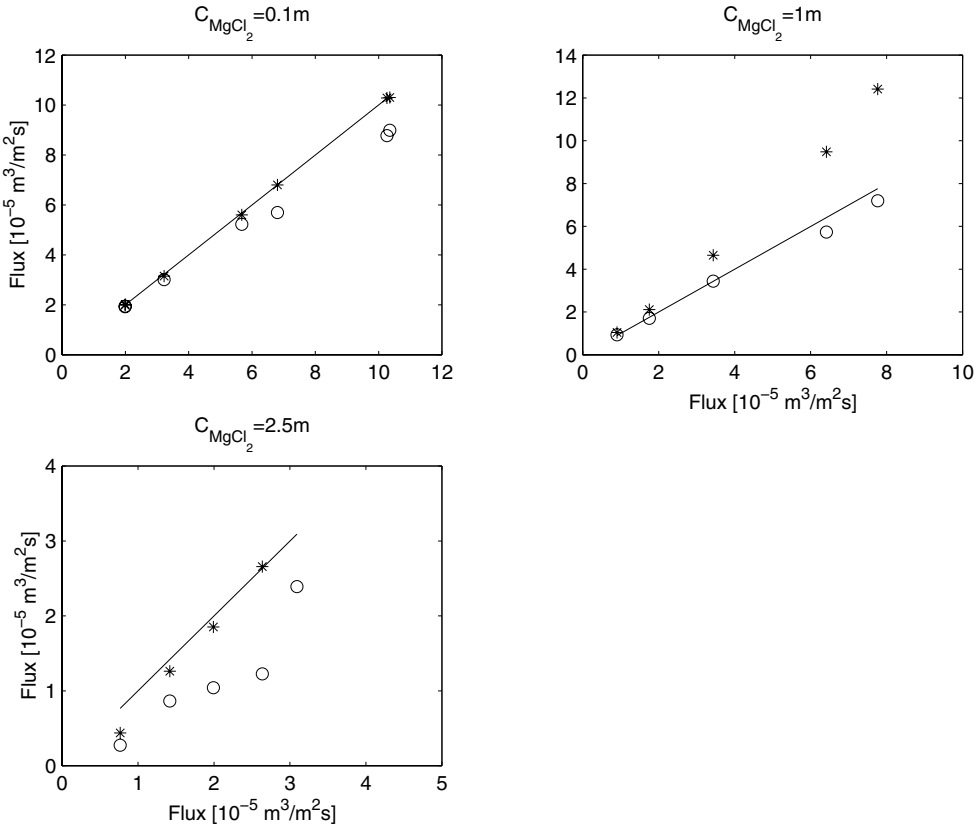

Figure 7.16: The predicted and observed volume fluxes at different magnesium chloride concentrations, 298 K and Desal 5 DK as a function of the observed volume fluxes. The solid lines are the observed fluxes versus the observed fluxes and deviations from this lines means that the predictions are either too high or too low. (-) observed volume flux, (*) predicted volume flux from the Hagen-Poiseuille equation with viscosity, water activity and omsotic pressure difference corrections, (o) predicted volume flux from the Hagen-Poiseuille equation with viscosity, water activity and osmotic pressure difference corrections, where the osmotic pressure difference is based on the concentration polarisation model of Brian (1966).

7.2.2 Splitting the volume flux into water and salt fluxes

The mass fluxes at different magnesium chloride concentrations using the Desal 5 DK membrane at 298 K are shown in Figure 7.17, where also the salt and the water mass fluxes are shown. The figure illustrates that with increasing salt concentration the salt flux share of the total mass flux increases and the assumption that the volume flux equals the water flux fails.

Further, the number of water molecules per ion inside the membrane has been calculated as a function of the bulk salt concentration and the result is shown in Figure 7.18. At the 5 molal magnesium chloride solution the number equals 3, which means that the ions only partially have filled hydration shells, refer Table 4.2.

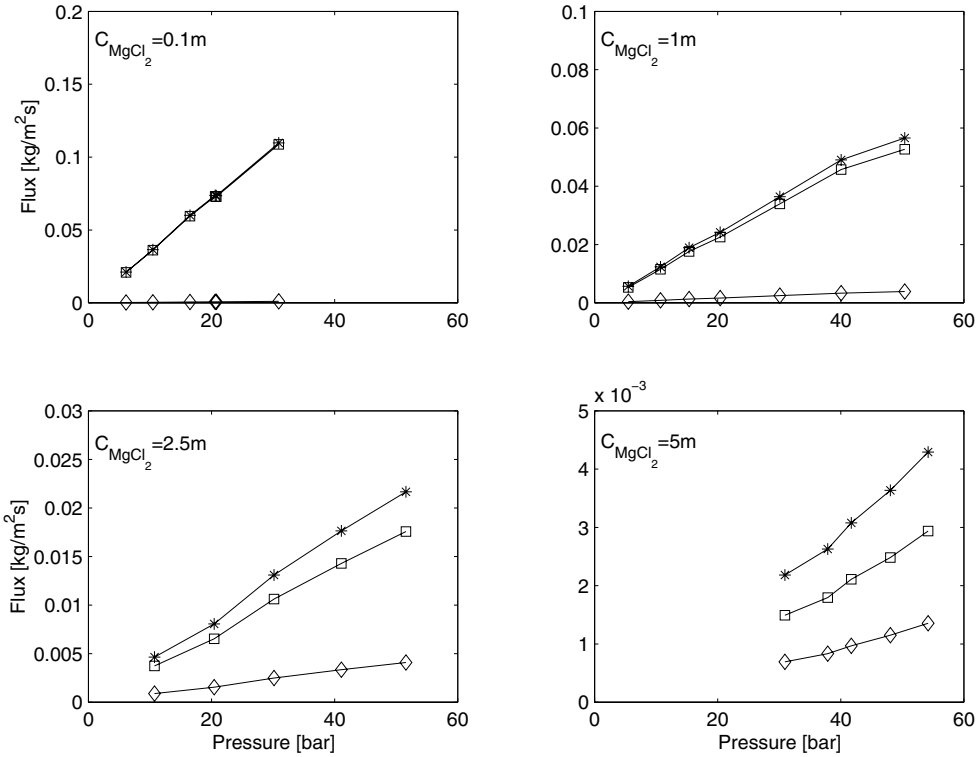

Figure 7.17: The total, salt and water mass fluxes as function of the pressure and different magneisum chloride concentrations at 298 K. (∗) total mass flux, (□) water mass flux, and, (◇) magnesium chloride mass flux.

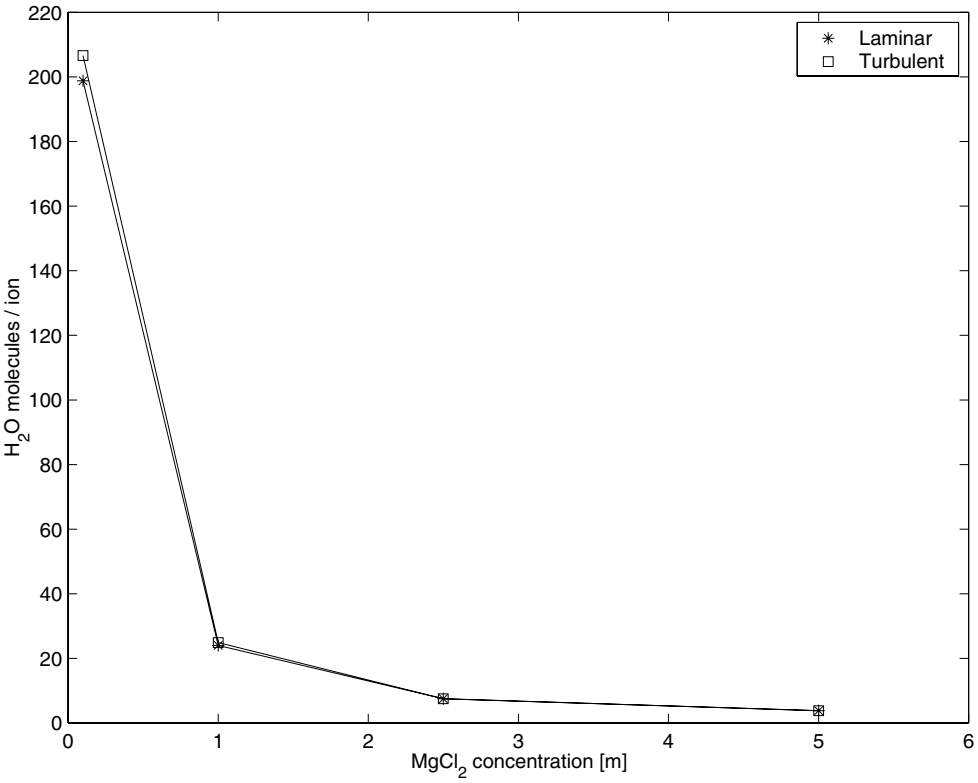

Figure 7.18: The number of water molecules per ion inside the membrane as a function of the magnesium chloride concentration calculated from the water and salt fluxes measured in experiments with pure magnesium chloride solutions.

7.3 Transport models in single $MgCl_2$ solutions

7.3.1 Election of transport models

The observed retentions will be used in the estimation of the model parameters, since the determination of the concentrations at the membrane surface and hence the intrinsic retentions are so uncertain. This will especially influence the results where the concentration polarisation is believed to be significant, *i.e.* at low concentration and in the laminar flow region. The discussion in the following sections will focus on the results obtained using the Desal 5 DK membrane at 298 K and 300 ppm sulphate concentration, unless stated otherwise. In the calculations the influence of the sulphate ions on the chloride ions are neglected, since no evidence of the contrary was found in Chapter 6. The discussion of the sulphate ion retentions is postponed until Section 7.4.

The flux and retention results presented in Chapter 6 were fitted to the different transport models presented in Chapter 3. The fitting results of the sieve model, Glueckauf dielectric exclusion equation and the solution-diffusion model were not good and the obtained models did not predict the retention patterns satisfactorily. The solution-diffusion-imperfection model gave reasonable results in the 0.1 molal magnesium chloride solution and the turbulent flow, but at the other concentrations the model predictions became only vertical lines giving the average retention. On the other hand, the Spiegler-Kedem model, the Pusch's model and the finely-porous model gave good models, which fitted the observed retentions nicely.

7.3.2 Retention predictions using the Spiegler-Kedem model

The observed magnesium chloride retentions were fitted using the Spiegler-Kedem equation given by Equation 3.54 and the parameters σ and $P_s/\Delta x$ were found using a non-linear least square regression procedure. The results for different magnesium chloride solutions are shown in Figure 7.19 and the calculated ASR-values[2] are very small and of the order $2 * 10^{-6}$.

[2]The averaged square resdidual (ASR) can be used as a measure of how good the model prediction is. The ASR can be calculated from the formula $ASR = 1/n \sum_n (y_{obs} - y_{pred})^2$, where n is the number of observations.

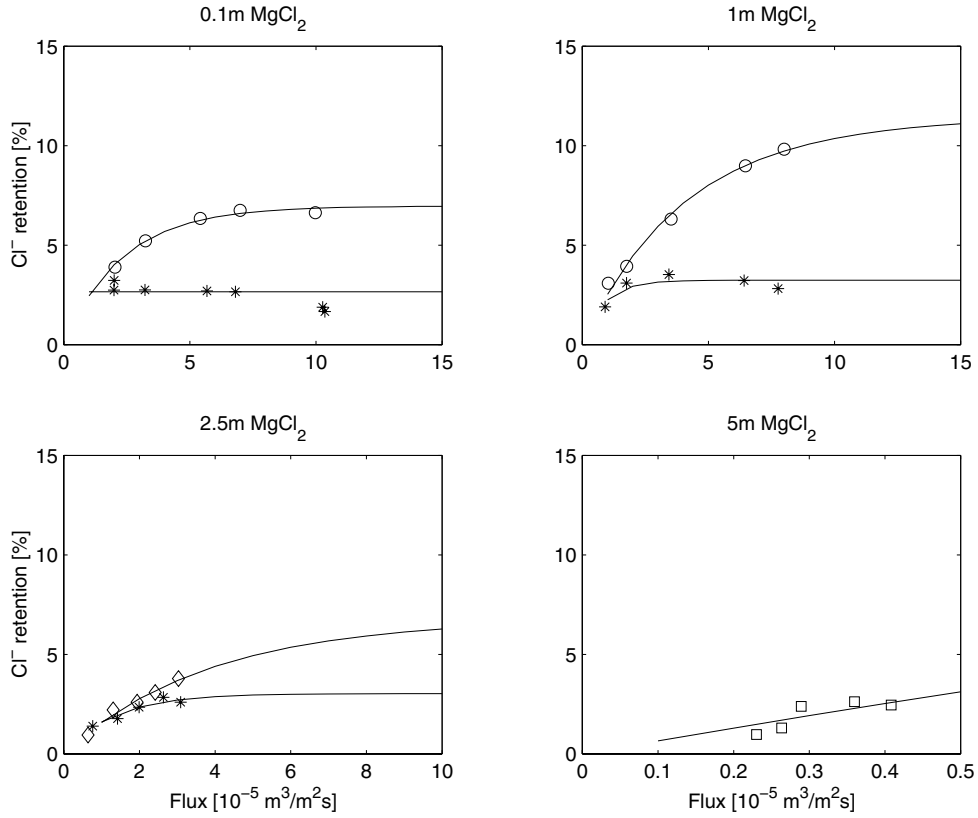

Figure 7.19: The observed and predicted chloride retentions using the Spiegler-Kedem model at different magnesium chloride concentrations, 298 K and Desal 5 DK membrane. Observed retentions at Reynolds number: (□) 750, (*) 1000, (◇) 2500, (o) 4500, and, (-) model predictions.

The local reflection coefficient, σ, is approximately equal to 0.03 at laminar flow and 0.1-2.5 molal magnesium chloride concentrations, whereas it increases to 0.3 at 5 molal. At turbulent flow the coefficient equals 0.07 at 0.1 and 2.5 molal, whereas at 1 molal magnesium chloride concentration the reflection coefficient is 0.11, probably due to the increased retention observed for this membrane sheet. If we focus on the laminar results it seems that something happens to the membrane process when the concentration changes from 2.5 molal to 5 molal, *i.e.* the membrane increases its salt reflection. First of all, this could be a result of bad model estimation, since we have very low retentions and a very small flux region at the highest concentration, which makes the parameter estimation uncertain. For example, the limiting retention predicted by the model obtained at 5 molal

is 25%, whereas the other models predict a retention around 4%.

If the increase in the reflection coefficient is real, it would be interesting to see what could be the reason according to Equation 3.68, which relates the reflection coefficient to an exclusion term and a kinetic term. The increase in the reflection coefficient can be caused by a decrease in the salt partition coefficient or an increase in the water partition coefficent, but most likely both of these coefficients are close to one. This leads to the conclusion that the change in the reflection coefficient is due to changes in the friction factors, where the friction factor between the membrane and the salt must increase more than the friction factor between the water and the membrane when the concentration increases.

The local solute permeability increases with increasing concentration at laminar flow, whereas at turbulent flow it is constant at 1 and 2.5 molal and twice as large as it is at 1 molal magnesium chloride. The permeability divided by the membrane thickness is equal to $4 * 10^{-5}$ m/s at a concentration of 5 molal and Reynolds number 750, which is also the value at the 1 and 2.5 molal solutions and Reynolds number 4500. The increase in the solute permeability with the concentration can be explained by increasing the friction factors between the salt and the membrane and the salt and the water. The salt partition coefficient will also increase with increasing concentration.

7.3.3 Retention predictions using the Pusch model

The magnesium chloride retentions were fitted using the Pusch's equation given in Equation 3.35 and the parameters R_∞ and $(L_{22}/L_p - (R^\infty)^2)L_p\pi_R/R^\infty$ were found using a non-linear least square regression procedure. The results for 0.1, 1 and 2.5 molal magnesium chloride solutions are shown in Figure 7.20 and the ASR-values are very small and of the order $2 * 10^{-5}$. The prediction at 5 molal magnesium chloride concentration was not good and is not shown.

The $(L_{22}/L_p - (R^\infty)^2)L_p\pi_R/R^\infty$ became negative at 0.1 molal magnesium chloride concentration and a Reynolds number of 1000, whereas the coefficients at all the other conditions was of the order 10^{-4} with the highest values at a concentration of 2.5 molal. The infinite retentions were 1.9, 3.7 and 3.8% at 0.1, 1 and 2.5 molal solutions and a Reynolds number of 1000, respectively, whereas the infinite retentions were 9.0, 12.9 and 24.0% at the same conditions and a Reynolds number of 4500 (2500 at 2.5 molal).

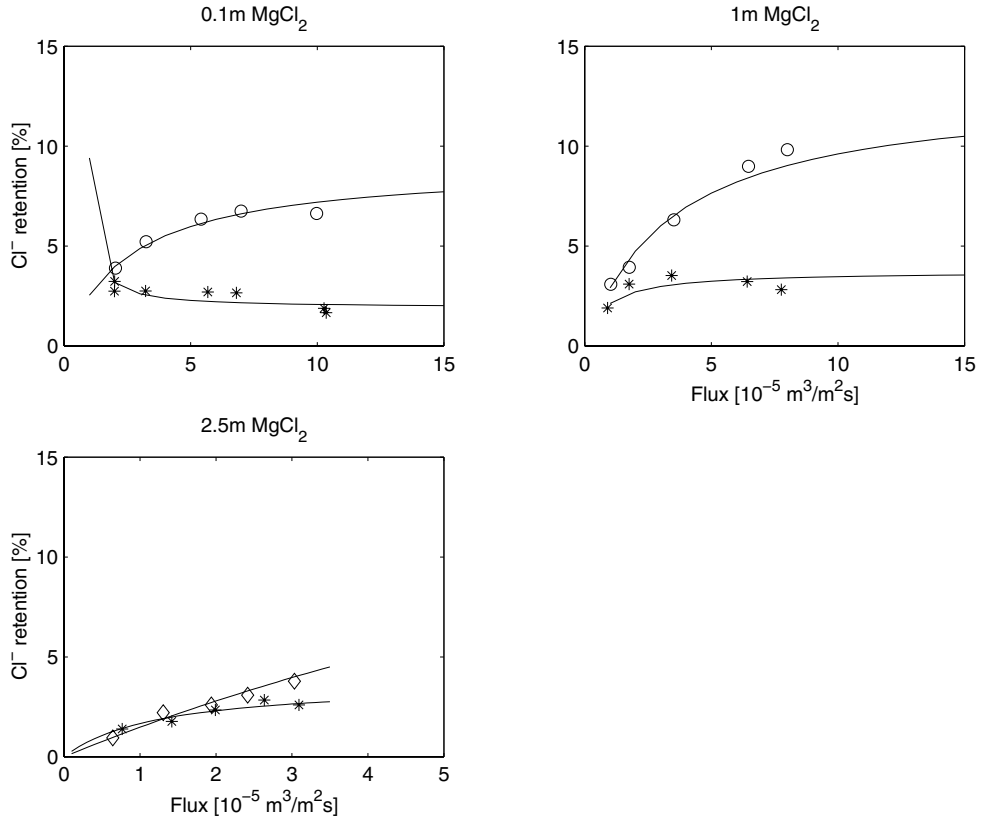

Figure 7.20: The observed and predicted chloride retentions using the Pusch model at different magnesium chloride concentrations, 298 K and Desal 5 DK membrane. Observed retentions at Reynolds number: (*) 1000, (◇) 2500, (o) 4500, and, (-) model predictions.

7.3.4 Retention prediction using the finely-porous model

The magnesium chloride retentions were fitted using the finely-porous model given in Equation 3.105 and the parameters $\tau\Delta x/\epsilon^*$ and $b\epsilon^*/k_s$ were found using a non-linear least square regression procedure. The results for different magnesium chloride solutions are shown in Figure 7.21 and the ASR-values are very small and of the order $2 * 10^{-6}$. The magnesium chloride diffusion coefficient varied with the concentration as shown in Figure 4.8. The model estimation at low concentrations and laminar flow gave negative model coefficients which can not be explained physically. Again it should be emphasized that we are using the

observed retentions in the regression analysis, which can give strange values in the theoretical models. The results at Reynolds number 1000 and 0.1, 1 and 2.5 molal are therefore omitted and the discussion will focus on the results at higher Reynolds number were the error in not taking the concentration polarisation into account is less.

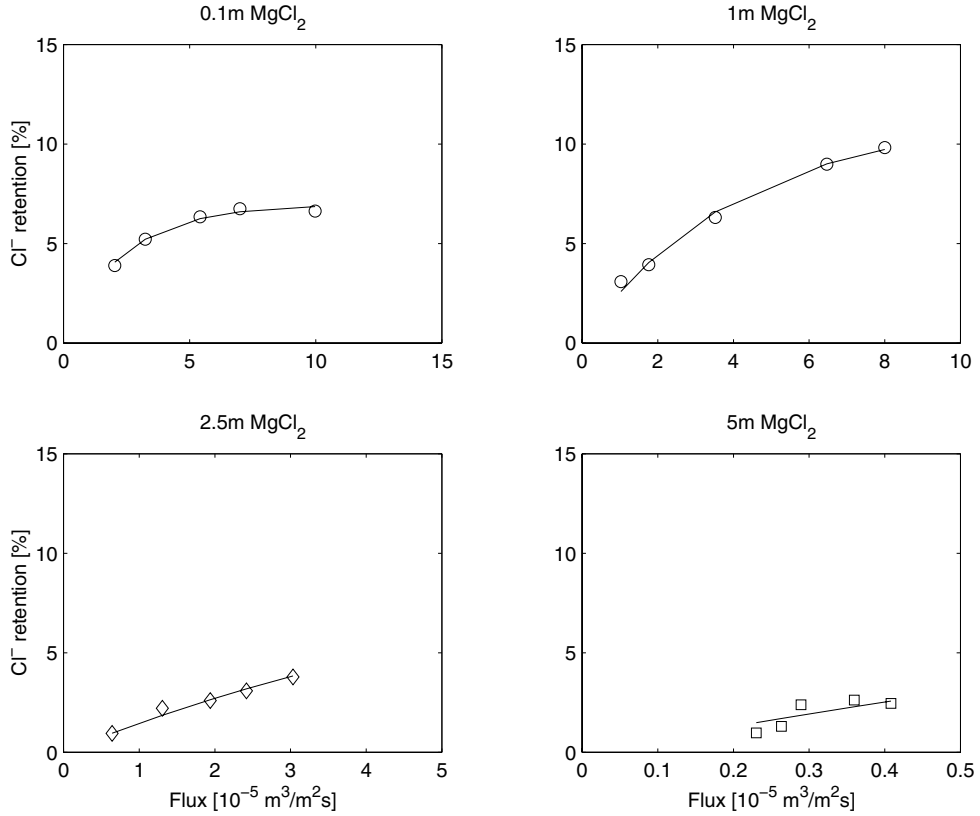

Figure 7.21: The observed and predicted chloride retentions using the finely-porous model at different magnesium chloride concentrations, 298 K and Desal 5 DK membrane. Observed retentions at Reynolds number: (□) 750, (◇) 2500, (o) 4500, and, (-) model predictions.

The estimated parameters are given in Table 7.2, where the parameter $\tau\Delta x/\epsilon^*$ decreases and the parameter $b\epsilon^*/k_s$ increases with increasing concentration. The surface porosity is constant and independent of the salt concentration, therefore the decrease in the $\tau\Delta x/\epsilon^*$-parameter indicates a decrease in the effective thickness of the membrane, which can be regarded as a membrane shrinkage as

discussed by Freger *et al.* (2000) and Heyde *et al.* (1975). Freger *et al.* proposed that the shrinkage of the membrane was caused by either a reduction in the water activity inside the membrane or a screening of the repulsion effect of the fixed charges in the skin layer, or a combination of these.

The increase in the $b\epsilon^*/k_s$-parameter is due to either an increase in the salt partition coefficient or an increase in the b-factor defined in Equation 3.103. The salt partition coefficient will most likely increase and approach 1 as the salt concentration increases, whereas the b-parameter increases when the friction factor between the salt and the membrane increases, which is reasonable when the concentration increases. Also a reduction in the friction factor between the salt and the water molecules will give an increase in the $b\epsilon^*/k_s$-parameter, but most likely this friction factor will also increase, but not as strongly as the friction factor between the salt and the membrane.

7.4 Multicomponent solutions

7.4.1 General remark about the multicomponent models

The discussion of the multicomponent models will concentrate on the Donnan-steric-pore model decribed in Section 3.3.9 and the use of single salt versions of the Spiegler-Kedem model, the Pusch's model and the finely-porous model. The models discussed in Section 3.4 can not be used since we have not done any pure magnesium sulphate experiments.

7.4.2 Ion retention prediction by the DSPM

The effective membrane charge can be calculated from an iteration procedure using the Donnan-steric-pore model described in Section 3.3.9 and the pure magnesium chloride retention results, where the membrane charge and the membrane thickness are used as the iteration variables. The iteration procedure did not converge to any stable values for any of the magnesium chloride solutions used. The membrane surface charge density can, on the other hand, be estimated assuming that it is close to the electrokinetic charge density at the plan of shear, which is related to the zeta potential by the equation (Hunter 1981, Hagmeyer and Gimbel 1998)

$$\sigma_e = \left[2\epsilon_0 \epsilon kT \sum_i c_i N_A \left[exp\left(-\frac{z_i e \zeta}{kT} \right) - 1 \right] \right]^{0.5} \tag{7.5}$$

which gives the effective volumetric membrane charge as

$$X_d = \frac{-2\sigma_e}{r_p F} \tag{7.6}$$

From Figure 5.7 in Chapter 5, the zeta potential for the Desal 5 DK membrane at pH 6 is around -5 mV, which gives an effective membrane charge equal to -15 mol/m^3.

The retention of the membrane was calculated by the DSPM using the measured permeate concentrations and the fluxes at different magnesium chloride solutions, 300 ppm sulphate concentration, Desal 5 DK and 298 K, where the effective membrane charge and the membrane thickness were set to reasonable values. The

procedure integrates from the permeate side through the membrane to the feed side, where the bulk concentrations are calculated using the Donnan exclusion potential. It was found that the effective membrane charge had little or no influence at all on the calculated retentions, whereas the results varied with the membrane thickness or equivalently the diffusion coefficients. An example of the concentration profile through the membrane is given in Figure 7.22, where the feed sulphate ion concentration increases with increasing flux. The retention predictions given for different magnesium chloride solutions are shown in Figure 7.23, from where we can see that the sulphate retention predictions are not good.

In order to better explain the sulphate retention results, some calculations were done varying the pore radius and using both the crystallic and hydrated radii given in Table 4.2. There was no significant difference in using the crystallic radii compared with the hydrated radii, whereas a decrease in the pore radius of course led to higher retention values for all ions, but it did not improve the sulphate model predictions.

Since the membrane charge did not have any effect on the retentions, the use of the DSPM in multicomponent solution is of less value, since the coupling between the ions is related to the electrical potential. Further, as for all the other models the DSPM is only valid in dilute solutions, which is not the case in these experiments.

7.4.3 The use of the Spiegler-Kedem, Pusch and finely-porous models in multicomponent solutions

The observed sulphate retentions were fitted using the Spiegler-Kedem equation given by Equation 3.54 and the parameters σ and $P_s/\Delta x$ were found using a non-linear least square regression procedure. The results for different magnesium chloride solutions are shown in Figure 7.24 and the calculated ASR-values in the turbulent flow region are small and of the order $1 * 10^{-3}$, whereas the model predictions at laminar flow and low concentrations are not so good.

The local reflection coefficient at turbulent flow decreases with magnesium chloride concentration, whereas for the local solute permeability only a small decrease is observed. The sulphate permeability values are an order of magnitude lower than the chloride permeabilities, which can be explained by a lower partition coefficient and a higher friction factor between the sulphate ions and the membrane compared to the friction factor between the chloride ions and the membrane.

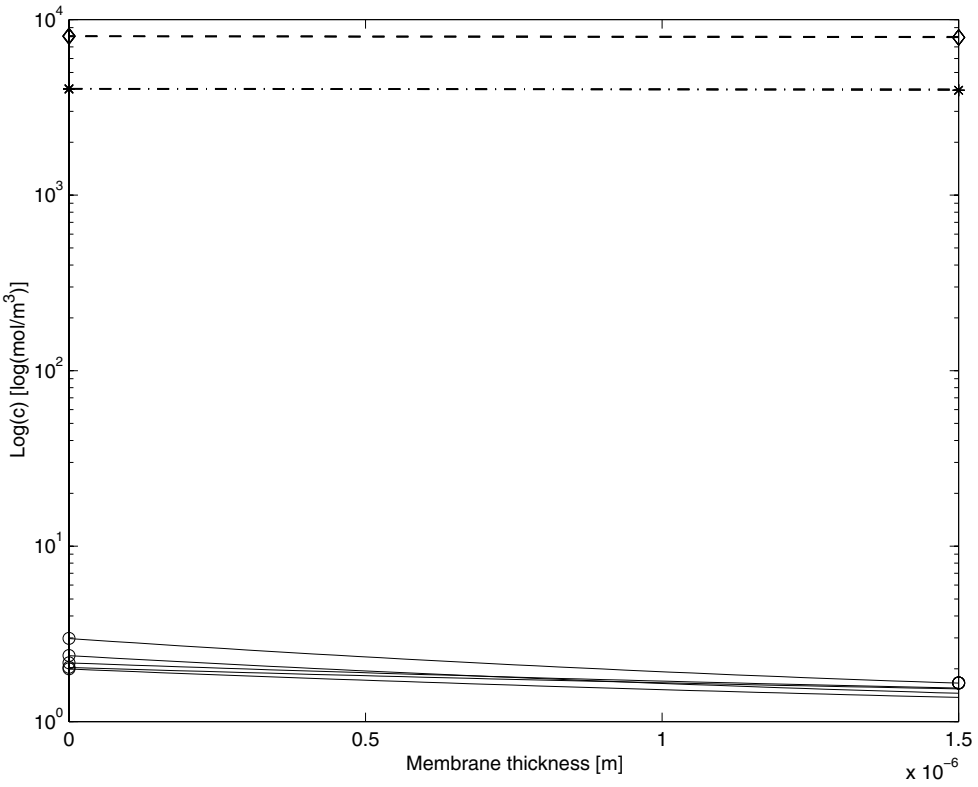

Figure 7.22: The calculated concentration profile through the membrane at 5 molal magnesium chloride solution, 300 ppm sulphate concentration, 298 K, Reynolds number 4500 and Desal 5 DK. (- -) chloride ion concentration, (-.) magnesium ion concentration, and, (-) sulphate ion concentration.

The observed sulphate retentions were fitted using the Pusch's equation given in Equation 3.35 and the parameters R_∞ and $(L_{22}/L_p - (R^\infty)^2)L_p\pi_R/R^\infty$ were found using a non-linear least square regression procedure. The results for 0.1, 1 and 2.5 molal magnesium chloride solutions are shown in the Figure 7.25 and the ASR-values for the turbulent flows are small and of the order $1*10^{-3}$. The prediction at laminar flow and the results at 5 molal magnesium chloride concentration were not good and are not shown.

The $(L_{22}/L_p - (R^\infty)^2)L_p\pi_R/R^\infty$ became negative at laminar flow conditions, whereas the coefficients at the turbulent conditions were of a magnitude lower compared with the corresponding chloride values discussed in Section 7.3.3. The

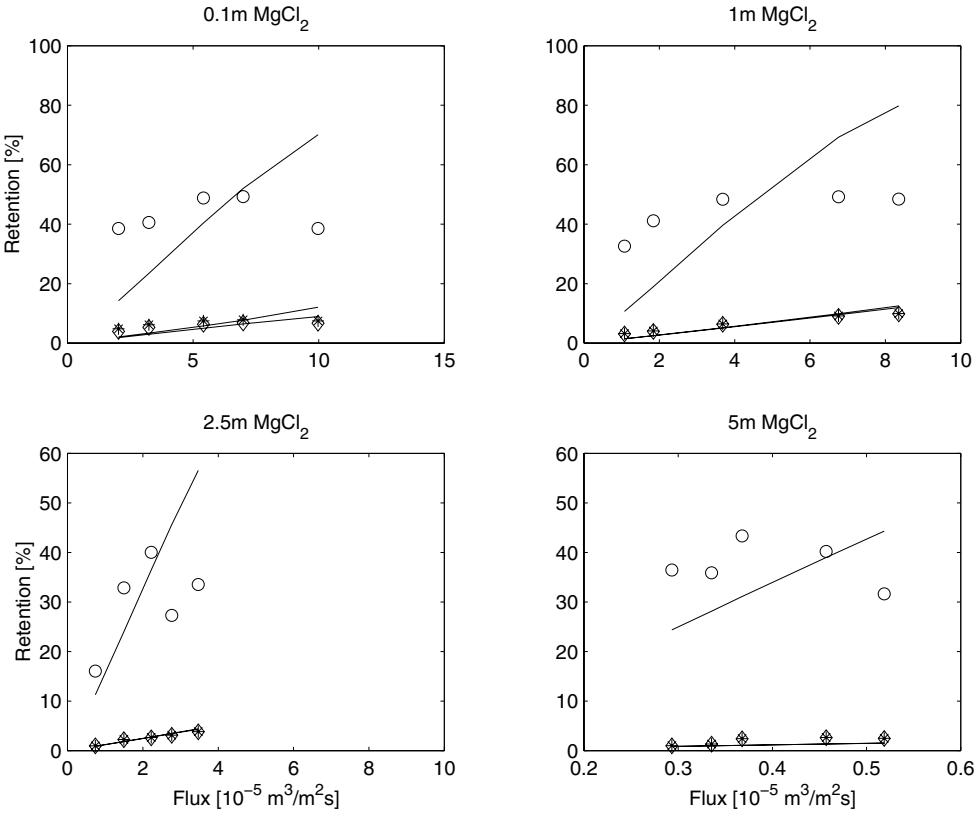

Figure 7.23: The ion retention predictions calculated from the DSPM. (*) observed magnesium ion retentions, (◇) observed chloride ion retentions, (o) observed sulphate ion retentions, and, (-) model predictions.

infinite retentions at turbulent flow increased to a limiting value of 55%. The values at high magnesium chloride concentration are measured at considerable lower fluxes and an extension of the model to the infinite flux limit will of course be more inaccurate when only a small range of the flux is used to make the models.

The finely-porous model was also used to fit the observed sulphate retention data, but in this case the $\tau\Delta x/\epsilon^*$-parameters found in the chloride regression analysis discussed in Section 7.3.4 were used and held constant at each magnesium chloride level. This means that all the information of the sulphate ion retention should be hidden in the $b\epsilon^*/k_s$-parameter. The finely-porous model is given in Equation 3.105 and the parameter $b\epsilon^*/k_s$ was found using a non-linear least

square regression procedure. The diffusion coefficient for the sulphate was set equal to the value that corresponded to a magnesium sulphate concentration equal to the magnesium chloride concentration in the actual solution. The results for different magnesium chloride solutions and turbulent flows are shown in Figure 7.26 and the ASR-values are small and of the order $1 * 10^{-3}$.

The sulphate $b\epsilon^*/k_s$-parameters are given in Table 7.2 and one can see that the parameter increases as the magnesium chloride concentration increases. The increase in the $b\epsilon^*/k_s$-parameter is due to either an increase in the sulphate partition coefficient or an increase in the b-factor defined in Equation 3.103. The sulphate partition coefficient will increase when the salt concentration increases because the retention decreases, whereas the b-parameter will decrease since the friction between the sulphate ions and the membrane will most likely decrease due to the shielding effects of the increasing and very high chloride concentration and at the same time the friction between the sulphate and the rest of the salt solution will increase.

Table 7.2: The estimated $\tau\Delta x/\epsilon^*$- and $b\epsilon^*/k_s$-parameters in the finely-porous model as function of magnesium chloride concentration and 300 ppm sulphate concentration at 298 K and Reynolds number 4500 (2500 at 2.5 molal and 750 at 5 molal).

c_{MgCl_2} [molal]	0.1	1	2.5	5
$\tau\Delta x/\epsilon^*$ [10^5 m]	4.31	2.46	1.19	0.85
$(b\epsilon^*/k_s)_{MgCl_2}$	1.075	1.129	1.131	1.395
$(b\epsilon^*/k_s)_{SO_4^{-2}}$	1.820	2.004	1.963	8.077
$(b\epsilon^*/k_s)_{SO_4^{-2}}/(b\epsilon^*/k_s)_{MgCl_2}$	1.69	1.77	1.74	5.79

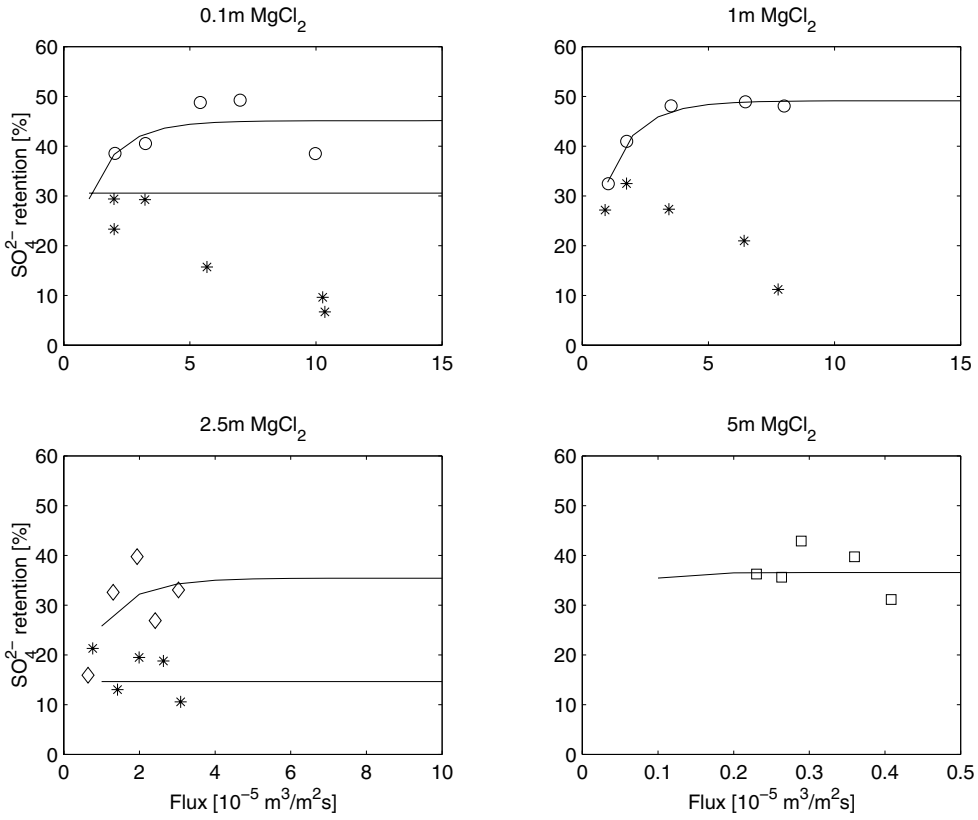

Figure 7.24: The observed and predicted sulphate retentions using the Spiegler-Kedem model at different magnesium chloride concentrations, 300 ppm sulphate concentration, 298 K and Desal 5 DK membrane. Observed retentions at Reynolds number: (□) 750, (*) 1000, (◇) 2500, (o) 4500, and, (-) model predictions. Note that there is no prediction line at 1 molal and Re=1000.

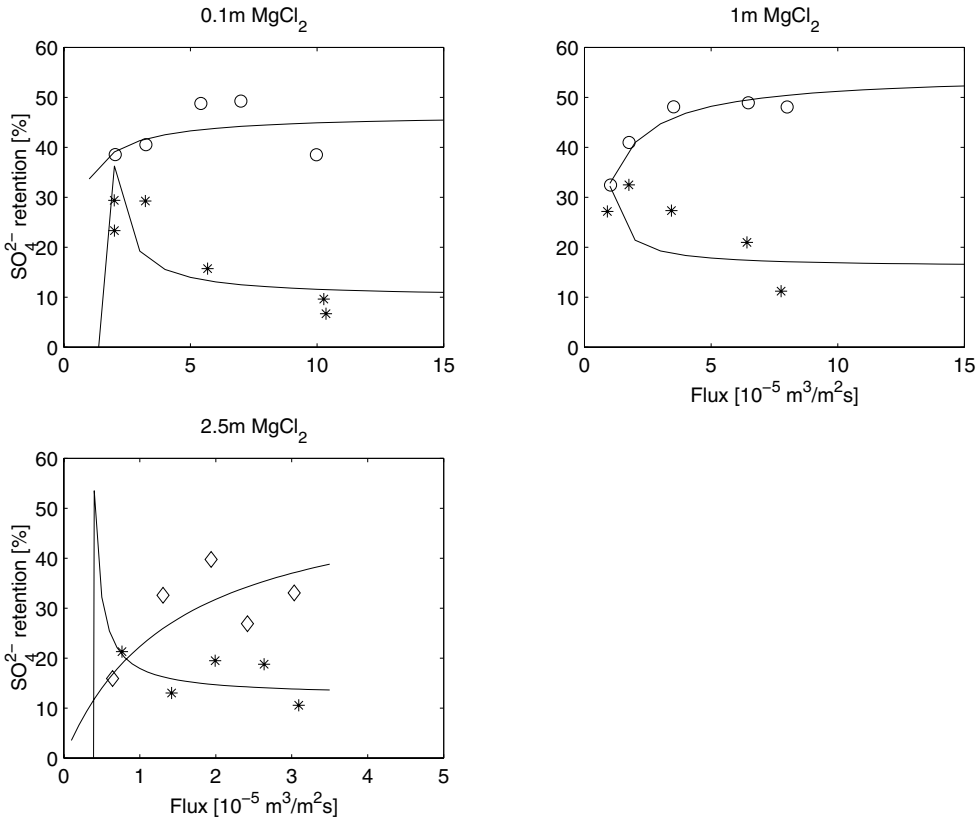

Figure 7.25: The observed and predicted sulphate retentions using the Pusch model at different magnesium chloride concentrations, 300 ppm sulphate concentration, 298 K and Desal 5 DK membrane. Observed retentions at Reynolds number: (*) 1000, (◇) 2500, (o) 4500, and, (-) model predictions.

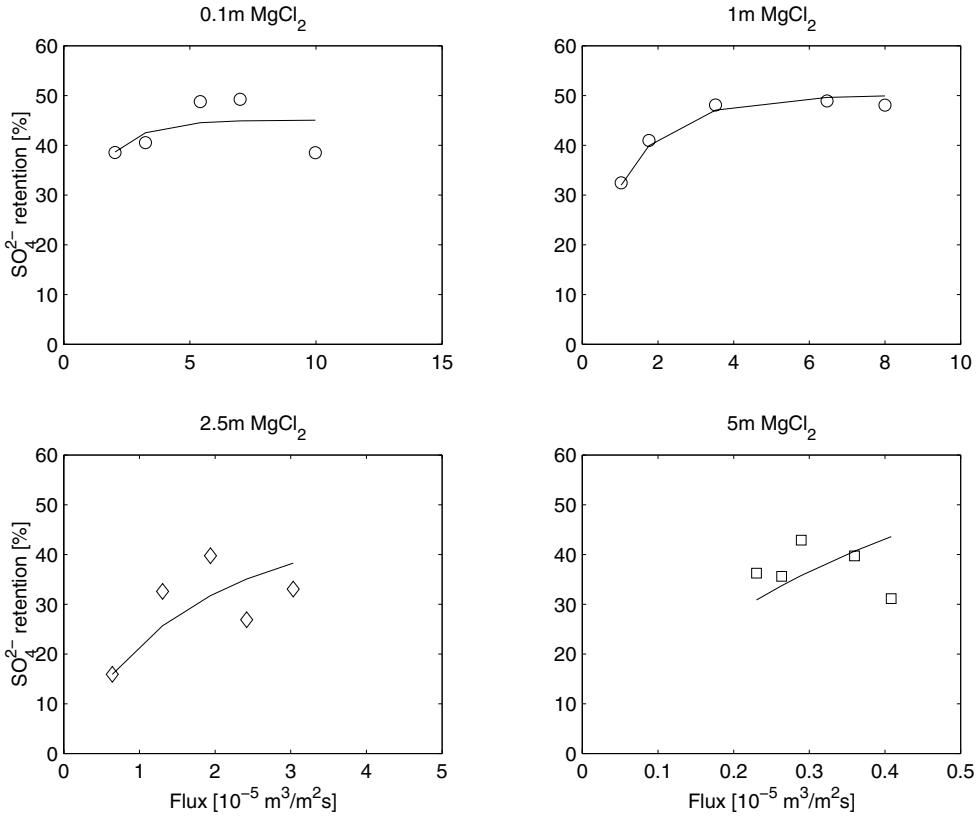

Figure 7.26: The observed and predicted sulphate retentions using the finely-porous model at different magnesium chloride concentrations, 300 ppm sulphate concentration, 298 K and Desal 5 DK membrane, when the parameter $\tau\Delta x/\epsilon^*$ estimated for the chloride retentions are held constant at each magnesium chloride level. Observed retentions at Reynolds number: (□) 750, (◇) 2500, (o) 4500, and, (-) model predictions.

7.5 Separation mechanisms

The interaction between the ions and the membrane is discussed in Section 3.3.7 and the Donnan potential is belived to be one of the separation mechanisms in nanofiltration of salt solutions (Peeters *et al.* 1998, Hagmeyer and Gimbel 1998, Nystrøm *et al.* 1995). The Donnan potential has been successfully applied in many salt systems as part of the Donnan-steric-pore model (Peeters *et al.* 1998, Hagmeyer and Gimbel 1998, Bowen and Mohammad 1998*b*), and Peeters *et al.* (1998) found that the 15 membranes they investigated could be divided into two categories, where the retention in the first type of membranes followed a typical Donnan exclusion mechansim, whereas in the second type of membranes the retention was determined by both Donnan exclusion and size effects. However, the concentration in all these systems has been very low compared to the magnesium chloride concentration discussed here. On the other hand, Sabbatovskii *et al.* (1993) claimed that the electrostatic separation mechanisms vanish at higher concentrations and related the retention characteristics to structural mechanisms or to ion pairing.

It is a well-known fact that the Debye length will decrease and the surface charges will be more effectively shielded with increasing concentration. Bowen *et al.* (1997) have shown how the electrical potential varies across a membrane pore with pore diameter and concentration, and, at 0.1 molar sodium chloride a significant decrease in the potential across the pore was found. The retention calculations of the Donnan-steric-pore model discussed in Section 7.4.2 also showed no effect of the membrane charge, which was varied between -150 - +150 mol/m^3. But even if the membrane charge has no or little effect on the separation at higher salt concentrations, the membrane itself will merely due to its presence have influence on the activity of the ions and the water.

Since it has been difficult to use any analytical expressions for the dielectric exclusion mechanism, the discussion will focus on the qualitative effects seen from the Born's model in Equation 3.135. From this equation one can see that the separation of an ion is caused by the difference in the dielectric constants in the membrane pore and in the bulk solution and valence and radius of the ion, *i.e.* higher valence and bigger ion give better separation of the ion. The decrease in the retention when the concentration of magnesium chloride increases can be explained by the decrease in the dielectric constant of the bulk solution, which at really high concentrations will approach the dielectric constant of the solution in the membrane pores. The separation between the chloride and sulphate ions will then of course be a result of the different ionic radiuses and valences. The

effect of temperature is difficult to predict, since the dielectric constants at higher temperatures will most likely be higher due to the higher water activity at a given concentration, which may level out the inverse temperature dependency.

The original preferential-sorption model presented by Sourirajan (1963) suggested that the retention of a membrane could be correlated with the Gibbs adsorption isotherm

$$\frac{\Gamma}{c} = -\frac{1}{RT}\frac{d\gamma}{dc} \tag{7.7}$$

where Γ is the surface excess concentration and γ is the surface tension. Also Heyde *et al.* (1975) discussed the validity of this simple correlation and were surprised how well it worked. The surface tension of magnesium chloride and magnesium sulphate at 393 K can be found in Lide (1990) and the surface tension for both salts are linear dependent with the concentration and the $d\gamma/dc$-slope of the magnesium chloride is 1.5 times higher than the slope of the magnesium sulphate. This means that the chloride ions will have a larger partition coefficient than the sulphate ions (Friebe and Moritz 1994).

The surface potential at the air/water interface of different salts is given by Conway (1977) and reprinted in Figure 7.27. The surface potential gives information about the surface structure of the fluid and the orientation of the water and ion molecules near the interface. The figure shows that the surface potential of magnesium chloride is negative and decreasing with concentration, whereas the surface potential of magnesium sulphate is positive and increasing with concentration. The surface potential can be related to the hydration energies, where smaller hydration energies give greater decreases in the potential, and the conclusion is that the sulphate ions will have a greater hydration energy than the chloride ions and according to the separation mechanisms proposed by Luck (1984), the sulphate ions should be better retained than the chloride.

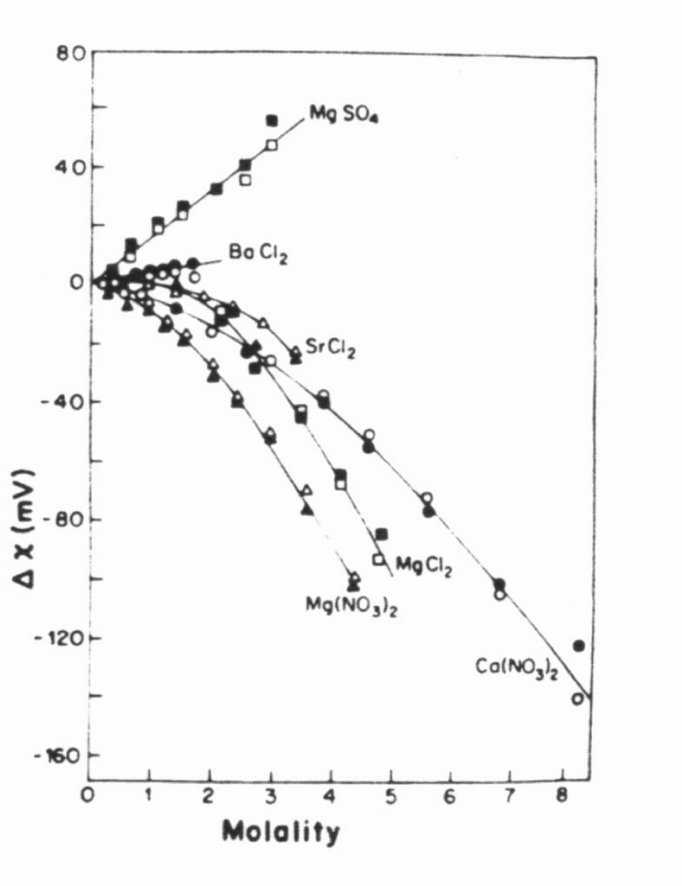

Figure 7.27: The change in the surface potential plotted as a function of the salt concentration (Conway 1977).

Chapter 8

Conclusions

8.1 Main results

This thesis has focused on the separation of sulphate ions from concentrated magnesium chloride solutions using nanofiltration. The magnesium chloride concentrations varied from 0.1 to 5 molal, whereas the sulphate concentration took three levels, *i.e.* 0, 300 ppm and 3000 ppm. An extensive database containing experimentally measured chloride and sulphate ion retentions and volume fluxes has been established using the Osmonics/Desal membranes Desal 5 DK and Desal G5. The effect of Reynolds number, temperature and pressure has been investigated, and the experimental results are in qualitative agreement with the results found in the literature.

The observed chloride retentions are relatively low, less than 10%, whereas the observed sulphate retentions are somewhat higher, around 20-60%. Both ion retentions decrease with increasing magnesium chloride concentration and to some extent increasing temperature, whereas the ion retentions increase with increasing Reynolds number and pressure.

The ions are separated due to the difference in the physical-chemical properties between the solution outside the membrane and the solution inside the membrane, which can be related to the dielectric exclusion mechanism. Both the chloride and the sulphate retentions fitted the Spiegler-Kedem model and the finely-porous model nicely and gave parameters, which can be given a physical interpretation.

The observed volume fluxes decrease with increasing magnesium chloride concentrations, which can at least partially be explained by the increase in the viscosity, the decrease in the water activity inside the membrane and the osmotic pressure difference between the feed side and the permeate side of the membrane.

At low concentrations the retention varied with the Reynolds number, which indicates the presence of a concentration polarisation phenomena. In order to make quantitative calculations of the membrane surface concentration different models were used, that gave very different answers. None of the models are believed to be good. However, the concentration polarisation decreases with increasing salt concentration and at 5 molal the concentration polarisation of the chloride ion is negligible, but the concentration polarisation of the sulphate ions is still significant.

8.2 Further research

Further research should include more experiments using high salt concentrations and different types of membranes, but the experiments can be limited to only one (high) Reynolds number and one sulphate concentration. For instance, it would be interesting to see the ion retentions of a highly charged membrane in a concentrated electrolyte.

The concentration polarisation phenomena should be more thoroughly discussed in order to use the results at low Reynolds numbers and low concentrations. A verification of the existing correlations or a development of new ones should be stressed unless future retention experiments are performed at high Reynolds numbers. Anyway, the concentration polarisation in multicomponent solutions should get some attention in the future.

The Maxwell-Stefan model provides a general approach to multicomponent transport without any restrictions in the concentration, and the model should get some attention in the future. The Pitzer model can be used to create the $\partial ln\gamma_i/\partial x_j$-relationship needed to calculate the Maxwell-Stefan diffusion coefficients.

Part II

Concentration polarisation measurements

Chapter 9

Direct measurements of the concentration polarisation phenomenon

Edvard Sivertsen, Vetle Misje, Mats Vingereid and Norvald Nesse
Department of Chemical Engineering, Norwegian University of Science and Technology, N-7491 Trondheim, Norway.

Parts of this chapter was presented at Euromembrane 2000, Jerusalem, Israel, September 24-27, 2000.

9.1 Introduction

The main idea of a membrane process is to separate a component from a solution by using a semi permeable membrane that allows some components to pass while other components are prohibited. The latter components will accumulate near the membrane surface and a concentration gradient is formed. The increase in the concentration at the membrane surface is referred to as concentration polarisation and may influence the separation process in several ways. First, an increase in the concentration polarisation will cause a reduction in the driving pressure difference since the osmotic pressure increases, and second, the solute flux increases since the concentration difference across the membrane increases. Both effects will in-

crease the solute concentration in the permeate and thereby lower the separation efficiency (Jonsson and Boesen 1984, Rautenbach and Albrecht 1989).

In concentrated solutions the concentration polarisation may cause super saturation of the liquid at the membrane surface, which may lead to precipitation on the membrane surface with the possibility of pore blocking. This will of course influence the product quality and production rate.

The problem with concentration polarisation was early brought into scientists attention when calculating the performance of membrane processes, *e.g.* Brian (1965), Sherwood *et al.* (1965), Sherwood *et al.* (1967) and Kimura and Sourirajan (1967), and it is now generally accepted that a quantitative knowlegde of the concentration polarisation is required in order to perform design and optimalisation of the membrane processes (Geraldes *et al.* 2000). In order to achive such knowlegde different methods have been used which can be divided into two main categories, direct and indirect. The direct methods measure the concentration as function of distance from the membrane and gives the concentration polarisation directly, while the indirect methods calculates the membrane surface concentration using measured retention and flux values together with a mathematical model of the mass transfer coefficient.

Direct measurement of the concentration profile can be made by optical devices or micro electrodes. Reported optical methods are based on laser interferograms (Dytnerskij *et al.* 1987, Mahlab *et al.* 1978, Kapur and Macleod 1975, Bollenbeck and Ramirez 1974, Johnson 1974, Lin *et al.* 1953) and on NMR micro-imaging (Pope *et al.* 1996), while in methods using micro-electrode measurements different properties such as conductivity (Hendricks and Williams 1971, Liu and Williams 1970), current transient (Tiravanti *et al.* 1985) and dielectric constants (Hanai *et al.* 1993) have been measured. Direct methods are often restricted to special membrane cells and flow conditions, which give less valuable results since they may be far from real process conditions.

Indirect methods have become the most important and widely used category of methods to calculate the concentration polarisation. The amount of available literature is enormous, with many different models and diversity of their use, *e.g.* Raridon *et al.* (1966), Ramani (1992), Bader and Jennings (1992) and Geraldes *et al.* (2000).

A new direct method to calculate the concentration polarisation is developed and the principle of the method will be explained. The method should be useful in

mapping the concentration polarisation in multi component solutions.

9.2 Film model

The film model is a widely used model to calculate the concentration polarisation in membrane separation (Mulder 1996, Jonsson and Boesen 1984). At steady state conditions the transport through the concentration boundary film equals the solute transport through the membrane[1], and using a mass balance over the film and integrating between the bulk solution and the membrane surface, the concentration polarisation modulus can be calculated from the film model by

$$\frac{C_m}{C_b} = \frac{\exp(J_v/k)}{R_{int} + (1 - R_{int})\exp(J_v/k)} \tag{9.1}$$

where J_v is the flux through the membrane, $k = D/\delta_c$ is the mass transfer number, D is the diffusion coefficient, δ_c is the concentration boundary layer thickness, C_b is the bulk concentration, C_m is the concentration at the membrane surface, $R_{int} = 1 - C_p/C_m$ is the intrinsic retention and C_p is the permeate concentration.

To use the equation above together with experimental results, a correlation for the mass transfer coefficient, k, has to be chosen. Gekas and Hallstrøm (1987) give a summary of mass transfer correlations based on Sherwood, Schmidt and Reynolds numbers, and suggest modifications in the correlations when they are used in membrane separation (*i.e.* walls with suction). The general correlation can be written

$$Sh = a\, Re^b\, Sc^c \left(\frac{d_h}{L}\right)^d \tag{9.2}$$

where $Sh = kd_h/D$ is the Sherwood number, $Re = d_h v\rho/\eta$ is the Reynolds number, $Sc = \eta/\rho D$ is the Schmidt number, $d_h = 4\,(\text{area})/(\text{wetted periphery})$ is the hydraulic diameter and a, b, c and d are constants. Further, D is the diffusion coefficient, v is the flow velocity, L is the length of the channel, ρ is the density and η is the viscosity. This study has used the coefficients given by Mulder (1996) as a first calculation of the mass transfer coefficient. For laminar flow in a channel the correlation is

$$Sh = 1.85\,(Re\, Sc\, d_h/L)^{0.33} \tag{9.3}$$

[1] Refer Figure 2.3 in Chapter 2.

while for turbulent flow it becomes

$$Sh = 0.04\, Re^{0.75}\, Sc^{0.33} \tag{9.4}$$

9.3 Principle of the new method

Three steel capillary tubes have been mounted on and through the top plate of a cross-flow flat-sheet membrane cell. The lower end of these tubes can be exactly positioned vertically in the membrane cell channel above the membrane using a micrometer screw with a scale of 1/100 mm. Micro valves connected to the capillary tubes allow very small samples to be drawn for analysis. The principle of the method is shown schematically in Figure 9.1. To the authors' knowledge, this is the first attempt to physically draw a sample of the solution near the membrane surface and analyze it.

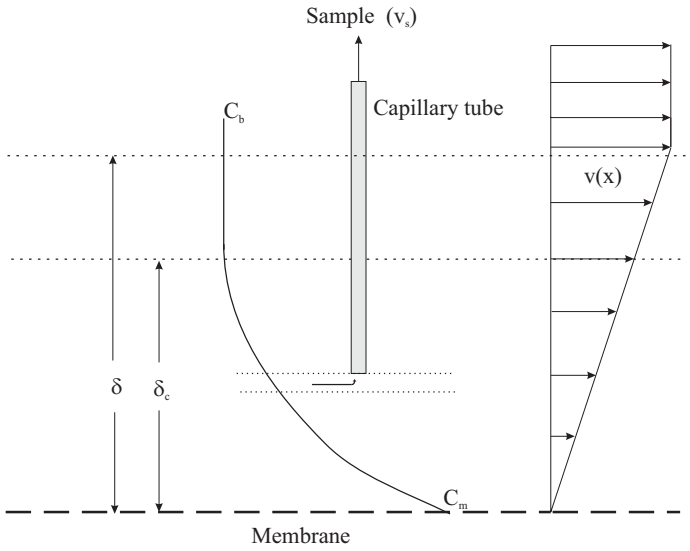

Figure 9.1: Principle of the new method measuring the concentration polarisation directly by adjusting a capillary tube inside the concentration boundary layer, δ_c, and drawing a sample of the solution for analysis. The fluid velocity profile in the hydrodynamic boundary layer, δ, is estimated by a linear velocity profile.

One important parameter to control is the sampling velocity defined as the veloc-

ity which the sample is drawn through the capillary tube. If samples are drawn with too high sampling velocity it will create suction also from the layers next to the layer under investigation, and the sample concentration will not be representative for that position in the concentration boundary layer. If all fluid in a height h below the probe tip should be drawn for analysis, the following mass balance could be set up (refer Figure 9.2)

$$\frac{\pi\, d_s^2}{4}\, v_s = b\, h\, v_i \quad \Rightarrow \quad \frac{v_s}{v_i} = \frac{4\, b\, h}{\pi\, d_s^2} \approx \frac{1}{10} \tag{9.5}$$

where the inner diameter of the capillary tube, d_s, equals 0.2 mm, the outer diameter, b, is 0.4 mm and the height of the layer under investigation, h, is set equal to 0.01 mm. The ratio between the sampling velocity and the fluid velocity in the channel above the membrane has been estimated with reasonable values and should not exceed 1/10.

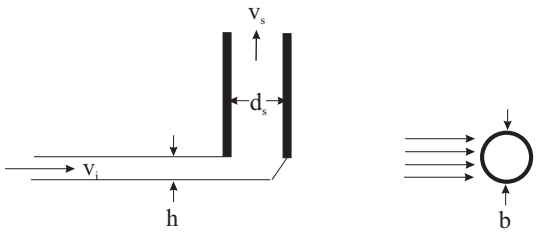

Figure 9.2: The sample drawn for analysis should be taken from the area $b \cdot h$, giving restrictions of the sampling velocity, v_s.

The fluid velocity in the boundary layer above the membrane is unknown, but as shown in Figure 9.1 this velocity has been approximated by a linear profile. Further, the sampling velocity profile inside the capillary tube will probably have a parabolic shape with a maximum velocity in the center of the tube with decreasing value towards the tube walls. To get the same amount of fluid into the tube as passing the area $b \cdot h$, the height of the concentration layer under investigation must be slightly higher than h.

9.4 Experimental

9.4.1 Apparatus

Experiments were carried out on the laboratory test unit shown schematically in Figure 9.3. The module consists of a feed tank (total volume 8 dm^3) with a temperature controller, a pump (Cat 5CP6121, engine effect 4 kW) with a bypass line and a membrane flat-sheet cell. The main line was controlled by a back pressure valve (Tescom), while the bypass line was controlled with a needle valve (Whitey union bonnet valve). All parts made of steel were of quality stainless steel (SS316) and the tubes were made of Teflon.

The pressure transmitter (Bourdon Sedeme Y763, 0-100 bar, current output 4-20 mA) was placed upstream of the membrane cell, while the flow meter (ADMAG SE magnetic flow meter, 0-20 dm^3/minute, current output 4-20 mA) was connected to the main line downstream the membrane cell. The accumulated permeate was weighed on a balance (Explorer, Ohaus, capacity 0.00-410.00 grams).

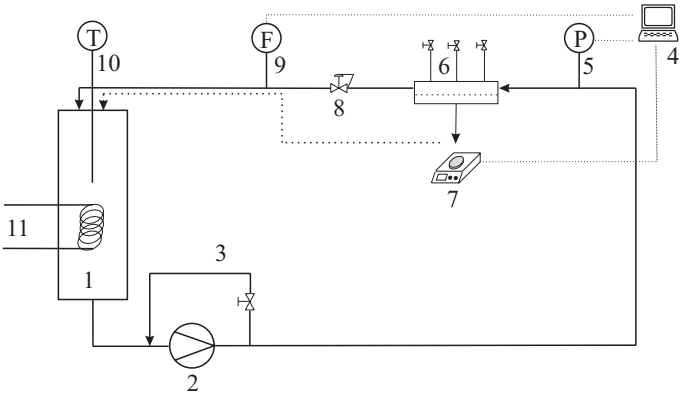

Figure 9.3: The laboratory test unit consists of (1) a feed tank, (2) a pump, (3) a bypass line, (4) a computer, (5) a pressure transmitter, (6) a membrane flat-sheet cell, (7) a weight balance, (8) a back pressure valve, (9) a flow meter, (10) a thermometer and (11) a water heat exchanger. Pressure, flow rate and flux were automatically measured and the data stored in the computer.

The pressure, flow rate and flux were automatically measured and the data stored

in a computer. The Field Point data acquisition system from National Instruments was used together with the program Labview. The process variables were normally sampled three times per minute.

The experimental conditions were limited to a maximum pressure of 100 bar, room temperature (20-25 degrees Celsius) and a maximum flow rate of 9 dm^3/minute.

The cross-flow flat-sheet membrane cell was made of stainless steel (SS316) and sketches are shown in Figures 9.4 and 9.5. The total active membrane area was 60 cm^2 (60 mm x 100 mm) and a porous sintered metal plate in stainless steel (SS316) was used as a membrane support. The height of the channel above the membrane was 3 mm and the placement of the capillary tubes are shown in Figure 9.4. The capillary tubes are placed on the diagonal of the flow direction to minimize the disturbance of the flow pattern around tubes downstream. A photo of the membrane cell showing the sampling system is given in Figure 9.6.

9.4.2 Response time

An important parameter of the apparatus is the dynamic behavior of the sampling system consisting of a capillary tube and a micro valve. The response time can be defined as the time elapsed from a change in the conditions at the inlet of the capillary tube inside the membrane cell till that change can be measured at the outlet of the capillary tube. The response time has been experimentally measured at different sampling velocities[2] by measuring the conductivity in the sample drawn from the membrane cell when the feed changed from water to 1 M magnesium chloride. The results are shown in Figure 9.7, where graph (a) shows two examples of the measured conductivity as a function of elapsed time after the change in feed, whereas graph (b) shows the response time as function of the sampling velocity. The response time increases almost exponentially with decreasing sampling velocities.

[2]The sampling velocity is given as drops/minute which is an appropriate number to control in the laboratory. One drop/minute equals a linear velocity of 4.1 mm/s.

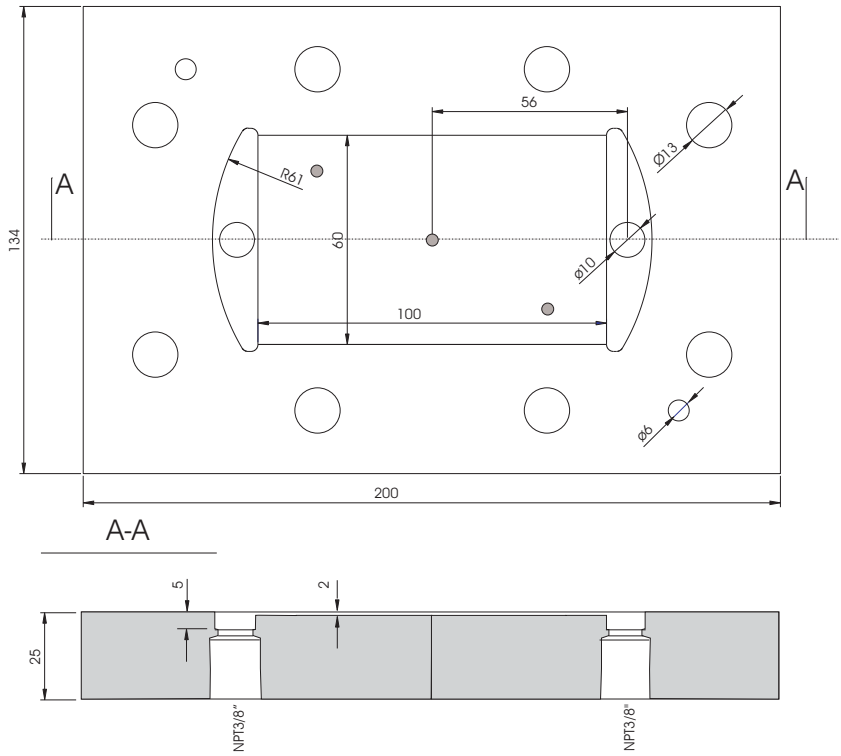

Figure 9.4: The top plate of the cross-flow flat-sheet membrane cell. The position of the three capillary tubes are shown as shaded dots. All lengths in mm.

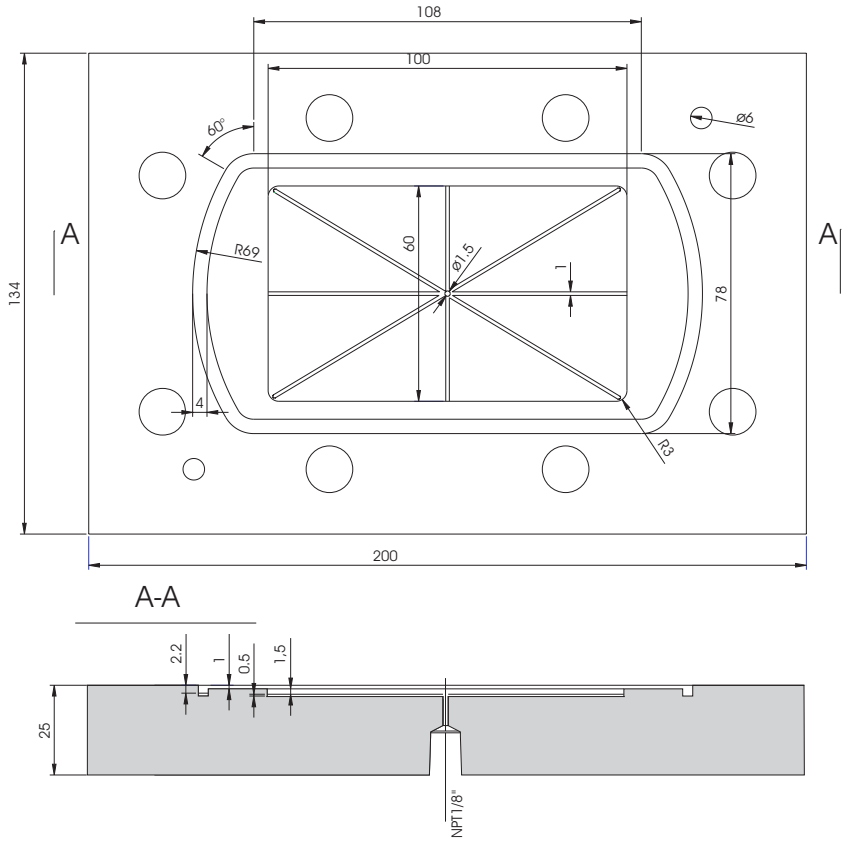

Figure 9.5: The bottom plate of the cross-flow flat-sheet membrane cell. All lengths in mm.

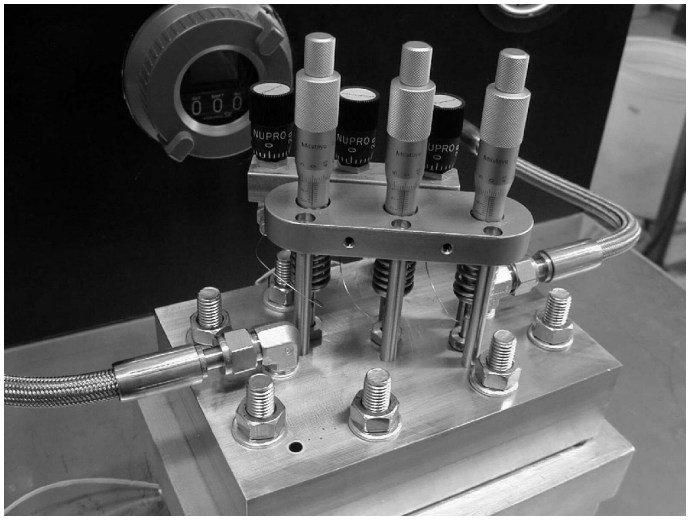

Figure 9.6: Top view of the cross-flow flat-sheet membrane cell showing the concentration polarisation measuring device consisting of three micrometer screws (in front) and three micro valves (back) mounted on the membrane cell top plate.

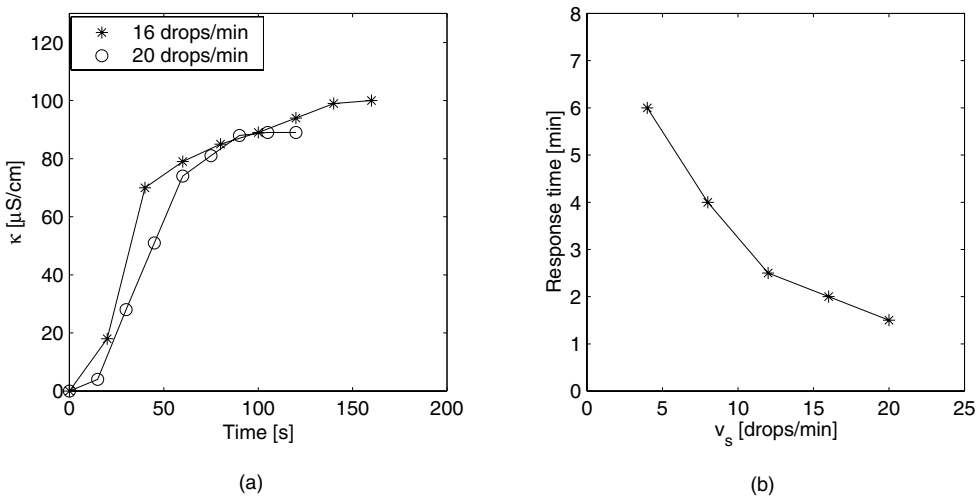

Figure 9.7: (a) The measured conductivity is plotted as a function of elapsed time after a change in the feed for two different sampling velocities. (b) The response time is plotted as a function of the sampling velocity.

9.4.3 Experimental conditions and procedure

The experiments were carried out on a NF-45 membrane from Danish Separation Systems, using a 0.1 M magnesium chloride solution, temperature 20 degrees Celsius and pressure 20 bar unless otherwise stated. At these conditions an average flux of $1.72 \cdot 10^{-5}$ m/s and approximately 80% retention were measured.

Unless otherwise stated, the center capillary tube and a sampling velocity of 4 drops/minute were used during the concentration polarisation measurements. The capillary tube was adjusted and solution was drawn through the capillary tube at the sampling velocity 4 drops/minute in a period of time equal to the response time which at a sampling velocity of 4 drops/minute equals 6 minutes. Then 5 or 10 drops of sample were collected, weighted and diluted with 10 grams of deionized water, before the conductivity was measured and the concentration in the diluted solution was determined from a calibration curve. Finally, the concentration in the sample was calculated.

The normal procedure was to start measuring the concentration in the middle of the cell (1.5 mm from the membrane surface), and then approach the membrane surface measuring the concentration at different positions. In some cases the experiment proceeded after reaching the membrane surface by also measuring the concentration when the distance from the membrane was increasing.

The magnesium chloride concentration was usually determined by measuring the conductivity by a conductivity meter (712 Conductometer, Metrohm, uncertainty $\pm 1\%$), and then determine the concentration from a calibration curve. In one experiment the magnesium ion concentration was measured with atomic absorption spectroscopy (Varian apparatus, model 400). The accuracy of the magnesium concentration analysis was found to be better than 1%. SINTEF Inorganic Process Chemistry and Analysis performed the atomic absorption spectroscopy measurements.

9.5 Results and discussion

9.5.1 Experimentally measured concentration profiles

Two concentration profiles are shown in Figure 9.8 for Reynolds number 1065, pressure 20 bar and temperature 20 degrees Celsius. Actually they are from the same measurements but the samples were diluted and split in two parallels, where the concentration in the first parallel was determined by conductivity measurements and the second parallel by atomic absorption spectroscopy. The two profiles follow the same pattern, but there is a shift in the concentration level. The ratio between the measured concentrations by conductivity and atomic absorption spectroscopy is constant and equals 1.10 ± 0.01. Since it is the relative concentration difference between the bulk and positions near the membrane surface that is of interest and the two methods measure the same relative concentrations, the rest of the concentrations were determined by conductivity measurements.

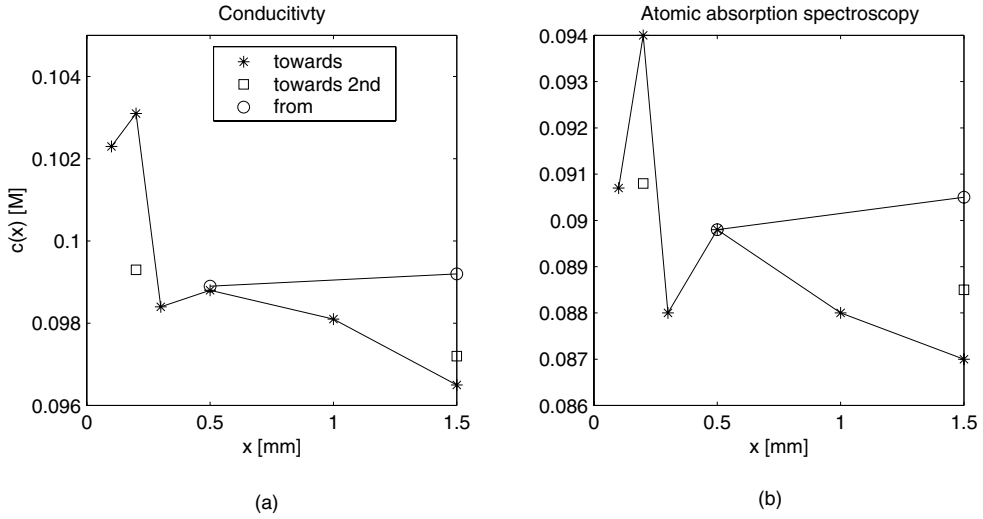

Figure 9.8: The concentration profile plotted as a function of the distance from the membrane; (a) shows the result when the concentration was determined by conductivity measurements, while (b) shows the result when the concentration was determined by atomic absorption spectroscopy. The process variables were Reynolds number 1065, pressure 20 bar and temperature 20 degrees Celsius and the samples were drawn from the center capillary tube.

Figure 9.8 also shows the results from two different samples drawn in succession for analysis at two different heights above the membrane. The measured concentrations at distance 1.5 mm from the surface are within the limits of uncertainties, whereas the difference in concentrations at distance 0.2 mm from the surface is too large to be explained by the uncertainty in the concentration measurements. There could be an experimental error in the dilution of the second sample at this position.

A decrease in the measured concentration profile near the membrane surface is observed in several experiments and can also be seen in Figure 9.8. The phenomenon occurs when measuring the concentration at positions around 0.07-0.1 mm from the membrane surface, and a possible explanation can be in the hydro dynamical flow pattern around the capillary tube as discussed below.

The results obtained for the center tube and at four different Reynolds numbers are given in Figure 9.9. For Reynolds number 1083, the samples were drawn for analysis both when the capillary tube was adjusted towards and from the membrane, and the circles in the figure indicate the average concentration at that position from the membrane. The concentration profiles at all Reynolds numbers shows a characteristic jump down around 0.3-0.4 mm from the membrane just after the concentration started to increase.

Figure 9.10 shows profiles obtained at all three capillary tubes at the same time. Two different sampling velocities have been applied at Reynolds number 1065, whereas the other experimental conditions are the same as before. There are small differences between the profiles taken from different positions along the flow direction over the membrane, indicating that the profile should be fully developed already 20 mm from the inlet. Another interpretation of the result is that the presence of the capillary tube inside the boundary layer disturbs the profile and acts as a turbulence promoter and make all three profiles equal.

The average concentration in the bulk was calculated from the three concentration measurements at positions 1.5, 1.0 and 0.5 mm from the membrane surface. From this average a dimensionless concentration profile can be calculated and the profiles for the different Reynolds numbers given in Figure 9.9 can be compared. The dimensionless concentration profiles are given in Figure 9.11, and as can be seen all four profiles follow the same pattern. The lowest Reynolds number has a very low concentration at 0.05 mm from the membrane surface, but the three other concentrations measured at this position increase with decreasing Reynolds number. The latter pattern is expected since higher Reynolds number

means more turbulent flow with more mixing of the solution causing a lower concentration polarisation.

The relative concentration polarisation measured at Reynolds number 630 is lower than the other concentration polarisations at higher Reynolds number. From the discussion above a lower Reynolds number should give a higher concentration polarisation, and this deviation between theory and experiment can be explained by calculating the ratio between sampling velocity and fluid velocity at that particular position in the boundary layer. In Figure 9.11 the change in the concentration starts approximately at position 0.5 mm from the membrane surface and the fluid velocity in the boundary layer can be estimated by a linear velocity profile between the bulk value and position 0.5 mm from the membrane surface and zero velocity at the membrane surface. The ratio between the sampling velocity and the fluid velocity at position 0.05 mm from the membrane then becomes 1.5 for the Reynolds number 630, 0.8 for the Reynolds number 1083 (1065), 0.6 for the Reynolds number 1559 and 0.2 for the Reynolds number 4267. Since none of the ratios are less than 1/10 all the concentration profiles are expected to be underestimated, and this underestimation is worse for the case at the lowest Reynolds number where the suction from the capillary tube should be noticeable.

When increasing the Reynolds number a thinner concentration boundary layer is expected due to the increased mixing effect. There are not observed any significant difference in the concentration boundary layer for the three cases of laminar flows in Figure 9.11 (or Figure 9.9). The increase in concentration starts around 0.45-0.50 mm from the membrane surface. A small decrease in this concentration boundary layer can be observed when the flow is turbulent, where the thickness of the layer becomes approximately 0.3 mm.

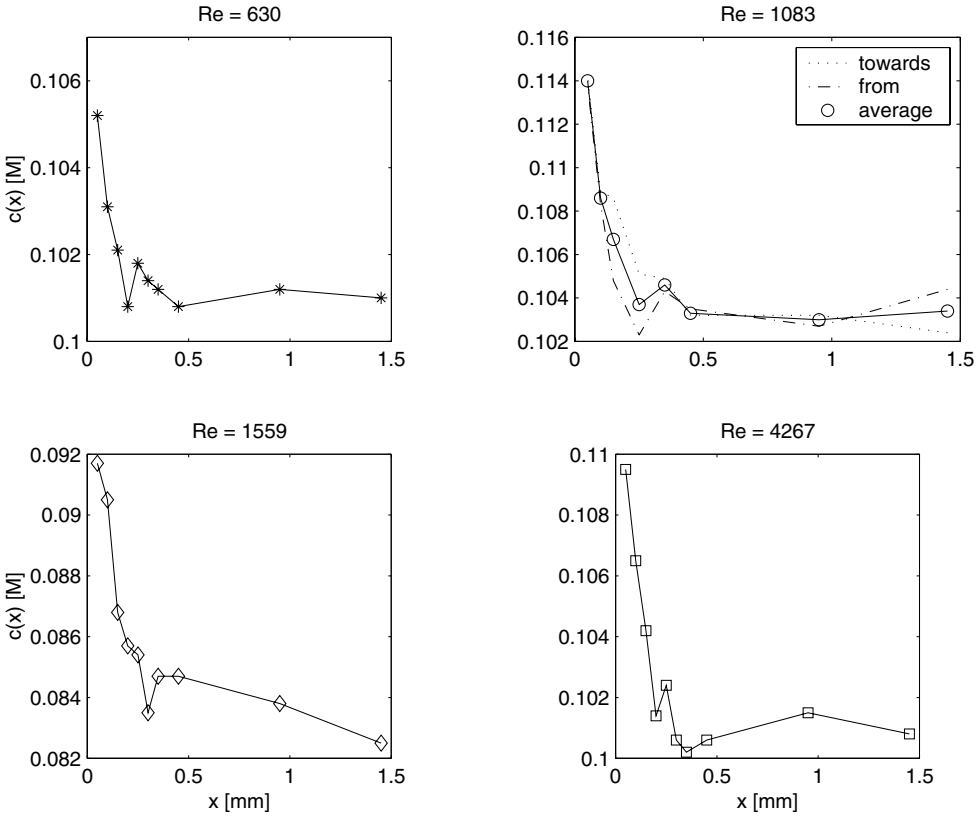

Figure 9.9: The concentration profile plotted as a function of the distance from the membrane at four different Reynolds number. The pressure was 20 bar, the temperature was 20 degrees Celsius and the samples were drawn from the center capillary tube.

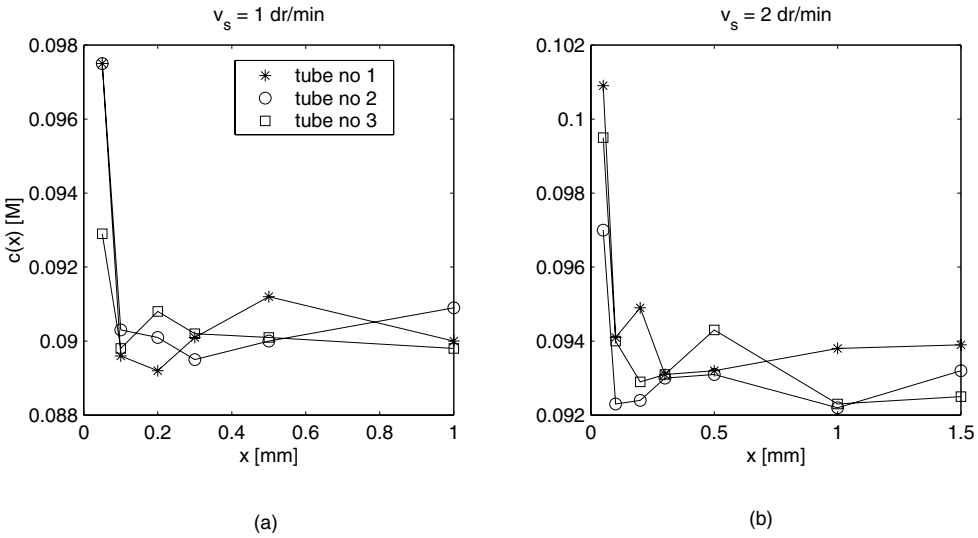

Figure 9.10: The concentration profile plotted as a function of the distance from the membrane; (a) shows the result when the sampling velocity was 1 drop/minute, while (b) shows the result when the sampling velocity was 2 drops/minute. The pressure was 20 bar, the temperature was 20 degrees Celsius and the Reynolds number was 1065. Capillary tube no 1 is located closest to the entrance to the membrane cell, no 2 is the center tube and no 3 are the capillary tube closest to the exit.

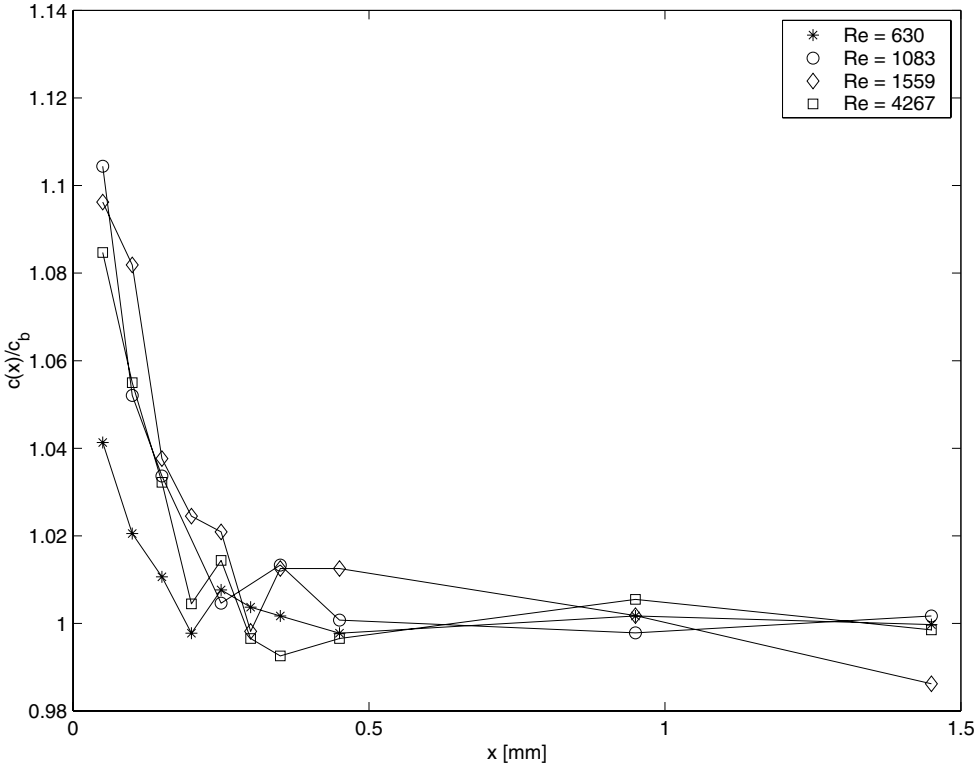

Figure 9.11: The dimensionless concentration profile plotted as a function of the distance from the membrane surface for various Reynolds numbers calculated using the average of the three concentrations at 0.5, 1.0 and 1.5 mm from the membrane surface as the bulk concentration. The pressure was 20 bar and the temperature was 20 degrees Celsius.

9.5.2 Experimental results versus the film model and literature data

The concentration profiles in Figures 9.9 and 9.10 can be used to estimate the concentration at the membrane surface by fitting the data points to a 2nd order polynom and extrapolate to zero distance. The calculated concentration polarisation modulus for different Reynolds numbers are given in Table 9.1 together with the results calculated using the film model (Equation 9.1). As can be seen from the table the experimental results underestimate the concentration polarisation modulus compared with the film model. This result is in accordance to the statement in the previous subsection, and the reasons are probably hidden in the hydrodynamic flow pattern around the capillary tube.

Table 9.1: The concentration polarisation modulus calculated from both experimental concentration profiles and the film model and mass transfer coefficients calculated from both experimental results and literature correlations are shown as a function of the Reynolds number. The experimental values at Reynolds number 1065 are calculated using the concentration profile at the center tube and sampling velocity 1 drop/minute (refer Figure 9.10).

Re	$(C_m/C_b)_{\text{exp}}$	$(C_m/C_b)_{\text{film}}$	$k_{\text{exp}}10^5$ [m/s]	$k_{\text{corr}}10^5$ [m/s]
630	1.07	3.93	1.96	2.15
1065	1.13	3.27	1.14	2.56
1083	1.19	2.77	0.69	2.57
1559	1.13	3.17	1.26	2.90
4267	1.13	1.51	1.24	3.77

Since the concentration polarisation calculated using the film model depends heavily on the mass transfer coefficient, the result can not be better than the mass transfer correlation used. Correlations are often based on experiments under special conditions, and when these correlations are used on other systems large uncertainties may be introduced. In membrane separations corrections to account for the change in viscosity due to higher concentration at the membrane surface and membrane surface roughness has been suggested (Gekas and Hallstrøm 1987). Other factors that have been discussed are the membrane porosity and the flux. In some cases it has been found that the porosity of the membrane stabilizes the laminar flow and onsets the turbulent region to a Reynolds number around 4000 and enhances the mass transfer coefficients (Gekas and Hallstrøm 1987). A larger mass transfer coefficient would give a smaller concentration polarisation

modulus calculated from the film model and give a smaller deviation between the experimental results and the model. If the mass transfer coefficient is doubled the calculated concentration polarisation modulus from the film model becomes 1.77 for Reynolds number 1065.

Dytnerskij *et al.* (1987) have used an optical method to measure the concentration polarisation in sodium chloride solutions. At 25 bar, 20 degrees Celsius and 0.1 M concentration they found a concentration polarisation modulus between 1.2 and 1.4 depending on the Reynolds number comparable with the results at Reynolds number 630, 1065 and 1083. Geraldes *et al.* (2000) have used a numerical model to predict the concentration polarisation in nanofiltration systems and tested the model on experimental results. For a 0.034 M sodium chloride solution at 20 bar, 25 degrees Celsius, and Reynolds number 1000, which gave a permeation velocity of the same order as the one used in this study, the calculated concentration polarisation modulus became 1.4.

The concentration boundary layer can be calculated through the relationship with the mass transfer coefficient and the diffusion coefficient, $k = D/\delta_c$. Table 9.1 shows both the mass transfer coefficient calculated from the experimental results and the film model and the mass transfer coefficient calculated from the correlations given in Equation 9.3 or Equation 9.4. The two mass transfer coefficients differ by an order of magnitude and give concentration boundary layer thicknesses between 0.005-0.01 mm and 0.02-0.05 mm, respectively. These values are much lower than the concentration boundary layer thicknesses found experimentally from the concentration profiles given in the previous section. If the concentrations near the membrane surface are assumed to be underestimated by the experimental method, increasing the estimated surface concentration would give a thicker calculated concentration boundary layer which is closer to the experimentally found values.

After the work by Blasius the hydro dynamical boundary layer can be approximated by (Geankoplis 1993)

$$\delta = 5.0\sqrt{\frac{\eta x}{\rho v_\infty}} \qquad \text{laminar} \tag{9.6}$$

$$\delta = 0.376\left(\frac{L v_\infty \rho}{\eta}\right)^{-1/5} \qquad \text{turbulent} \tag{9.7}$$

where η is the viscosity, ρ is the density, x is the position relative to the inlet, v_∞ is the fluid velocity in the bulk region and L is the length of the membrane cell. When the hydro dynamical boundary layer is known the concentration boundary

layer can be calculated by the approximation (Rautenbach and Albrecht 1989)

$$\frac{\delta_c}{\delta} = Sc^{-1/3} \tag{9.8}$$

which is valid for a third order concentration profile. Using these approximations, the hydro dynamical boundary layer in laminar flow becomes 3.4 mm, and with a Schmidt number equal to 1000, the concentration boundary layer is approximately 0.34 mm. In turbulent flow the calculated hydro dynamical boundary layer is 2.3 mm, which gives a concentration boundary layer of 0.23 mm. These concentration boundary layers are in good agreement with the experimentally found values which are 0.45 mm for laminar flow and 0.3 mm for turbulent flow.

Geraldes *et al.* (2000) have used a numerical method to calculate the concentration polarisation in nanofiltration and takes into account the mass transfer, hydrodynamics and the permeation and accumulation at the membrane surface. For typical nanofiltration conditions and laminar flow their calculated concentration boundary layer thicknesses are between 0.3-0.45 mm.

9.5.3 Problems with the new method

As emphasized before, the main problem with the method can be related to the probe and its ability to work as a turbulence promoter. Therefore, before the method can be used to map the concentration polarisation in different environments, a thorough study of the hydrodynamic behavior around a capillary tube with suction should be done.

The exact position of the probe in relation to the membrane surface has also been an issue for discussion. It has been shown that the position of the probes change due to different tightening of the cell, different membrane thicknesses and applied pressure.

9.6 Conclusions

A new method to measure the concentration polarisation in membrane separation has been developed, and the principles of the method, results and problems are discussed. The main idea of the method is that a capillary tube which can be positioned vertically with an accuracy of 1/100 mm, draw small samples from the concentration boundary layer for analysis. This gives the opportunity to measure the concentration polarisation for complex and multi component solutions.

Experimental results are in qualitative agreement with results from the film theory, *i.e.* the concentration polarisation decreases with increasing Reynolds number. The experimental results are not in quantitative agreement with the expected results from the film theory.

The lack of quantitative agreement can be caused by several factors. The most important disadvantage of the method is due to the capillary tube itself, since it may act as a turbulence promoter in the boundary layer and give a lower concentration at the membrane surface. Another question is the accuracy of the estimated mass transfer coefficient.

Before the method is used in a more systematic way to determine concentration polarisation data, a thorough study of the hydrodynamic flow and flow pattern around the capillary tube inside the boundary layer should be completed.

Bibliography

Afonso, M.D. and M.N. de Pinho (2000). Transport of $MgSO_4$, $MgCl_2$ and $NaSO_4$ across an amphoteric nanofiltration membrane. *J. Membr. Sci.* **179**, 137–154.

Agrawal, J.P. and S. Sourirajan (1969). Specification, selectivity, and performance of porous cellulose acetate membranes in reverse osmosis. *I & E C Proc. Des. & Dev.* **8**, 439–449.

Agrawal, J.P. and S. Sourirajan (1970). Reverse osmosis separation of some inorganic salts in aqueous solution containing mixed solutes with a common ion. *I & E C Proc. Des. & Dev.* **9**, 12–18.

Aitkuliev, K., V.D. Sobolev and N.V. Churaev (1984). Influence of the flow rate and concentration of the electrolyte on the selectivity of reverse-osmosis membranes. *Colloid J. USSR* **46**, 179–184.

Applegate, L.E. and C.R. Antonson (1972). The phenomenological characterization of DP-1 membranes. In: *Reverse osmosis membrane research* (H.K. Lonsdale and H.E. Podall, Eds.). pp. 243–252. Plenum Press. New York.

Bader, M.S.H. and P.A. Jennings (1992). Concentration polarization phenomena in turbulent flow: Review and modification. *J. Environ. Sci. Health* **27**, 463–483.

Banks, W. and A. Sharples (1966). Studies on desalination by reverse osmosis III. Mechanism of solute rejection. *J. Appl. Chem.* **16**, 153–158.

Bean, C.P. (1972). The physics of porous membranes - neutral pores. In: *Membranes, a series of advances* (G. Eisenman, Ed.). Vol. 1. pp. 1–54. Marcel Dekker. New York.

Belfort, G. (1976). A molecular friction model for transport of uncharged solutes in neutral hyperfiltration and ultrafiltration membranes containing bound water. *Desalination* **18**, 259–281.

Benavente, J. and G. Jonsson (1993). Transport of Na_2SO_4 and $MgSO_4$ solutions through a composite membrane. *J. Membr. Sci.* **80**, 275–283.

Berezkin, V.V., A.N. Nechaev, S.V. Fomichev, B.V. Mchedlishvili and N.I. Zhitaryuk (1991). Nuclear filters with ion-selective properties. *Colloid J. USSR* **53**, 292–295.

Bingham, E.C. (1941). Fluidity of electrolytes. *J. Phys. Chem.* **45**, 885–903.

Bird, R.B., W.E. Stewart and E.W. Lightfoot (1960). *Transport phenomena*. John Wiley & Sons. New York.

Bockris, J.O'M. and P.P.S. Saluja (1972). Ionic solvation numbers from compressibilities and ionic vibration potential measurements. *J. Phys. Chem.* **76**, 2140–2151.

Boesen, C.E. and G. Jonsson (1978). Solute-solute interactions by reverse osmosis of three component solutions. In: *Proceedings of the 6th International Symposium of Fresh Water from the Sea*. Vol. 3. pp. 157–164.

Bollenbeck, P.H. and W.F. Ramirez (1974). Use of a Rayleigh interferometer for membrane transport studies. *Ind. Eng. Chem. Fundam.* **13**, 385–393.

Bontha, J.R. and P.N. Pintauro (1994). Water orientation and ion solvation effects during multicomponent salt partitioning in a Nafion cation exchange membrane. *Chem. Eng. Sci.* **49**, 3835–3851.

Bowen, W.R. and A.W. Mohammad (1998*a*). Characterization and prediction of nanofiltration membrane performance: A general assessment. *Trans. IChemE.* **76**, 885–893.

Bowen, W.R. and A.W. Mohammad (1998*b*). Diafiltration by nanofiltration: Prediction and optimization. *AIChE J.* **44**, 1799–1812.

Bowen, W.R. and H. Mukhtar (1996). Characterization and prediction of separation performance of nanofiltration membranes. *J. Membr. Sci.* **112**, 263–274.

Bowen, W.R., A.W. Mohammad and N. Hilal (1997). Characterization of nanofiltration membranes for predictive purposes: Use of salts, uncharged solutes and atomic force microscopy. *J. Membr. Sci.* **126**, 91–105.

Brian, P.L.T. (1965). Concentration polarization in reverse osmosis desalination with variable flux and incomplete salt rejection. *Ind. Eng. Chem. Fundam.* **4**, 439–445.

Brian, P.L.T (1966). Mass transport in reverse osmosis. In: *Desalination by reverse osmosis* (U. Merten, Ed.). pp. 161–202. MIT Press. Cambridge.

Burgess, J. (1988). *Ions in Solution.* Ellis Horwood Limited. Chichester.

Chialvo, A.A., P.T. Cummings, J.M. Simonson, R.E. Mesmer and H.D. Cochran (1998). Interplay between molecular simulation and neutron scattering in developing new insights into the structure of water. *Ind. Eng. Chem. Res.* **37**, 3021–3025.

Comstock, D.L. (1989). Desal-5 membrane for water softening. *Desalination* **76**, 61–72.

Conway, B.E. (1977). The state of water and hydrated ions at interfaces. *Adv. Colloid Interface Sci.* **8**, 91–211.

Conway, B.E. (1981). *Ionic Hydration in Chemistry and Biophysics.* Elsevier. New York.

Deen, W.M. (1987). Hindered transport of large molecules in liquid-filled pores. *AIChE J.* **33**, 1409–1425.

Dey, T.K., V. Ramachandhran and B.M. Misra (2000). Selectivity of anionic species in binary mixed electrolyte systems for nanofiltration membranes. *Desalination* **127**, 165–175.

Dickson, J.M., T. Matsuura, P. Blais and S. Sourirajan (1975). Reverse osmosis separations of some organic and inorganic solutes in aqueous solutions using aromatic polyamide membranes. *J. Appl. Polym. Sci.* **19**, 801–819.

Dickson, J.M., T. Matsuura, P. Blais and S. Sourirajan (1976). Some transport characteristics of aromatic polyamide membranes in reverse osmosis. *J. Appl. Polym. Sci.* **20**, 1491–1499.

Dresner, L. (1972). Some remarks on the integration of the extended Nernst-Planck equation in the hyperfiltration of multicomponent solutions. *Desalination* **10**, 27–46.

Dresner, L. (1974). Ion exclusion from neutral and slightly charged pores. *Desalination* **15**, 39–57.

Dytnerskii, Y.N., G.V. Polyakov and L.S. Lukavyi (1972). The mechanism of separating aqueous salt solutions by reverse osmosis. *Theor. Found. Chem. Eng.* **6**, 565–568.

Dytnerskij, J.J., J.A. Dmitrijev, I.A. Scerev, P. Lutzsch and E. Weiss (1987). Eine optische Methode zur Untersuchung der Konzentrationspolarisation bei der Trenung von Salzlösungen durch Umkerosmose. *Chem. Techn.* **39**, 302–305.

Ernst, M., A. Bismarck, J. Springer and M. Jekel (2000). Zeta-potential and rejection rates of a polyethersulfone nanofiltration membrane in single salt solutions. *J. Membr. Sci.* **165**, 251–259.

Frank, H.S. and A.L. Robinson (1940). The entropy of dilution of strong electrolytes in aqueous solutions. *J. Chem. Phys.* **8**, 933–938.

Frank, H.S. and M.W. Evans (1945). Free volume and entropy in condensed systems. III. Entropy in binary liquid mixtures; partial molal entropy in dilute solutions; structure and thermodynamics in aqueous electrolytes. *J. Chem. Phys.* **13**, 507–532.

Frank, H.S. and W.-Y. Wen (1957). III. Ion-solvent interaction. Structural aspects of ion-solvent interaction in aqueous solutions: A suggested picture of water structure. *Disc. Faraday Soc.* **24**, 133–140.

Freger, V., T.C. Arnot and J.A. Howell (2000). Separation of concentrated organic/inorganic salt mixtures by nanofiltration. *J. Membr. Sci.* **178**, 185–193.

Friebe, A. and W. Moritz (1994). Influence of electrolyte on electrical properties of thin cellulose acetate membranes. *J. Appl. Polym. Sci.* **51**, 625–634.

Galey, W.R. and J.T. van Bruggen (1970). The coupling of solute fluxes in membranes. *J. Gen. Physiol.* **55**, 220–242.

Geankoplis, C.J. (1993). *Transport Processes and Unit Operations.* 3rd ed. Prentice-Hall International, Inc. London.

Gekas, V. and B. Hallstrøm (1987). Mass transfer in the membrane concentration polarization layer under turbulent cross flow. 1. Critical literature review and adaption of existing Sherwood correlations to membrane operations. *J. Membr. Sci.* **30**, 153–170.

Geraldes, V.M., V.A. Semiao and M.N. de Pinho (2000). Numerical modelling of mass transfer in slits with semi-permeable membrane walls. *Engineering Computations* **17**, 192–217.

Glueckauf, E. (1967). On the mechanism of osmotic desalting with porous membranes. In: *Proceedings of the First International Symposium on Water Desalination, Washington, DC, 1965.* Vol. 1. pp. 143–156.

Glueckauf, E. (1976). The distribution of electrolytes between cellulose acetate membranes and aqueous solutions. *Desalination* **18**, 155–172.

Govindan, T.S. and S. Sourirajan (1966). Reverse osmosis separation of some inorganic salts in aqueous solution using porous cellulose acetate membranes. *I & E C Proc. Des. & Dev.* **5**, 422–429.

Gurney, R.W. (1960). *Ionic Processes in Solution.* Dover Publications, Inc. New York.

Haase, R. (1969). *Thermodynamics of Irreversible Processes.* Dover Publications, Inc. New York.

Hagmeyer, G. and R. Gimbel (1998). Modelling the salt rejection of nanofiltration membranes for ternary ion mixtures and for single salts at different pH values. *Desalination* **117**, 247–256.

Hagmeyer, G. and R. Gimbel (1999). Modelling the rejection of nanofiltration membranes using zeta potential measurements. *Sep. Purif. Technol.* **15**, 19–30.

Hanai, T., K. Zhao and K. Asami (1993). Theoretical approach and the practice to the evaluation of structural parameters characterizing concentration polarization alongside ion-exchange membranes by means of dielectric measurement. *Colloid Polym. Sci.* **271**, 766–773.

Harvie, C.E., N. Møller and J.H. Weare (1984). The prediction of mineral solubilities in natural waters: The Na-K-Mg-Ca-H-Cl-SO_4-OH-HCO_3-CO_3-H_2O system to high ionic strenghts at 25^oC. *Geochim. Cosmochim. Acta* **48**, 723–751.

Hasted, J.B., D.M. Ritson and C.H. Collie (1948). Dielectric properties of aqueous ionic solutions. *J. Chem. Phys.* **16**, 1–21.

Hendricks, T.J. and F.A. Williams (1971). Diffusion-layer structure in reverse osmosis channel flow. *Desalination* **9**, 155–180.

Heyde, M.E., C.R. Peters and J.E. Anderson (1975). Factors influencing reverse osmosis rejection of inorganic solutes from aqueous solution. *J. Colloid Interface Sci.* **50**, 467–487.

Higa, M., A. Tanioka and K. Miyasaka (1990). A study of ion permeation across a charged membrane in multicomponent ion systems as a function of membrane charge density. *J. Membr. Sci.* **49**, 145–169.

Higa, M., A. Tanioka and K. Miyasaka (1991). An experimental study of ion permeation in multicomponent ion systems as a function of membrane charge density. *J. Membr. Sci.* **64**, 255–262.

Hodgson, T.D. (1970). Selective properties of cellulose acetate membranes towards ions in aqueous solutions. *Desalination* **8**, 99–138.

Hunter, R.J. (1981). *Zeta potential in colloid science: Principles and Applications.* Academic Press. London.

Jagur-Grodzinski, J. and O. Kedem (1966). Transport coefficients and salt rejection in uncharged hyperfiltration membranes. *Desalination* **1**, 327–341.

Johnson, A.R. (1974). Experimental investigation of polarization effects in reverse osmosis. *AIChE J.* **20**, 966–974.

Johnson, R.A. and D.W. Wichern (1992). *Applied Multivariate Statistical Analysis.* Prentice-Hall International, Inc. London.

Jonsson, G. and C.E. Boesen (1975). Water and solute transport through cellulose acetate reverse osmosis membranes. *Desalination* **17**, 145–165.

Jonsson, G. and C.E. Boesen (1977). Concentration polarization in a reverse osmosis test cell. *Desalination* **21**, 1–10.

Jonsson, G. and C.E. Boesen (1984). Polarization phenomena in membrane processes. In: *Synthetic Membrane Processes* (G. Belfort, Ed.). pp. 101–130. Academic Press, Inc. Orlando.

Jonsson, G. and J. Benavente (1992). Determination of some transport coefficients for the skin and porous layer of a composite membrane. *J. Membr. Sci.* **69**, 29–42.

Kaminsky, M. (1957). Ion-solvent interaction and the viscosity of strong-electrolyte solutions. *Disc. Faraday Soc.* **24**, 171–179.

Kapur, D.N. and N. Macleod (1975). Holographic determination of local mass transfer coefficients at a solid-liquid boundary. *AIChE J.* **21**, 184–187.

Kargol, A. (2000). Modified Kedem-Katchalsky equations and their applications. *J. Membr. Sci.* **174**, 43–53.

Kedem, O. and A. Katchalsky (1958). Thermodynamic analysis of the permeability of biological membranes to non-electrolytes. *Biochim. Biophys. Acta* **27**, 229–246.

Kedem, O. and A. Katchalsky (1963). Permeability of composite membranes. I. Electric current, volume flow and flow of solute through membranes. *Trans. Faraday Soc.* **59**, 1918–1930.

Kimura, S. and S. Sourirajan (1967). Analysis of data in reverse osmosis with porous cellulose acetate membranes used. *AIChE J.* **13**, 497–503.

Kornyshev, A.A., G.I. Tsitsuashvili and A.E. Yaroshchuk (1989). Effects of polar solvent structure in the theory of dielectric exclusion of ions from polymer membrane pores: Formulation of the problem, calculation of potential. *Soviet Electrochemistry* **25**, 923–931.

Krasne, S. and G. Eisenman (1973). The molecular basis of ion selectivity. In: *Membranes, a series of advances* (G. Eisenman, Ed.). Vol. 2. pp. 277–328. Marcel Dekker. New York.

Krishna, R. and J.A. Wesselingh (1997). The Maxwell-Stefan approach to mass transfer. *Chem. Eng. Sci.* **52**, 861–911.

Laidler, K.J. and J.H. Meiser (1982). *Physical Chemistry.* The Benjamin/Cummings Publishing Company, Inc. London.

Lakshminarayanaiah, N. (1969). *Transport phenomena in membranes.* Academic Press. New York.

Lide, D.R. (1990). *Handbook of Chemistry and Physics.* 71st ed. CRC Press. Boca Raton.

Lin, C.S., R.W. Moulton and G.L. Putnam (1953). Interferometric measurements of concentration profiles in turbulent and streamline flow. *Ind. Engng. Chem.* **45**, 640–646.

Liu, M.K. and F.A. Williams (1970). Concentration polarization in an unstirred batch cell: Measurments and comparison with theory. *Int. J. Heat Mass Transfer.* **13**, 1441–1457.

Lobo, V.M.M. and J.L. Quaresma (1989). *Handbook of electrolyte solutions.* Elsevier. New York.

Loeb, S. and S. Sourirajan (1962). Sea water demineralization by means of osmotic membranes. *Adv. Chem. Ser.* **38**, 117.

Loehe, J.R. and M.D. Donohue (1997). Recent advances in modeling thermodynamic properties of aqueous strong electrolyte systems. *AIChE J.* **43**, 180–195.

Lonsdale, H.K., U. Merten and R.L. Riley (1965). Transport properties of cellulose acetate osmotic membranes. *J. Appl. Polym. Sci.* **9**, 1341–1362.

Lonsdale, H.K., W. Push and A. Walch (1974). Donnan-membrane effects in hyperfiltration of ternary systems. *J. Chem. Soc. Faraday Trans. I* **71**, 501–514.

Luck, W.A.P. (1984). Structure of water and aqueous systems. In: *Synthetic Membrane Processes* (G. Belfort, Ed.). pp. 21–72. Academic Press, Inc. Orlando.

Mahlab, D., N.B. Yosef and G. Belfort (1978). Concentration polarization profile for dissolved species in unstirred batch hyperfiltration (reverse osmosis) - II Transient case. *Desalination* **24**, 297–303.

Mänttäri, M. (1999). Fouling management and retention in nanofiltration of integrated paper mill effluents. PhD thesis. Lappeenranta University of Technology, Finland.

Marcus, Y. (1997). *Ion Properties.* Marcel Dekker, Inc. New York.

Mariñas, B.J. and R.E. Selleck (1992). Reverse osmosis treatment of multicomponent electrolyte solutions. *J. Membr. Sci.* **72**, 211–229.

Martens, H. and T. Næs (1989). *Multivariate calibration.* John Wiley and Sons. Chichester.

Merten, U. (1966). *Desalination by reverse osmosis.* MIT Press. Cambridge.

Meyer, K.H. and J.-F. Sievers (1936). La perméabilité des membranes. I. Théorie de la perméabilité ionique. *Helv. Chim. Acta* **19**, 649–664.

Millero, F.J. (2001). *Physical chemistry of natural waters.* Wiley Interscience. New York.

Millero, F.J., R.J. Ricco and D.R. Schreiber (1982). PVT properties of concentrated aqueous electrolytes. II. Compressibilities and apparent molar compressibilities of aqueous NaCl, Na_2SO_4, $MgCl_2$ and $MgSO_4$ from dilute solution to saturation and from 0 to 50 ^{o}C. *J. Solution Chem.* **11**, 671–686.

Min, B.R. and K.B. Im (1990). The energy of an ion in a cylindrical pore of a low dielectric membrane. *J. Membr. Sci.* **52**, 89–95.

Mørk, P.C. (1994). *Overflate og Kolloidkjemi.* 4th ed. Tapir. Trondheim.

Morrison, F.A. and J.F. Osterle (1965). Electrokinetic energy conversion in ultrafine capillaries. *J. Chem. Phys.* **43**, 2111–2115.

Mulder, M. (1996). *Basic Principles of Membrane Technology.* 2nd ed. Kluwer Academic Publishers. Dordrecht.

Narten, A.H., M.D. Danford and H.A. Levy (1967). X-ray diffraction study of liquid water in the temperature range 4-200 degrees Celsius. *Disc. Faraday Soc.* **43**, 97–107.

Nystrøm, M., L. Kaipia and S. Luque (1995). Fouling and retention of nanofiltration membranes. *J. Membr. Sci.* **98**, 249–262.

Nystrøm, M., M. Lindstrøm and E. Matthiasson (1989). Streaming potential as a tool in the characterization of ultrafiltration membranes. *Colloid Surf.* **36**, 297–312.

Onsager, L. (1931a). Reciprocal relations in irreversible processes, part I. *Phys. Rev.* **37**, 405–425.

Onsager, L. (1931b). Reciprocal relations in irreversible processes, part II. *Phys. Rev.* **38**, 2265–2279.

Orofino, T.A., H.B. Hopfenberg and V. Stannett (1969). Charaterization of penetrant clustering in polymers. *J. Macromol. Sci. Phys.* **B3**, 777–788.

Pabalan, R.T. and K.S. Pitzer (1987). Thermodynamics of concentrated electrolyte mixtures and the prediction of mineral solubilities to high temperatures for mixtures in the system Na-K-Mg-Cl-SO_4-OH-H_2O. *Geochim. Cosmochim. Acta* **51**, 2429–2443.

Palacio, L., J.I. Calvo, P. Prádanos, A. Hernández, P. Väisänen and M. Nystrøm (1999). Contact angles and external protein adsorption onto UF membranes. *J. Membr. Sci.* **152**, 189–201.

Parsegian, A. (1969). Energy of an ion crossing a low dieletric membrane: Solutions to four relevant electrostatic problems. *Nature* **221**, 844–846.

Peeters, J.M.M., J.P. Boom, M.H.V. Mulder and H. Strathmann (1998). Retention measurements of nanofiltration membranes with electrolyte solutions. *J. Membr. Sci.* **145**, 199–209.

Petersen, R.J. (1993). Composite reverse osmosis and nanofiltration membranes. *J. Membr. Sci.* **83**, 81–150.

Pihlajamäki, A. (1998). Electrochemical characterisation of filter media properties and their exploitation in enhanced filtration. PhD thesis. Lappeenranta University of Technology, Finland.

Pitzer, K.S. (1973). Thermodynamics of electrolytes. I. Theoretical basis and general equations. *J. Phys. Chem.* **77**, 268–277.

Pitzer, K.S. (1975). Thermodynamics of electrolytes. V. Effects of higher-order electrostatic terms. *J. Solution Chem.* **4**, 249–265.

Pitzer, K.S. (1995). *Thermodynamics*. 3rd ed. McGraw-Hill International Editions. New York.

Pope, J.M., S. Yao and A.G. Fane (1996). Quantitative measurements of the concentration polarisation layer thickness in membrane filtration of oil-water emulsions using NMR micro-imaging. *J. Membr. Sci.* **118**, 247–257.

Prigogine, I. (1955). *Introduction to thermodynamics of irreversible processes.* Thomas Springfield. Illinois.

Pusch, W. (1977a). Determination of transport parameters of synthetic membranes by hyperfiltration experiments; Part I: Derivation of transport relationship from the linear relations of thermodynamics of irreversible processes. *Ber. Bunsenges. Phys. Chem.* **81**, 269–276.

Pusch, W. (1977b). Determination of transport parameters of synthetic membranes by hyperfiltration experiments; Part II: Membrane transport parameters independent of pressure and/or pressure difference. *Ber. Bunsenges. Phys. Chem.* **81**, 854–864.

Pusch, W. (1980). Characterization of transport across synthetic membranes for ternary and quaternary salt solutions in hyperfiltration. In: *Proceedings of the 7th International Symposium of Fresh Water from the Sea.* Vol. 2. pp. 207–223.

Ramani, M.P.S. (1992). Mass transport mechanism on the high-pressure side in reverse osmosis: An analysis. *Chem. Eng. Sci.* **47**, 4099–4105.

Rangarajan, R., T. Matsuura and S. Sourirajan (1985). Predictability of membrane performance in reverse osmosis systems involving mixed ionized solutes in aqueous solutions. In: *Reverse osmosis and ultrafiltration* (S. Sourirajan and T. Matsuura, Eds.). pp. 167–185. American Chemical Society.

Raridon, R.J., L. Dresner and K.A. Kraus (1966). Hyperfiltration studies V. Salt rejection of membranes by a concentration polarization method. *Desalination* **1**, 210–224.

Rautenbach, R. and R. Albrecht (1989). *Membrane Processes.* John Wiley & Sons. Chichester.

Reid, C.E. and E.J. Breton (1959). Water and ion flow across cellulosic membranes. *J. Appl. Poly. Sci.* **1**, 133–143.

Reid, R.C., J.M. Prausnitz and B.E. Poling (1987). *The Properties of Gases and Liquids.* 4th ed. McGraw-Hill Book Company. New York.

Sabbatovskii, K.G., V.D. Sobolev and N.D. Churaev (1993). Rejection of concentrated electrolytes by reverse osmosis membranes. *Colloid J.* **55**, 738–743.

Saracco, G. (1997). Transport properties of monovalent-ion-permselective membranes. *Chem. Eng. Sci.* **52**, 3019–3031.

Sata, T., K. Mine and M. Higa (1998). Change in permselectivity between sulfate and chloride ions through anion exchange membrane with hydrophilicity of the membrane. *J. Membr. Sci.* **141**, 137–144.

Schaep, J., B. van der Bruggen and C. Vandecasteele (2000). Ion adsorption on nanofiltration membranes. In: *Euromembrane 2000, Poster session.*

Schaep, J., B. van der Bruggen, C. Vandecasteele and D. Wilms (1998*a*). Influence of ion size and charge in nanofiltration. *Sep. Purif. Technol.* **14**, 155–162.

Schaep, J., C. Vandecasteele, A.W. Mohammad and W.R. Bowen (1999). Analysis of the salt retention of nanofiltration membranes using the Donnan-steric partitioning pore model. *Sep. Sci. Technol.* **34**, 3009–3030.

Schaep, J., C. Vandecasteele, R. Leysen and W. Doyen (1998*b*). Salt retention of Zirfon membranes. *Sep. Purif. Technol.* **14**, 127–133.

Schlögl, R. (1964). *Stofftransport durch Membranen.* Dr. Dietrich Steinkopff Verlag. Darmstadt.

Shenase, A., E. Staude and Yaroshchuk (1995). Separation of counterions during pressure-driven transport of electrolyte mixture across charged porous membranes. *Sep. Sci. Technol.* **30**, 2865–2876.

Sherwood, T.K., P.L.T. Brian and R.E. Fisher (1967). Desalination by reverse osmosis. *Ind. Eng. Chem. Fundam.* **6**, 2–12.

Sherwood, T.K., P.L.T. Brian, R.E. Fisher and L. Dresner (1965). Salt concentration at phase boundaries in desalination by reverse osmosis. *Ind. Eng. Chem. Fundam.* **4**, 113–118.

Smith, F.G. and W.M. Deen (1983). *Electrostatic Effects on the Partitioning of Spherical Colloids between Dilute Bulk Solution and Cylindrical Pores.* Vol. 91.

Soltanieh, M. and S. Sahebdelfar (2001). Interaction effects in multicomponent separation by reverse osmosis. *J. Membr. Sci.* **183**, 15–27.

Soltanieh, M. and W.N. Gill (1981). Review of reverse osmosis membranes and transport models. *Chem. Eng. Commun.* **12**, 279–363.

Sourirajan, S. (1963). The mechanism of demineralization of aqueous sodium chloride solutions by flow, under pressure, through porous membranes. *Ind. Eng. Chem. Fundam.* **2**, 51–55.

Spiegler, K.S. (1958). Transport processes in ionic membranes. *Trans. Faraday Soc.* **54**, 1409.

Spiegler, K.S. and O. Kedem (1966). Thermodynamics of hyperfiltration (reverse osmosis): Criteria for efficient membranes. *Desalination* **1**, 311–326.

Starov, V.M. and N.V. Churaev (1993). Separation of electrolyte solutions by reverse osmosis. *Adv. Colloid Interface Sci.* **43**, 145–167.

Stegen, J.H.G. van der, H. Weerdenburg, A.J. van der Veen, J.A. Hogendoorn and G.F. Versteeg (1999). Application of the Pitzer model for the estimation of activity coefficients of electrolytes in ion selective membranes. *Fluid Phase Equilib.* **157**, 181–196.

Stegen, J.H.G. van der, J. Görtzen, J.A.M. Kuipers, J.A. Hogendoorn and G.F. Versteeg (2001). Radial distribution of ions in pores with a surface charge. *J. Membr. Sci.* **183**, 61–74.

Stokes, R.H. and R.A. Robinson (1973). Solvation equilibria in very concentrated electrolyte solutions. *J. Solution Chem.* **2**, 173–184.

Surdo, A.L., E.M. Alzola and F.J. Millero (1982). The (P, V, T) properties of concentrated aqueous electrolytes. I. Densities and apparent molar volumes of NaCl, Na_2SO_4, $MgCl_2$ and $MgSO_4$ solutions from 0.1 mol kg^{-1} to saturation and from 273.15 to 323.15 K. *J. Chem. Thermodyn.* **14**, 649–662.

Teorell, T. (1935). An attempt to formulate a quantitative theory of membrane permeability. *Proc. Soc. Exp. Biol.* **33**, 282–285.

Thomas, D.G. (1973). Forced convection mass transfer in hyperfiltration at high fluxes. *Ind. Eng. Chem. Fundam.* **12**, 396–405.

Tiravanti, G., G. Boari and R. Passino (1985). Concentration polarization and Nernst-Planck equations. *NATO ASI Ser.* **98**, 468–483.

Tsuru, T., S.-I. Nakao and S. Kimura (1991*a*). Calculation of ion rejection by extended Nernst-Planck equation with charged reverse osmosis membranes for single and mixed electrolyte solutions. *J. Chem. Eng. Jpn.* **24**, 511–517.

Tsuru, T., S.-I. Nakao and S. Kimura (1991*b*). Reverse osmosis of single and mixed electrolytes with charged membranes: Experiment and analysis. *J. Chem. Eng. Jpn.* **24**, 518–524.

Turek, M. and M. Gonet (1996). Nanofiltration in the utilization of coal-mine brines. *Desalination* **108**, 171–177.

Vonk, M.W. and J.A.M. Smit (1983). Positive and negative ion retention curves of mixed electrolytes in reverse osmosis with a cellulose acetate membrane. An analysis on the basis of the generalized Nernst-Planck equation. *J. Colloid Interface Sci.* **96**, 121–134.

Wang, X.-L., T. Tsuru, M. Togoh, S.-I. Nakao and S. Kimura (1995*a*). Evaluation of pore structure and electrical properties of nanofiltration membranes. *J. Chem. Eng. Jpn.* **28**, 186–192.

Wang, X.-L., T. Tsuru, S.-I. Nakao and S. Kimura (1995*b*). Electrolyte transport through nanofiltration membranes by the space-charge model and the comparison with Teorell-Meyer-Sievers model. *J. Membr. Sci.* **103**, 117–133.

Wang, X.-L., T. Tsuru, S.-I. Nakao and S. Kimura (1997). The electrostatic and steric-hindrance model for the transport of charged solutes through nanofiltration membranes. *J. Membr. Sci.* **135**, 19–32.

Westermann-Clark, G.B. and J.L. Anderson (1983). Experimental verification of the space-charge model for electrokinetics in charged microporous membranes. *J. Electrochem. Soc.* **130**, 839–847.

Wood, J.R. (1975). Thermodynamics of brine-salt equlilibria. I. The systems NaCl-KCl-$MgCl_2$-$CaCl_2$-H_2O and NaCl-$MgSO_4$-H_2O at 25^oC. *Geochim. Cosmochim. Acta* **39**, 1147–1163.

Xu, Y. and R.E. Leburn (1999). Investigation of the solute separation by charged nanofiltration membrane: effect of pH, ionic strength and solute type. *J. Membr. Sci.* **158**, 93–104.

Yaroshchuk, A.E. (1995). Osmosis and reverse osmosis in fine-porous charged diaphragms and membranes. *Adv. Colloid Interface Sci.* **60**, 1–93.

Yaroshchuk, A.E. (2000*a*). Asymptotic behaviour in the pressure-driven separations of ions of different mobilities in charged porous membranes. *J. Membr. Sci.* **167**, 163–185.

Yaroshchuk, A.E. (2000*b*). Optimal charged membranes for the pressure-driven separation of ions of different mobilites: theoretical analysis. *J. Membr. Sci.* **167**, 149–161.

Yaroshchuk, A.E. and Y.A. Vovkogon (1994*a*). Phenomenological theory of pressure-driven transport of ternary electrolyte solutions with a common coion and its specification for capillary space-charge model. *J. Membr. Sci.* **86**, 1–18.

Yaroshchuk, A.E. and Y.A. Vovkogon (1994*b*). Pressure-driven transport of ternary electrolyte solutions with a common coion through charged membranes. Numerical analysis. *J. Membr. Sci.* **86**, 19–27.

Appendix A

Pitzer parameters for the system Mg-Cl-SO_4-H_2O

A.1 Main parameters for $MgCl_2$ and $MgSO_4$

The temperature dependency of the magnesium chloride main parameters are given by the equation

$$f(T) = Q_1 T^2 + Q_2 T + Q_3 \tag{A.1}$$

whereas the main parameters of magnesium sulphate are given by the equation

$$\begin{aligned} f(T) = \; & Q_1 \left(\tfrac{T}{2} + \tfrac{298^2}{2T} - 298 \right) + Q_2 \left(\tfrac{T^2}{6} + \tfrac{298^3}{3T} - \tfrac{298^2}{2} \right) \\ & + Q_3 \left(\tfrac{T^3}{12} + \tfrac{298^4}{4T} - \tfrac{298^3}{3} \right) + Q_4 \left(\tfrac{T^4}{20} + \tfrac{298^5}{5T} - \tfrac{298^4}{4} \right) \\ & + Q_5 \left(298 - \tfrac{298^2}{T} \right) + Q_6 \end{aligned} \tag{A.2}$$

The coefficients, Q_i, are given in Tables A.1 and A.2 for the magnesium chloride and magnesium sulphate, respectively, and are valid in the temperature range 298-473 K and from infinite dilution to the saturation concentrations (Pitzer 1995).

Table A.1: Coefficients for the main parameters of magnesium chloride valid in the temperature range 298-473 K, taken from Pitzer (1995).

	β_0	β_1	C^ϕ
Q_1	5.93915e-07	2.60169e-05	2.41831e-07
Q_2	-9.31654e-04	-1.09438e-02	-2.49949e-04
Q_3	0.576066	2.60135	5.95320e-02

Table A.2: Coefficients for the main parameters of magnesium sulphate valid in the temperature range 298-473 K, taken from Pitzer (1995).

	β_0	β_1	β_2	C^ϕ
Q_1	-1.0282	-2.9596e-01	-1.3764e-01	1.0541e-01
Q_2	8.4790e-03	9.4564e-04	1.2121e-01	-8.9316e-04
Q_3	-2.33667e-05	0	-2.7642e-04	2.51e-06
Q_4	2.1575e-04	0	0	-2.3436e-09
Q_5	6.8402e-04	1.028e-02	-2.1515e-01	-8.7899e-05
Q_6	0.21499	3.3646	-32.743	0.006993

A.2 Mixing parameters for the system Mg-Cl-SO_4

The temperature function of the mixing parameters can be given by the equation

$$f(T) = a + b(T - T_r) + c(T^2 - T_r^2) + d\left(\frac{1}{T} - \frac{1}{T_r}\right) + e\ln\left(\frac{T}{T_r}\right) + f\left(\frac{1}{T^2} - \frac{1}{T_r^2}\right) \tag{A.3}$$

where a, b, c, d, e and f are adjustable coefficients. Known values are given in Table A.3 (Harvie *et al.* 1984, Pabalan and Pitzer 1987), where the θ_{Cl-SO_4}-parameter is independent of the temperature when the temperature is below 473 K and the coefficients of the $\psi_{Mg-Cl-SO_4}$-parameter are valid in the temperature range 298-373 K. The parameters are valid up to the saturation concentrations.

Table A.3: Coefficients for the mixing parameters for the system Mg-Cl-SO_4, taken from Harvie et al. (1984) and Pabalan and Pitzer (1987).

	a	b	c	d	e	f
θ_{Cl-SO_4}	0.02000	0	0	0	0	0
$\psi_{Mg-Cl-SO_4}$	-0.00796	0	0	32.63	0	0

Appendix B

Measured water fluxes and permeabilities

Figures B.1-B.6 show the water flux measurements before and after running experiment with salt solutions. The water flux measurements were carried out at temperature 298 K and the Reynolds number between 1000-3000, unless otherwise stated. The standard deviation is 0.5 K for the temperature; 6% of the Reynolds number values; 2% of the pressure values; and, 5% of the flux values.

The water flux, the water permeability and the pressure is related by Equation 5.1 in Chapter 5, which gives the water permeability as the slope in a flux-pressure diagram. For each new membrane sample the slope was calculated with a least square method and the result was divided by the water density to convert the permeability unit from g $m^{-2}s^{-1}bar^{-1}$ to $m^3m^{-2}s^{-1}bar^{-1}$. The water density values 996.96 kg m^{-3} at 298 K and 977.8 kg m^{-3} at 343 K (Lide 1990) was used. The results using the Desal 5 DK membrane are given in Table B.1, whereas Table B.2 shows the results using the Desal G5 membrane.

The salt retention using a 0.1 molal magnesium chloride solution at Reynolds number 1000, temperature 298 K and pressure 30 bar was measured for each membrane sample in order to compare the retention characteristics. The results are given in Tables B.1 and B.2.

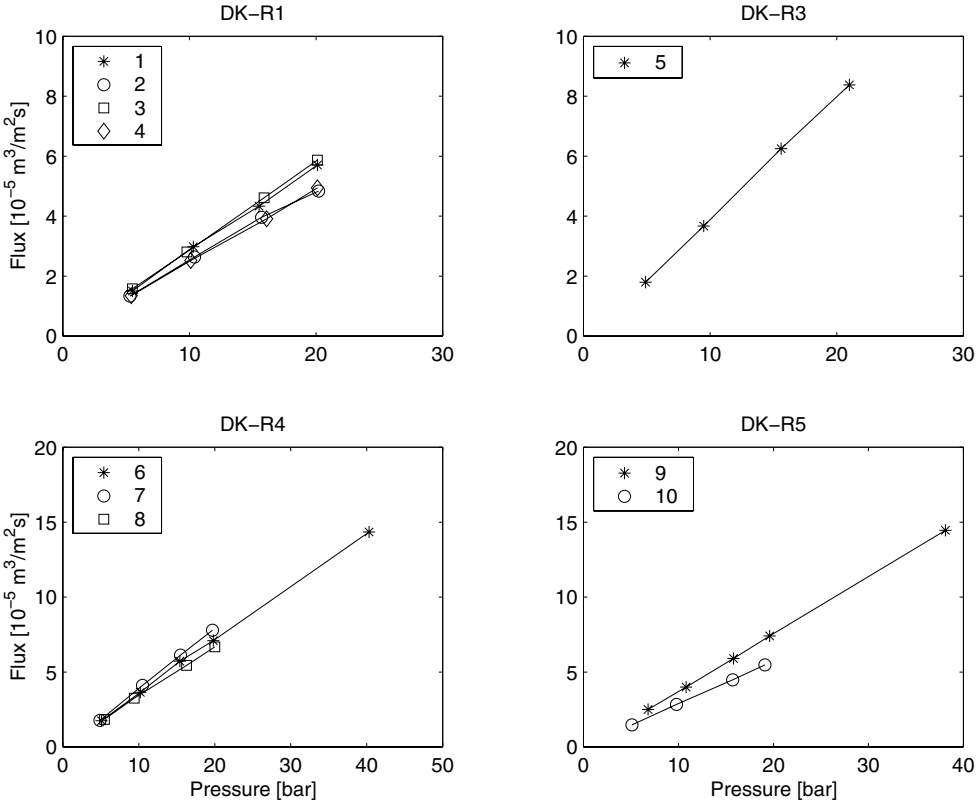

Figure B.1: Measured water fluxes using the membrane samples DK-R1, DK-R3, DK-R4 and DK-R5. Legends: (1) new after pretreatment, (2) after experiment with 2.5 m solution, (3) after 24 h, (4) after experiment with 5 m solution, (5) new after pretreatment, (6) new after pretreatment, (7) after experiment with 0.1 m solution, (8) after experiment with 2.5 m solution, (9) new after pretreatment, (10) after experiment with 5 m solution.

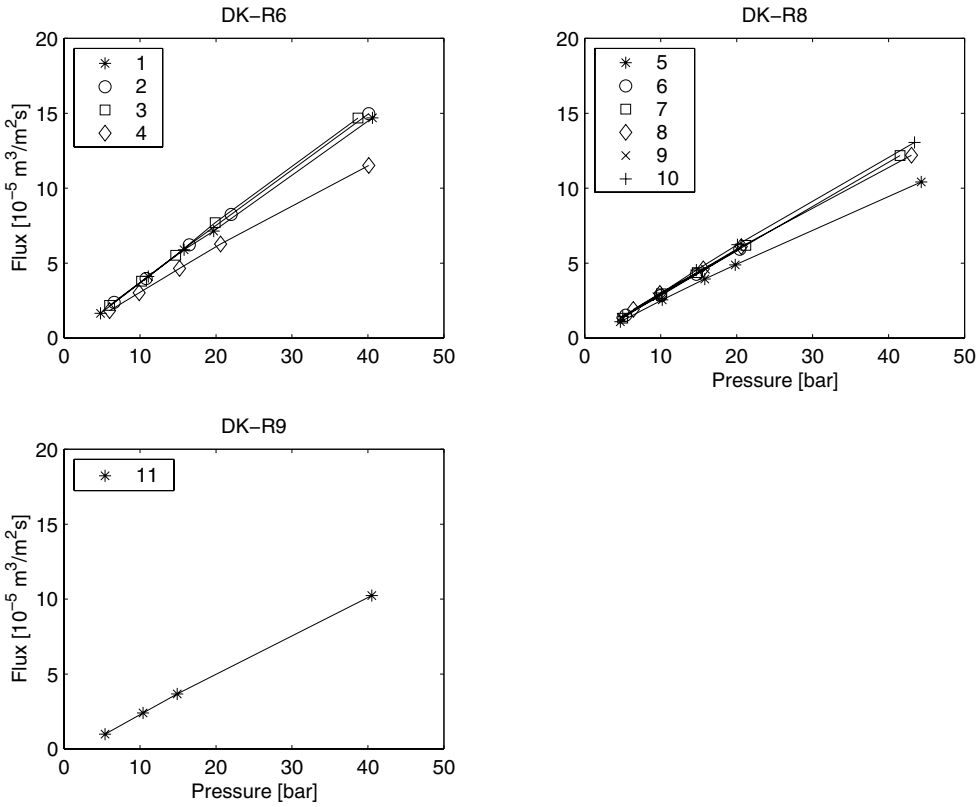

Figure B.2: Measured water fluxes using the membrane samples DK-R6, DK-R8 and DK-R9. Legends: (1) new after pretreatmemt, (2) after experiment with 0.1 m solution, (3) after experiment with 0.1 m solution, (4) after experiment with 5 m solution, (5) new after pretreatment (6) after experiment with 1 m solution, (7) after 10 days of storage in destilled water, (8) after experiment with 1 m solution, (9) after experiment with 1 m solution, (10) after experiment with 1 m solution, (11) new after pretreatment.

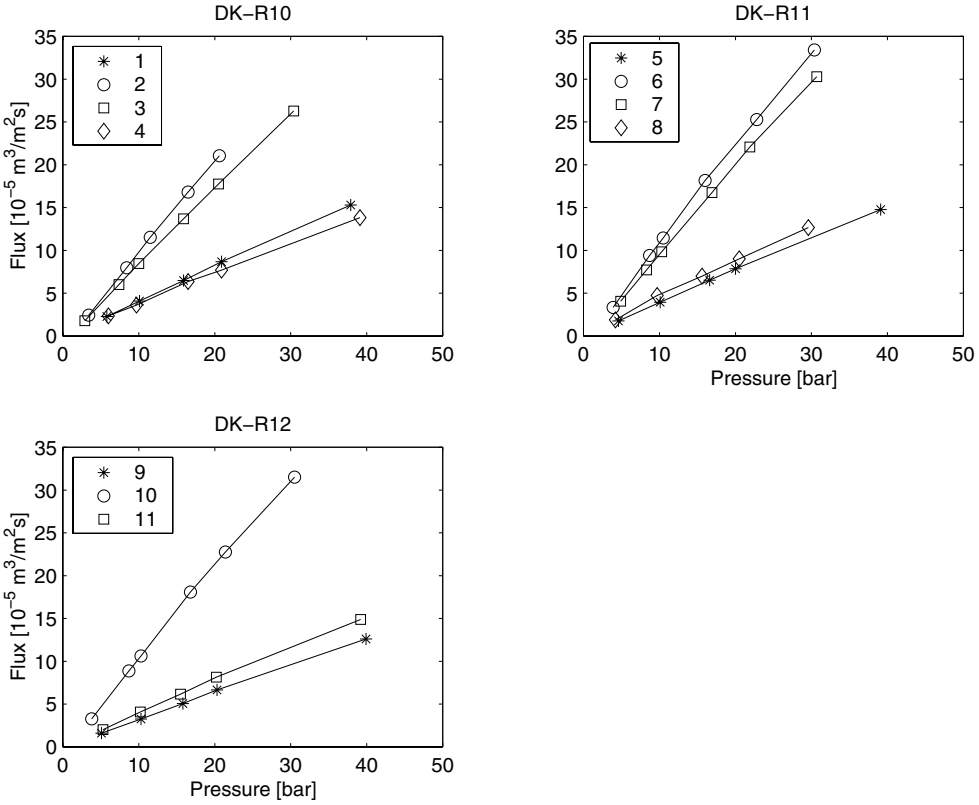

Figure B.3: Measured water fluxes using the membrane samples DK-R10, DK-R11 and DK-R12. Legends: (1) new at 298 K after pretreatment, (2) immediately after reaching 343 K, (3) after 3.5 h at 343 K and 30 bar, (4) immediately after cooling to 298 K, (5) new at 298 K after pretreatment, (6) immediately after reaching 343 K, (7) after 1.5 h at 343 K and 30 bar, (8) immediately after cooling to 298 K, (9) new at 298 K after pretreatment, (10) immediately after reaching 343 K, (11) immediately after cooling to 298 K.

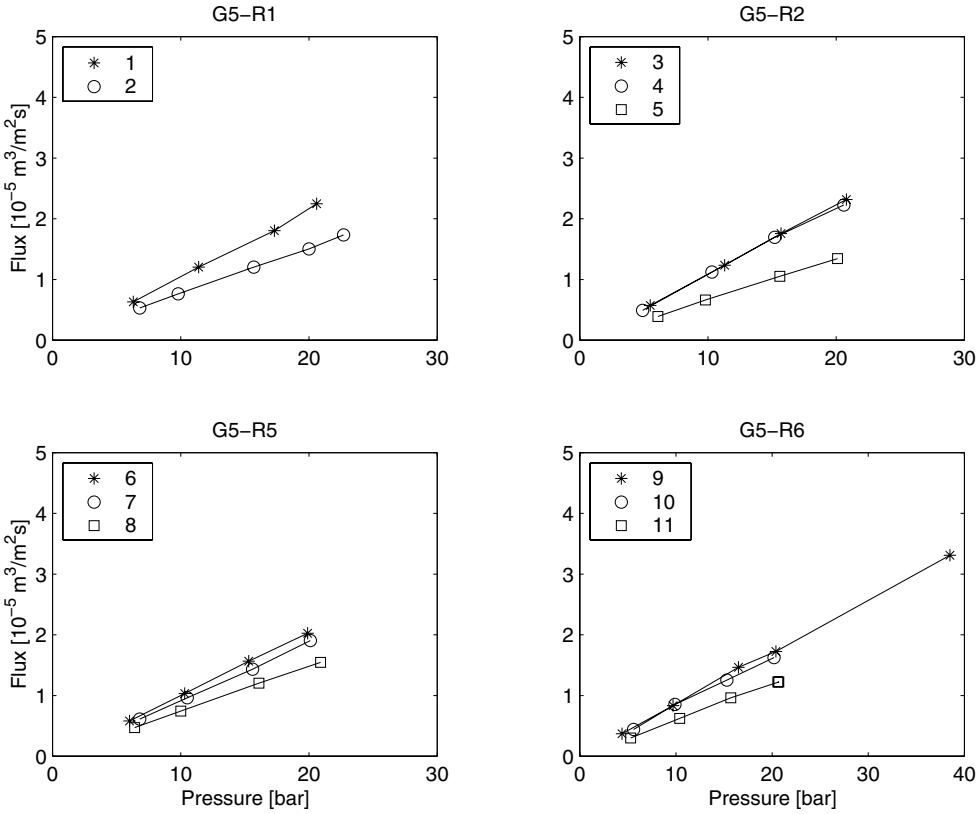

Figure B.4: Measured water fluxes using the membrane samples G5-R1, G5-R2, G5-R5 and G5-R6. Legends: (1) new after pretreatment, (2) after experiment with 2.5 m solution, (3) new after pretreatment, (4) after experiment with 0.1 m solution, (5) after experiment with 1 and 5 m solutions, (6) new after pretreatment, (7) after experiment with 0.1 m solution, (8) after experiment with 1 m solution, (9) new after pretreatment, (10) after experiment with 0.1 m solution, (11) after experiment with 5 m solution.

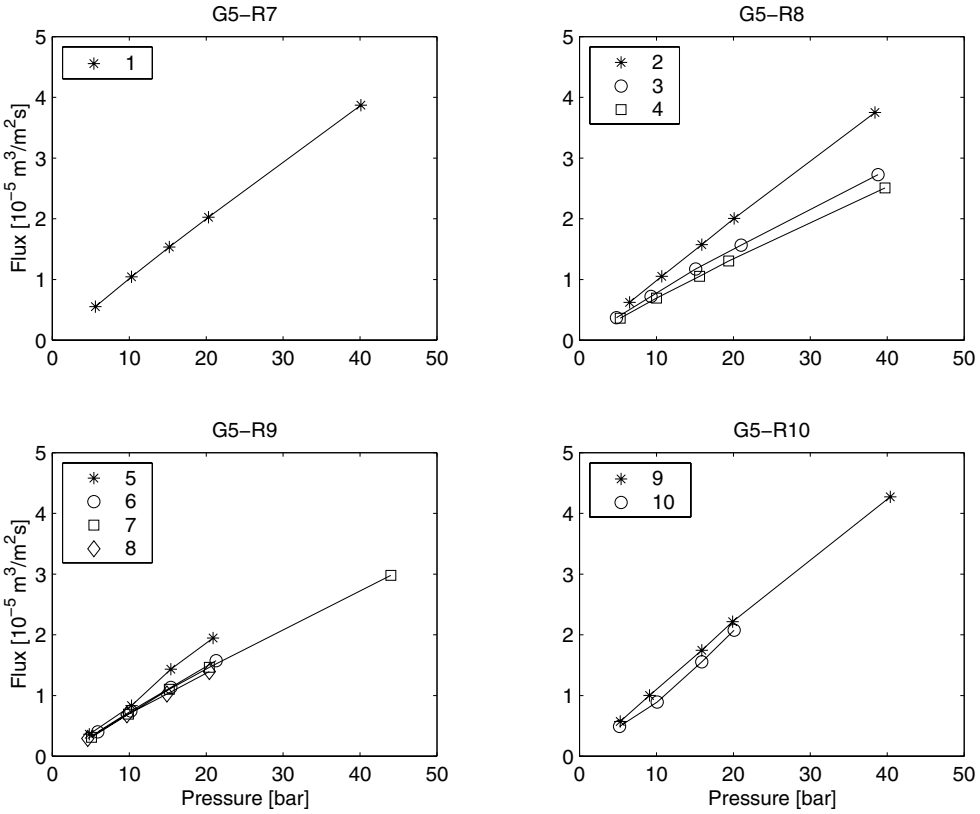

Figure B.5: Measured water fluxes using the membrane samples G5-R7, G5-R8, G5-R9 and G5-R10. Legends: (1) new after pretreatment, (2) new after pretreatment, (3) after experiment with 2.5 m solution, (4) after experiment with 5 m solution, (5) new after pretreatment, (6) after experiment with 1 m solution, (7) after experiment with 1 m solution, (8) after experiment with 1 m solution, (9) new after pretreatment, (10) after experiment with 1 m solution.

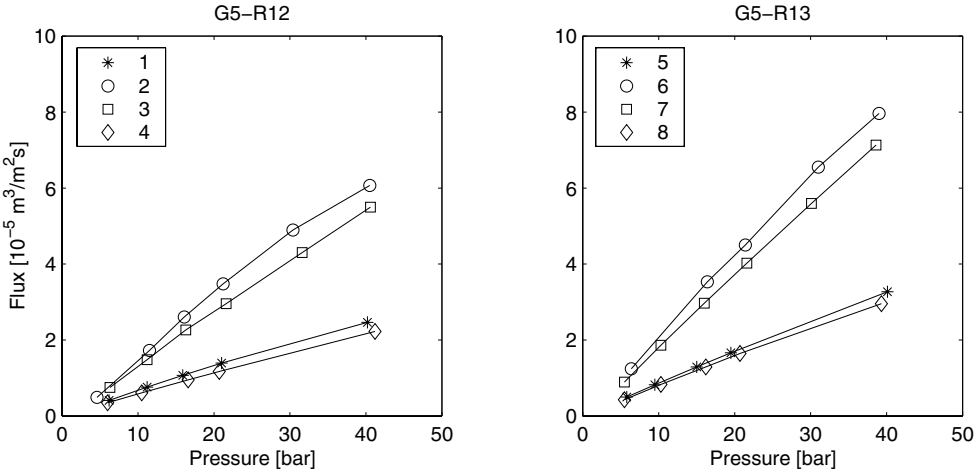

Figure B.6: Measured water fluxes using the membrane samples G5-R12 and G5-R13. Legends: (1) new at 298 K after pretreatment, (2) immediately after reaching 343 K, (3) after 4 h at 343 K and 40 bar, (4) immediately after cooling to 298 K, (5) new at 298 K after pretreatment, (6) immediately after reaching 343 K, (7) after 1.5 h at 343 K and 40 bar, (8) immediately after cooling to 298 K.

Table B.1: Measured water permeabilities at 298 and 343 K and the salt retention using a 0.1 molal magnesium chloride solution at 30 bar for different Desal 5 DK membrane samples.

Sample	L_p^{298} [10^{-6} m^3/m^2s^1bar]	L_p^{343} [10^{-5} m^3/m^2s^1bar]	R_{test} [%]
DK-R1	2.861	na	3.80
DK-R3	4.116	na	4.35
DK-R4	3.562	na	2.63
DK-R5	3.816	na	3.60
DK-R6	3.619	na	3.20
DK-R8	3.011	na	3.62
DK-R9	2.611	na	na
DK-R10	4.053	1.107	na
DK-R11	3.764	1.151	na
DK-R12	3.213	1.082	na
Average	3.5	1.11	3.53
Std	0.5	0.03	0.58

Table B.2: Measured water permeabilities at 298 and 343 K and the salt retention using a 0.1 molal magnesium chloride solution at 30 bar for different Desal G5 membrane samples.

Sample	L_p^{298} [10^{-6} m^3/m^2s^1bar]	L_p^{343} [10^{-6} m^3/m^2s^1bar]	R_{test} [%]
G5-R1	1.113	na	8.50
G5-R2	1.139	na	5.82
G5-R5	1.043	na	7.60
G5-R6	0.859	na	na
G5-R7	0.956	na	11.72
G5-R8	0.979	na	10.90
G5-R9	0.998	na	na
G5-R10	1.053	na	6.30
G5-R11	0.599	1.596	na
G5-R12	0.886	1.981	na
G5-R13	0.804	2.156	na
Average	1.0	1.9	8.47
Std	0.1	0.1	2.41

Appendix C

Experiment operation procedure

The experiments were carried out as described in the detailed operation procedure given below.

1. The salt solution was added to the feed tank.
2. The computer was turned on and the logging-program started.
3. The temperature set point was given to the computer and the feed was pumped through the system at low pressure until this temperature was reached.
4. The flow rate was adjusted until the acquired value was obtained.
5. The pressure was adjusted until the acquired value was obtained.
6. The experiment was run for at least 0.5 hour and to the accumulated permeate exceeded 75 grams.
7. Two samples of the feed and one sample of the permeate were taken out for analysis (approximately 20 grams/sample).
8. The pressure was adjusted to a new acquired value.
9. The experiment was run for at least 10 minutes and the accumulated permeate exceeded 75 grams.

10. One sample of the permeate was taken out for analysis.
11. The experiment continued at point 8 until measurements on all pressure levels were done.
12. The flow rate was adjusted until the new acquired value was obtained, and the experiment proceeded at point 8 until measurements on all flow rate levels were done.
13. The temperature set point was changed and the experiment proceeded at point 3 until measurements on all temperature levels were done.
14. Two samples of the feed were taken out for analysis.
15. The feed was cooled and the system was emptied and shut down.

Appendix D

Results using Desal 5 DK

The following tables give the results from experiments done with samples of Desal 5 DK membrane. The code in brackets in the table headings, *e.g.* DK-R3, refers to the membrane sample used in the experiments. The tables include the following columns: temperature [K]; Reynolds number; pressure [bar]; flux [g/m^{2}s]; chloride ion concentration [m]; sulphate ion concentration [ppm]; pH and, finally, the experimental order the experiments were run[1].

The standard deviations of the measured variables are calculated and only the maximum values are given. The standard deviation for the temperature is 0.5 K; for laminar Reynolds numbers 6% and for turbulent Reynolds numbers 2% of the value; for pressures 2% of the value; for fluxes 5% of the value; for chloride concentration 0.5% of the value, and for sulphate concentrations 3% of the value when the concentrations were around 300 ppm and 1% of the value when the sulphate concentrations were around 3000 ppm. The uncertainty in the pH measurements is 0.05 units.

[1]Number 2 is normally missing in this column because this sample was a parallel to sample number 1 and only the averaged value is given.

Table D.1: Results using 0.1 m $MgCl_2$ (DK-R3).

T [K]	Re	Pressure [bar]	Flux [g/m^{2}s]	C_{Cl^-} [m]	pH	Exp order
	feed	-	-	0.193	na	1
298.0	1000	6.1	21.1	0.185	6.77	5
		10.5	36.5	0.184	6.76	4
		16.5	60.0	0.186	6.85	6
		20.5	73.7	0.187	6.69	3
		20.8	73.5	0.186	6.85	7
		30.9	109.7	0.188	6.56	2
297.8	4400	6.7	22.0	0.183	6.84	12
		11.4	39.3	0.179	6.88	9
		16.6	59.6	0.177	6.86	10
		20.4	73.3	0.177	6.82	8
		30.5	107.4	0.178	6.89	11
	feed	-	-	0.192	6.48	13

Table D.2: Results using 0.1 m $MgCl_2$ and 300 ppm $MgSO_4$ (DK-R4).

T [K]	Re	Pressure [bar]	Flux [g/m^{2}s]	C_{Cl^-} [m]	$C_{SO_4^{2-}}$ [ppm]	pH	Exp order
	feed	-	-	0.189	299	6.47	1
297.9	1020	6.0	20.0	0.184	211	6.67	4
		6.1	20.1	0.183	229	6.83	8
		9.3	32.4	0.184	212	6.77	5
		16.5	57.0	0.184	252	6.69	3
		20.0	68.3	0.184	na	6.77	6
		30.1	104.0	0.186	279	6.72	2
		30.0	103.0	0.186	270	6.77	7
297.9	4400	6.3	20.4	0.182	296	6.75	12
		9.8	32.5	0.179	292	6.76	11
		15.9	54.3	0.177	299	6.74	13
		20.6	70.2	0.176	285	6.81	9
		29.3	100.2	0.177	289	6.78	10
	feed	-	-	0.189	299	6.71	14

Table D.3: Results using 0.1 m $MgCl_2$ and 3000 ppm $MgSO_4$ (DK-R6).

T [K]	Re	Pressure [bar]	Flux [g/m^{2}s]	C_{Cl^-} [m]	$C_{SO_4^{2-}}$ [ppm]	pH	Exp order
	feed	-	-	0.178	2848	6.42	1
298.2	1030	5.1	13.7	0.174	2044	6.58	6
		10.0	29.7	0.173	1999	6.60	5
		9.9	29.3	0.174	1993	6.55	8
		15.9	45.6	0.173	2063	6.56	4
		20.7	60.3	0.174	2205	6.56	7
		30.7	86.3	0.174	2459	6.60	3
297.9	4450	7.0	20.1	0.171	1694	6.52	13
		7.3	21.1	0.171	1696	6.55	14
		10.8	31.2	0.168	1537	6.56	9
		15.8	47.7	0.168	1515	6.52	12
		20.4	60.6	0.167	1530	6.54	11
		29.3	88.1	0.166	1605	6.54	10
	feed	-	-	0.179	2861	6.51	15

Table D.4: Results using 1.0 m $MgCl_2$ (DK-R8 and DK-R9).

T [K]	Re	Pressure [bar]	Flux [g/m^{2}s]	C_{Cl^-} [m]	pH	Exp order
DK-R8	feed	-	-	1.609	6.01	1
298.4	900	5.5	5.7	1.568	6.21	4
		10.7	12.4	1.548	6.26	5
		15.4	18.9	1.535	6.27	6
		20.4	24.2	1.528	6.15	2
		30.1	36.4	1.531	6.19	3
		40.0	49.0	1.529	6.29	8
		50.4	56.5	1.544	6.28	7
298.2	4380	4.8	4.6	1.568	6.30	14
		10.3	12.3	1.544	6.30	12
		15.3	19.3	1.505	6.30	13
		21.4	27.0	1.490	6.27	9
		31.5	39.0	1.454	6.32	10
		40.0	49.1	1.428	6.33	11
		50.7	59.6	1.427	6.33	15
DK-R9	feed	-	-	1.643	6.68	1
343.0	1980	5.2	15.4	1.615	5.23	3
		10.1	35.0	1.589	6.02	2
		15.4	50.6	1.587	6.57	5
		20.4	58.2	1.570	7.24	15
		30.4	102.6	1.555	7.25	4
		39.8	114.4	1.547	7.35	6
		48.8	127.7	1.549	7.38	7
343.0	9820	5.1	13.7	1.604	7.11	9
		9.9	27.4	1.583	6.03	8
		15.9	46.3	1.546	6.93	11
		19.3	54.4	1.530	7.22	14
		29.5	86.2	1.487	7.28	10
		40.5	112.5	1.458	7.41	12

Table D.5: Results using 1.0 m $MgCl_2$ (DK-R3).

T [K]	Re	Pressure [bar]	Flux [g/m^{2}s]	C_{Cl^-} [m]	pH	Exp order
	feed	-	-	1.931	5.80	1
343.0	980	5.8	33.6	1.907	6.03	3
		10.7	67.2	1.901	6.00	2
		16.3	106.8	1.917	6.13	4
		20.7	133.1	1.916	6.13	5
		30.1	181.2	1.910	6.24	6
343.0	4260	5.7	30.6	1.910	6.28	11
		11.2	63.7	1.888	6.30	10
		15.7	91.6	1.875	6.23	9
		20.1	117.6	1.870	6.31	8
		31.0	180.0	1.867	6.28	7
	feed	-	-	1.929	6.35	12

Table D.6: Results using 1.0 m $MgCl_2$ and 175 ppm $MgSO_4$ (DK-R8).

T [K]	Re	Pressure [bar]	Flux [g/m^{2}s]	C_{Cl^-} [m]	$C_{SO_4^{2-}}$ [ppm]	pH	Exp order
	feed	-	-	1.687	175	6.31	1
298.1	900	4.9	5.9	1.659	118	6.52	7
		10.2	14.3	1.626	152	na	6
		15.8	22.6	1.603	134	6.69	3
		20.6	29.6	1.599	119	6.59	4
		31.4	42.4	1.582	140	na	2
		40.6	56.6	1.608	151	na	5
		50.8	69.3	1.615	141	na	8
298.1	4320	5.9	7.6	1.642	168	6.42	12
		10.8	15.2	1.611	134	na	11
		14.8	22.0	1.587	120	6.41	13
		21.9	32.4	1.559	97	na	9
		29.8	44.8	1.533	99	na	14
		40.5	59.4	1.505	89	6.46	10
		52.4	76.3	1.485	102	na	15
	feed	-	-	1.688	na	na	16

Table D.7: Results using 1.0 m $MgCl_2$ and 300 ppm $MgSO_4$ (DK-R8).

T [K]	Re	Pressure [bar]	Flux [g/m^{2}s]	C_{Cl^-} [m]	$C_{SO_4^{2-}}$ [ppm]	pH	Exp order
	feed	-	-	1.557	290	na	1
298.3	850	5.7	9.5	1.527	211	6.46	4
		11.0	18.4	1.508	196	na	3
		21.6	36.1	1.502	211	na	5
		41.1	67.5	1.506	229	6.47	2
		52.8	81.7	1.513	258	na	6
298.3	4310	6.9	10.8	1.508	196	6.39	9
		11.2	18.5	1.495	171	na	10
		22.1	37.0	1.458	151	na	7
		41.1	67.8	1.417	148	6.35	11
		52.2	83.9	1.404	151	na	8
	feed	-	-	1.688	300	na	1
343.0	2140	4.1	14.7	1.674	268	6.79	6
		11.0	50.6	1.650	242	na	7
		15.2	68.3	1.646	256	6.97	5
		21.1	100.2	1.654	269	na	2
		29.5	139.4	1.652	264	na	3
		41.0	183.6	1.642	279	6.96	4
		50.2	209.4	1.667	305	na	8
343.0	10080	6.0	22.7	1.664	251	6.96	11
		9.9	39.9	1.648	234	na	10
		15.6	66.1	1.624	204	6.90	14
		20.4	85.6	1.612	185	na	9
		29.7	129.2	1.596	202	na	13
		41.1	174.8	1.576	199	7.00	12
		53.3	221.8	1.584	217	na	15
	feed	-	-	1.695	311	na	16

Table D.8: Results using 1.0 m $MgCl_2$ and 300 ppm $MgSO_4$ (DK-R6).

T [K]	Re	Pressure [bar]	Flux [g/m^{2}s]	C_{Cl^-} [m]	$C_{SO_4^{2-}}$ [ppm]	pH	Exp order
	feed	-	-	1.819	316	6.00	1
343.0	930	5.3	25.1	1.799	290	6.06	6
		10.1	52.8	1.795	300	6.05	5
		16.1	88.5	1.802	302	6.08	7
		19.6	105.6	1.794	293	5.99	3
		29.8	157.2	1.807	307	6.04	4
343.1	4420	6.8	33.8	1.792	271	6.22	11
		10.4	54.4	1.783	255	6.17	9
		16.0	89.1	1.774	252	6.19	10
		20.1	112.0	1.773	257	6.12	8
		29.7	165.3	1.771	262	6.25	12
	feed	-	-	1.820	320	6.30	13

Table D.9: Results using 1.0 m $MgCl_2$ and 3000 ppm $MgSO_4$ (DK-R6).

T [K]	Re	Pressure [bar]	Flux [g/m^{2}s]	C_{Cl^-} [m]	$C_{SO_4^{2-}}$ [ppm]	pH	Exp order
	feed	-	-	1.820	3052	6.28	1
343.0	950	5.5	26.4	1.804	2819	6.37	6
		9.9	53.1	1.802	2810	na	7
		16.0	87.6	1.806	2919	na	3
		20.0	107.1	1.800	2962	na	5
		29.8	158.1	1.810	2974	6.34	4
343.1	4430	5.9	29.3	1.801	2691	6.00	9
		10.7	57.9	1.786	2646	6.36	8
		15.6	88.5	1.778	2588	na	10
		20.3	113.6	1.777	2614	na	11
		30.5	166.7	1.769	2691	6.40	12
	feed	-	-	1.825	3087	6.36	13

Table D.10: Results using 1.0 m $MgCl_2$ and 3000 ppm $MgSO_4$ (DK-R8).

T [K]	Re	Pressure [bar]	Flux [g/m^{2}s]	C_{Cl^-} [m]	$C_{SO_4^{2-}}$ [ppm]	pH	Exp order
	feed	-	-	1.558	3065	5.56	1
298.3	900	6.2	9.8	1.524	3065	5.85	2
		10.2	16.4	1.508	3066	na	3
		15.5	24.8	1.512	3067	5.95	4
		20.9	33.0	1.516	3068	na	5
		30.5	47.1	1.518	3069	na	6
		39.6	60.2	1.510	3070	6.04	7
		51.2	74.4	1.524	3071	na	8
298.3	4440	6.0	9.3	1.534	3072	6.11	9
		10.5	16.8	1.510	3073	na	10
		15.5	25.2	1.490	3074	6.16	11
		22.2	36.8	1.460	3075	na	12
		31.6	51.4	1.444	3076	na	13
		43.7	71.3	1.432	3077	6.22	14
		52.4	83.9	1.420	3078	na	15
	feed	-	-	1.569	3079	6.15	16
343.0	2080	5.1	20.8	1.553	2656	6.07	20
		10.8	46.6	1.547	2562	na	19
		15.3	66.5	1.547	2589	5.98	18
		21.2	91.4	1.535	2601	na	17
		29.5	126.1	1.543	2698	na	22
		41.7	176.8	1.537	2683	6.20	21
		50.8	206.1	1.550	2937	na	23
343.0	10030	6.2	25.3	1.541	2468	6.18	26
		9.7	41.1	1.532	2312	na	29
		14.9	66.6	1.508	2075	6.19	25
		20.6	93.2	1.493	1963	na	24
		30.1	137.2	1.477	1913	na	27
		41.7	181.8	1.466	1900	6.30	28
		48.9	206.8	1.473	1939	na	30
	feed	-	-	1.575	3090	6.11	31

Table D.11: Results using 2.5 m $MgCl_2$ (DK-R1).

T [K]	Re	Pressure [bar]	Flux [g/m^{2}s]	C_{Cl^-} [m]	pH	Exp order
	feed	-	-	5.07	5.43	1
298.0	840	10.7	4.6	5.02	5.48	6
		20.4	8.1	4.97	5.52	5
		30.1	13.1	4.92	5.50	2
		41.1	17.6	4.92	5.48	3
		51.6	21.7	4.89	5.45	4
298.4	2460	10.7	4.3	5.02	5.46	9
		19.8	8.2	4.96	5.43	8
		31.9	14.0	4.94	5.45	7
		42.5	18.4	4.92	5.42	10
		51.0	22.3	4.86	5.43	11
	feed	-	-	4.86	5.47	12
343.1	1130	8.8	16.6	4.83	5.25	14
		19.5	38.9	4.81	5.46	13
		29.2	56.9	4.82	5.31	15
		39.8	72.3	4.76	5.34	16
		50.1	84.1	4.78	5.34	17
343.0	2680	9.5	15.3	4.83	5.36	22
		22.3	37.1	4.79	5.39	21
		31.2	52.0	4.77	5.41	20
		40.3	65.9	4.79	5.47	19
		50.5	81.7	4.77	5.35	18
343.1	5000	10.5	17.1	4.81	5.36	23
		20.6	35.2	4.77	5.34	24
		30.8	52.6	4.76	5.38	25
		41.3	69.2	4.74	5.36	26
		50.9	83.0	4.72	5.38	27
	feed	-	-	4.86	5.36	28

Table D.12: Results using 2.5 m $MgCl_2$ and 300 ppm $MgSO_4$ (DK-R4).

T [K]	Re	Pressure [bar]	Flux [g/m^{2}s]	C_{Cl^-} [m]	$C_{SO_4^{2-}}$ [ppm]	pH	Exp order
	feed	-	-	4.63	270	5.47	1
298.2	910	11.3	8.8	4.56	226	5.60	4
		20.6	16.4	4.54	250	5.61	5
		28.9	22.9	4.52	231	5.43	2
		38.7	30.3	4.49	233	5.48	3
		50.6	35.6	4.50	257	5.60	6
298.4	2540	10.2	7.4	4.58	241	5.64	9
		20.6	15.0	4.52	193	5.65	8
		30.7	22.3	4.50	173	5.67	7
		38.5	27.8	4.48	210	5.64	10
		48.3	34.8	4.45	192	5.64	11
	feed	-	-	4.62	304	5.63	12
343.1	1140	5.9	14.0	4.61	277	5.58	17
		9.8	25.0	4.61	232	5.61	14
		20.8	54.6	4.60	250	5.62	13
		30.5	81.7	4.60	237	5.55	15
		40.3	104.6	4.60	246	5.58	16
343.0	2850	6.2	14.8	4.61	265	5.62	19
		10.3	26.5	4.60	253	5.65	18
		19.8	53.4	4.58	267	5.62	20
		30.0	79.0	4.58	260	5.65	22
		39.3	103.6	4.54	271	5.64	21
343.2	5190	6.7	15.8	4.61	277	5.63	26
		10.7	26.7	4.59	232	5.63	25
		21.4	55.8	4.57	250	5.64	24
		29.7	77.5	4.57	237	5.67	23
		39.7	105.1	4.55	246	5.61	27
	feed	-	-	4.62	290	5.62	28

Table D.13: Results using 5.0 m $MgCl_2$ (DK-R1).

T [K]	Re	Pressure [bar]	Flux [g/m^{2}s]	C_{Cl^-} [m]	pH	Exp order
	feed	-	-	9.74	5.41	1
299.0	750	30.9	2.2	9.74	5.43	2
		37.9	2.6	9.74	5.33	4
		41.7	3.1	9.65	5.36	3
		48.0	3.6	9.73	5.35	5
		54.2	4.3	9.70	5.26	6
343.1	630	11.2	5.2	9.77	5.07	9
		21.2	10.3	9.82	5.25	8
		30.8	14.8	9.77	5.29	7
		42.6	21.1	9.71	5.21	10
		52.2	24.6	9.85	5.23	11
343.1	1320	10.2	4.5	9.84	5.11	21
		19.1	8.9	9.81	5.17	20
		32.1	15.2	9.88	5.11	17
		41.7	19.8	9.84	5.15	18
		50.9	23.9	9.76	5.14	19
343.0	2580	10.6	4.6	9.82	5.17	13
		20.0	9.4	9.84	5.24	12
		30.3	14.0	9.85	5.15	16
		39.4	19.0	9.80	5.21	14
		50.7	24.0	9.72	5.21	15
	feed	-	-	9.92	5.38	22

Table D.14: Results using 5.0 m $MgCl_2$ and 300 ppm $MgSO_4$ (DK-R5).

T [K]	Re	Pressure [bar]	Flux [g/m^{2}s]	C_{Cl^-} [m]	$C_{SO_4^{2-}}$ [ppm]	pH	Exp order
	feed	-	-	9.29	232	5.21	1
297.6	800	29.7	2.9	9.20	148	5.37	2
		36.0	3.4	9.17	149	5.43	3
		39.8	3.7	9.07	132	5.26	4
		49.0	4.6	9.05	140	5.18	5
		54.8	5.2	9.06	160	5.28	6
343.0	770	11.7	7.5	9.26	260	5.38	11
		19.6	12.8	9.26	233	5.30	7
		20.6	13.9	9.27	260	5.50	25
		30.8	20.6	9.29	249	5.34	10
		40.7	27.9	9.22	245	na	8
		40.2	27.1	9.20	272	5.49	24
		50.0	33.5	9.26	261	5.33	9
		50.5	34.3	9.25	263	5.49	23
343.1	1530	11.6	7.5	9.20	255	5.42	15
		20.7	13.8	9.26	258	5.39	14
		27.7	18.9	9.26	250	5.45	16
		40.4	27.3	9.23	257	5.35	13
		50.8	34.5	9.20	243	5.37	12
	feed	-	-	9.26	298	5.44	17
343.2	2650	12.3	8.3	9.20	249	5.50	20
		20.3	14.1	9.21	254	5.47	19
		29.3	20.9	9.19	250	5.48	18
		39.1	27.5	9.20	252	5.47	21
		47.8	33.0	9.17	252	5.49	22
	feed	-	-	9.28	306	5.44	26

Table D.15: Results using 5.0 m $MgCl_2$ and 3000 ppm $MgSO_4$ (DK-R6).

T [K]	Re	Pressure [bar]	Flux [g/m^{2}s]	C_{Cl^-} [m]	$C_{SO_4^{2-}}$ [ppm]	pH	Exp order
	feed	-	-	9.67	2879	5.00	1
298.2	710	32.0	3.6	9.52	1963	5.09	3
		41.4	4.3	9.64	1888	5.01	4
		47.3	4.9	9.57	1855	5.08	5
		52.9	5.3	9.46	na	5.07	6
	feed	-	-	9.60	2927	na	7
343.2	720	11.2	6.4	9.65	2635	5.08	12
		20.7	13.2	9.64	2568	5.12	8
		30.7	17.9	9.61	2509	5.09	11
		40.2	24.9	9.55	2538	5.11	9
		50.2	28.8	9.62	2562	5.11	10
343.2	1420	10.2	5.7	9.70	2609	5.10	13
		21.4	12.3	9.65	2449	5.06	17
		30.1	18.3	9.58	2416	5.08	14
		29.7	17.0	9.67	2420	5.05	18
		40.1	23.0	9.51	2406	5.07	16
		50.6	28.9	9.55	2402	5.07	15
	feed	-	-	9.68	2962	5.09	19

Appendix E

Results using Desal G5

The following tables give the results from experiments done with samples of Desal G5 membrane. The code in brackets in the table headings, *e.g.* G5-R2, refers to the membrane sample used in the experiments. The tables include the following columns: temperature [K]; Reynolds number; pressure [bar]; flux [g/m^{2}s]; chloride ion concentration [m]; sulphate ion concentration [ppm]; pH and, finally, the experimental order the experiments were run[1].

The standard deviations of the measured variables are calculated and only the maximum values are given. The standard deviation for the temperature is 0.5 K; for laminar Reynolds numbers 6% and for turbulent Reynolds numbers 2% of the value; for pressures 2% of the value; for fluxes 5% of the value; for chloride concentration 0.5% of the value, and for sulphate concentrations 3% of the value when the concentrations were around 300 ppm and 1% of the value when the sulphate concentrations were around 3000 ppm. The uncertainty in the pH measurements is 0.05 units.

[1]Number 2 is normally missing in this column because this sample was a parallel to sample number 1 and only the averaged value is given.

Table E.1: Results using 0.1 m $MgCl_2$ (G5-R2).

T [K]	Re	Pressure [bar]	Flux [g/m^{2}s]	C_{Cl^-} [m]	pH	Exp order
	feed	-	-	0.190	6.43	1
298.0	980	10.0	10.4	0.182	na	3
		15.5	16.5	0.181	6.46	4
		20.2	21.6	0.179	6.43	2
		27.2	27.6	0.177	6.51	5
		37.5	36.7	0.177	6.48	6
298.0	4430	9.8	9.2	0.186	na	10
		15.9	15.1	0.177	6.48	11
		20.0	18.5	0.174	6.46	9
		28.5	26.8	0.170	6.45	8
		38.2	36.4	0.156	6.46	7
	feed	-	-	0.189	6.43	12

Table E.2: Results using 0.1 m $MgCl_2$ and 300 ppm $MgSO_4$ (G5-R5).

T [K]	Re	Pressure [bar]	Flux [g/m^{2}s]	C_{Cl^-} [m]	$C_{SO_4^{2-}}$ [ppm]	pH	Exp order
	feed	-	-	0.185	325	6.23	1
297.8	970	6.8	5.5	0.180	na	6.34	7
		10.5	8.7	0.178	172	6.33	6
		15.5	13.1	0.175	144	6.33	5
		19.8	16.7	0.174	129	6.34	4
		30.0	25.7	0.173	144	6.32	3
		29.7	24.2	0.173	138	6.35	8
297.7	4500	7.3	5.4	0.179	171	6.36	13
		10.6	8.2	0.177	189	6.34	12
		15.5	12.0	0.174	142	6.40	11
		19.8	15.8	0.171	144	6.40	10
		20.9	17.0	0.171	148	6.37	14
		30.2	24.3	0.166	128	6.39	9
	feed	-	-	0.186	291	6.38	15

Table E.3: Results using 0.1 m $MgCl_2$ and 3000 ppm $MgSO_4$ (G5-R6).

T [K]	Re	Pressure [bar]	Flux [g/m^{2}s]	C_{Cl^-} [m]	$C_{Mg^{2+}}$ [m]	$C_{SO_4^{2-}}$ [ppm]	pH	Exp order
	feed	-	-	0.180	0.117	2876	6.52	1
298.4	980	6.3	4.4	0.176	0.107	1954	6.50	6
		10.2	7.6	0.174	0.105	1826	6.51	5
		16.5	12.3	0.172	0.101	1696	6.49	7
		21.0	16.1	0.171	0.100	1687	6.57	3
		30.2	22.0	0.168	0.098	1590	6.53	4
297.9	4450	7.7	4.9	0.176	0.104	1845	6.47	12
		10.3	7.1	0.174	0.103	1670	6.49	11
		16.5	12.1	0.171	0.100	1524	6.44	8
		20.6	14.9	0.169	0.098	1425	6.42	9
		30.6	21.3	0.164	0.094	1408	6.48	10
	feed	-	-	0.181	0.117	2896	6.36	13

Table E.4: Results using 1.0 m $MgCl_2$ (G5-R2).

T [K]	Re	Pressure [bar]	Flux [g/m^{2}s]	C_{Cl^-} [m]	pH	Exp order
	feed	-	-	1.897	5.64	1
343.0	950	6.2	8.0	1.866	6.17	3
		9.8	13.5	1.854	6.05	2
		16.4	25.1	1.844	6.34	4
		21.1	30.7	1.825	6.52	6
		30.3	45.5	1.812	6.47	5
343.0	4290	5.9	7.0	1.868	6.59	10
		10.2	14.0	1.850	6.59	9
		14.6	20.9	1.824	6.57	11
		20.2	29.4	1.799	6.47	7
		29.9	44.0	1.770	6.58	8
	feed	-	-	1.901	6.61	12

Table E.5: Results using 1.0 m $MgCl_2$ (G5-R9).

T [K]	Re	Pressure [bar]	Flux [g/m^{2}s]	C_{Cl^-} [m]	pH	Exp order
	feed	-	-	1.607	6.40	1
298.2	770	5.4	2.3	1.583	6.63	5
		10.2	4.9	1.556	6.91	7
		15.3	7.8	1.537	6.96	6
		20.2	10.0	1.514	6.93	3
		31.2	16.7	1.494	6.92	2
		41.5	20.0	1.459	6.88	4
		51.9	22.8	1.435	6.85	8
	feed	-	-	1.579	6.68	1
298.2	4360	6.0	2.4	1.541	6.63	4
		10.0	4.3	1.531	6.88	5
		15.5	7.0	1.496	6.52	3
		21.4	9.3	1.462	6.85	7
		32.9	14.7	1.404	5.92	2
		43.0	18.6	1.363	6.97	6
		52.0	21.3	1.322	6.98	8
	feed	-	-	1.677	7.06	1
342.9	1860	5.5	5.7	1.649	4.68	7
		9.9	11.5	1.625	5.97	6
		15.0	18.6	1.606	6.11	8
		21.3	28.1	1.585	6.39	2
		29.7	38.2	1.568	6.95	3
		40.3	47.4	1.542	6.88	4
		48.3	53.8	1.526	7.05	5
	feed	-	-	1.652	7.18	9
343.0	9930	5.3	5.3	1.652	4.97	14
		11.4	12.9	1.622	5.76	16
		15.9	18.8	1.594	6.12	15
		20.9	24.2	1.575	6.49	13
		30.6	36.4	1.536	6.64	10
		40.9	45.6	1.488	6.84	11
		48.8	54.3	1.457	6.97	12

Table E.6: Results using 1.0 m $MgCl_2$ and 300 ppm $MgSO_4$ (G5-R10).

T [K]	Re	Pressure [bar]	Flux [g/m^{2}s]	C$_{Cl^-}$ [m]	C$_{SO_4^{2-}}$ [ppm]	pH	Exp order
	feed	-	-	1.513	294	5.99	1
298.2	960	5.9	3.7	1.577	230	6.27	7
		9.4	6.1	1.563	219	na	5
		16.6	10.7	1.538	200	6.13	6
		20.8	13.3	1.529	194	na	3
		30.2	19.8	1.599	183	na	2
		41.6	24.0	1.473	157	5.85	4
		52.5	27.6	1.464	166	na	8
298.2	4520	6.8	4.2	1.569	222	6.57	11
		11.4	7.0	1.552	203	na	13
		16.2	9.9	1.528	187	6.63	12
		20.4	12.1	1.511	173	na	9
		30.9	17.7	1.462	155	na	14
		40.1	21.9	1.436	140	6.41	10
		53.4	27.8	1.388	130	na	15
342.9	1970	5.8	7.0	1.580	251	5.96	20
		10.6	14.7	1.569	233	na	19
		16.6	24.2	1.559	217	5.90	18
		22.3	33.6	1.540	214	na	16
		31.0	46.1	1.518	200	na	17
		41.3	59.2	1.506	189	6.30	21
		52.0	99.0	1.537	230	na	22
342.9	10250	7.0	9.5	1.578	247	6.30	27
		10.7	15.2	1.569	223	na	28
		15.4	22.4	1.546	211	6.37	29
		21.4	31.2	1.544	196	na	26
		30.1	42.4	1.508	183	na	24
		40.8	59.3	1.480	181	6.49	23
		53.4	77.3	1.454	172	na	25
	feed	-	-	1.579	279	na	30

Table E.7: Results using 1.0 m $MgCl_2$ and 300 ppm $MgSO_4$ (G5-R5).

T [K]	Re	Pressure [bar]	Flux [g/m^{2}s]	C_{Cl^-} [m]	$C_{SO_4^{2-}}$ [ppm]	pH	Exp order
	feed	-	-	1.861	299	6.10	1
343.0	950	6.0	6.2	1.839	252	6.02	7
		11.3	14.3	1.821	218	6.03	3
		15.6	19.3	1.812	213	6.05	6
		20.1	25.3	1.796	208	6.04	5
		30.4	38.6	1.776	194	6.03	4
343.0	4390	6.4	6.6	1.835	240	6.15	12
		11.3	13.2	1.812	214	6.08	10
		16.1	19.6	1.794	183	6.14	11
		18.9	23.6	1.781	177	6.07	8
		29.1	36.4	1.744	159	6.11	9
		-	-	1.865	290	6.19	13

Table E.8: Results using 1.0 m $MgCl_2$ and 3000 ppm $MgSO_4$ (G5-R7).

T [K]	Re	Pressure [bar]	Flux [g/m^{2}s]	C_{Cl^-} [m]	$C_{SO_4^{2-}}$ [ppm]	pH	Exp order
	feed	-	-	1.750	3055	5.61	1
343.0	1000	5.4	5.5	1.722	2496	na	6
		11.1	13.8	1.699	2287	5.84	5
		16.2	21.4	1.686	2146	na	7
		20.7	28.6	1.679	2093	5.81	3
		30.9	41.3	1.664	2082	na	4
343.0	4500	5.2	5.0	1.718	2454	5.90	10
		10.7	13.1	1.695	2145	na	11
		15.3	19.7	1.678	1968	na	8
		20.9	27.5	1.654	1847	na	9
		30.6	40.2	1.622	1683	5.97	12
	feed	-	-	1.750	3055	6.01	13

Table E.9: Results using 1.0 m $MgCl_2$ and 3000 ppm $MgSO_4$ (G5-R10).

T [K]	Re	Pressure [bar]	Flux [g/m^{2}s]	C_{Cl^-} [m]	$C_{SO_4^{2-}}$ [ppm]	pH	Exp order
	feed	-	-	1.575	3090	6.11	1
298.2	910	5.7	2.5	1.546	2298	6.27	7
		9.9	4.6	1.530	2084	na	6
		15.5	7.3	1.507	1919	6.22	5
		20.3	9.8	1.492	1846	na	4
		31.1	15.2	1.462	1751	na	2
		41.2	21.1	1.453	1674	6.03	3
		52.4	30.4	1.465	1988	na	8
298.2	4490	6.3	2.8	1.544	2281	na	12
		10.8	5.1	1.526	2080	na	13
		15.6	7.6	1.504	1820	na	14
		20.5	10.2	1.481	1760	na	15
		29.1	14.4	1.446	1590	na	9
		39.0	19.1	1.415	1514	na	10
		50.1	26.4	1.392	1485	na	11
	feed	-	-	1.574	3091	6.31	16
343.0	2080	5.8	7.4	1.561	2697	6.21	23
		10.2	19.8	1.553	2681	na	22
		15.5	31.5	1.544	2599	6.23	21
		20.2	42.8	1.536	2515	na	20
		31.3	73.9	1.524	2707	na	18
		41.2	89.6	1.518	2453	6.10	19
		51.6	148.4	1.536	2697	na	17
343.0	10170	6.0	8.9	1.560	2745	na	30
		10.4	16.9	1.539	2486	na	29
		15.1	24.9	1.509	2380	na	28
		19.5	41.9	1.522	2408	na	27
		30.7	84.5	1.519	2485	na	25
		41.9	108.0	1.510	2389	na	26
		51.3	151.7	1.511	2389	na	24
	feed	-	-	1.565	3056	na	31

Table E.10: Results using 2.5 m $MgCl_2$ (G5-R1).

T [K]	Re	Pressure [bar]	Flux [g/m^{2}s]	C_{Cl^-} [m]	pH	Exp order
	feed	-	-	4.74	5.31	1
298.0	910	21.5	5.2	4.65	5.22	3
		30.5	7.3	4.62	5.22	2
		40.1	8.7	4.61	5.32	4
		50.4	10.3	4.57	5.39	5
298.7	2680	18.9	4.4	4.68	5.45	7
		31.4	6.8	4.64	5.47	8
		41.3	8.5	4.57	5.43	6
		51.3	10.6	4.54	5.50	9
	feed	-	-	4.79	5.45	10
343.1	1110	10.5	6.9	4.74	5.45	11
		22.4	16.0	4.68	5.37	12
		30.2	20.9	4.66	5.40	13
		41.7	27.3	4.65	5.41	14
		51.4	31.9	4.63	5.44	15
343.0	2730	10.5	6.4	4.73	5.43	17
		22.8	14.5	4.67	5.46	16
		32.8	20.9	4.66	5.43	18
		41.0	25.7	4.61	5.41	19
		52.8	31.7	4.58	5.46	20
342.7	5020	11.3	6.6	4.72	5.47	23
		20.7	12.8	4.69	5.48	24
		29.3	18.2	4.66	5.51	25
		42.7	25.6	4.61	5.48	22
		51.0	30.3	4.59	5.52	21
	feed	-	-	4.78	5.49	26

Table E.11: Results using 2.5 m $MgCl_2$ and 300 ppm $MgSO_4$ (G5-R8).

T [K]	Re	Pressure [bar]	Flux [g/m^{2}s]	C_{Cl^-} [m]	$C_{SO_4^{2-}}$ [ppm]	pH	Exp order
	feed	-	-	4.26	383	5.09	1
298.2	1000	14.7	4.1	4.23	282	5.16	7
		19.4	6.2	4.19	282	5.14	4
		30.4	9.0	4.15	252	5.09	3
		40.0	11.2	4.12	238	5.15	5
		50.8	13.0	4.11	235	5.18	6
	feed	-	-	4.29	384	5.14	8
	feed	-	-	4.56	352	5.09	9
343.0	1130	10.5	6.5	4.51	303	5.07	15
		20.7	15.4	4.48	282	5.09	11
		30.6	20.0	4.46	265	5.08	14
		40.8	26.7	4.45	260	5.10	13
		49.6	32.9	4.42	258	5.12	12
343.1	5000	11.0	6.7	4.49	285	5.08	16
		20.0	12.9	4.47	259	5.07	20
		29.6	19.7	4.45	265	5.09	17
		39.4	25.3	4.41	234	5.10	19
		50.0	32.1	4.38	223	5.06	18
	feed	-	-	4.53	354	5.08	21

Table E.12: Results using 5.0 m $MgCl_2$ (G5-R1 and G5-R2).

T [K]	Re	Pressure [bar]	Flux [g/m^{2}s]	C_{Cl^-} [m]	pH	Exp order
G5-R1	feed	-	-	10.82	5.30	1
343.1	1100	32.8	4.0	10.69	5.16	2
		42.9	4.6	10.62	5.19	3
		52.0	4.8	10.61	6.01	4
		61.9	5.4	na	na	5
G5-R2	feed	-	-	9.63	4.64	1
343.0	720	32.6	5.8	9.55	4.86	2
		40.1	6.7	9.54	5.01	3
		48.5	7.4	9.50	5.05	4
		55.6	8.2	9.47	5.04	5
343.0	1410	28.0	3.9	9.48	5.15	15
		32.0	4.8	9.51	5.02	6
		41.5	6.0	9.54	5.01	8
		48.0	7.0	9.55	5.01	7
		55.1	7.8	9.50	5.09	9
		59.8	8.2	9.59	5.24	14
343.2	2400	30.1	4.2	9.54	5.19	11
		39.9	5.7	9.55	5.16	10
		43.1	6.0	9.51	5.19	13
		51.0	7.2	9.55	5.18	12
	feed	-	-	9.68	5.28	16

Table E.13: Results using 5.0 m $MgCl_2$ and 300 ppm $MgSO_4$ (G5-R6).

T [K]	Re	Pressure [bar]	Flux [g/m^{2}s]	C_{Cl^-} [m]	$C_{Mg^{2+}}$ [m]	$C_{SO_4^{2-}}$ [ppm]	pH	Exp order
	feed	-	-	9.84	4.20	357	5.37	1
343.3	1350	31.0	3.7	9.76	4.22	2484	4.98	6
		36.6	4.8	9.74	4.13	2463	4.97	3
		35.4	4.2	9.76	4.22	2507	4.96	7
		46.2	5.5	9.76	4.18	2396	4.90	4
		53.6	6.0	9.76	4.18	2253	4.95	5
	feed	-	-	9.83	4.22	339	5.03	8

Table E.14: Results using 5.0 m $MgCl_2$ and 3000 ppm $MgSO_4$ (G5-R8).

T [K]	Re	Pressure [bar]	Flux [g/m^{2}s]	C_{Cl^-} [m]	$C_{SO_4^{2-}}$ [ppm]	pH	Exp order
	feed	-	-	9.62	3046	4.74	1
343.5	1440	30.8	5.2	9.54	2253	4.87	3
		31.0	4.3	9.53	2119	4.95	7
		40.5	5.7	9.54	1984	4.94	6
		47.4	7.0	9.48	1934	4.89	4
		53.1	7.3	9.43	1928	4.95	5

Appendix F

Multivariate statistical analysis

F.1 General multivariate regression

Detailed information about multivariate statistical analysis can be found in Martens and Næs (1989) or Johnson and Wichern (1992), and the following discussion will just formulate the statistical problem and give the idea behind the partial least squares regression method.

The multivariate regression analysis seeks to extract information from a set of observations to formulate a model depending on a set of variables. To measure how good the model fits the observed data the expected mean squared prediction error (MSPE) can be calculated from

$$MSPE \equiv E[(Y - \widehat{Y}(\mathbf{Z}))^2] \tag{F.1}$$

where Y is the observation and $\widehat{Y}(\mathbf{Z})$ is the predicted response depending on the variables given in the vector $\mathbf{Z} = [Z_1\ Z_2\ ...\ Z_r]^T$. The regression analysis can then be reduced to the mathematical problem of finding the predictor (model) that minimizes the MSPE. It can be shown that if the observation and the set of variables

$$\begin{pmatrix} Y \\ \mathbf{Z} \end{pmatrix} \tag{F.2}$$

have a multivariate normal distribution with the mean vector

$$\begin{pmatrix} \eta \\ \boldsymbol{\mu} \end{pmatrix} \tag{F.3}$$

and the covariance matrix

$$\begin{pmatrix} \tau^2 & \boldsymbol{\sigma}^T \\ \boldsymbol{\sigma} & \boldsymbol{\Sigma} \end{pmatrix} \tag{F.4}$$

the best result is obtained by the linear least squares predictor given by

$$\widehat{Y}_{LS} = \eta + \boldsymbol{\sigma}^T \boldsymbol{\Sigma}^{-1} (\mathbf{Z} - \boldsymbol{\mu}) \tag{F.5}$$

The statistical parameters are defined by

$$\boldsymbol{\mu} = E(\mathbf{Z}) \tag{F.6}$$

$$\boldsymbol{\Sigma} = Cov(\mathbf{Z}) = E[(\mathbf{Z} - \boldsymbol{\mu})(\mathbf{Z} - \boldsymbol{\mu})^T] \tag{F.7}$$

$$\eta = E(Y) \tag{F.8}$$

$$\tau^2 = Var(Y) \tag{F.9}$$

$$\boldsymbol{\sigma} = Cov(\mathbf{Z}, Y) = E[(\mathbf{Z} - \boldsymbol{\mu})(Y - \eta)^T] \tag{F.10}$$

where their unbiased estimators from n independent observations can be calculated from

$$\widehat{\boldsymbol{\mu}} = \frac{1}{n} \sum_{j=1}^{n} \mathbf{Z_j} \tag{F.11}$$

$$\widehat{\boldsymbol{\Sigma}} = \frac{1}{n-1} \sum_{j=1}^{n} (\mathbf{Z}_j - \widehat{\boldsymbol{\mu}})(\mathbf{Z}_j - \widehat{\boldsymbol{\mu}})^T \tag{F.12}$$

$$\widehat{\eta} = \frac{1}{n} \sum_{j=1}^{n} Y_j \tag{F.13}$$

$$\widehat{\tau}^2 = \frac{1}{n-1} \sum_{j=1}^{n} (Y_j - \widehat{\eta})^2 \tag{F.14}$$

$$\widehat{\boldsymbol{\sigma}} = \frac{1}{n-1} \sum_{j=1}^{n} (\mathbf{Z}_j - \widehat{\boldsymbol{\mu}})(Y - \widehat{\eta})^T \tag{F.15}$$

In practice the observations and variables are standardized and replaced by

$$\widetilde{Y}_j = \frac{Y_j - \widehat{\eta}}{\widehat{\tau}} \tag{F.16}$$

$$\widetilde{Z}_{ij} = \frac{Z_{ij} - \widehat{\mu}_i}{\sqrt{s_{ii}}} \tag{F.17}$$

where s_{ii} are the diagonal elements of the matrix $\widehat{\Sigma}$. Further, to test the estimated model a cross validation procedure can be used. In full cross validation one sample at a time is left out from the regression analysis and used to calculate the prediction residual. Then at the end all prediction residuals are combined to compute the validation residual variance and MSPE.

Lack of selectivity, collinearity[1] and lack of knowledge of the mechanisms behind the data are common problems that may rise when Y is predicted from a set of variables $\mathbf{Z}$. To handle these problems flexible methods have been developed, *e.g.* data compression methods such as principal component regression (PCR) and partial least squares regression (PLSR)(Martens and Næs 1989). These methods try to extract the information in the many observed variables $\mathbf{Z}$ onto a few underlying latent variables $\mathbf{T}$[2]. The transformation done by these so-called bivariate methods can be written

$$\mathbf{Z} = \mathbf{T}\mathbf{P}^T + \mathbf{E} \tag{F.18}$$

where $\mathbf{T}$ and $\mathbf{P}$ are some sort of matrix decomposition and $\mathbf{E}$ is the residual matrix. PCR uses the m ($m \leq r$) first principal components of the matrix $\mathbf{Z}$ to perform the prediction instead of the matrix $\mathbf{Z}\mathbf{Z}^T$ itself, whereas PLSR uses the linear combinations of the variables which gives the largest possibly dependency (largest covariance) with the observations.

F.2 PLSR algorithm

The PLSR method can be summarized by the algorithm:

1. Find the eigenvector corresponding to the largest eigenvalue in the matrix $\mathbf{Y}^T\mathbf{Z}$, and name it $\mathbf{w}_1$.

2. Calculate the score vector for the first latent variable, $\mathbf{t}_1 = \mathbf{Z}\mathbf{w}_1$.

[1] Collinearity means that the columns in the design matrix $\mathbf{Z}$ are linear or almost linear dependent of each other and will make the inverse of the matrix $\mathbf{Z}\mathbf{Z}^T$ singular or close to singular. In the first case no solution will exists whereas in the latter case the numerical solution can give wrong regression coefficients.

[2] Also called components, scores, regression factors or just factors.

3. Calculate the loading vector to $\mathbf{Z}$: $\mathbf{p}_1 = \frac{\mathbf{Z}^T\mathbf{t}_1}{\mathbf{t}_1^T\mathbf{t}_1}$.

4. Calculate the loading vector to $\mathbf{Y}$: $\mathbf{q}_1 = \frac{\mathbf{Y}^T\mathbf{t}_1}{\mathbf{t}_1^T\mathbf{t}_1}$.

5. Calculate the residual matrix to $\mathbf{Z}$: $\mathbf{E}_1 = \mathbf{Z} - \mathbf{t}_1\mathbf{p}_1^T$.

6. Calculate the residual matrix to $\mathbf{Y}$: $\mathbf{F}_1 = \mathbf{Y} - \mathbf{t}_1\mathbf{q}_1^T$.

Repeat this procedure with $\mathbf{E}_1$ and $\mathbf{F}_1$ instead of $\mathbf{X}$ and $\mathbf{Y}$ and continue to repeat the procedure with new latent variables until k latent variables have been found and the eigenvalues of the matrix $\mathbf{F}_k^T\mathbf{E}_k$ are small. The prediction from a set of variables $\mathbf{Z}_{\text{new}}$ can now be found by the algorithm:

1. Calculate the score for the first latent variable: $t_1 = \mathbf{w}_1\mathbf{Z}_{\text{new}}$.

2. Calculate the residual: $\mathbf{e}_1 = \mathbf{Z}_{\text{new}} - t_1\mathbf{p}_1^T$.

3. Use $\mathbf{e}_1$ instead of $\mathbf{Z}_{\text{new}}$ to calculate the score for the second latent variable, t_2, and so on until all k t-scores have been calculated.

4. Estimate the response: $\widehat{Y}_{\text{new}} = \mathbf{Q}^T\mathbf{t}$.

F.3 PLSR results

The PLSR method was chosen because it seeks to find the largest covariance between the variables and the observations. The regression analysis was done with the computer program Unscrambler (version 6.1). Models obtained from separate calculations of the measured retention data and the modified retention data[3] showed no significant differences.

[3] The measured retentions have been modified by the equation $R_{\text{mod}} = R_{\text{obs}}\frac{R^t_{\text{ave}}}{R^t_{\text{sample}}}$, where R^t_{sample} is the chloride retention measured in the test experiment run on each new membrane sample and R^t_{ave} is their average.

The results from the PLSR analysis are shown in the Figures F.1-F.4, where each figure consists of six different plots which show (a) the scores, (b) the loadings, (c) the normal probability plot of the residuals, (d) the predicted versus measured retentions, (e) the regression coefficients, and (f) the residual validation variance. The score plot (a) reveals the main pattern in the set of observations according to the new coordination system and the loading plot (b) shows the relationships between the variables and the latent variables. Both plots use the first latent variable as the x-axis and the second latent variable as the y-axis. The normal probability plot of the residuals (c) is used as an indicator of whether nonlinearities are covered in the model or not. Deviations from a straight line can be an indication that the model used is not sufficient to describe all the information in the observations. Single points deviating from the straight line can be outliers. The residual validation variance plot (f) shows how the residual changes when the number of latent variables used in the model increases.

The four models presented in this appendix are the models that gave the best fit to the modified retention data. The models were made to depend on the main variables (temperature, Reynolds number, chloride concentration, sulphate concentration and pressure), their two-factor interactions and the squared main variables. Most of the predicted retentions are too low and the models can only explain around 65-70% of the variation in the observations. The residual validation variance plots (f) show that only two latent variables in each model are needed in order to extract the information in the observed retentions available for the chosen models. Further, the normal probability plots of the residuals (c) show some curvature which also indicates that other variables or interactions should be included in the models. Some of the points which deviate strongly at the ends of the line can be an indication of the presence of outliers. For example, the point to the far left in Figure F.2c, has been identified as the sulphate retention point at 175 ppm sulphate concentration, Reynolds number 1000 and pressure around 5 bar in Figure 6.2, Chapter 6. This point do not fit into the rest of the same experimental data series and most likely something went wrong in the laboratory.

Figure F.1b show the loadings for the latent variables in the case of chloride retention measured on the Desal 5 DK membrane. The first latent variable is negatively correlated with the chloride concentration and temperature and positively correlated with the Reynolds number. The second latent variable is positively correlated with the pressure and to some extent with the chloride concentration. The regression coefficients given in Figure F.1e shows that the temperature and the chloride concentration have a large negative effect on the chloride retention whereas the Reynolds number, the pressure and their interaction have a relatively

large positive effect. The loadings for the latent variables found in the case of sulphate retentions, shown in Figure F.2b, indicate that the first latent variable is mainly positively correlated with the temperature squared and Reynolds number and negatively correlated with the temperature. The second latent variable is positively correlated with the Reynolds number and the chloride concentration and negatively correlated with the interaction between the Reynolds number and the chloride concentration. The regression coefficients in Figure F.2e show that it is mainly the temperature, the Reynolds number and the interaction between the Reynolds number and the chloride concentration that influence the sulphate retention predictions.

The separation process should be operated at low Reynolds number and low pressure in order to increase the separation between the sulphate and chloride ions which can be seen when the loadings from the chloride and sulphate models are compared. The pressure has almost no influence on the sulphate retention whereas the chloride retention increases when the pressure increases. Both the chloride and sulphate retentions will increase when the Reynolds number increases but the Reynolds number also has a strong negative effect on the sulphate retention through the interaction with the chloride concentration and should therefore be kept as low as possible.

A similar analysis of the results obtained on the Desal G5 membrane show that the first latent variable in the chloride retention predictions is positively correlated with the pressure, the Reynolds number and their interaction and negatively correlated with the temperature and the chloride concentration, refer Figure F.3b. On the other hand, the second latent variable is mainly correlated with the pressure. The regression coefficients show that the temperature, the chloride concentration and the pressure dominate the chloride retention predictions. In the case of sulphate, the first latent variable is negatively correlated with the temperature and the chloride concentration, whereas the second latent variable is mainly correlated with the pressure, refer Figure F.4b. The regression coefficients show that the temperature and the pressure dominate the model but neither the Reynolds number, the chloride concentration and the sulphate concentration can be excluded from the model. The results give no clear differences between the two models, but there are indications that an increased chloride concentration has a stronger negative effect on the chloride retention than on the sulphate retention.

It should be emphasized that the models used in the regression analysis are purely stochastic without any mechanistic foundations which makes it difficult to explain some of the terms appearing in the models, *e.g.* the squared pressure

and temperature terms.

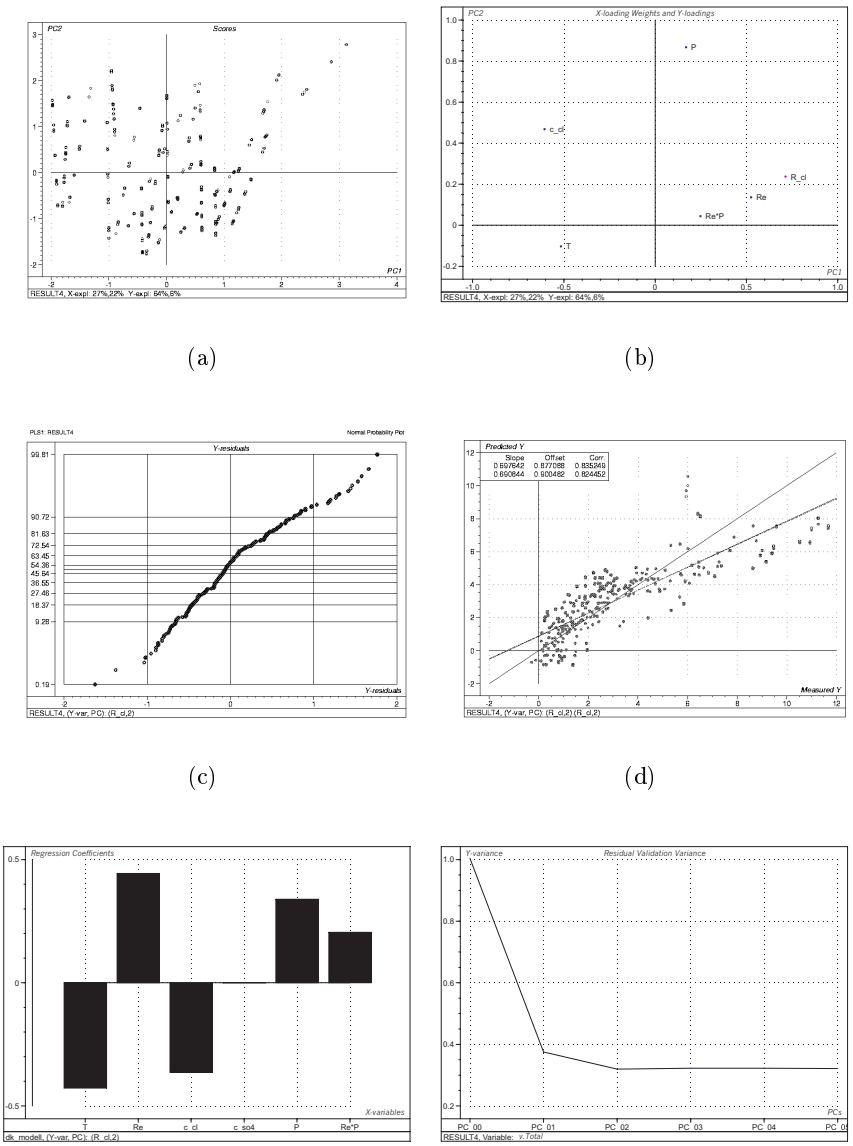

(a) (b)

(c) (d)

(e) (f)

Figure F.1: PLSR results of the chloride retentions obtained using the Desal 5 DK membrane. (a) scores, (b) loadings, (c) residual normal probability plot, (d) predicted versus measured retentions, (e) regression coefficients, (f) residual validation variance.

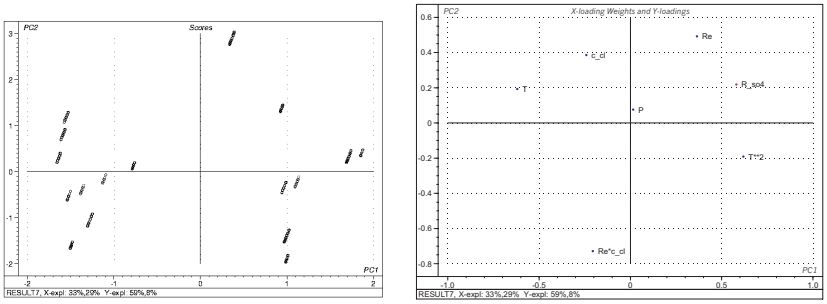

(a) (b)

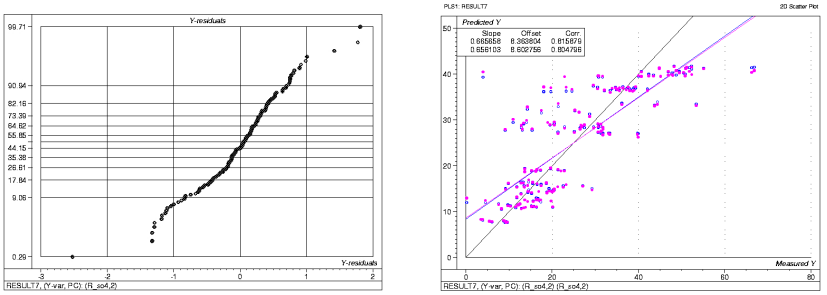

(c) (d)

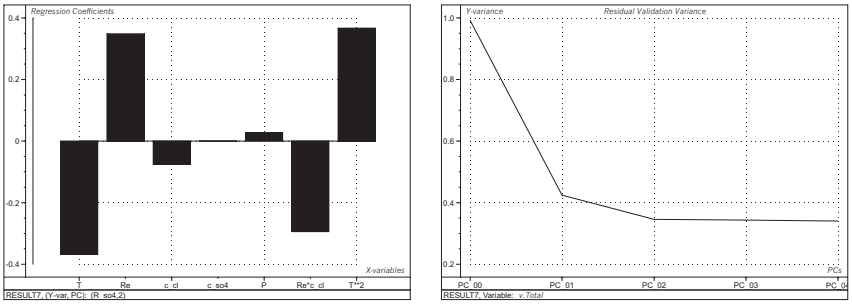

(e) (f)

Figure F.2: PLSR results of the sulphate retentions obtained using the Desal 5 DK membrane. (a) scores, (b) loadings, (c) residual normal probability plot, (d) predicted versus measured retentions, (e) regression coefficients, (f) residual validation variance.

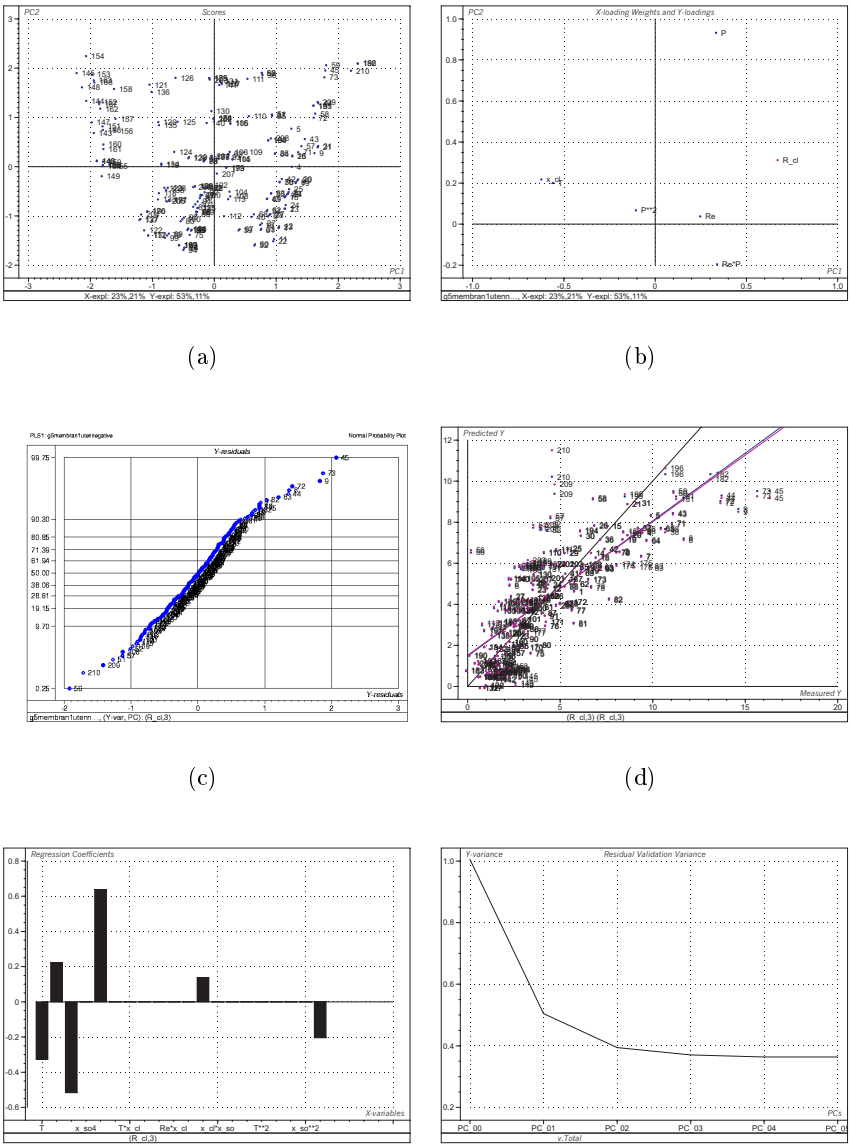

(a) (b)

(c) (d)

(e) (f)

Figure F.3: PLSR results of the chloride retentions obtained using the Desal G5 membrane. (a) scores, (b) loadings, (c) residual normal probability plot, (d) predicted versus measured retentions, (e) regression coefficients (from left to right: T, Re, c_{Cl^-}, P, Re x P and P^2), (f) residual validation variance.

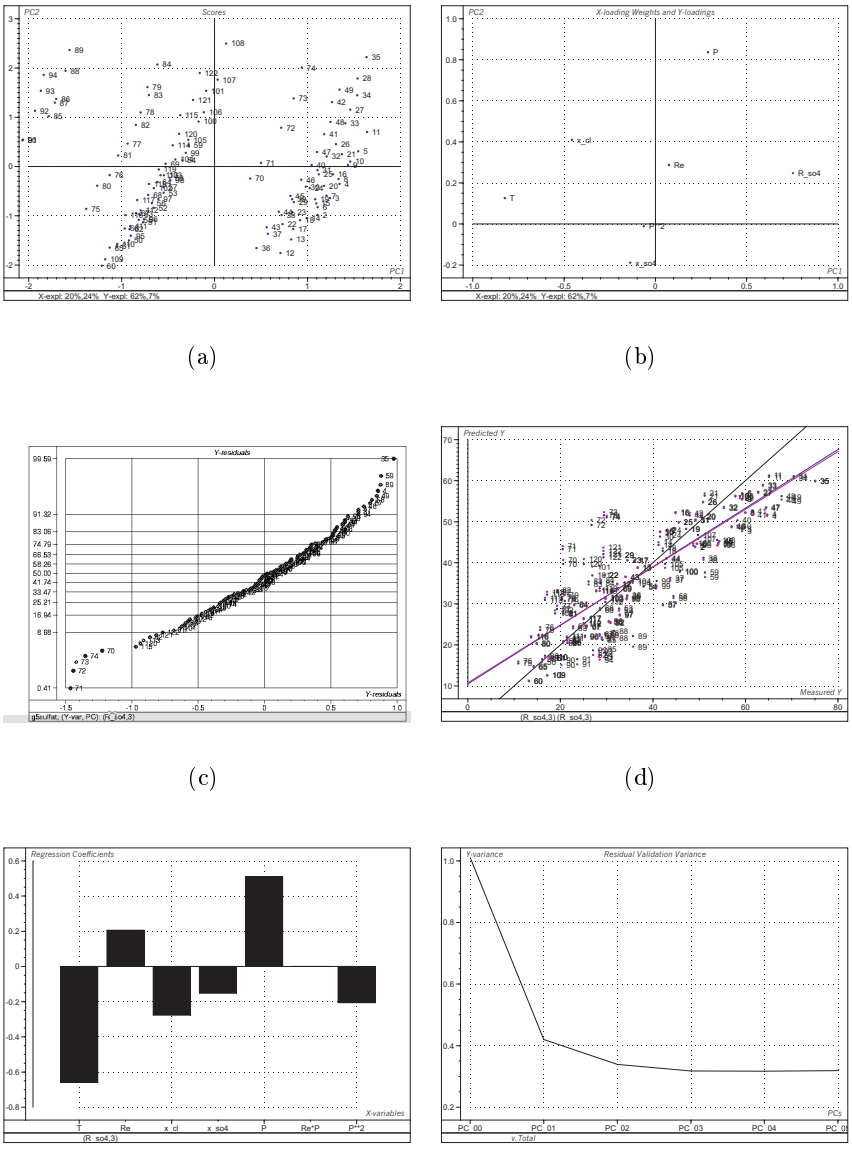

Figure F.4: PLSR results of the sulphate retentions obtained using the Desal G5 membrane. (a) scores, (b) loadings, (c) residual normal probability plot, (d) predicted versus measured retentions, (e) regression coefficients, (f) residual validation variance.